# SYNTHESIS AND PHOTOPHYSICS OF ORGANOGOLD COMPLEXES BEARING EITHER A BENZOTHIAZOLE FLUORENYL OR DIPHENYL AMINO FLUORENYL MOIETY: A STUDY IN STRUCTURE-PROPERTY RELATIONSHIPS

by

JOSEPH J. MIHALY

Submitted in partial fulfillment of the requirements for

the degree of Doctor of Philosophy

Department of Chemistry

**CASE WESTERN RESERVE UNIVERSITY**

August 2020

CASE WESTERN RESERVE UNIVERSITY

SCHOOL OF GRADUATE STUDIES

We hereby approve the thesis/dissertation of

Joseph J. Mihaly

candidate for the degree of Doctor of Philosophy *.

Committee Chair

John Protasiewicz

Committee Member

Thomas G. Gray

Committee Member

Anna Cristina Samia

Committee Member

Ica Manas-Zloczower

Date of Defense

6/25/20

*We also certify that written approval has been obtained

for any proprietary material contained therein.

**Copyright Information.**

*Chapter 2*
The work described within chapter 2 was published in Dalton Transactions, 2019, 48, 15917 – 15927. https://doi.org/10.1039/C9DT02312G.The Royal Society of Chemistry states "If you are the author of this article you still need to obtain permission to reproduce the whole article in a third party publication with the exception of reproduction of the whole article in a thesis or dissertation."

*Chapter 3*
The work described within chapter 3 was published in Physical Chemistry Chemical Physics (2020): https://doi.org/10.1039/D0CP01539C. "From PCCP's website: If you are the author of this article you do not need to formally request permission to reproduce figures, diagrams etc. contained in this article in a thesis or dissertation provided that the correct acknowledgement is given."

*Chapter 4*
The work described within chapter 4 was published in Organometallics (2020): https://doi.org/10.1021/acs.organomet.9b00768. "From the Organometallics website:"Reuse/Republication of the Entire Work in Theses or Collections: Authors may reuse all or part of the Submitted, Accepted or Published Work in a thesis or dissertation that the author writes and is required to submit to satisfy the criteria of degree-granting institutions."

Table of Contents

# List of Tables

Chapter 2:



Chapter 3:



Chapter 4:

Chapter 5:



Chapter 6:

# List of Figures

Introduction:



Chapter 2:

Chapter 3:

Chapter 4:

Chapter 5:

Chapter 6:

List of Schemes:

## A Dedication/Acknowledgments

### A Dedication

To my fiancée and my parents, the love I have for you knows no bounds.

### Acknowledgements

First, I would like to thank my parents. They taught me from an early age how to take responsibility for myself and how to not blame other people for my failures. Both of you have exhaustively sacrificed body and mind so that your children could have a chance to chase their dreams. It would be an insult to your sacrifices to not strive every day for greatness, and that is exactly what I have done. I love you both and I'll never be able to repay you for everything you have given up. To my fiancée, you have shown me unwavering support while simultaneously being in the trenches of this thing called doctorate school. The fact that you can put up with me and my far-fetched dreams surprises me every day. You have seen my triumphs as well as my failures, and have stood by me through it all. I guess the Marlboro man was right, "The right women can make you, and the wrong one can break you." I am excited for everything the future holds for us, and taking it on together. I feel overwhelming gracious that I've had you through this journey, and I love you for that and everything else.

Dr. Thomas Gray, I am truly sorry you've had to put up with me for the last four to five years. I know my insatiable appetite for success coupled with my ability to exhibit little patience and understanding has driven you close to madness. I am truly grateful for everything I have learned from you, because it has been a lot, and like Jim Heckler…"I'll be lucky to retain half of it." I will miss my conversations with you as my mentor, but I look forward to having some with you as my peer. Dr. Tod Grusenmeyer, I think we have worked so well together because we are both hard-headed, win at all costs type men. We don't believe in excuses and are both highly ambitious. I've learned more about photophysics from listening to you speak then any text book has taught me. I was fortunate that you were willing to be a co-mentor to me, and I did take advantage of it every chance I could. I've always enjoyed and appreciated your mentorship on career advancement as well as managing personalities and collaborations, and really anything else that has to do with the business of chemistry. **To both of you, thank you**. I would not be the chemist I am today with the guidance I received.

Being very important to me: I would like to thank anyone who has ever doubted me or told me I would never accomplish certain goals, dreams, or visions. Your doubts have fueled this flame since the beginning and I can recite everything negative ever said about me as a person but more importantly as a chemist, to this day.

Lastly, as all great athletes do. I would like to thank God. Without the possibility of an eternity in hell, only you know where I would be.

People/Quotes that have helped me along the way

"I knew what was gonna happen. I knew I was gonna get here. They didn't. There was a lot of stressful years. A lot of tough times, but I proved them wrong. I proved myself right."
-Conor McGregor

"This is not arrogance, this is belief"
-Conor McGregor

"You can only have two things in life: reasons or results. Folks will always point out reasons on why they are not living their dreams, on why they are not manifesting their greatness. They will always be able to point those things out, but none of those things count. The only thing that counts are results; and results don't lie, they tell it all. Judge a tree by the fruit that it bears. Not the ones that it might talk. Not the ones that it might wish for, or think about, or firm about. But by the fruit that it actually bears."
-Les Brown

"When you have something you want to do. If you don't develop the courage to do that which has been given you to do; and you spend a lot of time trying to convince other people or get their approval. What will happen is that you will lose your nerve. And other people will convince you that what you're doing doesn't have any value. And you'll give up on your dreams."
-Les Brown

Synthesis and Photophysics of Organogold Complexes Bearing Either a Benzothiazole Fluorenyl or Diphenyl Amino Fluorenyl Moiety: A Study in Structure-Property Relationships


Abstract

By

JOSEPH J. MIHALY

This dissertation describes the synthesis, photophysics, and computations for a library gold(I)/(III) organometallics bearing either a benzothiazole fluorenyl (BTF) or diphenyl amino fluorenyl (DPA) moiety. Three different series of gold(I) BTF complexes were synthesized with variation in ancillary ligand, gold-chromophore linkage, and number of metal centers. It was found that all three of these parameters have an effect on photophysical properties and excited-state dynamics. Computations support the observed photophysical phenomena for those complexes. Gold(I) complexes bearing the DPA moiety were isolated and photophysical analyzed. Both ancillary ligand, gold-chromophore linkage, and amine capping moiety were found to have an effect on absorption and emission properties. Lastly, gold(III) complexes bearing either the DPA or BTF moiety were isolated and photophysical analyzed. The effect of both capping moiety, gold-chromophore linkage, and oxidation state on photophysical properties is drawn. Overall, structure-property relationships for gold organometallics concerning oxidation state, ancillary ligand, gold-chromophore linkage, and capping moiety are discussed.

# Chapter 1: Introduction

Triplet photoactive compounds have been of continued interest in a variety of fields due to their long-live triplet excited states coupled with the possibility of increased luminescence efficiency. Often, these compounds consist of late *d*-block transition metals bound to conjugated organic fluorophores. Introduction of metals like copper, palladium, iridium, platinum, and gold endow organic chromophores with spin-orbit coupling; which relaxes the orthogonality between close lying singlet and triplet excited states, allowing for intersystem crossing to occur (Figure 1.1).[1-7] If the metal itself contributes to the frontier orbitals of the ligand, spin-orbit coupling is enhanced and population of triplet excited states ensues.[8,9]

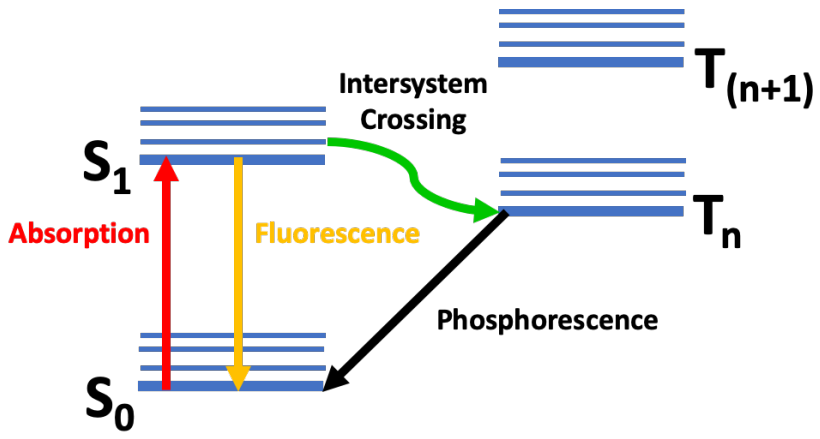


**Figure 1.1.** Jablonski diagram showing the photophysical processes of absorption (red), fluorescence (yellow), intersystem crossing (green), and phosphorescence (black).

Triplet-state photoproperties are desirable for a variety of applications, including organic light-emitting diodes (OLEDs),[10-24] photoredox sensitization and catalysis,[25-31] photodynamic therapy (PDT),[32-37] nonlinear optical materials (NLO),[38-46] and bioimaging agents,[47-51] as well as others.[52-55] Iridium(III) and platinum(II) complexes have been extensively studied from a fundamental, structure-property standpoint. A brief discussion regarding the complexes of those metals and the applications they are implemented for is now appropriate.

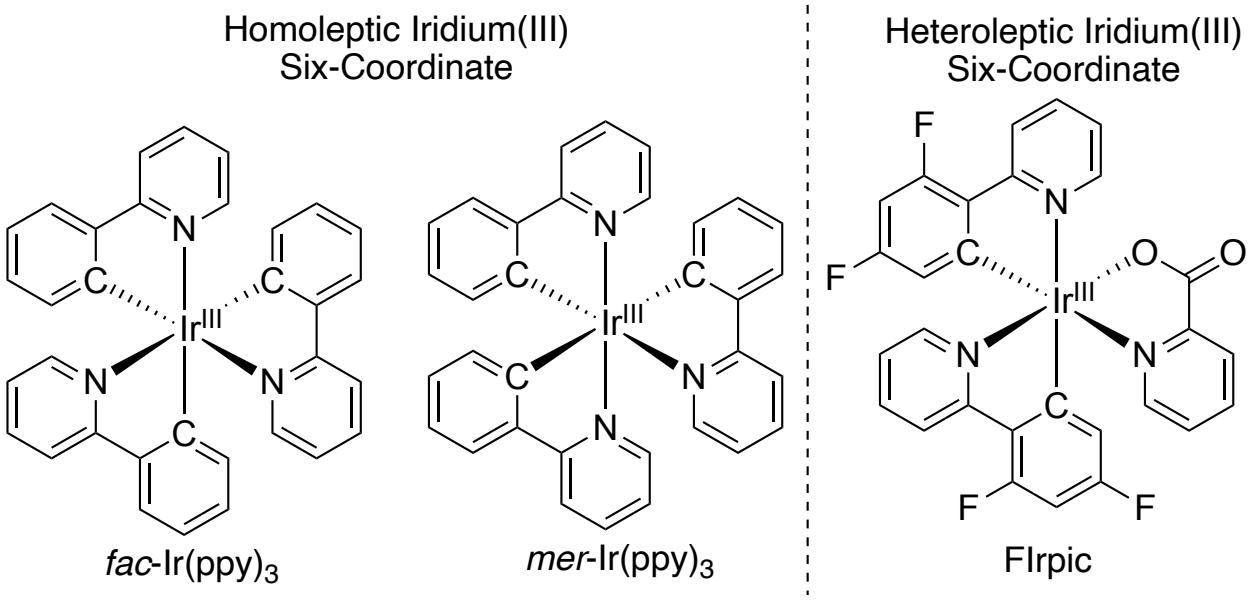


**Figure 1.2.** Examples of neutral iridium(III) complexes.

Cyclometallated iridium(III) complexes are most widely used in light-emitting applications and photoredox catalysis, though they have been employed for other purposes (Figure 1.2).[12-16, 18-19, 21-22, 56-58] Iridium(III), $d^6$, has a spin-orbit coupling constant $\zeta_{soc}$ = 3909 $cm^{-1}$; the complexes are generally six coordinate and octahedral.[56] Iridium(III) complexes are commonly used in OLED devices for a plethora of reasons (Figure 1.3).[58] The first is that triplet emitters can theoretically yield a unity internal quantum efficiency via electroluminescence. Second, these complexes generally have high phosphorescence quantum yields both in solution and the solid state, as well as relatively short phosphorescence lifetimes. Third, the emission color of the complex can be easily tuned through cyclometallate (C^N) ligand variation or addition of electron withdrawing or electron donating groups to said ligand. A range of charge transfer states are also available, though the triplet state is usually some blend of ligand centered ($^3$LC) and metal-to-ligand charge transfer ($^3$MLCT) character. The combination of these qualities make iridium(III) complexes good candidates for red, green, and blue emitters. Much literature exits on the synthesis,

photophysical characterization, and OLED device performance of iridium(III) compounds. Some are even commercially used in OLED televisions and displays.[57]

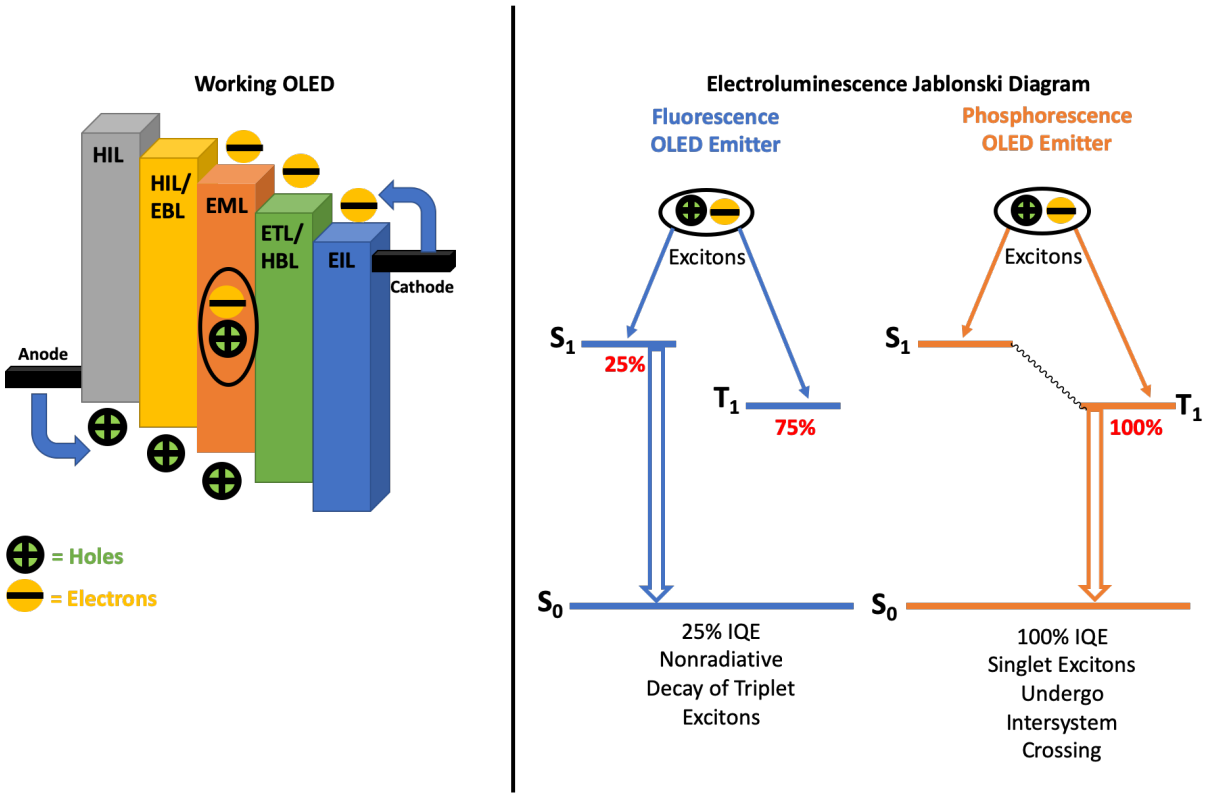


**Figure 1.3.** (Left) Working OLED depiction, adapted from reference 58. (Right) Electroluminescence Jablonski diagram displaying the advantages of using a triplet-state emitter.

Iridium(III) complexes have been extensively studied as photoredox catalysts as well. They exhibit a number of desirable qualities that make them suitable for this purpose (Figure 1.4).[27-29,56] Iridium(III) complexes strongly absorb visible light at select wavelengths where many organic reactants do not. Once this light is absorbed, a MLCT occurs where the metal center is formally oxidized and the ligand is formally reduced. This excited-state can then readily undergo an outer-sphere electron transfer. As discussed for OLEDs, iridium(III) complexes display near unit phosphorescence quantum yields and short phosphoresce lifetimes (nanoseconds to milliseconds). These qualities allow iridium(III) complexes to undergo bimolecular reactions in many organic

solvents efficiently. That attribute, in combination with desirable redox potentials and the ability to absorb selective visible light yields photoreactive molecules prime for use as photoredox catalysts.

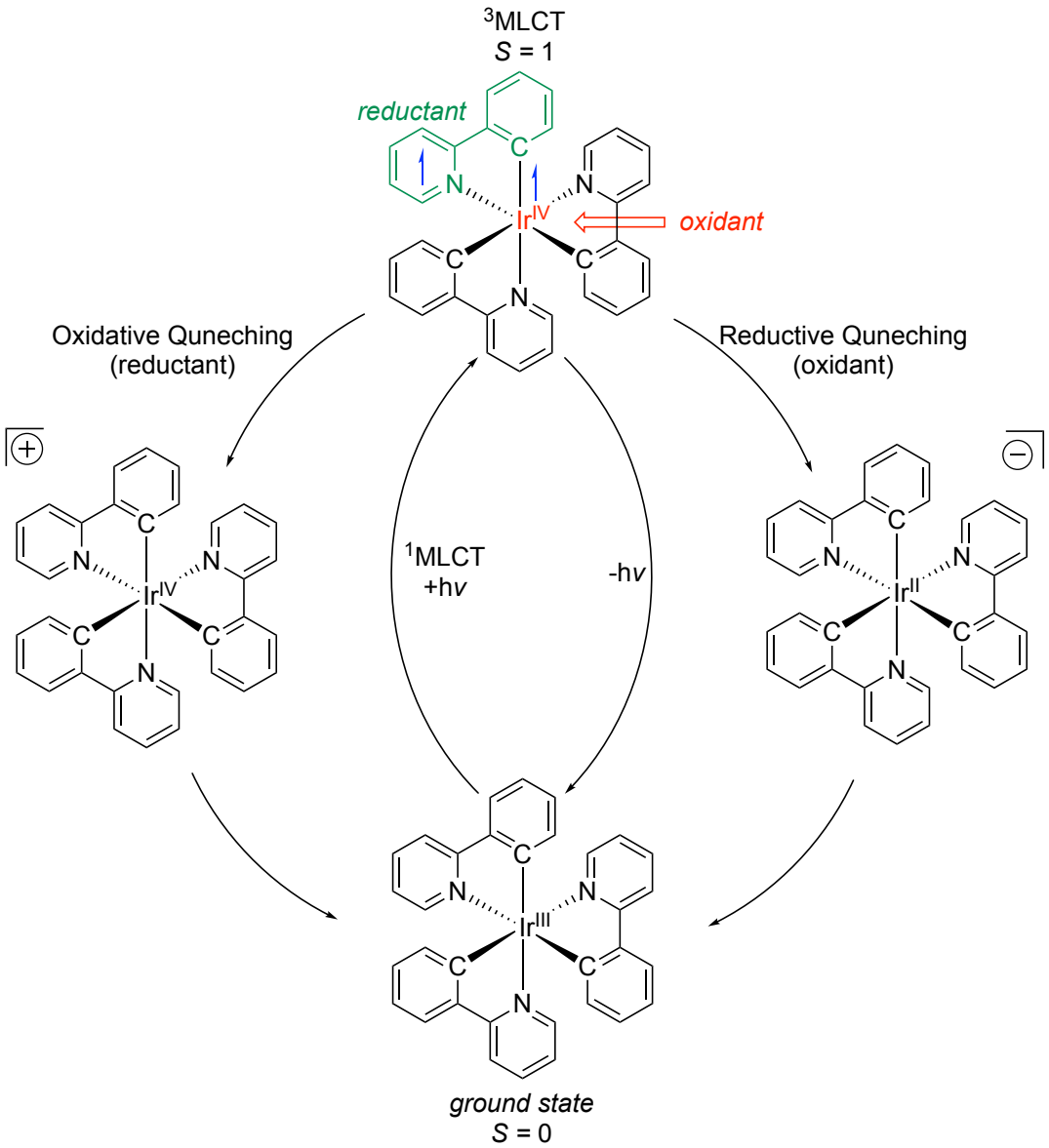


**Figure 1.4.** Photophysical and photochemical pathways of an iridium(III) complex in regards to photoredox catalysis. Adapted from reference 56.

Platinum(II) complexes, like iridium(III) compounds are exploited as triplet photoactive materials. Platinum(II) is a $d^8$ metal and has an ($\zeta_{SOC}$ =4500 $cm^{-1}$); the complexes are square planar

(Figure 1.5).[59,60] Platinum compounds have found widespread use in bioimaging and sensing and as nonlinear optical materials.[61-75] However, platinum(II) complexes are most widely used as OLED emitters for reasons previously described regarding iridium(III) complexes.[3,14-16,18,23] The impact of platinum(II) compounds on the field of OLEDs cannot be understated; many reviews exist on this topic and commercial use has been realized.[59,60,76]

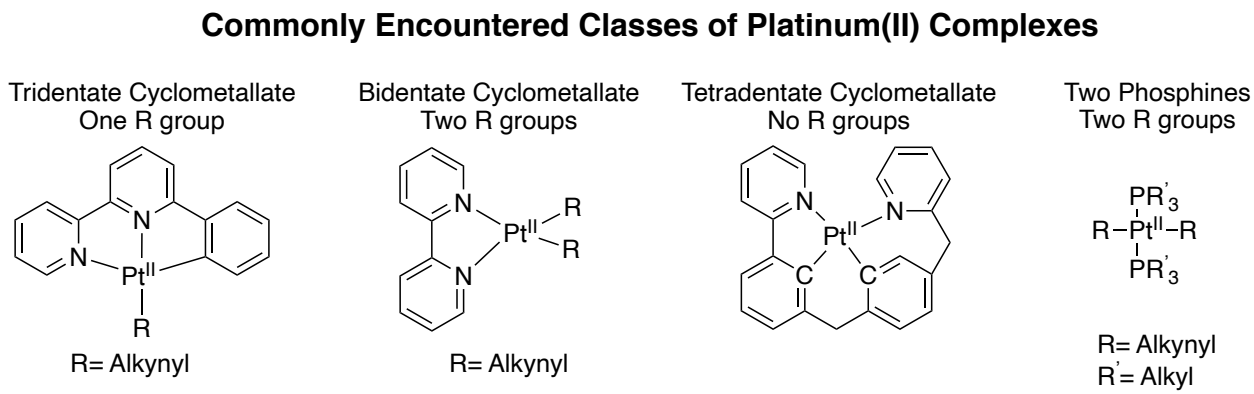


**Figure 1.5.** Examples of neutral Platinum(II) complexes.

Platinum(II) complexes have desirable qualities for bioimaging, since they tend to produce high quantum yields and long lifetimes.[61] Emission via triplet parentage also guarantees larger stoke-shifts which can eliminate undesirable quenching pathways. Like iridium(III) complexes, emission as well as excitation wavelengths can be easily altered through well-established structure modification. This, being particularly important since red or near infra-red (650-1350 nm) excitation is desirable for bioimaging. Platinum(II) crown ethers have been implemented as analyte sensors through a variety "turn-on" and "turn off" mechanisms (Figure 1.6).[62] Platinum(II) triplet emitters are particularly useful for sensing because of their emission sensitivity, large stokes shifts, and greater temporal resolution compared to singlet fluorophores. Metallophilicity is another emission phenomenon that can be exploited in sensing, compared to fluorescence molecules.

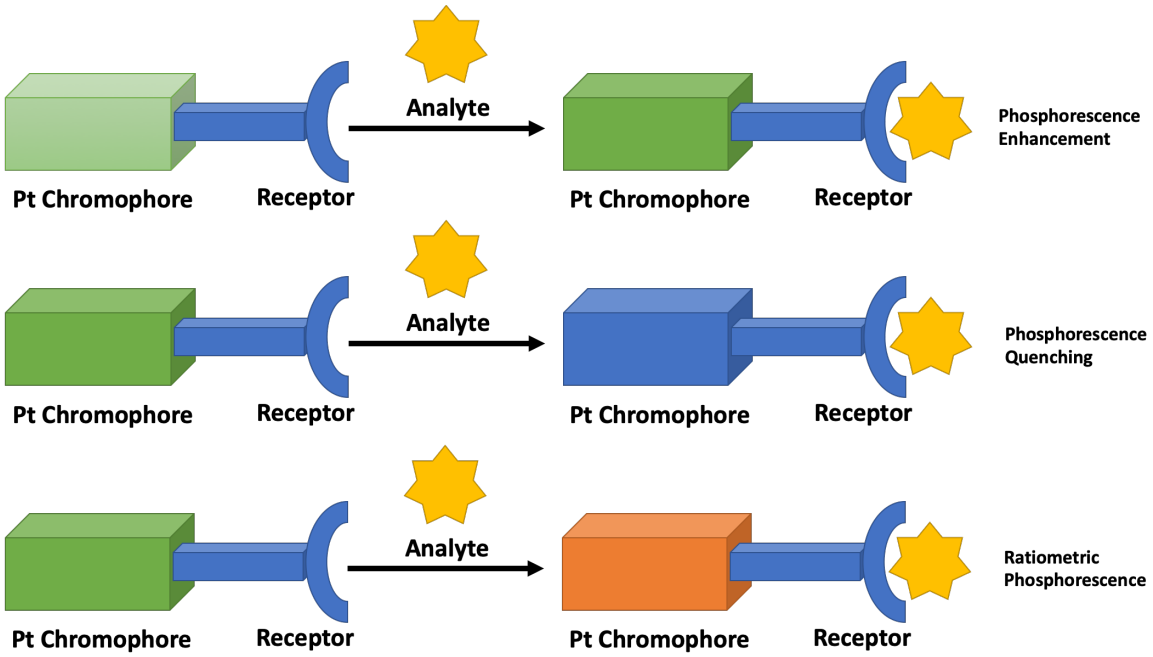


**Figure 1.6.** Possible analyte sensing pathways by a platinum chromophore.[62]

Lastly, platinum(II) compounds have been extensively studied as triplet-state nonlinear optical materials (NLOs) (Figure 1.7).[61-75] Obviously, gaining access to triplet excited states is imperative for achieving excited-state absorption. Two-photon absorption is inherent in the organometallic by use of organic ligands with large two-photon absorption cross sections. Schanze, Rodgers, and others have pioneered this topic; however, one drawback to platinum(II) complexes is that they are highly colored and impractical for applications that require visible light transparency.

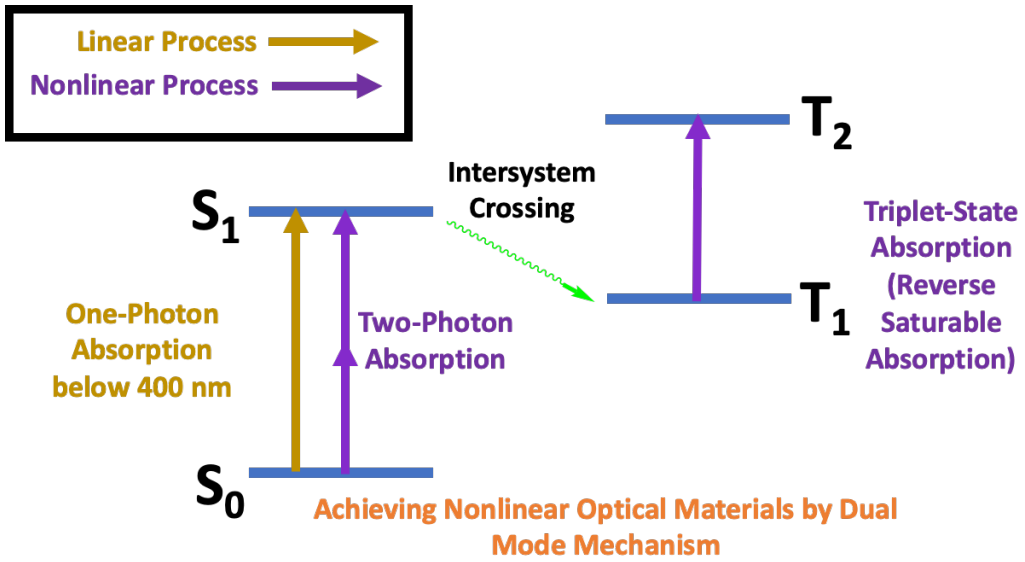


**Figure 1.7.** Jablonski Diagram showing both linear and nonlinear absorption processes.

In summation, iridium(III) and platinum(II) complexes have seen much success as triplet photoactive materials because there is a breadth of structure-property knowledge concerning these organometallics. The ability to alter excitation and emission wavelength as well as photophysical properties is well understood. This allows for the synthesis of complexes with a specific set of photophysical characteristics to be implemented for an exact application. While iridium(III) and platinum(II) complexes have been suitable triplet photoactive materials for some applications; they have not been able to solve specific problems in others, and alternative solutions are being pursued.

Understanding of structure-property relationships is crucial to successful implementation in any application space. Gold organometallics have been comparatively understudied regarding both structure-property relationships and as triplet photoactive materials. Facile synthetic accessibility to gold organometallics in the plus (III) and (I) oxidation states coupled with unique luminescence properties warrants their continued investigation. Arguably, more is known about the core luminescence principles of gold(III) complexes compared to its reduced comrade, gold(I).

A brief discussion about gold(III) and an in-depth discussion about gold(I) organometallics, their luminescence properties, and the applications they are employed for follows.

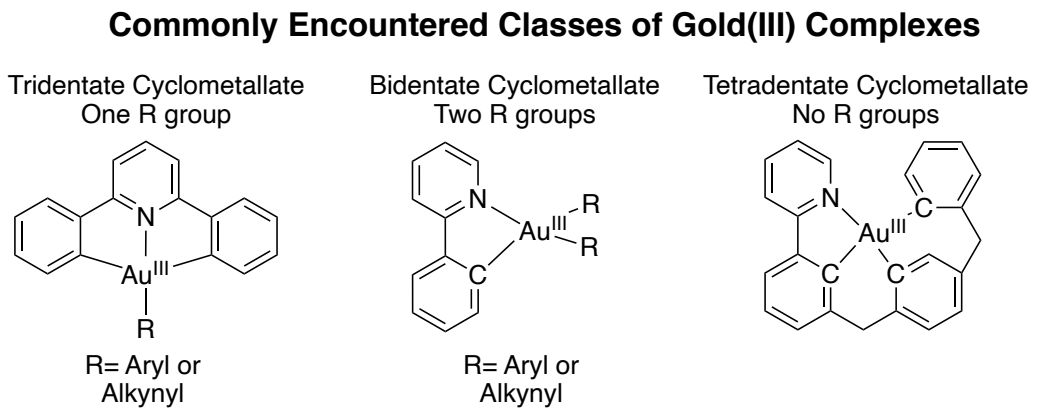


**Figure 1.8.** Examples of neutral gold(III) complexes.

Gold(III) is a $d^8$ metal and is isoelectronic to platinum(II), its complexes are square-planar and four coordinate; Generally, gold(III) complexes are of two types: [Au(C^N^C)-(R)] and [Au(C^N)-$(R)_2$] where R is either an organic alkyne or aryl ligand(s); however, gold(III) bound to tetradentate cyclometallates have been reported (Figure 1.8).[5,14,17,59,60] Vivian Yam, Chi-Ming Che, and others have developed the synthesis, photophysics, and OLED application of gold(III) complexes.[3,9,10-11,17,30,77-84] Numerous, fundamental reports on the synthesis of gold(III) complexes, focused on the alteration of the electronics in both cyclometallate as well as R group exist. Because of this, structure-property relationships in gold(III) compounds are becoming well understood. Most gold(III) complexes are phosphorescent emitters with microsecond lifetimes. Excitation wavelength and emission color can be strategically tuned through variation in structure; which in turn changes corresponding HOMO and LUMO energies. Two different types of metal perturbed emission are commonly observed for gold(III) complexes: highly structured phosphorescence that is derived from an intraligand charge transfer of the cyclometallate, or structureless phosphorescence originating from a ligand-to-ligand charge transfer (LLCT) from the R group to cyclometallate. The electronic nature of the cyclometallate as well as the R group

(i.e. donor and acceptor capability) ultimately dictate the nature of emission. More recently, there has been a shift towards the study of gold(III) complexes with tridentate cyclometallates and N-coordinating R groups such as carbazole.[85-87]

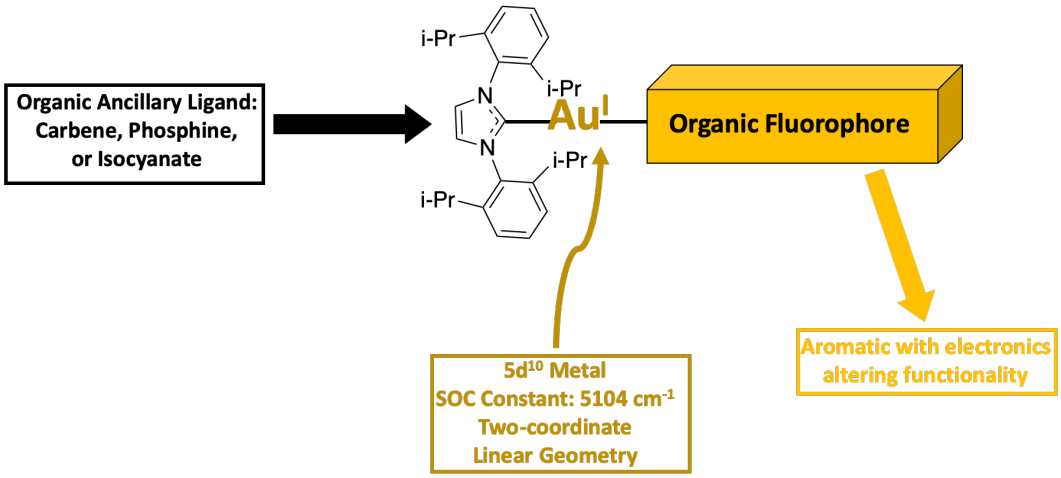


**Figure 1.9.** Typical neutral gold(I) chromophore.

Gold(I) complexes behave differently than their gold(III) counterparts. Complexes of gold(I) are isolated by different synthetic methodology and unique light-matter phenomena are observed.[88-99] Neutral gold(I) complexes are linear and two-coordinate. The gold atom generally bears a chromophoric organic ligand on one side and an ancillary ligand (phosphine or carbene) on the other (Figure 1.9). Gold(I) is a closed-shell, $5d^{10}$ metal. Gold(I) ($\zeta_{soc}$ =5104 $cm^{-1}$) renders ligand-based transitions with spin-orbit coupling; thereby enabling the population of triplet-excited states.[100] Investigations of photophysical properties for gold(I) chromophores has lacked in comparison to correlative gold(III) complexes.

Gold(I) chemistry and photophysics gained prominence in the 1990's. Much of the work through that decade focused on the isolation of new compounds and fundamental photophysical properties; such as, absorption and emission profiles as well as origin of emission; studies on aurophilic interactions were also conducted during this time.[101-111] The 2000's and early 2010's

focused on the continued synthesis of novel gold(I) complexes as well as fundamental photophysics.[112-138] Emphasis on how variation in the chromophoric organic ligand changed photophysical properties became customary. Excited-state lifetime and quantum yield data were more commonly reported, and structure-property relationships became of interest. During this time, Gray and co-workers put forward a number of studies on the synthesis and photophysical analysis of both mono-and-dinuclear gold(I) aryls, alkynyls, and triazolyls.[88,89,139-146] These complexes often exhibit dual-luminescence (both fluorescence and phosphorescence) at room temperature with microsecond lifetimes.

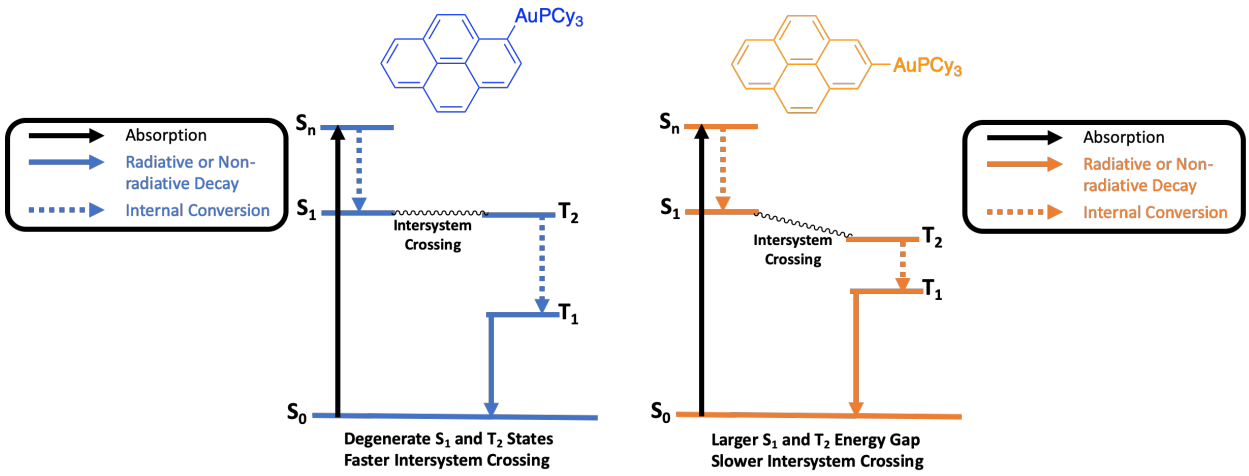


**Figure 1.10.** Jablonski diagram for pyrenyl gold(I) isomers that supports photophysical results.

Crespo-Hernández, Gray, and co-workers published transient absorption studies on gold(I) substituted pyrenyls and naphthyls (Figure 1.10). It was demonstrated that femto-to-picosecond rates of intersystem crossing occur and that cite of metalation affects excited-state dynamics.[140,143] In both studies photophysics and computations support excitation to an $S_n$ state followed by internal conversion to the $S_1$ state. Intersystem crossing to a $T_2$ state is then followed by internal conversion to the $T_1$ state and radiative/non-radiative relaxation back to the ground state. The

metalation site is shown to affect the energy gap between the $S_1$ and $T_2$ states, therefore affecting intersystem crossing rate (Figure 10).

In the mid-2010's Schanze, Wu, Chou, their respective co-workers produced a series of publications focusing on structure-property relationships in digold(I) alkynyl complexes.[147-151] Chou and co-workers demonstrated that the effective distance between gold(I) atoms has marked effect on emission and excited-state dynamics. Increasing the effective distance between gold atoms is a viable pathway to vary the ratio between fluorescence and phosphorescence as well as rate of intersystem crossing.

Schanze and co-workers reported two separate studies on digold(I) complexes with two different bridging ligands: In 2014, a digold(I) alkynyl complex containing a thiophene/carbazole bridging ligand and phosphine ancillary ligands was disclosed. This complex demonstrated low fluorescence and triplet-state quantum yields and short fluorescence and phosphorescence lifetimes. A year later, Schanze reported two new digold(I) alkynyl complexes, this time bearing a thiophene/benzothiadiazole bridging ligand and phosphine ancillary ligands. These complexes exhibited much larger fluorescence quantum yields and similar triplet state quantum yields and lifetimes. The rates of intersystem crossing were on the order of $10^7$. As a result of these studies, it was demonstrated that these gold(I) complexes undergo both two-photon absorption and excited-state absorption. Nonlinear optical capabilities were exhibited with enhanced visible light transparency (Figure 1.11).

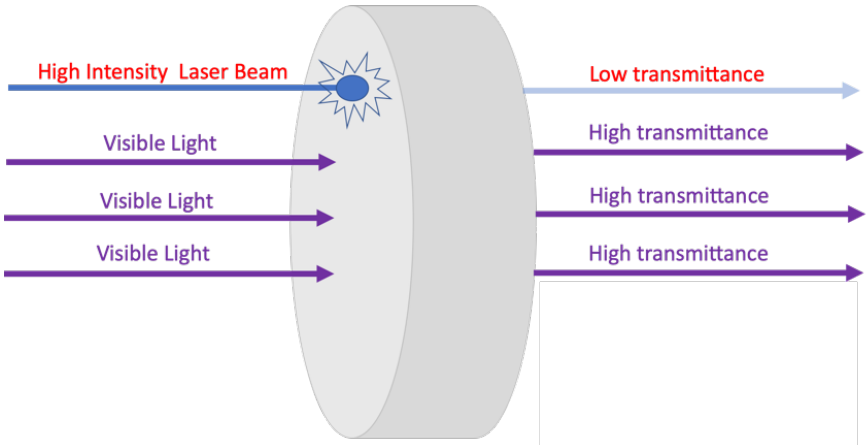


**Figure 1.11.** Transparent nonlinear optical chromophore.

In the last few years, there has been a renaissance regarding the investigation of excited state dynamics and photophysical properties of gold(I) complexes. Bachmann, Thompson, and their respective co-workers have both reported on the synthesis and photophysical analysis of carbene-metal-amide (CMA) complexes.[152-156] Bochmann has demonstrated that emission color of CMAs can be modified through variation in the electronics of the amide ligand itself, and that excited-state properties can be fine-tuned by gaining access to both ligand-to-ligand charge transfer (LLCT) and privileged molecular geometries (Figure 1.12). This combination leads to an increase in luminescence efficiency, particularly in regards to OLEDs. Thompson and co-workers have also demonstrated that gaining access to ligand-to-ligand charge transfer excited-states in CMAs and gold(I) aryls has a marked effect on excited-state dynamics. LLCT excited-states reduce the rate of non-radiative decay in gold(I) aryls by limiting geometric distortion; further reductions in the non-radiative decay rate was achieved via addition of sterically bulky amide ligands that limit bond rotation (Figure 1.12 (right)).[157] Lastly, Schanze and Veige have recently demonstrated the effect of aurophilic bonding on the photophysical properties of di-and-tetranuclear gold(I) triazolyls. Their initial findings showed aurophilic interactions and size of the phosphine ancillary ligand affect photophysical properties.[158] When the phosphine ancillary ligand

is small, white light emission is achieved via dimerization of the dinuclear species leading to aurophilic interactions. A follow up report discloses that aurophilic bonding in dinuclear gold(I) triazolyls can be invoked in the excited-state via a ligand-to-metal charge transfer (LMCT).[159]

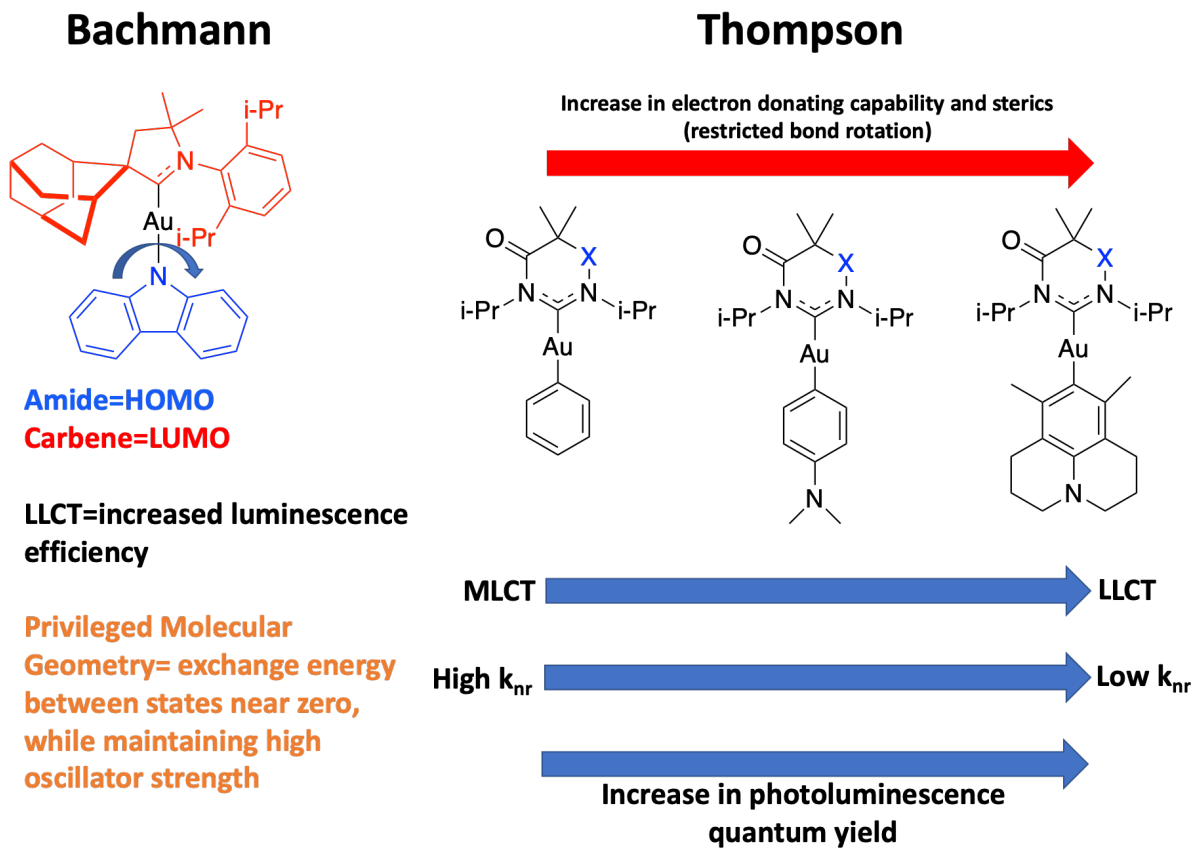


**Figure 1.12.** Summary of recent results by Bachmann and co-workers (left) and Thompson and co-workers (right) (X= CO or $CH_2$).

Despite recent efforts in the photophysical properties of gold(I) complexes; a complete understanding of structure-property relationships in gold(I) complexes is still lacking. Due to this deficiency in understanding, application of gold(I) complexes as triplet-photoactive materials lags. This dissertation serves to add to the knowledge of structure-property relationships for gold(I) as well as gold(III) complexes. Of particular interest are the effects ancillary ligand, gold-chromophore linkage, and organic ligand have on structure-property relationships. Specifically,

trends in absorption and emission spectra, lifetime and quantum yield data, and excited-state rate constants will be discussed and structure-property relationships are drawn for gold complexes containing either a benzothiazole fluorenyl or diphenyl amino fluorenyl moiety.

**References.**


1 D. M. Arias-Rotondo and J. K. Mccusker, in *Visible Light Photocatalysis in Organic Chemistry*, Wiley-VCH Verlag GmbH & Co. KGaA, Weinheim, Germany, 2017, pp. 1–24.

2 E. Zysman-Colman, Ed., *Iridium(III) in Optoelectronic and Photonics Applications*, John Wiley & Sons, Ltd, Chichester, UK, 2017.

3 H. Yersin, *Highly Efficient OLEDs with Phosphorescent Materials*, Wiley-VCH Verlag GmbH & Co. KGaA, Weinheim, Germany, 2008.

4 T. Y. Li, J. Wu, Z. G. Wu, Y. X. Zheng, J. L. Zuo and Y. Pan, *Coord. Chem. Rev.*, 2018, 374, 55–92.

5 C. M. Che, C. C. Kwok, C. F. Kui, S. L. Lai and K. H. Low, in *Comprehensive Inorganic Chemistry II (Second Edition): From Elements to Applications*, Elsevier, 2013, vol. 8, pp. 607–655.

6 C. K. Prier, D. A. Rankic and D. W. C. MacMillan, *Chem. Rev.*, 2013, **113**, 5322–5363.

7 Y. You and W. Nam, *Chem. Soc. Rev.*, 2012, 41, 7061–7084.

8 K. T. Chan, G. S. M. Tong, W. P. To, C. Yang, L. Du, D. L. Phillips and C. M. Che, *Chem. Sci.*, 2017, **8**, 2352–2364.

9 G. S. Ming Tong, K. T. Chan, X. Chang and C. M. Che, *Chem. Sci.*, 2015, **6**, 3026–3037.

10 M. C. Tang, C. H. Lee, M. Ng, Y. C. Wong, M. Y. Chan and V. W. W. Yam, Highly Emissive Fused Heterocyclic Alkynylgold(III) Complexes for Multiple Color Emission Spanning from Green to Red for Solution-Processable Organic Light-Emitting Devices, *Angew. Chemie - Int. Ed.*, 2018, **57**, 5463–5466.

11 M. C. Tang, M. Y. Leung, S. L. Lai, M. Ng, M. Y. Chan and V. Wing-Wah Yam, Realization of Thermally Stimulated Delayed Phosphorescence in Arylgold(III) Complexes and Efficient Gold(III) Based Blue-Emitting Organic Light-Emitting Devices, *J. Am. Chem. Soc.*, 2018, **140**, 13115–13124.

12 Y. Yuan, P. Gnanasekaran, Y. W. Chen, G. H. Lee, S. F. Ni, C. S. Lee and Y. Chi,

Iridium(III) Complexes Bearing a Formal Tetradentate Coordination Chelate: Structural Properties and Phosphorescence Fine-Tuned by Ancillaries, *Inorg. Chem.*, 2019, **59**, 523–532.

13 Z. Hao, K. Zhang, P. Wang, X. Lu, Z. Lu, W. Zhu and Y. Liu, Deep Red Iridium(III) Complexes Based on Pyrene-Substituted Quinoxaline Ligands for Solution-Processed Phosphorescent Organic Light-Emitting Diodes, *Inorg. Chem.*, 2019, **59**, 332–342.

14 R. C. Evans, P. Douglas and C. J. Winscom, Coordination complexes exhibiting room-temperature phosphorescence: Evaluation of their suitability as triplet emitters in organic light emitting diodes, *Coord. Chem. Rev.*, 2006, **250**, 2093–2126.

15 G. M. Farinola and R. Ragni, Electroluminescent materials for white organic light emitting diodes, *Chem. Soc. Rev.*, 2011, **40**, 3467–3482.

16 M. E. Thompson, P. E. Burrows and S. R. Forrest, Electrophosphorescence in organic light emitting diodes, *Curr. Opin. Solid State Mater. Sci.*, 1999, **4**, 369–372.

17 M. C. Tang, C. H. Lee, S. L. Lai, M. Ng, M. Y. Chan and V. W. W. Yam, Versatile Design Strategy for Highly Luminescent Vacuum-Evaporable and Solution-Processable Tridentate Gold(III) Complexes with Monoaryl Auxiliary Ligands and Their Applications for Phosphorescent Organic Light Emitting Devices, *J. Am. Chem. Soc.*, 2017, **139**, 9341–9349.

18 P. T. Furuta, L. Deng, S. Garon, M. E. Thompson and J. M. J. Fréchet, Platinum-functionalized random copolymers for use in solution-processible, efficient, near-white organic light-emitting diodes, *J. Am. Chem. Soc.*, 2004, **126**, 15388–15389.

19 S. Lamansky, P. Djurovich, D. Murphy, F. Abdel-Razzaq, H. E. Lee, C. Adachi, P. E. Burrows, S. R. Forrest and M. E. Thompson, Highly phosphorescent bis-cyclometalated iridium complexes: Synthesis, photophysical characterization, and use in organic light emitting diodes, *J. Am. Chem. Soc.*, 2001, **123**, 4304–4312.

20 W. P. To, D. Zhou, G. S. M. Tong, G. Cheng, C. Yang and C. M. Che, Highly Luminescent Pincer Gold(III) Aryl Emitters: Thermally Activated Delayed Fluorescence and Solution-Processed OLEDs, *Angew. Chemie - Int. Ed.*, 2017, **56**, 14036–14041.

21 M. A. Baldo, D. F. O. an dY. You, A. Shoustikov, S. Sibley, M. E. Thompson and S. R. Forrest, Highly efficient phosphorescent emission from organic electroluminescent

devices, *Nature*, 1998, **395**, 151.

22 C. Adachi, M. A. Baldo, M. E. Thompson and S. R. Forrest, Nearly 100% internal phosphorescence efficiency in an organic light emitting device, *J. Appl. Phys.*, 2001, **90**, 5048–5051.

23 J. Kalinowski, V. Fattori, M. Cocchi and J. A. G. Williams, Light-emitting devices based on organometallic platinum complexes as emitters, *Coord. Chem. Rev.*, 2011, **255**, 2401–2425.

24 Q. Zeng, F. Li, Z. Chen, K. Yang, Y. Liu, T. Guo, G.-G. Shan and Z.-M. Su, Rational Design of Efficient Organometallic Ir(III) Complexes for High-Performance Flexible Monochromatic and White Light-Emitting Electrochemical Cells, *ACS Appl. Mater. Interfaces*, 2020, **12**, 4649–4658.

25 X. Z. Shu, M. Zhang, Y. He, H. Frei and F. D. Toste, Dual visible light photoredox and gold-catalyzed arylative ring expansion, *J. Am. Chem. Soc.*, 2014, **136**, 5844–5847.

26 O. Reiser, G. Kachkovskyi, V. Kais, P. Kohls, S. Paria, M. Pirtsch, D. Rackl and H. Seo, Walter de Gruyter GmbH, 2013, p. 139.

27 M. H. Shaw, J. Twilton and D. W. C. MacMillan, Photoredox Catalysis in Organic Chemistry, *J. Org. Chem.*, 2016, **81**, 6898–6926.

28 Y. You and W. Nam, Photofunctional triplet excited states of cyclometalated Ir(III) complexes: Beyond electroluminescence, *Chem. Soc. Rev.*, 2012, **41**, 7061–7084.

29 C. K. Prier, D. A. Rankic and D. W. C. MacMillan, Visible light photoredox catalysis with transition metal complexes: Applications in organic synthesis, *Chem. Rev.*, 2013, **113**, 5322–5363.

30 M. D. Levin, S. Kim and F. D. Toste, Photoredox catalysis unlocks single-electron elementary steps in transition metal catalyzed cross-coupling, *ACS Cent. Sci.*, 2016, **2**, 293–301.

31 M. N. Hopkinson, A. Tlahuext-Aca and F. Glorius, Merging Visible Light Photoredox and Gold Catalysis, *Acc. Chem. Res.*, 2016, **49**, 2261–2272.

32 J. Zhao, W. Wu, J. Sun and S. Guo, Triplet photosensitizers: From molecular design to applications, *Chem. Soc. Rev.*, 2013, **42**, 5323–5351.

33 J. F. Longevial, K. El Cheikh, D. Aggad, A. Lebrun, A. van der Lee, F. Tielens, S. Clément, A. Morère, M. Garcia, M. Gary-Bobo and S. Richeter, Porphyrins Conjugated with Peripheral Thiolato Gold(I) Complexes for Enhanced Photodynamic Therapy, *Chem. - A Eur. J.*, 2017, **23**, 14017–14026.

34 L. Zhou, X. Ge, J. Liu, J. Zhou, S. Wei, F. Li and J. Shen, Internal heavy atom effect of Au(III) and Pt(IV) on hypocrellin A for enhanced in vitro photodynamic therapy of cancer, *Bioorganic Med. Chem. Lett.*, 2013, **23**, 5317–5324.

35 E. Baggaley, J. A. Weinstein and J. A. G. Williams, Lighting the way to see inside the live cell with luminescent transition metal complexes, *Coord. Chem. Rev.*, 2012, **256**, 1762–1785.

36 L. K. McKenzie, H. E. Bryant and J. A. Weinstein, Transition metal complexes as photosensitisers in one- and two-photon photodynamic therapy, *Coord. Chem. Rev.*, 2019, **379**, 2–29.

37 X. Jiang, N. Zhu, D. Zhao and Y. Ma, New cyclometalated transition-metal based photosensitizers for singlet oxygen generation and photodynamic therapy, *Sci. China Chem.*, 2016, **59**, 40–52.

38 R. Vestberg, R. Westlund, A. Eriksson, C. Lopes, M. Carlsson, B. Eliasson, E. Glimsdal, M. Lindgren and E. Malmström, Dendron decorated platinum(II) acetylides for optical power limiting, *Macromolecules*, 2006, **39**, 2238–2246.

39 N. J. Long, Organometallic Compounds for Nonlinear Optics—The Search for En-light-enment!, *Angew. Chemie Int. Ed. English*, 1995, **34**, 21–38.

40 M. J. Miller, A. G. Mott and B. P. Ketchel, General optical limiting requirements, *Nonlinear Opt. Liq. Power Limiting Imaging*, 2003, **3472**, 24.

41 S. R. Marder, B. Kippelen, A. K. Y. Jen and N. Peyghambarian, Design and synthesis of chromophores and polymers for electro-optic and photorefractive applications, *Nature*, 1997, **388**, 845–851.

42 G. J. Zhou and W. Y. Wong, Organometallic acetylides of PtII, AuI and Hg II as new generation optical power limiting materials, *Chem. Soc. Rev.*, 2011, **40**, 2541–2566.

43 G. S. He, L.-S. Tan, Q. Zheng and P. N. Prasad, Multiphoton Absorbing Materials: Molecular Designs, Characterizations, and Applications, *Chem. Rev.*, 2008,

**108**, 1245–1330.

44 B. Liu, Z. Tian, F. Dang, J. Zhao, X. Yan, X. Xu, X. Yang, G. Zhou and Y. Wu, Photophysical and optical power limiting behaviors of Au(I) acetylides with diethynyl aromatic ligands showing different electronic features, *J. Organomet. Chem.*, 2016, **804**, 80–86.

45 P. B. Jacques Simon, Design of Molecular Materials: Supramolecular Engineering, *Wiley*, 2001, **15**, 197–199.

46 Y. Lin, C. Jiang, F. Hu, J. Yin, G. A. Yu and S. H. Liu, Synthesis, characterization, and properties of some bisacetylide and binuclear acetylide gold(I) compounds based on the photochromic dithienylethene unit, *Dye. Pigment.*, 2013, **99**, 995–1003.

47 Q. Zhao, C. Huang and F. Li, Phosphorescent heavy-metal complexes for bioimaging, *Chem. Soc. Rev.*, 2011, **40**, 2508–2524.

48 H. Xiang, J. Cheng, X. Ma, X. Zhou and J. J. Chruma, *Near-infrared phosphorescence: Materials and applications*, 2013, vol. 42.

49 K. K. W. Lo, A. W. T. Choi and W. H. T. Law, Applications of luminescent inorganic and organometallic transition metal complexes as biomolecular and cellular probes, *Dalt. Trans.*, 2012, **41**, 6021–6047.

50 D. L. Ma, H. Z. He, K. H. Leung, D. S. H. Chan and C. H. Leung, Bioactive luminescent transition-metal complexes for biomedical applications, *Angew. Chemie - Int. Ed.*, 2013, **52**, 7666–7682.

51 K. Li, G. S. Ming Tong, Q. Wan, G. Cheng, W. Y. Tong, W. H. Ang, W. L. Kwong and C. M. Che, Highly phosphorescent platinum(ii) emitters: photophysics, materials and biological applications, *Chem. Sci.*, 2016, **7**, 1653–1673.

52 M. Mydlak, C. Bizzarri, D. Hartmann, W. Sarfert, G. Schmid and L. De Cola, Positively charged iridium(lll) triazole derivatives as blue emitters for light-emitting electrochemical cells, *Adv. Funct. Mater.*, 2010, **20**, 1812–1820.

53 C. Ulbricht, B. Beyer, C. Friebe, A. Winter and U. S. Schubert, Recent developments in the application of phosphorescent iridium(III) complex systems, *Adv. Mater.*, 2009, **21**, 4418–4441.

54 H. C. Su, H. F. Chen, F. C. Fang, C. C. Liu, C. C. Wu, K. T. Wong, Y. H. Liu and S. M.

Peng, Solid-state white light-emitting electrochemical cells using iridium-based cationic transition metal complexes, *J. Am. Chem. Soc.*, 2008, **130**, 3413–3419.

55 R. D. Costa, E. Ortí, H. J. Bolink, F. Monti, G. Accorsi and N. Armaroli, Luminescent ionic transition-metal complexes for light-emitting electrochemical cells, *Angew. Chemie - Int. Ed.*, 2012, **51**, 8178–8211.

56 T. M. Monos and C. R. J. Stephenson, Photoredox Catalysis of Iridium(III)-Based Photosensitizers, *Iridium(III) Optoelectron. Photonics Appl.*, 2017, 541–581.

57 K. Teegardin, J. I. Day, J. Chan and J. Weaver, Advances in Photocatalysis: A Microreview of Visible Light Mediated Ruthenium and Iridium Catalyzed Organic Transformations, *Org. Process Res. Dev.*, 2016, **20**, 1156–1163.

58 C. Adachi, S. Lee, T. Nakagawa, K. Shizu, K. Goushi and W. Potscavage, 2015, pp. 43–73.

59 I. Eryazici, C. N. Moorefield and G. R. Newkome, Square-planar Pd(II), Pt(II), and Au(III) terpyridine complexes: Their syntheses, physical properties, supramolecular constructs, and biomedical activities, *Chem. Rev.*, 2008, **108**, 1834–1895.

60 V. W. W. Yam and A. S. Y. Law, Luminescent d8 metal complexes of platinum(II) and gold(III): From photophysics to photofunctional materials and probes, *Coord. Chem. Rev.*, 2020, **414**, 213298.

61 Q. Zhao, F. Li and C. Huang, Phosphorescent chemosensors based on heavy-metal complexes, *Chem. Soc. Rev.*, 2010, **39**, 3007–3030.

62 Q. Zhao, H. Huang and F. Li, Phosphorescent heavy-metal complexes for bioimaging, *Chem. Soc. Rev.*, 2011, **40**, 2508–2524.

63 G. S. He, L.-S. Tan, Q. Zheng and P. N. Prasad, Multiphoton Absorbing Materials: Molecular Designs, Characterizations, and Applications, *Chem. Rev.*, 2008, **108**, 1245–1330.

64 B. Liu, Z. Tian, F. Dang, J. Zhao, X. Yan, X. Xu, X. Yang, G. Zhou and Y. Wu, Photophysical and optical power limiting behaviors of Au(I) acetylides with diethynyl aromatic ligands showing different electronic features, *J. Organomet. Chem.*, 2016, **804**, 80–86.

65 S. Cekli, R. W. Winkel, E. Alarousu, O. F. Mohammed and K. S. Schanze, Triplet excited state properties in variable gap π-conjugated donor-Acceptor-donor chromophores, *Chem.*

*Sci.*, 2016, **7**, 3621–3631.

66 S. Goswami, G. Wicks, A. Rebane and K. S. Schanze, Photophysics and non-linear absorption of Au(i) and Pt(ii) acetylide complexes of a thienyl-carbazole chromophore, *Dalt. Trans.*, 2014, **43**, 17721–17728.

67 S. Goswami, R. W. Winkel and K. S. Schanze, Photophysics and Nonlinear Absorption of Gold(I) and Platinum(II) Donor-Acceptor-Donor Chromophores, *Inorg. Chem.*, 2015, **54**, 10007–10014.

68 R. Vestberg, R. Westlund, A. Eriksson, C. Lopes, M. Carlsson, B. Eliasson, E. Glimsdal, M. Lindgren and E. Malmström, Dendron decorated platinum(II) acetylides for optical power limiting, *Macromolecules*, 2006, **39**, 2238–2246.

69 W. Wu, C. Cheng, W. Wu, H. Guo, S. Ji, P. Song, K. Han, J. Zhao, X. Zhang, Y. Wu and G. Du, Tuning the emission colour of triphenylamine-capped cyclometallated platinum(II) complexes and their application in luminescent oxygen sensing and organic light-emitting diodes, *Eur. J. Inorg. Chem.*, 2010, 4683–4696.

70 R. Westlund, E. Malmström, C. Lopes, J. Öhgren, T. Rodgers, Y. Saito, S. Kawata, E. Glimsdal and M. Lindgren, Efficient nonlinear absorbing platinum(II) acetylide chrompphores in solid PMMA matrices, *Adv. Funct. Mater.*, 2008, **18**, 1939–1948.

71 T. M. Cooper, D. M. Krein, A. R. Burke, D. G. McLean, J. E. Rogers and J. E. Slagle, Asymmetry in platinum acetylide complexes: Confinement of the triplet exciton to the lowest energy ligand, *J. Phys. Chem. A*, 2006, **110**, 13370–13378.

72 J. E. Rogers, J. E. Slagle, D. M. Krein, A. R. Burke, B. C. Hall, A. Fratini, D. G. McLean, P. A. Fleitz, T. M. Cooper, M. Drobizhev, N. S. Makarov, A. Rebane, K. Y. Kim, R. Farley and K. S. Schanze, Platinum acetylide two-photon chromophores, *Inorg. Chem.*, 2007, **46**, 6483–6494.

73 K. D. Belfield, M. V. Bondar, F. E. Hernandez and O. V. Przhonska, Photophysical characterization, two-photon absorption and optical power limiting of two fluorenylperylene diimides, *J. Phys. Chem. C*, 2008, **112**, 5618–5622.

74 K. Y. Kim, A. H. Shelton, M. Drobizhev, N. Makarov, A. Rebane and K. S. Schanze, Optimizing simultaneous two-photon absorption and transient triplet-triplet absorption in platinum acetylide chromophores, *J. Phys. Chem. A*, 2010, **114**, 7003–7013.

75 E. Glimsdal, M. Carlsson, B. Eliasson, B. Minaev and M. Lindgren, Excited states and

two-photon absorption of some novel thiophenyl Pt(II)-ethynyl derivatives, *J. Phys. Chem. A*, 2007, **111**, 244–250.

76 J. Kalinowski, V. Fattori, M. Cocchi and J. A. G. Williams, Light-emitting devices based on organometallic platinum complexes as emitters, *Coord. Chem. Rev.*, 2011, **255**, 2401–2425.

77 K. M. Wong, X. Zhu, L. Hung, N. Zhu, V. W. Yam and H. Kwok, A novel class of phosphorescent gold ( III ) alkynyl-based organic light-emitting devices with tunable colour, 2005, **2**, 2906–2908.

78 V. W. Yam, Bipolar Gold(III) Complexes for Solution-Processable Organic Light-Emitting Devices with a Small E ffi ciency Roll-O ff, 2014, 17861–17868.

79 L. Li, M. Tang, W. Cheung, S. Lai, M. Ng, C. K. Chan, M. Chan and V. W. Yam, Rational Design Strategy for the Realization of Red- to Near- Infrared-Emitting Alkynylgold(III) Complexes and Their Applications in Solution-Processable Organic Light-Emitting Devices, , DOI:10.1021/acs.chemmater.9b01208.

80 C. H. Lee, M. C. Tang, W. L. Cheung, S. L. Lai, M. Y. Chan and V. W. W. Yam, Highly luminescent phosphine oxide-containing bipolar alkynylgold(iii) complexes for solution-processable organic light-emitting devices with small efficiency roll-offs, *Chem. Sci.*, 2018, **9**, 6228–6232.

81 V. K. M. Au, K. M. C. Wong, D. P. K. Tsang, M. Y. Chan, N. Zhu and V. W. W. Yam, High-efficiency green organic light-emitting devices utilizing phosphorescent bis-cyclometalated alkynylgold(III) complexes, *J. Am. Chem. Soc.*, 2010, **132**, 14273–14278.

82 M. C. Tang, D. P. K. Tsang, Y. C. Wong, M. Y. Chan, K. M. C. Wong and V. W. W. Yam, Bipolar gold(III) complexes for solution-processable organic light-emitting devices with a small efficiency roll-off, *J. Am. Chem. Soc.*, 2014, **136**, 17861–17868.

83 M. Tang, C. Lee, S. Lai, M. Ng, M. Chan and V. W. Yam, Versatile Design Strategy for Highly Luminescent Vacuum-Evaporable and Solution-Processable Tridentate Gold(III) Complexes with Monoaryl Auxiliary Ligands and Their Applications for Phosphorescent Organic Light Emitting Devices, *J. Am. Chem. Soc.*, 2017, **139**, 9341–9349.

84 M. C. Tang, D. P. K. Tsang, M. M. Y. Chan, K. M. C. Wong and V. W. W. Yam, Dendritic luminescent gold(III) complexes for highly efficient solution-processable

organic light-emitting devices, *Angew. Chemie - Int. Ed.*, 2013, **52**, 446–449.

85 D. Zhou, W. P. To, G. S. M. Tong, G. Cheng, L. Du, D. L. Phillips and C. M. Che, Tetradentate Gold(III) Complexes as Thermally Activated Delayed Fluorescence (TADF) Emitters: Microwave-Assisted Synthesis and High-Performance OLEDs with Long Operational Lifetime, *Angew. Chemie - Int. Ed.*, 2020, **59**, 6375–6382.

86 C. H. Lee, M. C. Tang, F. K. W. Kong, W. L. Cheung, M. Ng, M. Y. Chan and V. W. W. Yam, Isomeric Tetradentate Ligand-Containing Cyclometalated Gold(III) Complexes, *J. Am. Chem. Soc.*, 2020, **142**, 520–529.

87 M. Y. Leung, M. C. Tang, W. L. Cheung, S. L. Lai, M. Ng, M. Y. Chan and V. Wing-Wah Yam, Thermally Stimulated Delayed Phosphorescence (TSDP)-Based Gold(III) Complexes of Tridentate Pyrazine-Containing Pincer Ligand with Wide Emission Color Tunability and Their Application in Organic Light-Emitting Devices, *J. Am. Chem. Soc.*, 2020, **142**, 2448–2459.

88 D. V. Partyka, A. J. Esswein, M. Zeller, A. D. Hunter and T. G. Gray, Gold(I) pyrenyls: Excited-state consequences of carbon-gold bond formation, *Organometallics*, 2007, **26**, 3279–3282.

89 L. Gao, M. A. Peay, D. V. Partyka, J. B. Updegraff, T. S. Teets, A. J. Esswein, M. Zeller, A. D. Hunter and T. G. Gray, Mono- and di-gold(I) naphthalenes and pyrenes: Syntheses, crystal structures, and photophysics, *Organometallics*, 2009, **28**, 5669–5681.

90 Y. Dong, J. Zhang, A. Li, J. Gong, B. He, S. Xu, J. Yin, S. H. Liu and B. Z. Tang, Structure-tuned and thermodynamically controlled mechanochromic self-recovery of AIE-active Au( i ) complexes , *J. Mater. Chem. C*, 2020, 894–899.

91 I. D. Strelnik, V. V. Sizov, V. V. Gurzhiy, A. S. Melnikov, I. E. Kolesnikov, E. I. Musina, A. A. Karasik and E. V. Grachova, Binuclear Gold(I) Phosphine Alkynyl Complexes Templated on a Flexible Cyclic Phosphine Ligand: Synthesis and Some Features of Solid-State Luminescence, *Inorg. Chem.*, 2019, **59**, 244–253.

92 T. Seki, K. Kashiyama and H. Ito, Luminescent mechanochromism of gold N -heterocyclic carbene complexes with hypso- and bathochromic spectral shifts, *Dalt. Trans.*, 2019, **48**, 7105–7109.

93 N. M. W. Wu, M. Ng and V. W. W. Yam, Photochromic Benzo[b]phosphole

Alkynylgold(I) Complexes with Mechanochromic Property to Serve as Multistimuli-Responsive Materials, *Angew. Chemie - Int. Ed.*, 2019, **58**, 3027–3031.

94 V. Fernández-Moreira, C. Val-Campillo, I. Ospino, R. P. Herrera, I. Marzo, A. Laguna and M. C. Gimeno, Bioactive and luminescent indole and isatin based gold(i) derivatives, *Dalt. Trans.*, 2019, **48**, 3098–3108.

95 E. Y. H. Hong and V. W. W. Yam, Triindole-tris-alkynyl-bridged trinuclear gold(I) complexes for cooperative supramolecular self-assembly and small-molecule solution-processable resistive memories, *ACS Appl. Mater. Interfaces*, 2017, **9**, 2616–2624.

96 M. C. Blanco, J. Cámara, V. Fernández-Moreira, A. Laguna and M. C. Gimeno, Gold(I), Phosphanes, and Alkynyls: The Perfect Allies in the Search for Luminescent Compounds, *Eur. J. Inorg. Chem.*, 2018, **2018**, 2762–2767.

97 J. J. González, E. Ortega, M. Rothemund, M. Gold, C. Vicente, C. De Haro, D. Bautista, R. Schobert and J. Ruiz, Luminescent Gold(I) Complexes of 1-Pyridyl-3-anthracenylchalcone Inducing Apoptosis in Colon Carcinoma Cells and Antivascular Effects, *Inorg. Chem.*, 2019, **58**, 12954–12963.

98 M. Głodek, S. Pawlędzio, A. Makal and D. Plażuk, The Impact of Crystal Packing and Aurophilic Interactions on the Luminescence Properties in Polymorphs and Solvate of Aroylacetylide–Gold(I) Complexes, *Chem. - A Eur. J.*, 2019, **25**, 13131–13145.

99 K. T. Chan, G. S. M. Tong, W. P. To, C. Yang, L. Du, D. L. Phillips and C. M. Che, The interplay between fluorescence and phosphorescence with luminescent gold(i) and gold(iii) complexes bearing heterocyclic arylacetylide ligands, *Chem. Sci.*, 2017, **8**, 2352–2364.

100 Montalti, A. Credi, L. Prodi and M. Teresa Gandolfi, *Handbook of Photochemistry, Third Edition*, CRC Press, 3rd Editio., 2006.

101 V. W. W. Yam, S. W. K. Choi and K. K. Cheung, Synthesis, photophysics and thermal redox reactions of a [{Au(dppn)Cl}2]2+ dimer with an unsupported AuII-AuII bond, *Chem. Commun.*, 1996, **3**, 1173–1174.

102 V. W. W. Yam, S. W. K. Choi and K. K. Cheung, Synthesis and design of novel tetranuclear and dinuclear gold(I) phosphine acetylide complexes. First X-ray crystal structures of a tetranuclear ([Au4(tppb)(C≡CPh)4]) and a related dinuclear

([Au2(dppb)(C≡CPh)2]) complex, *Organometallics*, 1996, **15**, 1734–1739.

103 V. W. W. Yam, Luminescent coinage metal clusters of acetylides and chalcogenides, *J. Photochem. Photobiol. A Chem.*, 1997, **106**, 75–84.

104 V. W. W. Yam, C. K. Li and C. L. Chan, Proof of potassium ions by luminescence signaling based on weak gold - Gold interactions in dinuclear gold(I) complexes, *Angew. Chemie - Int. Ed.*, 1998, **37**, 2857–2859.

105 V. W. W. Yam and K. K. W. Lo, Luminescent polynuclear d10 metal complexes, *Chem. Soc. Rev.*, 1999, **28**, 323–334.

106 V. W. W. Yam, K. K. W. Lo and K. M. C. Wong, Luminescent polynuclear metal acetylides, *J. Organomet. Chem.*, 1999, **578**, 3–30.

107 B. C. Tzeng, K. K. Cheung and C. M. Che, Photoluminescent two-dimensional gold(I) polymers bearing a macrocyclic tetraaza cavity, *Chem. Commun.*, 1996, **0**, 1681–1682.

108 B. Tzeng and S. Pengb, Gl Y, 1996, 181–182.

109 B. C. Tzeng, C. M. Che and S. M. Peng, Luminescent gold(I) supermolecules with trithiocyanuric acid. Crystal structure, spectroscopic and photophysical properties, *Chem. Commun.*, 1997, **130**, 1771–1772.

110 Y. Ma, C. M. Che, H. Y. Chao, X. Zhou, W. H. Chan and J. Shen, High luminescence gold(I) and copper(I) complexes with a triplet excited state for use in light-emitting diodes, *Adv. Mater.*, 1999, **11**, 852–857.

111 K. H. Leung, D. L. Phillips, M. C. Tse, C. M. Che and V. M. Miskowski, Resonance raman investigation of the Au(I) - Au(I) interaction of the 1[dσ*pσ] Excited state of Au2(dcpm)2(ClO4)2 (dcpm = bis(dicyclohexylphosphine)methane), *J. Am. Chem. Soc.*, 1999, **121**, 4799–4803.

112 W. F. Fu, K. C. Chan, K. K. Cheung and C. M. Che, Substrate-binding reactions of the 3[dσ*pσ] excited state of binuclear gold(I) complexes with bridging bis(dicyclohexylphosphino)methane ligands: Emission and time-resolved absorption spectroscopic studies, *Chem. - A Eur. J.*, 2001, **7**, 4656–4664.

112 C. M. Che, H. Y. Chao, V. M. Miskowski, Y. Li and K. K. Cheung, Luminescent μ-ethynediyl and μ-butadiynediyl binuclear gold(I) complexes: Observation of 3(ππ*) emissions from bridging Cn2- units, *J. Am. Chem. Soc.*, 2001, **123**, 4985–4991.

114 W. Lu, H. F. Xiang, N. Zhu and C. M. Che, The 3(ππ*) Emission of

Cy3PAu(C≡C)nAuPCy3 (n = 3, 4). Effect of chain length upon acetylenic 3(ππ*) emission, *Organometallics*, 2002, **21**, 2343–2346.

115 W. Lu, N. Zhu and C. M. Che, Polymorphic Forms of a Gold(I) Arylacetylide Complex with Contrasting Phosphorescent Characteristics, *J. Am. Chem. Soc.*, 2003, **125**, 16081–16088.

116 B. H. Xia, H. X. Zhang, C. M. Che, K. H. Leung, D. L. Phillips, N. Zhu and Z. Y. Zhou, Metal-metal interactions in heterobimetallic d8-d10 complexes. Structures and spectroscopic investigation of [M′M″(μ-dcpm)2(CN)2]+ (M′ = Pt, Pd; M″ = Cu, Ag, Au) and related complexes by UV-vis absorption and resonance Raman spectroscopy and ab initio calculations, *J. Am. Chem. Soc.*, 2003, **125**, 10362–10374.

117 T. Zou, C. T. Lum, C. N. Lok, W. P. To, K. H. Low and C. M. Che, A binuclear gold(I) complex with mixed bridging diphosphine and bis(N-heterocyclic carbene) ligands shows favorable thiol reactivity and inhibits tumor growth and angiogenesis in vivo, *Angew. Chemie - Int. Ed.*, 2014, **53**, 5810–5814.

118 X. S. Xiao, C. Zou, X. Guan, C. Yang, W. Lu and C. M. Che, Homoleptic gold(i) N-heterocyclic allenylidene complexes: Excited-state properties and lyotropic chromonics, *Chem. Commun.*, 2016, **52**, 4983–4986.

119 E. C. C. Cheng, K. H. Leung, V. M. Miskowski, V. W. W. Yam and D. L. Phillips, Electronic and resonance Raman spectra of [Au2(CS3)2]2-. Spectroscopic properties of a 'short' Au(I)-Au(I) bond, *Inorg. Chem.*, 2000, **39**, 3690–3695.

120 V. W. W. Yam, C. K. Li, C. L. Chan and K. K. Cheung, Synthesis, structural characterization, and photophysics of dinuclear gold(II) complexes [{Au(dppn)Br}2](PF6)2 and [{Au(dppn)I}2](PF6)2 with an unsupported AuII-AuII bond, *Inorg. Chem.*, 2001, **40**, 7054–7058.

121 V. W. W. Yam and E. C. C. Cheng, Design of luminescent sulfur-containing polynuclear gold(I) complexes for advanced nanomaterials and chemosensors, *Gold Bull.*, 2001, **34**, 20–23.

122 V. W. W. Yam, Molecular design of transition metal alkynyl complexes as building blocks for luminescent metal-based materials: Structural and photophysical aspects, *Acc. Chem. Res.*, 2002, **35**, 555–563.

123 V. W. W. Yam, K. L. Cheung, S. K. Yip and K. K. Cheung, Synthesis, characterization,

structure and luminescence studies of mono-, di- and trinuclear gold(I) phosphine alkynyl complexes, *J. Organomet. Chem.*, 2003, **681**, 196–209.

124 V. W. W. Yam, S. K. Yip, L. H. Yuan, K. L. Cheung, N. Zhu and K. K. Cheung, Synthesis, structure, and ion-binding properties of luminescent gold(I) alkynylcalix[4]crown-5 complexes, *Organometallics*, 2003, **22**, 2630–2637.

125 C. K. Li, X. X. Lu, K. M. C. Wong, C. L. Chan, N. Zhu and V. W. W. Yam, Molecular design of luminescence ion probes for various cations based on weak gold(I)···gold(I) interactions in dinuclear gold(I) complexes, *Inorg. Chem.*, 2004, **43**, 7421–7430.

126 V. W. W. Yam, Luminescent metal alkynyls - From simple molecules to molecular rods and materials, *J. Organomet. Chem.*, 2004, **689**, 1393–1401.

127 H. S. Tang, N. Zhu and V. W. W. Yam, Tetranuclear macrocyclic gold(I) alkynyl phosphine complex containing azobenzene functionalities: A dual-input molecular logic with photoswitching behavior controllable via silver(I) coordination/decoordination, *Organometallics*, 2007, **26**, 22–25.

128 X. He, F. Herranz, E. C. C. Cheng, R. Vilar and V. W. W. Yam, Design, synthesis, photophysics, and anion-binding studies of bis(dicyclohexylphosphino)methane-containing dinuclear gold(I) thiolate complexes with urea receptors, *Chem. - A Eur. J.*, 2010, **16**, 9123–9131.

129 X. He and V. W. W. Yam, Design, synthesis, photophysics, and ion-binding studies of a ditopic receptor based on goid(i) phosphine thiolate complex functionalized with crown ether and urea binding units, *Inorg. Chem.*, 2010, **49**, 2273–2279.

130 X. He and V. W. W. Yam, Luminescent gold(I) complexes for chemosensing, *Coord. Chem. Rev.*, 2011, **255**, 2111–2123.

131 E. Y. H. Hong, H. L. Wong and V. W. W. Yam, From spherical to leaf-like morphologies: Tunable supramolecular assembly of alkynylgold(I) complexes through variations of the alkyl chain length, *Chem. - A Eur. J.*, 2015, **21**, 5732–5735.

132 F. K. W. Hau and V. W. W. Yam, Synthesis and cation-binding studies of gold(i) complexes bearing oligoether isocyanide ligands with ester and amide as linkers, *Dalt. Trans.*, 2015, **45**, 300–306.

133 F. C. M. Leung and V. W. W. Yam, Cation- and Solvent-Induced Supramolecular Aggregation Studies of Crown Ether-Containing Dinuclear Alkynylgold(I) Isocyanide

Complexes, *Eur. J. Inorg. Chem.*, 2017, **2017**, 5271–5278.

134 A. Chu, F. K. W. Hau and V. W. W. Yam, AuI···AuI Interaction Assisted Host–Guest Interactions and Stimuli-Responsive Self-Assembly in Tetranuclear Alkynylgold(I) Calix[4]arene-Based Isocyanide Complexes, *Chem. - A Eur. J.*, 2017, **23**, 11076–11084.

135 E. Y. H. Hong and V. W. W. Yam, Triindole-tris-alkynyl-bridged trinuclear gold(I) complexes for cooperative supramolecular self-assembly and small-molecule solution-processable resistive memories, *ACS Appl. Mater. Interfaces*, 2017, **9**, 2616–2624.

136 F. C. M. Leung and V. W. W. Yam, Photophysical and ion-binding studies of a tetranuclear alkynylgold(I) isonitrile complex, *J. Photochem. Photobiol. A Chem.*, 2018, **355**, 212–219.

137 A. Chu, F. K.-W. Hau, L.-Y. Yao and V. W.-W. Yam, Decanuclear Gold(I) Sulfido Pseudopolymorphs Displaying Stimuli-Responsive RGBY Luminescence Changes, *ACS Mater. Lett.*, 2019, **1**, 277–284.

138 N. M. W. Wu, M. Ng and V. W. W. Yam, Photochromic Benzo[b]phosphole Alkynylgold(I) Complexes with Mechanochromic Property to Serve as Multistimuli-Responsive Materials, *Angew. Chemie - Int. Ed.*, 2019, **58**, 3027–3031.

139 J. E. Heckler, N. Deligonul, A. L. Rheingold and T. G. Gray, Gold(i) triazolyls: Organometallic synthesis in air and aqueous media, *Chem. Commun.*, 2013, **49**, 5990–5992.

140 R. A. Vogt, T. G. Gray and C. E. Crespo-Hernández, Subpicosecond intersystem crossing in mono- and Di(organophosphine)gold(I) naphthalene derivatives in solution, *J. Am. Chem. Soc.*, 2012, **134**, 14808–14817.

141 L. Gao, D. S. Niedzwiecki, N. Deligonul, M. Zeller, A. D. Hunter and T. G. Gray, Gold(I) styrylbenzene, distyrylbenzene, and distyrylnaphthalene complexes: High emission quantum yields at room temperature, *Chem. - A Eur. J.*, 2012, **18**, 6316–6327.

142 D. V. Partyka, T. S. Teets, M. Zeller, J. B. Updegraff, A. D. Hunter and T. G. Gray, Constrained digold(I) diaryls: Syntheses, crystal structures, and photophysics, *Chem. - A Eur. J.*, 2012, **18**, 2100–2112.

143 R. A. Vogt, M. A. Peay, T. G. Gray and C. E. Crespo-Hernández, Excited-state dynamics of (Organophosphine)gold(I) pyrenyl isomers, *J. Phys. Chem. Lett.*, 2010, **1**, 1205–1211.

144 D. V. Partyka, L. Gao, T. S. Teets, J. B. Updegraff, N. Deligonul and T. G. Gray, Copper-

catalyzed huisgen [3 + 2] cycloaddition of gold(I) alkynyls with benzyl azide. Syntheses, structures, and optical properties, *Organometallics*, 2009, **28**, 6171–6182.

145 L. Gao, M. A. Peay, D. V. Partyka, J. B. Updegraff, T. S. Teets, A. J. Esswein, M. Zeller, A. D. Hunter and T. G. Gray, Mono- and di-gold(I) naphthalenes and pyrenes: Syntheses, crystal structures, and photophysics, *Organometallics*, 2009, **28**, 5669–5681.

146 T. J. Robilotto, N. Deligonul, J. B. Updegraff and T. G. Gray, Azido, triazolyl, and alkynyl complexes of gold(I): Syntheses, structures, and ligand effects, *Inorg. Chem.*, 2013, **52**, 9659–9668.

147 K. T. Chan, G. S. M. Tong, W. P. To, C. Yang, L. Du, D. L. Phillips and C. M. Che, The interplay between fluorescence and phosphorescence with luminescent gold(i) and gold(iii) complexes bearing heterocyclic arylacetylide ligands, *Chem. Sci.*, 2017, **8**, 2352–2364.

148 S. Goswami, R. W. Winkel and K. S. Schanze, Photophysics and Nonlinear Absorption of Gold(I) and Platinum(II) Donor-Acceptor-Donor Chromophores, *Inorg. Chem.*, 2015, **54**, 10007–10014.

149 G. J. Zhou and W. Y. Wong, Organometallic acetylides of PtII, AuI and Hg II as new generation optical power limiting materials, *Chem. Soc. Rev.*, 2011, **40**, 2541–2566.

150 Y. Lin, C. Jiang, F. Hu, J. Yin, G. A. Yu and S. H. Liu, Synthesis, characterization, and properties of some bisacetylide and binuclear acetylide gold(I) compounds based on the photochromic dithienylethene unit, *Dye. Pigment.*, 2013, **99**, 995–1003.

151 B. Liu, Z. Tian, F. Dang, J. Zhao, X. Yan, X. Xu, X. Yang, G. Zhou and Y. Wu, Photophysical and optical power limiting behaviors of Au(I) acetylides with diethynyl aromatic ligands showing different electronic features, *J. Organomet. Chem.*, 2016, **804**, 80–86.

152 P. J. Conaghan, C. S. B. Matthews, F. Chotard, S. T. E. Jones, N. C. Greenham, M. Bochmann, D. Credgington and A. S. Romanov, Highly efficient blue organic light-emitting diodes based on carbene-metal-amides, *Nat. Commun.*, 2020, **11**, 1–8.

153 R. Hamze, S. Shi, S. C. Kapper, D. S. M. Ravinson, L. Estergreen, M. C. Jung, A. C. Tadle, R. Haiges, P. I. Djurovich, J. L. Peltier, R. Jazzar, G. Bertrand, S. E. Bradforth and M. E. Thompson, 'Quick-Silver' from a Systematic Study of Highly Luminescent, Two-Coordinate, d10 Coinage Metal Complexes, *J. Am. Chem. Soc.*, 2019, **141**, 8616–8626.

154 A. S. Romanov, S. T. E. Jones, Q. Gu, P. J. Conaghan, B. H. Drummond, J. Feng, F. Chotard, L. Buizza, M. Foley, M. Linnolahti, D. Credgington and M. Bochmann, Carbene metal amide photoemitters: Tailoring conformationally flexible amides for full color range emissions including white-emitting OLED, *Chem. Sci.*, 2020, **11**, 435–446.

155 C. R. Hall, A. S. Romanov, M. Bochmann and S. R. Meech, Ultrafast Structure and Dynamics in the Thermally Activated Delayed Fluorescence of a Carbene-Metal-Amide, *J. Phys. Chem. Lett.*, 2018, **9**, 5873–5876.

156 D. Di, A. S. Romanov, L. Yang, J. M. Richter, J. P. H. Rivett, S. Jones, T. H. Thomas, M. A. Jalebi, R. H. Friend, M. Linnolahti, M. Bochmann and D. Credgington, High-performance light-emitting diodes based on carbene-metal-amides, 2017, **163**, 159–163.

157 T. Y. Li, D. S. Muthiah Ravinson, R. Haiges, P. I. Djurovich and M. E. Thompson, Enhancement of the Luminescent Efficiency in Carbene-Au(I)-Aryl Complexes by the Restriction of Renner-Teller Distortion and Bond Rotation, *J. Am. Chem. Soc.*, 2020, **142**, 6158–6172.

158 C. C. Beto, C. J. Zeman, Y. Yang, J. D. Bullock, E. D. Holt, A. Q. Kane, T. A. Makal, X. Yang, I. Ghiviriga, K. S. Schanze and A. S. Veige, An Application Exploiting Aurophilic Bonding and iClick to Produce White Light Emitting Materials, *Inorg. Chem.*, 2020, **59**, 1893–1904.

159 C. J. Zeman, Y.-H. Shen, J. K. Heller, K. A. Abboud, K. S. Schanze and A. S. Veige, Excited-State Turn-On of Aurophilicity and Tunability of Relativistic Effects in a Series of Digold Triazolates Synthesized via iClick, *J. Am. Chem. Soc.*, 2020, **142**, 8331–8341.

# Chapter 2: Synthesis, Photophysics, and Computations for a Series of Gold(I) BTF Aryl Complexes (Au-BTF(0-2))

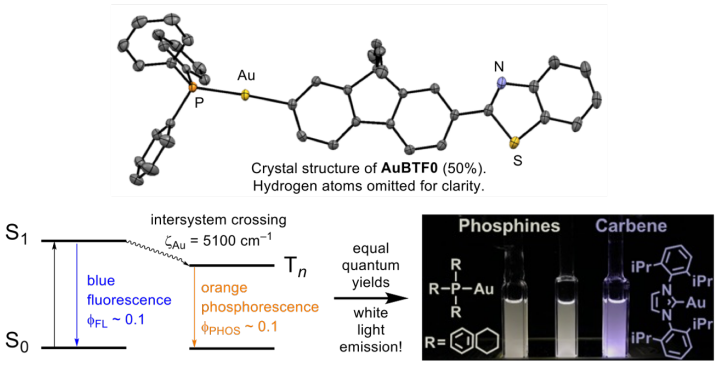


The interest of this dissertation is to expand the knowledge of structure-property relationships in gold organometallics while endowing the complexes with nonlinear absorption capabilities. In other words, an increased understanding of gold organometallics as triplet photoactive materials will support applications in nonlinear optics (NLO). A nonlinear optical material is one that attenuates high intensity light through nonlinear absorption processes. For other applications, it is desirable for a nonlinear optical material to be transparent (Figure 2.1).

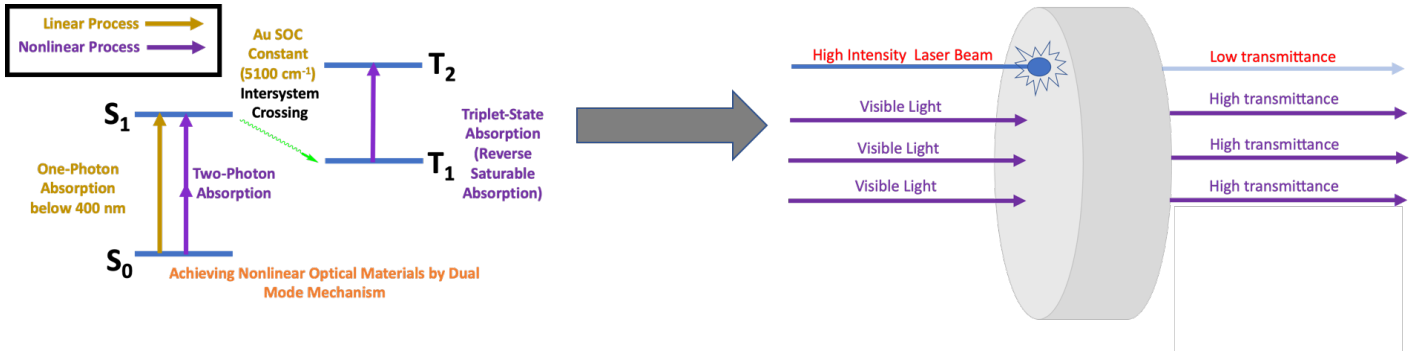


**Figure 2.1.** Achieving transparent nonlinear optical materials via the dual-mode mechanism.

The parameters to achieve a material with those properties appear in the Jablonski diagram of Figure 2.1. The nonlinear portion is achieved by the dual-mode mechanism of two-photon absorption (2PA) and triplet-excited state absorption, with transparency coming from a ground-state absorption profile confined to the ultraviolet region. To design nonlinear optical

chromophores rationally, we bind known two-photon chromophores to gold.[1] Ligands that contain the benzothiazole-2,7-fluorenyl or diphenylamino-2,7-fluorenyl moiety were chosen for a variety of reasons (Figure 2.2). First, those moieties have established syntheses and 2PA capability.[1] Second, synthetic modification of the terminal substituent labeled in dark blue is facile and the nature of the gold-chromophore linkage can be altered at will. Third, easy modification of the capping moiety (labeled in gray) on the other end of the fluorene is possible, which allows for tuning of the electronic properties of the ligand. Last, the alkyl arms (labeled in red) can be extended or shortened in the interest of solubility; there is also evidence that extended alkyl chains increase 2PA capability.[1]

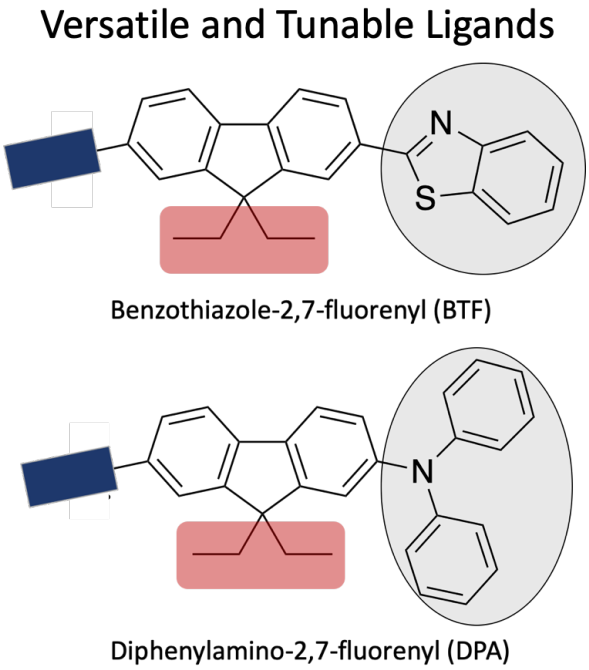


**Figure 2.2** Designation of chromophores.

In order to gain access to triplet excited states, we impart the gold atom. The spin-orbit coupling of gold ($\zeta_{SOC}$ = 5104 cm$^{-1}$) allows for the relaxation of the orthogonality between singlet and triplet exited-states allowing for intersystem crossing. This allows study of gold

organometallics as triplet photoactive materials and enables triplet excited-state absorption. With the rationale of that design principle in mind, the BTF-Bpin ligand was synthesized (Scheme 2.1).[1]

**Syntheses and Crystal Structures of Au-BTF(0-2):**

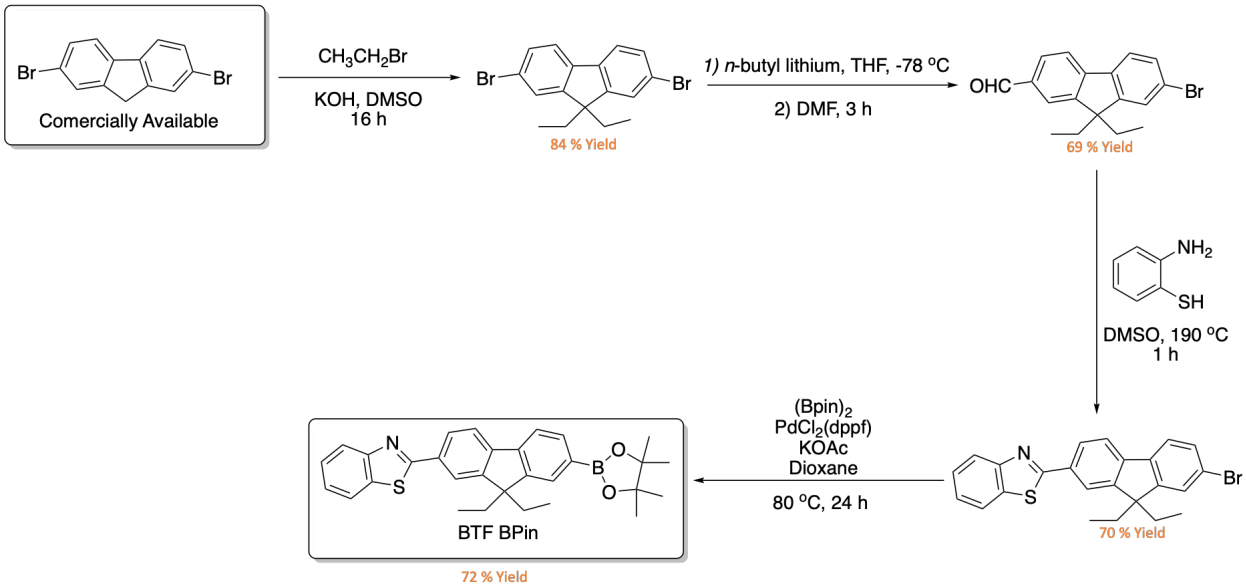


**Scheme 2.1.** Synthesis of benzothiazole-2,7- fluorenyl pinocolato ester (BTF Bpin). Isolated yields are indicated.

Ligand precursors were reacted with either *N*-heterocyclic carbene or organophosphine gold(I) halide starting materials.[2] Three new gold(I) BTF aryl complexes (**Au-BTF(0-2)**) were achieved in base-assisted boron transmetallation reactions (Scheme 2.2).[2] Vapor diffusion of pentane into concentrated dichloromethane solutions yielded the new complexes in 53-72% isolated yields as yellow crystalline solids.[3]

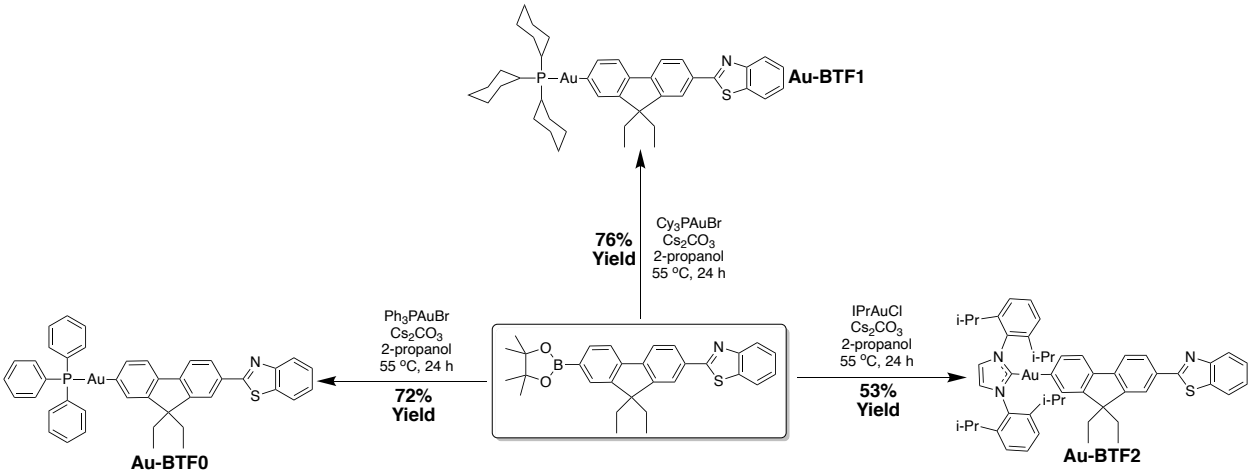


**Scheme 2.2** Synthesis of new **Au-BTF(0-2)**.

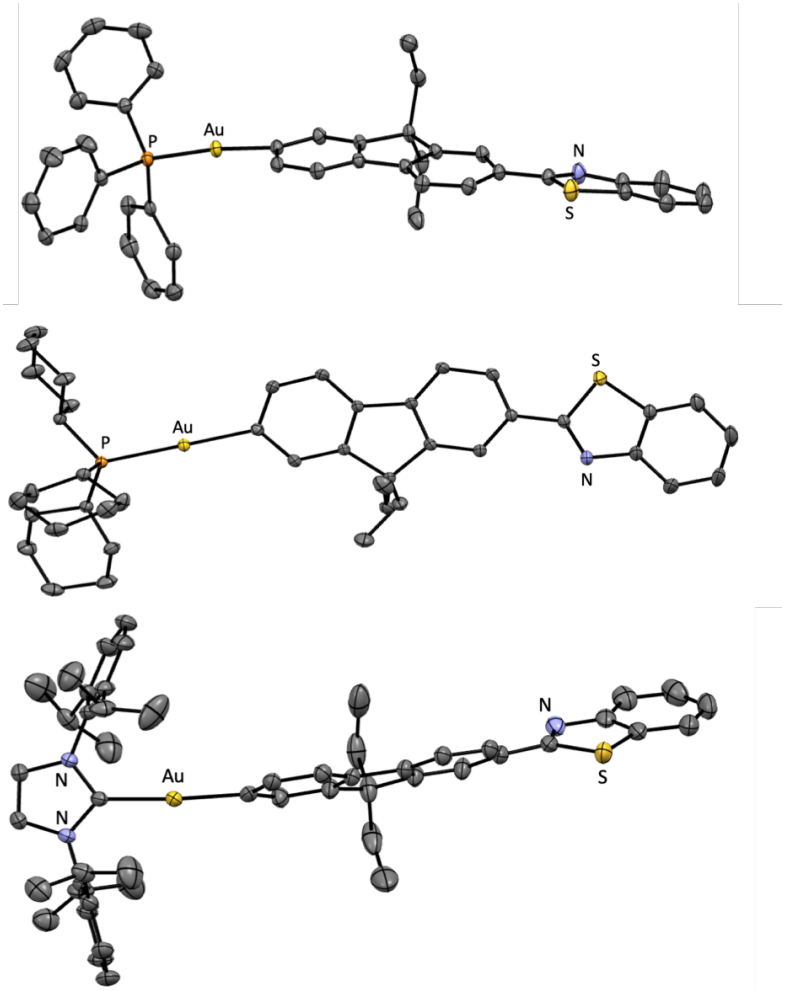

**Figure 2.3.** Crystal structures of **Au-BTF0** (top), **Au-BTF1** (middle), **Au-BTF2** (bottom) (50% probability level, 150 K). Hydrogen atoms are omitted for clarity. Partial atom labeling schemes are indicated; unlabeled atoms are carbon.

Thermal ellipsoid depictions of all three complexes appear in Figure 2.3. In all cases, gold(I) is linear; packing diagrams show no evidence of aurophilic interactions or π-π stacking. **Au-BTF0** has an Au-C bond length 2.053(2) Å and an Au-P length of 2.294(6) Å and **Au-BTF1** has an Au-C bond length of 2.050(2) Å and an Au-P length of 2.295(4) Å demonstrating little variation in the bond lengths between the two phosphine complexes. **Au-BTF2** has an Au-$C_{carbene}$ length of 2.029(3) Å and an Au-$C_{aryl}$ length of 2.033(3) Å.

**Photophysical Characterization of Au-BTF(0-2):**

Ground-state absorption spectra for **Au-BTF(0-2)** in molar absorptivity units appear in Figure 2.4. All three complexes exhibit structured absorption spectra with similar molar absorptivity values on the scale of (5-6) x $10^4$. The spectra are similar, with two distinct peaks and a high-energy shoulder. **Au-BTF0** and **Au-BTF1** exhibit maxima at 359 and 360 nm respectively. Varying the ancillary ligand from an organophosphine to an *N*-heterocyclic carbene in **Au-BTF2**, a red-shift in the spectrum maximum to 364 nm is observed.

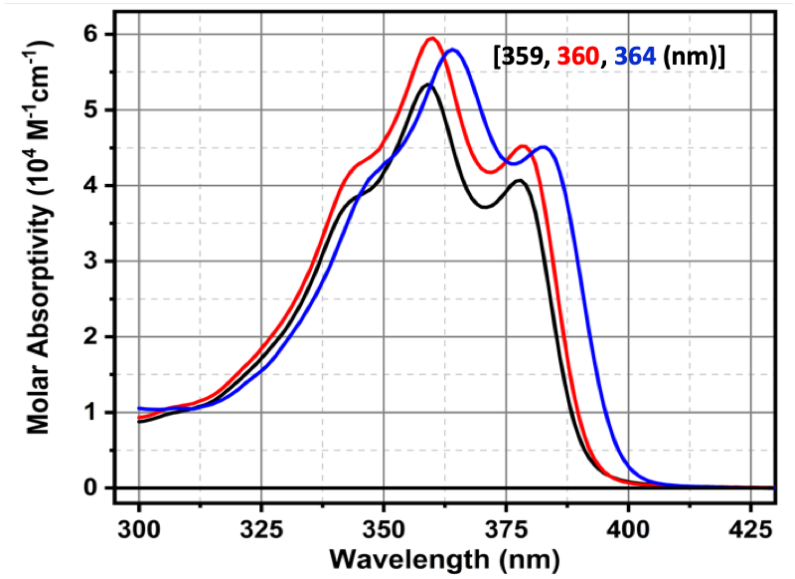


**Figure 2.4.** Ground-state absorption spectra for **Au-BTF0** (black), **Au-BTF1** (red), and **Au-BTF2** (blue).

Emission spectra collected in degassed toluene at room temperature are shown in Figure 2.5. All three complexes are characterized by dual-luminescence, fluorescence and phosphorescence emission. The energy trends follow that of the absorption spectra; namely, the carbene complex (**Au-BTF2**) is the most red-shifted. The two phosphine complexes **Au-BTF0**

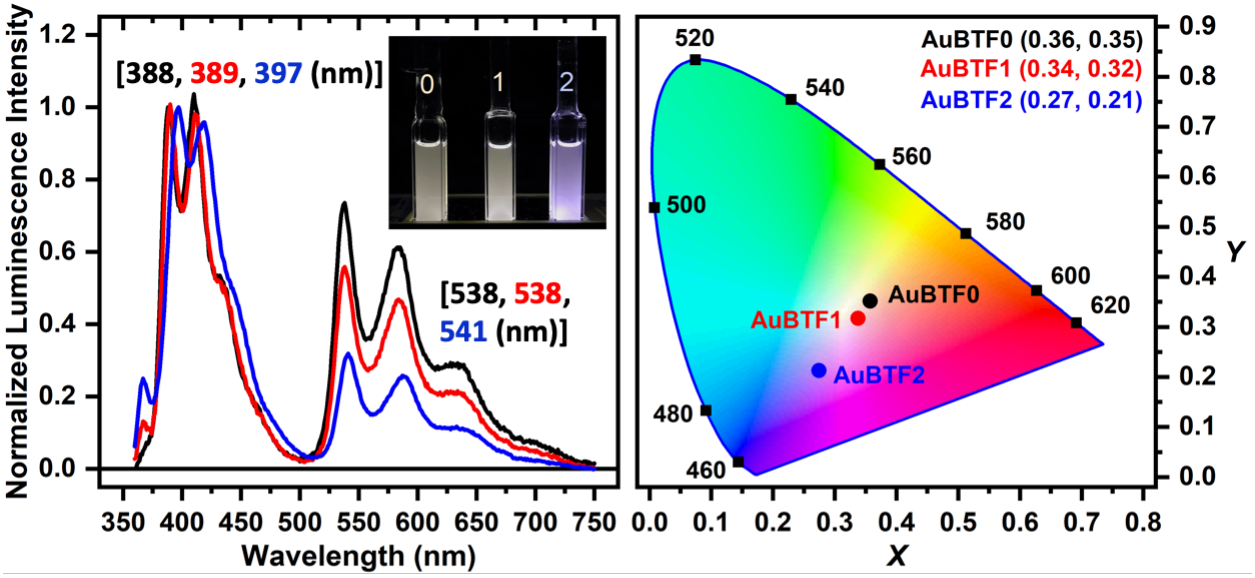

**Figure 2.5.** Emission spectra collected in toluene at room temperature following three freeze-pump-thaw cycles for **Au-BTF0** (black), **Au-BTF1** (red), and **Au-BTF2** (blue) in molar absorptivity units (left), Inset (emission color of complexes when subjected to UV irradiation). CIE 1931 chromaticity diagram (right).

and **Au-BTF1** exhibit larger phosphorescence intensities. The two phosphine complexes are white-light emitters when subjected to ultraviolet irradiation (Figure 2.5, inset) with corroboration by a CIE 1931 chromaticity diagram (Figure 2.5, right).

| Complex | AuBTF0 | AuBTF1 | AuBTF2 |
|---|---|---|---|
| $\lambda_{ABS}$/nm ($10^4$ $M^{-1}cm^{-1}$) | 359 (5.34 ± 0.68 ) | 360 (5.95 ± 0.18 ) | 364 (5.80 ± 0.18) |
| $^{A}\lambda_{FL}$ (nm) | 388 | 389 | 397 |
| $\varphi_{FL}$ | 0.08 ± 0.01 | 0.09 ± 0.03 | 0.22 ± 0.01 |
| $\tau_{FL}$ – TCSPC (ps) | 79.3 | 89.4 | 229 |
| $\tau_{FL}$ – TA (ps) | 84.5 ± 4.6 | 95.4 ± 2.3 | 279 ± 10 |
| $k_r$ ($s^{-1}$) | 9.4 x $10^8$ | 9.5 x $10^8$ | 7.9 x $10^8$ |
| $k_{nr}$ ($s^{-1}$) | 1.5 x $10^9$ | 1.1 x $10^9$ | 5.4 x $10^8$ |
| $k_{ISC}$ ($s^{-1}$) | 9.3 x $10^9$ | 8.5 x $10^9$ | 2.3 x $10^9$ |
| $^{B}\lambda_{PHOS}$ (nm) | 538 | 538 | 541 |
| $\varphi_{TRIPLET}$ | 0.79 ± 0.01 | 0.81 ± 0.02 | 0.63 ± 0.03 |
| $\varphi_{PHOS}$ | 0.09 ± 0.01 | 0.07 ± 0.01 | 0.11 ± 0.01 |
| $\tau_{PHOS}$ (μs) Vac. Pressure (mTorr) | 810 ± 70<br>89 | 766 ± 8<br>90 | 872 ± 59<br>87 |
| $k_T$ ($s^{-1}$) | 1,220 | 1,290 | 1,140 |
| $k_{TT}$ ($M^{-1}s^{-1}$) | 1.3 ± 0.1 x $10^{10}$ | 1.2 ± 0.1 x $10^{10}$ | 1.4 ± 0.1 x $10^{10}$ |
| $\Delta\varepsilon_{T_1-T_n}$/λ nm ($10^4$ $M^{-1}$ $cm^{-1}$) | 547 (9.14 ± 0.50 ) | 550 (10.1 ± 0.1 ) | 562 (9.40 ± 0.10 ) |
| $\Delta\varepsilon_{S_1-S_n}$/λ nm ($10^4$ $M^{-1}$ $cm^{-1}$) | 567 (13.7 ) | 588 (15.6 ) | 557 (15.0 ) |

**Table 2.1.** Summary of photophysical data for **Au-BTF(0-2)**.

All data collected in room temperature toluene. Legend: $\lambda_{FL}$ = wavelength of fluorescence; $\varphi_{FL}$ = emission quantum yield of fluorescence; $\tau_{FL}$ =lifetime of fluorescence; TCSPC = time-correlated single-photon counting; TA = transient absorption; $k_r$ = radiative decay rate constant; $k_{nr}$ = non-radiative decay rate constant; $k_{ISC}$ = rate constant of intersystem crossing; $\lambda_{PHOS}$ = wavelength of phosphorescence; $\varphi_{TRIPLET}$ = quantum yield of triplet state formation; $\varphi_{PHOS}$ = emission quantum yield of phosphorescence; $\tau_{PHOS}$ =

lifetime of phosphorescence; $k_T$ = rate constant for formation of triplet excited state; $k_{TT}$ = rate constant of triplet–triplet annihilation; $\Delta\varepsilon_{T1-Tn}$ = molar absorptivity of triplet–triplet absorption; $\Delta\varepsilon_{S1-Sn}$=molar absorptivity of excited-singlet–singlet absorption. [a]Estimated from the peak maximum of the dilute luminescence spectrum used for the reabsorption correction in fluorescence quantum yield experiments. b Estimated from the peak maximum of the phosphorescence signal.

Static and transient photophysical measurements were performed in order to gain insight into the nature of the excited-states for these complexes. Fluorescence and phosphorescence lifetimes and quantum yields as well as triplet-state quantum yields appear in Table 2.1. Phosphine complexes **Au-BTF0** and **Au-BTF1** display similar fluorescence and phosphorescence quantum yields (~0.1) leading to white light emission. **Au-BTF0 and Au-BTF1** display similar fluorescence lifetimes of ~90 ps, triplet-state quantum yields of ~0.80, and phosphoresce lifetimes of ~800 microseconds. Changing the ancillary ligand from an organophosphine to an *N*-heterocyclic carbene leads to sizable changes in lifetimes and quantum yields. **Au-BTF2** exhibits a fluorescence quantum yield and lifetime of 0.22 and 229 ps, a triplet state quantum yield of 0.63 and, a phosphoresce lifetime of 872 microseconds and quantum yield of 0.11. Changing the ancillary ligand from an organophosphine to an *N*-heterocyclic carbene leads to an increase in fluorescence quantum yield and lifetime by a factor of two, a decreased triplet-state quantum yield, and an increased phosphorescence lifetime; subtle changes in phosphorescence quantum yields are observed.

Emission lifetime and quantum yield data allows for calculation of excited-state rate constants for radiative decay ($k_r$), nonradiative decay ($k_{nr}$) and intersystem crossing ($k_{isc}$). **Au-BTF2** displays a $k_r$ value of $7.9 \times 10^8$, a $k_{nr}$ value of $5.4 \times 10^8$, and a $k_{isc}$ value of $2.3 \times 10^9$. When the ancillary ligand is changed from *N*-heterocyclic carbene to an organophosphine, we observe an increase in rate of intersystem crossing by a factor of 4, an increase in the nonradiative decay rate by a factor of 2, and an increase in radiative rate by a factor of ~1.2 (Table 2.1).

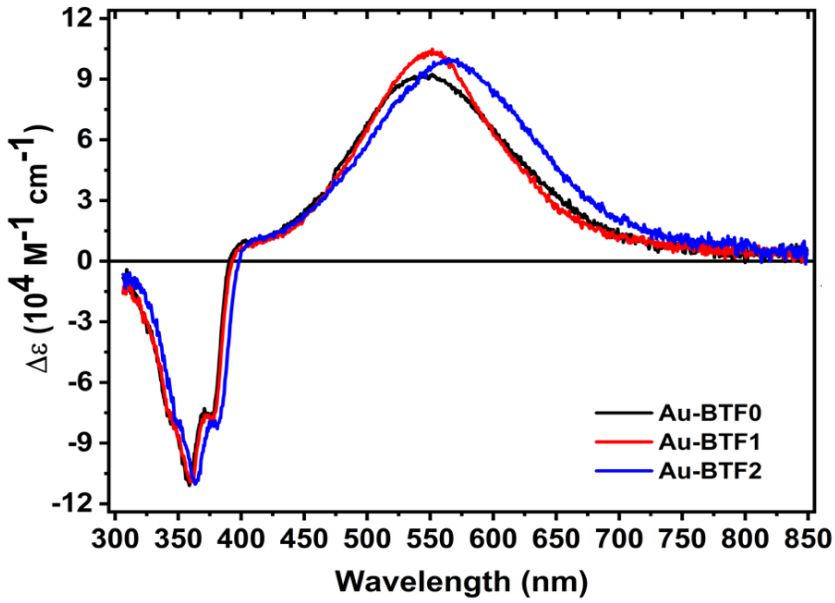


**Figure 2.6.** Nanosecond transient absorption difference spectra collected following three freeze-pump-thaw cycles in toluene. All samples were excited at 355 nm. The spectra were collected 100 ns after the laser pulse. Spectra were converted to units of Δε using relative actinometry measurements with a $[Ru(bpy)_3]^{2+}$ standard.

Nanosecond transient absorption spectra for **Au-BTF(0-2)** in units of Δε are shown in Figure 2.6. All three complexes are characterized by a bleach of the ground-state and strong, positive absorption throughout the visible spectrum attributed to the triplet state. All three complexes have excited-state extinction coefficients ($\Delta\varepsilon_{T_1\text{-}T_n}$) ~1 x $10^5$ $M^{-1}$ $cm^{-1}$. The energy trends seen in the ground state absorption and emission spectra extend to the excited-state absorption maxima. **Au-BTF0** and **AuBTF1** have maxima at 547 and 550 nm; a red-shift is observed when the ancillary ligand is changed in **Au-BTF2** to 562 nm.

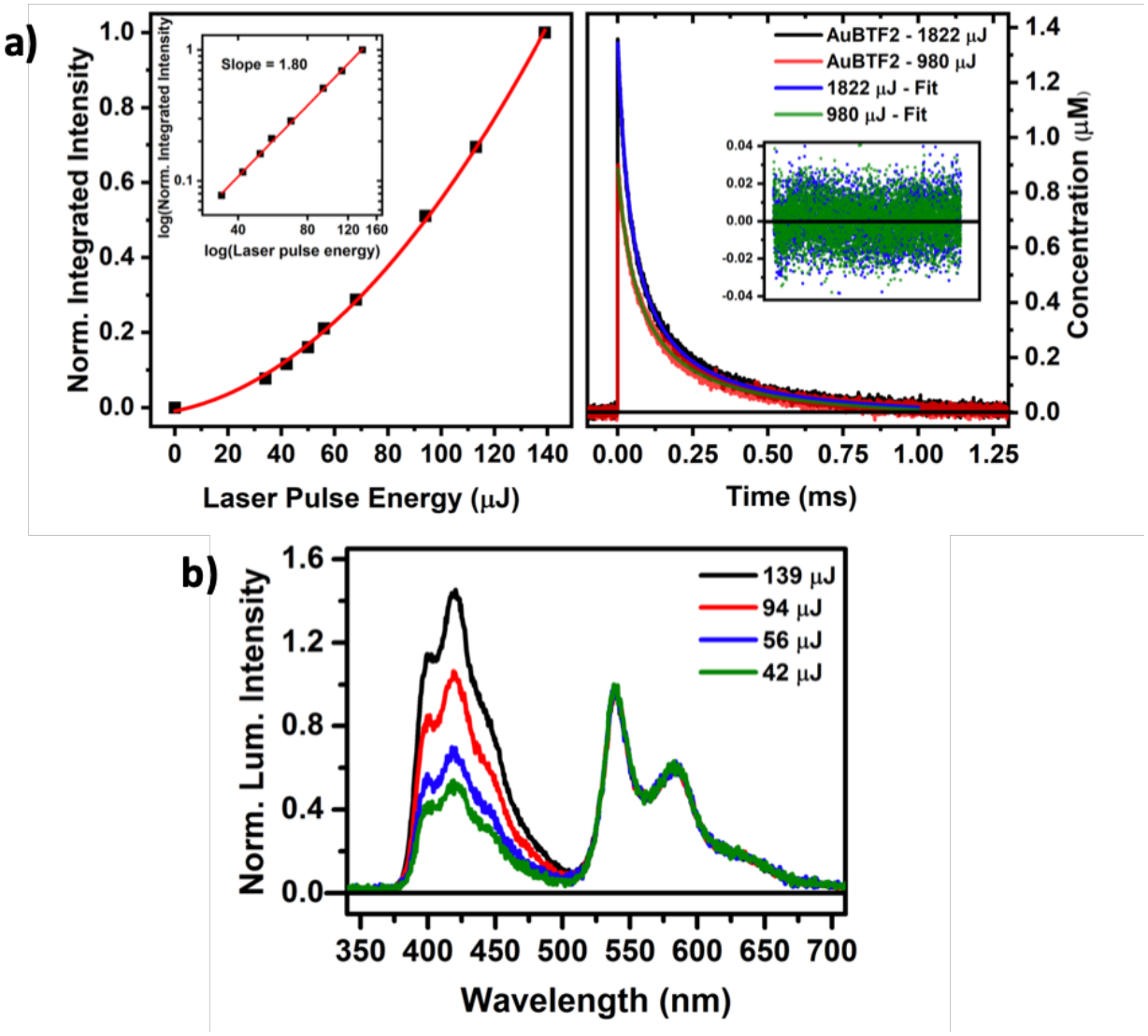


**Figure 2.7.** a) Fits of the normalized, integrated fluorescence intensity vs. laser pulse energy (left) and triplet-triplet annihilation fitting of excited-state decay traces in freeze-pump-thaw degassed toluene of **Au-BTF2** (right). b) Delayed fluorescence observed in **Au-BTF2**, the signal is normalized to the phosphorescence maximum. Data is representative of all complexes.

Delayed fluoresce was observed in all three complexes. Figure 2.7b (left) shows the normalized luminescence intensity vs. wavelength, where the signal is normalized to the phosphorescence maximum to demonstrate the effect laser pulse energy has on the fluorescence intensity. As laser pulse energy is increased, we observe a clear increase in fluorescence intensity.

Figure 2.7a displays the normalized integrated fluorescence intensity vs. laser pulse energy and the inset is the logarithmic plot. A slope of nearly two is observed demonstrating that the delayed fluorescence is a result of a bimolecular process (i.e. triplet-triplet annihilation). Dependence of delayed fluorescence on laser pulse energy also indicates a triplet-triplet annihilation decay pathway. It is believed that the slope is not exactly two in any of the complexes due to fast intersystem crossing, which efficiently depopulates the triplet state.

Triplet-triplet annihilation rate constants ($k_{TT}$) were obtained by fitting the nanosecond decay traces after conversion from ΔOD to concentration via Beer's law Figure 2.7b (right). A discussion of the process as well as the fit equation used can be found in the experimental section of this chapter. The fits were done at two different pulse energies with the parameter of $k_T$ being held constant; the values were then averaged, which appear in Table 2.1. All three complexes exhibit triplet-triplet annihilation rate constants ($k_{TT}$) ~1 x $10^{10}$ $M^{-1}$ $s^{-1}$. This value indicates that triplet-triplet annihilation is diffusion controlled in the solvent of toluene.

Picosecond transient absorption measurements were performed in order to paint a more complete picture of the excited-state dynamics in these complexes (Figure 2.8). All three complexes exhibit both singlet and triplet excited-state absorption. The transient progression of from singlet state to the triplet state can be seen at different time delays (Figure 2.8). Values for the singlet lifetimes were obtained via decay traces. The $S_1$ – $S_n$ absorption transitions are represented by shortest time delay spectra and the $T_1$ – $T_n$ absorption transitions are represented by the longest time delay spectra for each complex. Molar absorptivities of the $S_1 \rightarrow S_n$ absorption transitions are nearly twice those of the $T_1 \rightarrow T_n$ transitions. All three complexes have $\Delta\varepsilon_{S_1\text{-}S_n}$ ~1.5 x $10^5$ $M^{-1}$ $cm^{-1}$ and exhibit a single isosbestic point at ~ 475 nm.

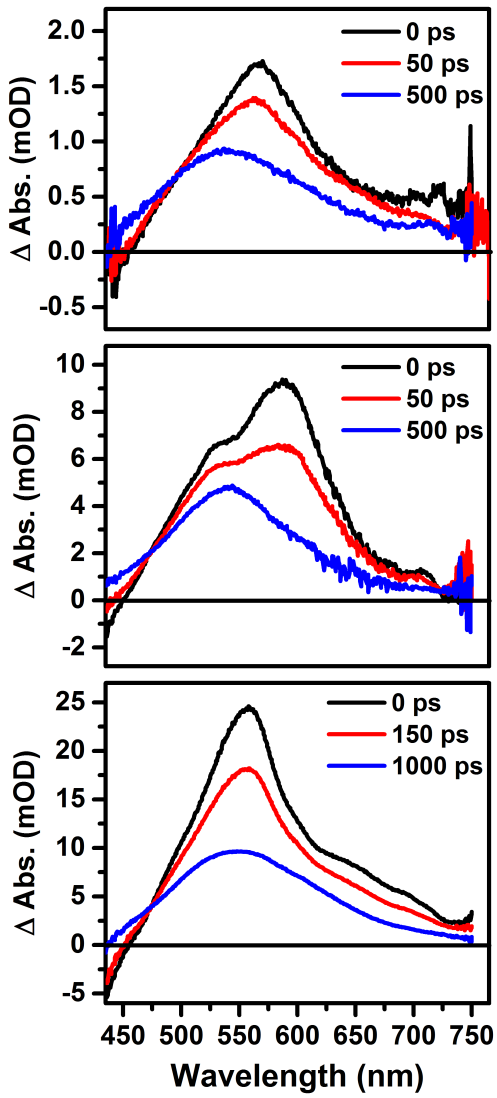


**Figure 2.8.** Picosecond transient absorption difference spectra collected at various probe times for (top) **AuBTF0**, (middle) **AuBTF1**, and (bottom) **AuBTF2** in deaerated toluene. The frequency doubled output of Ti:sapphire was used to excited the samples.

**Computations.**

Density-functional theory calculations were undertaken to gain insight into the origin of the photophysical behavior for the **Au-BTF** series. Details for the calculations can be found in the experimental section of this chapter. Figure 2.9 displays a frontier orbital energy level diagram

with Kohn-Sham orbital plots for both the highest-occupied Kohn-Sham orbital (HOMO) and the lowest unoccupied Kohn-Sham orbital (LUMO). Percentages of orbital density in the HOMO are of 4% Au, 79% fluorene, and 17% benzothiazole; for the LUMO, these are 50% fluorene and 48% benzothiazolyl.

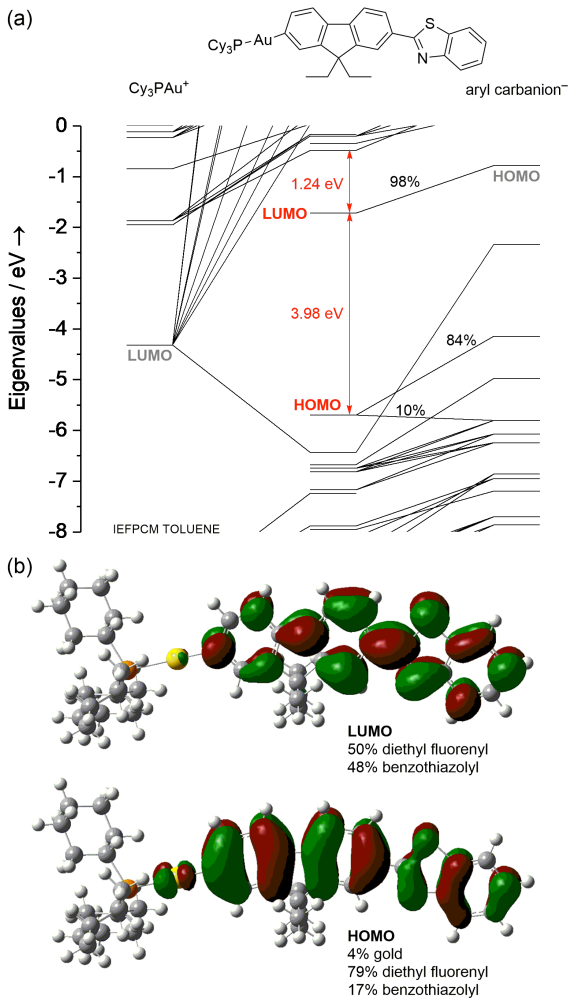


**Figure 2.9.** (a) Frontier orbital energy level diagram of **AuBTF1**. (b) Plots of frontier Kohn-Sham orbitals (HOMO) and (LUMO) (Percentages are of electron density).

The $S_1$ state derives primarily from a (98%) LUMO ← HOMO excitation; These results in conjunction with highly structed absorption spectra indicate that these transitions are π-π *in nature. Figure 2.10 displays a time-dependent density-functional theory state plot for **Au-BTF(0-**

**2)**. The results concur with the photophysical data obtained for the three complexes, particularly in regards to the rate of intersystem crossing.

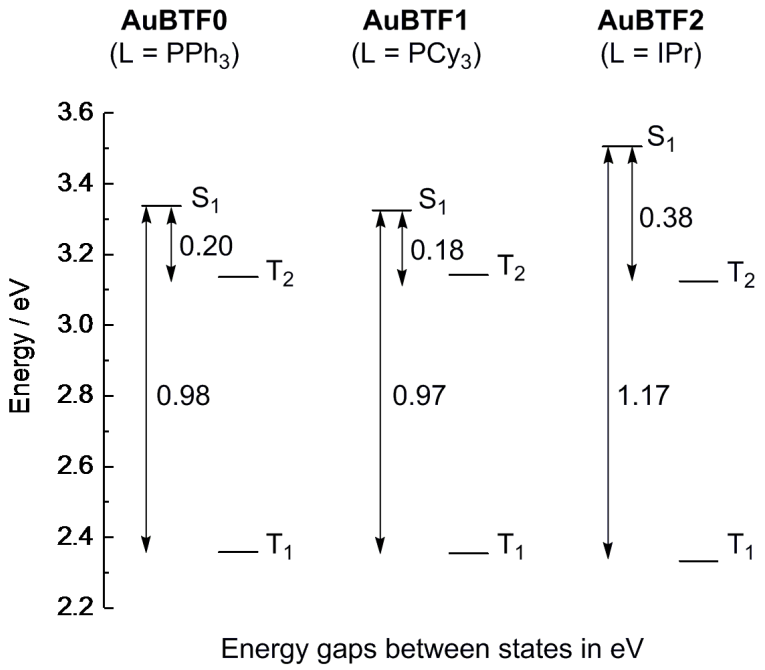


**Figure 2.10** Time-dependent density-functional theory (TD-DFT) state plot showing $S_1$, $T_1$, and $T_2$ states and their corresponding energies in electron volts (eV) for the three **Au-BTF** complexes.

The two phosphine complexes **Au-BTF0** and **Au-BTF1** exhibit rates of intersystem crossing almost four times that of the carbene complex, **Au-BTF2**. TD-DFT calculations show that **Au-BTF0** and **Au-BTF1** display $S_1$-to-$T_2$ energy gaps that are roughly half that of **Au-BTF2**. This is believed to be a contributing factor as to why the phosphine complexes have faster and more efficient intersystem crossing.

**Conclusions.**

Three new gold(I) BTF aryl complexes, **Au-BTF(0-2)** were synthesized and photophysically characterized. The complexes were synthesized via a base-assisted boron transmetallation in moderate to good yields (53-75%). Crystal structures were obtained for each complex, all are nearly linear in geometry. No evidence of aurophilic or π-π stacking interactions is found. The

three complexes are characterized by highly structured ground-state absorption and emission spectra following the energy trends **AuBTF0** ≈ **AuBTF1** > **AuBTF2**. These complexes emit via dual-luminescence; highly structured fluorescence and phosphorescence. The two phosphine complexes are white-light emitters by nearly equal fluorescence and phosphorescence quantum yields. General trends recur in the photophysical data: The two phosphine complexes (**Au-BTF 0,1**) exhibit shorter fluorescence lifetimes, higher triplet state quantum yields, and smaller fluorescence quantum yields compared to the carbene complex, **Au-BTF2**. **Au-BTF 0** and **1** also display rates of intersystem crossing four times that of **Au-BTF2** with higher rates of radiative and nonradiative decay as well. Strong and broad triplet-excited state absorption was established via nanosecond transient absorption measurements. Delayed fluorescence via triplet-triplet annihilation was also observed from laser pulse energy dependence studies. All three complexes exhibit triplet-triplet annihilation rate constants ($k_{TT}$) ~1 x $10^{10}$ $M^{-1}$ $s^{-1}$, suggesting that triplet-triplet annihilation is diffusion-controlled in toluene. Picosecond transient absorption data show that both the singlet and triplet states strongly absorb with $\Delta\varepsilon_{S_1\text{-}S_n}$ ~1.5 x $10^5$ $M^{-1}$ $cm^{-1}$ and $\Delta\varepsilon_{T_1\text{-}T_n}$ on the order of 1 x $10^5$ $M^{-1}$ $cm^{-1}$. A progression from the singlet to the triplet state is also visible and an isosbestic point around 475 nm is evident. Density-functional theory calculations show that both the HOMO and LUMO for all three complexes is localized on the BTF ligand and that the $S_1$ state derives from a (98%) LUMO ← HOMO excitation. We therefore assign the absorption transitions as π-π *in nature. TD-DFT computations broadly agree with the photophysical data. **Au-BTF 0** and **1** have computed $S_1$-to-$T_2$ energy gaps that are nearly half that of the carbene complex **Au-BTF2**, which is believed to be a contributing factor as to why **Au-BTF 0** and **1** have higher rates of intersystem crossing and larger triplet state quantum yields.

## Experimental Details

**General Considerations.** All experimental procedures were carried out under an inert atmosphere of argon using standard Schlenk line techniques. Microanalyses (C, H, and N) were undertaken by Midwest Microlab and Atlantic Microlab. Mass spectrometry was performed at the University of Cincinnati Mass Spectrometry facility. (Phosphine)gold(I) chloride and (i-$Pr_2$NHC)AuCl were prepared according to literature procedures.[2] The corresponding gold(I) bromides were prepared by reacting one equivalent of gold(I) chloride with five equivalents of potassium bromide in a 1:1 mixture of DCM/Water, extraction in DCM yielded the bromides quantitatively. 2-(9,9-Diethyl-7-(4,4,5,5-tetramethyl-1,3,2-dioxaborolan-2-yl)-9*H*-fluoren-2-yl)benzo[*d*]thiazole was synthesized via previously described literature.[1] Dry 2-propanol, benzene, dichloromethane, pentane, and cesium carbonate was purchased from Sigma Aldrich and used as received. $^1$H NMR experiments were performed on a Bruker-500 Ascend Advanced III HD NMR spectrometer operating at 500.24 MHz. All NMR experiments were run at a millimolar concentration.$^1$H chemical shifts are reported in parts per million ($\delta$) with integration and multiplicity (s = singlet, d = doublet, t = triplet, q = quartet, dd = doublet of doublets, dt = doublet of triplets, td = triplet of doublets, ddd = doublet of doublet of doublets, and m = multiplet), measured from tetramethylsilane (0 ppm) and are referenced to residual solvent in $CDCl_3$ (7.26 ppm). $^{31}$P{$^1$H} NMR, chemical shifts were determined relative to concentrated $H_3PO_4$.

**Instrumentation and photophysical measurements.**

Details regarding instrumentation and photophysical measurements can be found here:

http://www.rsc.org/suppdata/c9/dt/c9dt02312g/c9dt02312g1.pdf

**Synthesis, NMR, Mass Spectrometry and Elemental Analysis**

**AuBTF0:**

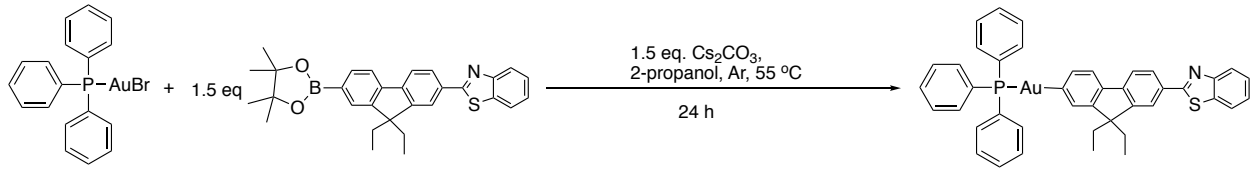


To a flame-dried 25 mL round bottom flask equipped with a stir bar was added (100 mg, 0.186 mmol) of $Ph_3PAuBr$, (134 mg, 0.278 mmol) of pinacolboronate ester, and (181 mg, 0.556 mmol) of $Cs_2CO_3$. The flask was purged with argon for 15 min, after which 5 mL of dry 2-propanol was added via syringe. The vessel was then shielded from light and heated at 55 °C for 24 h. The contents of the flask were then cooled to room temperature yielding a bright yellow suspension that was concentrated *in vacuo.* The crude product was dissolved in 5 X 5 mL portions of benzene and filtered over Celite to yield a yellow solution which was concentrated under reduced pressure. This crude product was then subjected to vapor diffusion crystallization using dichloromethane as the solvent and pentanes as the anti-solvent (111 mg, 72 %).$^1$H NMR (500 MHz, Chloroform-*d*) δ 8.08 (d, *J* = 10.8 Hz, 2H), 8.00 (d, *J* = 9.0 Hz, 1H), 7.90 (d, *J* = 7.9 Hz, 1H), 7.74 (d, *J* = 7.9 Hz, 1H), 7.70 (d, *J* = 7.2 Hz, 1H), 7.62 (dt, *J* = 14.7, 7.4 Hz, 8H), 7.49 (q, *J* = 7.7 Hz, 10H), 7.37 (t, *J* = 7.2 Hz, 1H), 2.16 – 2.10 (m, 4H), 0.37 (t, *J* = 7.3 Hz, 6H). $^{31}$P NMR (121 MHz, $CDCl_3$) δ (ppm): 43.58. HRMS (FT-ICR, $[M+H]^+$) m/z calcd for $MH^+$ $C_{42}H_{36}NPSAu^+$ 814.19661, found 814.19680. Anal. Calcd for: $C_{51}H_{56}AuN_3S$: C, (61.99); H, (4.34); N, (1.72). Found: C, (61.83); H, (4.54); N, (1.75).

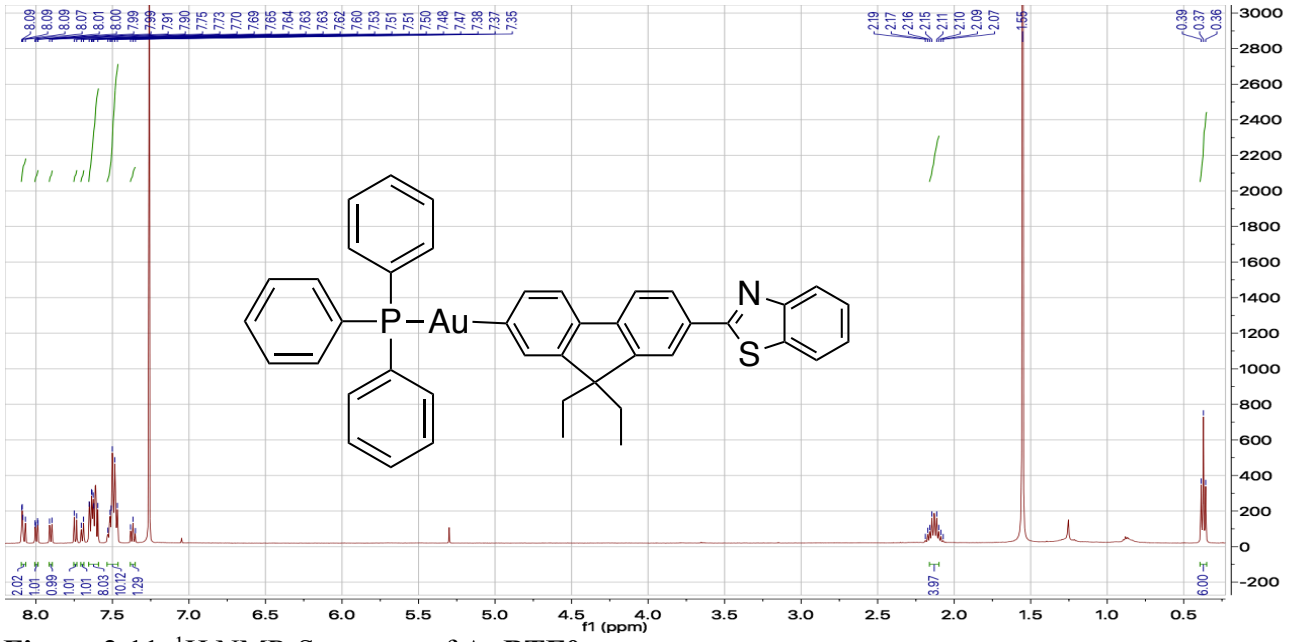


**Figure 2.11.** $^{1}$H NMR Spectrum of **AuBTF0**

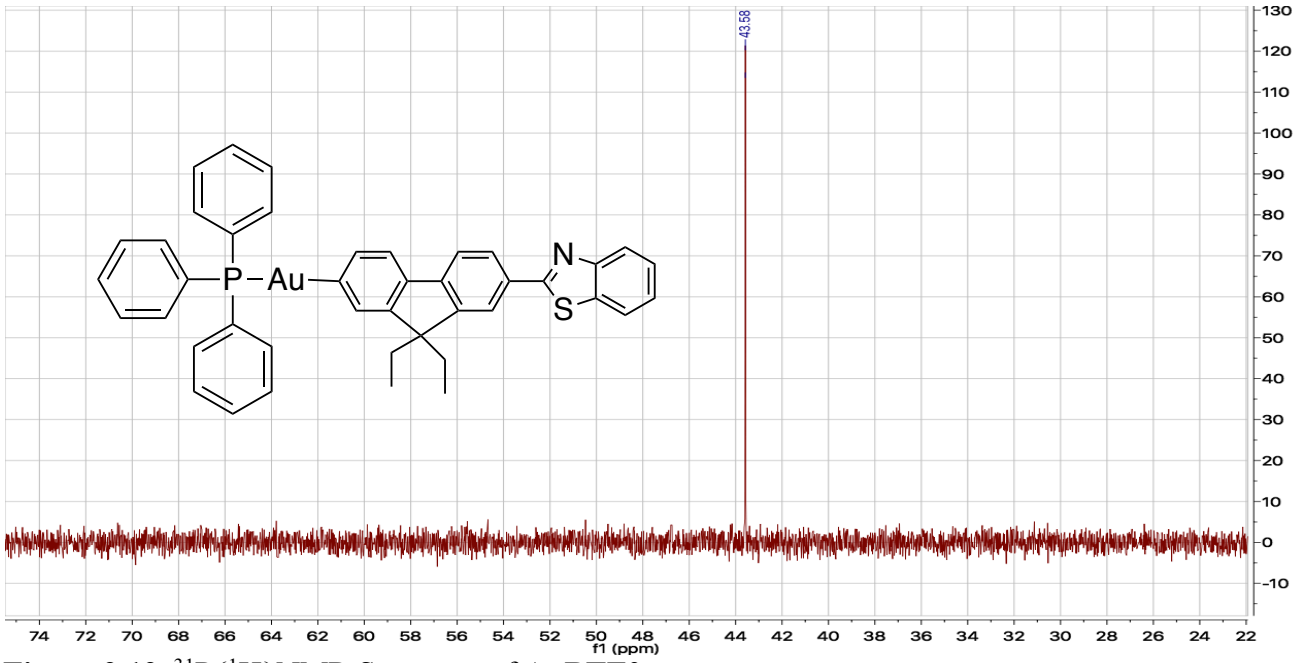


**Figure 2.12.** $^{31}$P{$^{1}$H}NMR Spectrum of **AuBTF0**

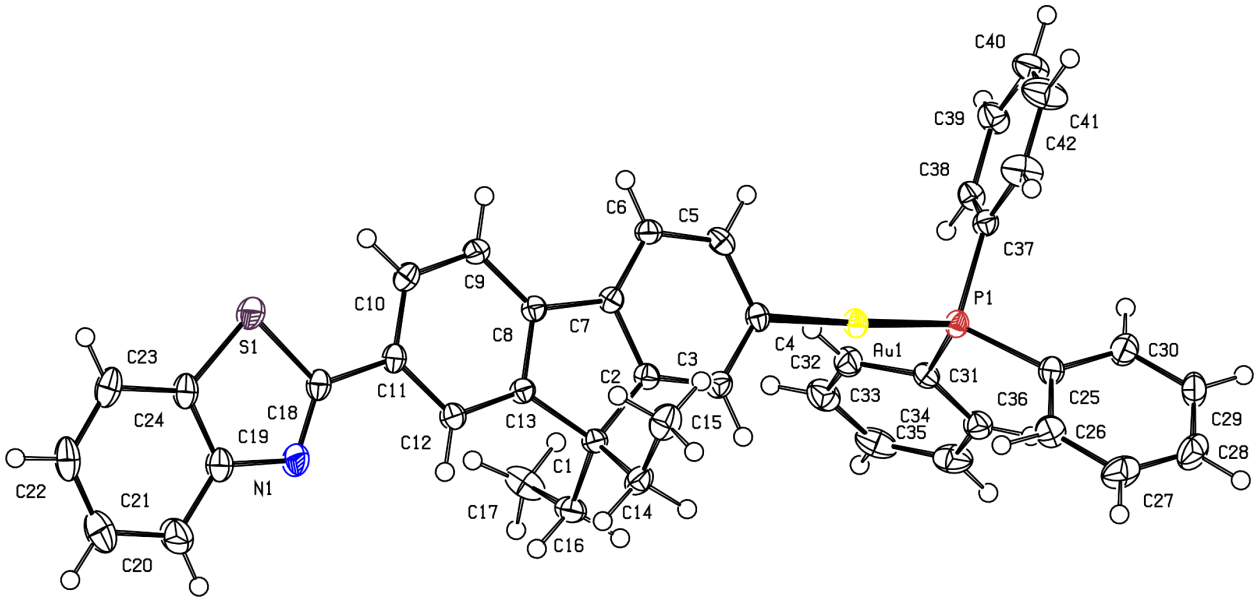


**Figure 2.13.** Crystal Structure of **AuBTF0** (50% probability level, 150 K).

**AuBTF1:**

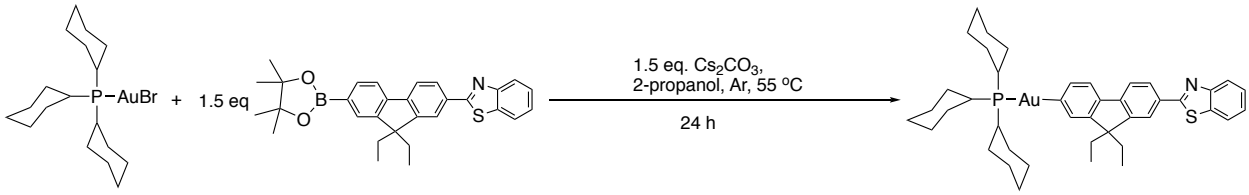


To a flame-dried 25 mL round bottom flask equipped with a stir bar was added 100 mg (0.180 mmol) of $Cy_3PAuBr$, 130 mg (0.270 mmol) of pinacolboronate ester, and 176 mg (0.540 mmol) of $Cs_2CO_3$. The flask was purged with argon for 15 min, after which 5 mL of dry 2-propanol was added via syringe. The vessel was then shielded from light and heated at 55 °C for 24 h. The contents of the flask were then cooled to room temperature yielding a bright yellow suspension that was concentrated *in vacuo*. The crude product was dissolved in 5 × 5 mL portions of benzene and filtered through Celite to yield a yellow solution which was concentrated under reduced pressure. This crude product was then subjected to vapor diffusion crystallization using dichloromethane as the solvent and pentanes as the anti-solvent. (111 mg, 76 %). $^1$H NMR (500 MHz, chloroform-*d*) δ 8.09 – 8.05 (m, 2H), 7.98 (dd, *J* = 7.8, 1.7 Hz, 1H), 7.90 (d, *J* = 7.9 Hz,

1H), 7.72 (d, $J$ = 7.9 Hz, 1H), 7.66 (d, $J$ = 7.3 Hz, 1H), 7.54 – 7.46 (m, 3H), 7.36 (t, $J$ = 7.5 Hz, 1H), 2.18 – 2.02 (m, 15H), 1.92 – 1.86 (m, 7H), 1.75 (d, $J$ = 9.0 Hz, 4H), 1.32 (h, $J$ = 12.7, 11.2 Hz, 11H), 0.38 (t, $J$ = 7.3 Hz, 6H). $^{31}$P NMR (121 MHz, $CDCl_3$) δ (ppm): 57.07. HRMS (FT-ICR, $[M+H]^+$) m/z calcd for $MH^+$ $C_{42}H_{54}NPSAu^+$ 832.33746, found 832.33739. Anal. Calcd for: $C_{42}H_{35}AuNPS$: C, (60.64); H, (6.42); N, (1.68). Found: C, (60.91); H, (6.56); N, (1.75).

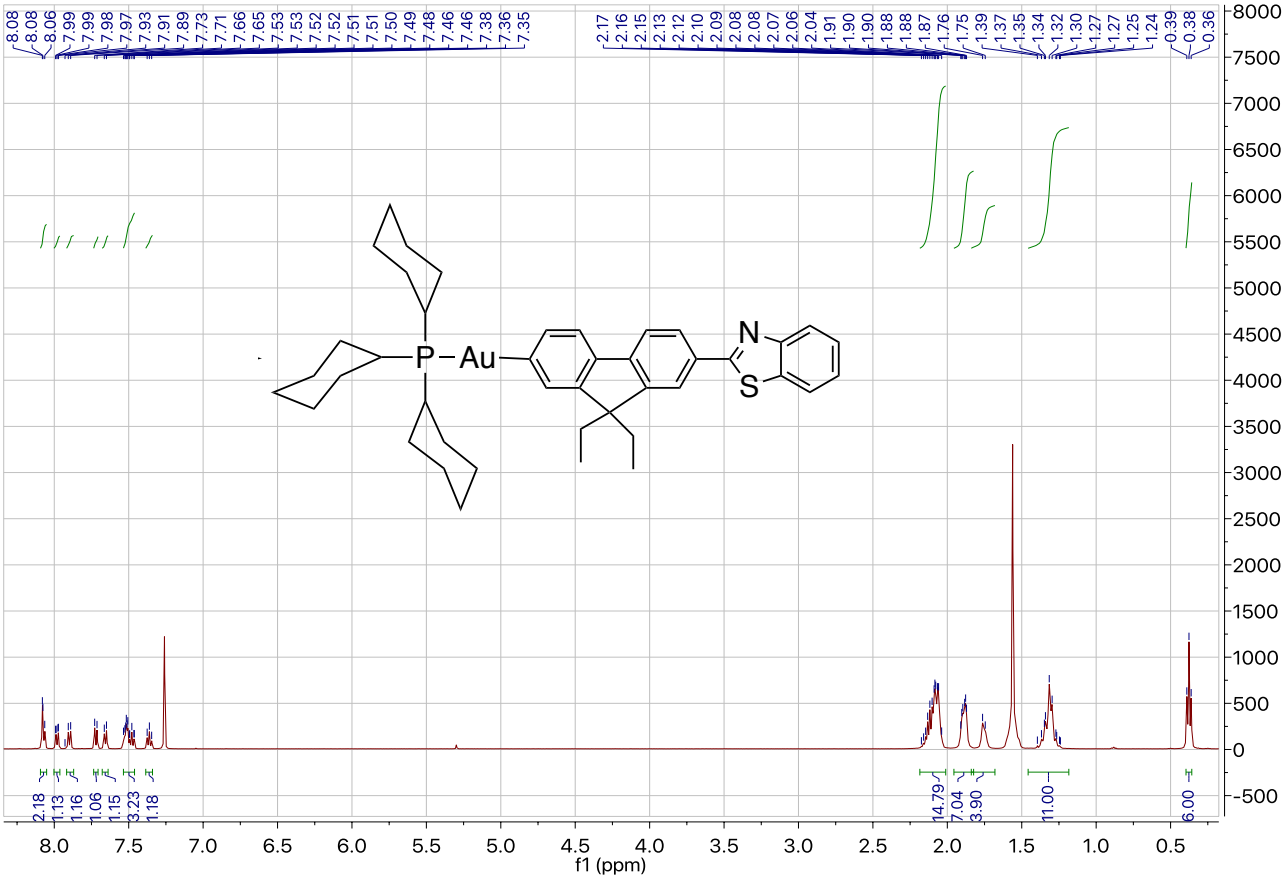


**Figure 2.14.** $^1$H NMR Spectrum of **AuBTF1**

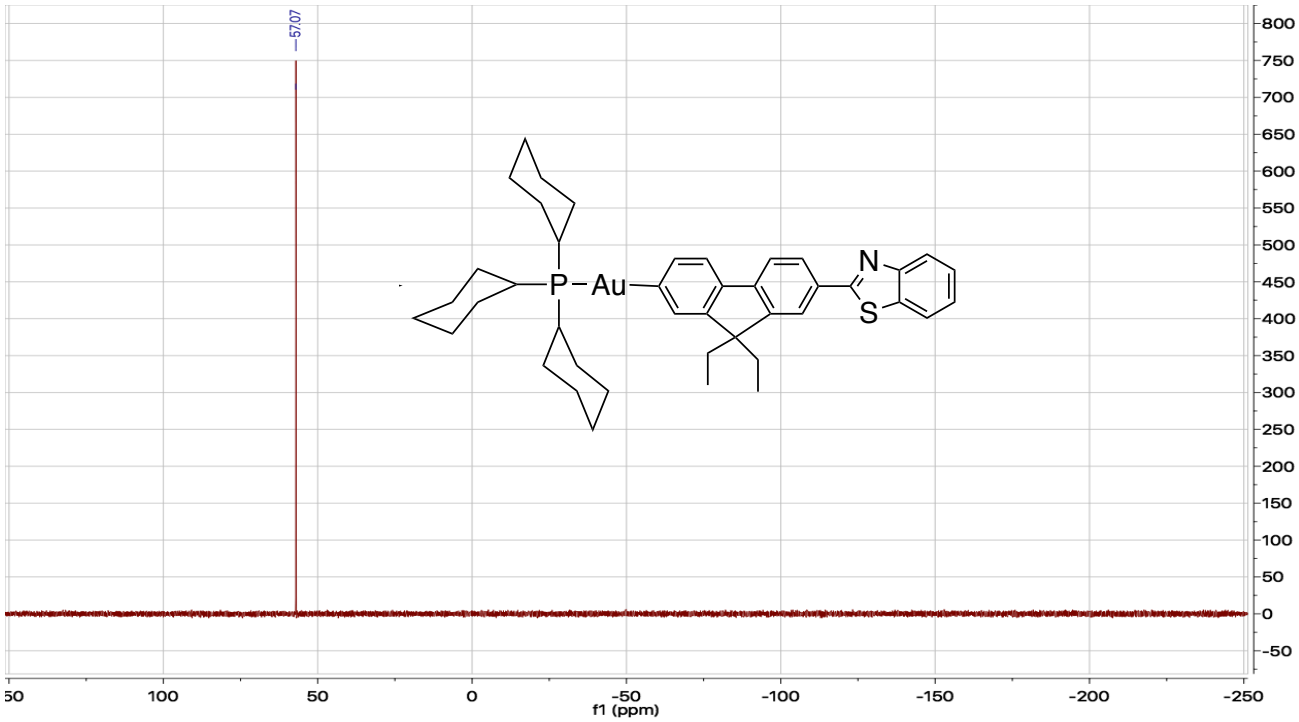


**Figure 2.15.** $^{31}P\{^{1}H\}$NMR Spectrum of **AuBTF1**

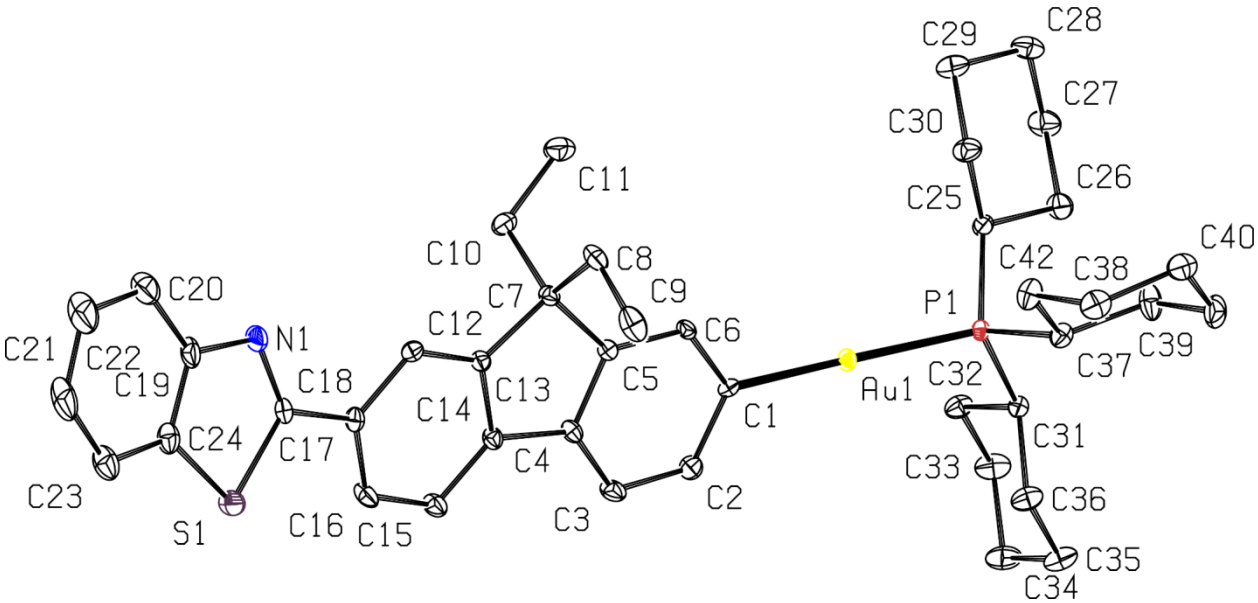


**Figure 2.16.** Crystal Structure of **AuBTF1** (50% probability level, 100 K). Hydrogen atoms are omitted for clarity.

**AuBTF2:**

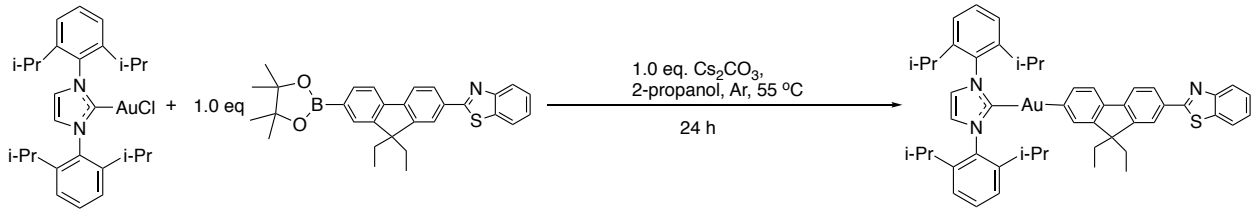


To a flame-dried 25 mL round bottom flask equipped with a stir bar was added 96 mg (0.155 mmol) of IPrAuCl, 74 mg (0.155 mmol) of pinacolboronate ester, and 101 mg (0.310 mmol) of $Cs_2CO_3$. The flask was then purged with argon for 15 min, after which 5 mL of dry 2-propanol was added via syringe. The vessel was then shielded from light and heated at 55 °C for 24 h. The contents of the flask were then allowed to cool to room temperature yielding a bright yellow suspension that was concentrated *in vacuo*. The crude product was dissolved in 5 × 5 mL portions of benzene and filtered through Celite to yield a yellow solution which was subsequently concentrated under reduced pressure. This crude product was then subjected to vapor diffusion crystallization using dichloromethane as the solvent and pentanes as the anti-solvent. (78 mg, 53 %) Yield.$^1$H NMR (500 MHz, chloroform-*d*) δ 8.04 (d, *J* = 8.2 Hz, 1H), 8.00 (d, *J* = 1.8 Hz, 1H), 7.95 – 7.80 (m, 2H), 7.60 (d, *J* = 7.9 Hz, 1H), 7.47 (dt, *J* = 16.1, 8.0 Hz, 3H), 7.40 (d, *J* = 7.4 Hz, 1H), 7.32 (dd, *J* = 21.2, 7.6 Hz, 5H), 7.16 (s, 2H), 7.09 (d, *J* = 7.3 Hz, 1H), 7.03 (s, 1H), 2.71 (hept, *J* = 7.1 Hz, 4H), 1.93 (qq, *J* = 14.1, 7.2 Hz, 4H), 1.42 (d, *J* = 6.8 Hz, 12H), 1.25 (d, *J* = 6.8 Hz, 12H), 0.33 (t, *J* = 7.3 Hz, 6H). HRMS (FT-ICR, $[M+H]^+$) m/z calcd for $MH^+$ $C_{51}H_{57}N_3SAu^+$ 940.39332, found 940.39341. Anal. Calcd for: $C_{51}H_{56}AuN_3S$: C, (65.16); H, (6.00); N, (4.47). Found: C, (65.11); H, (6.19); N, (4.44).

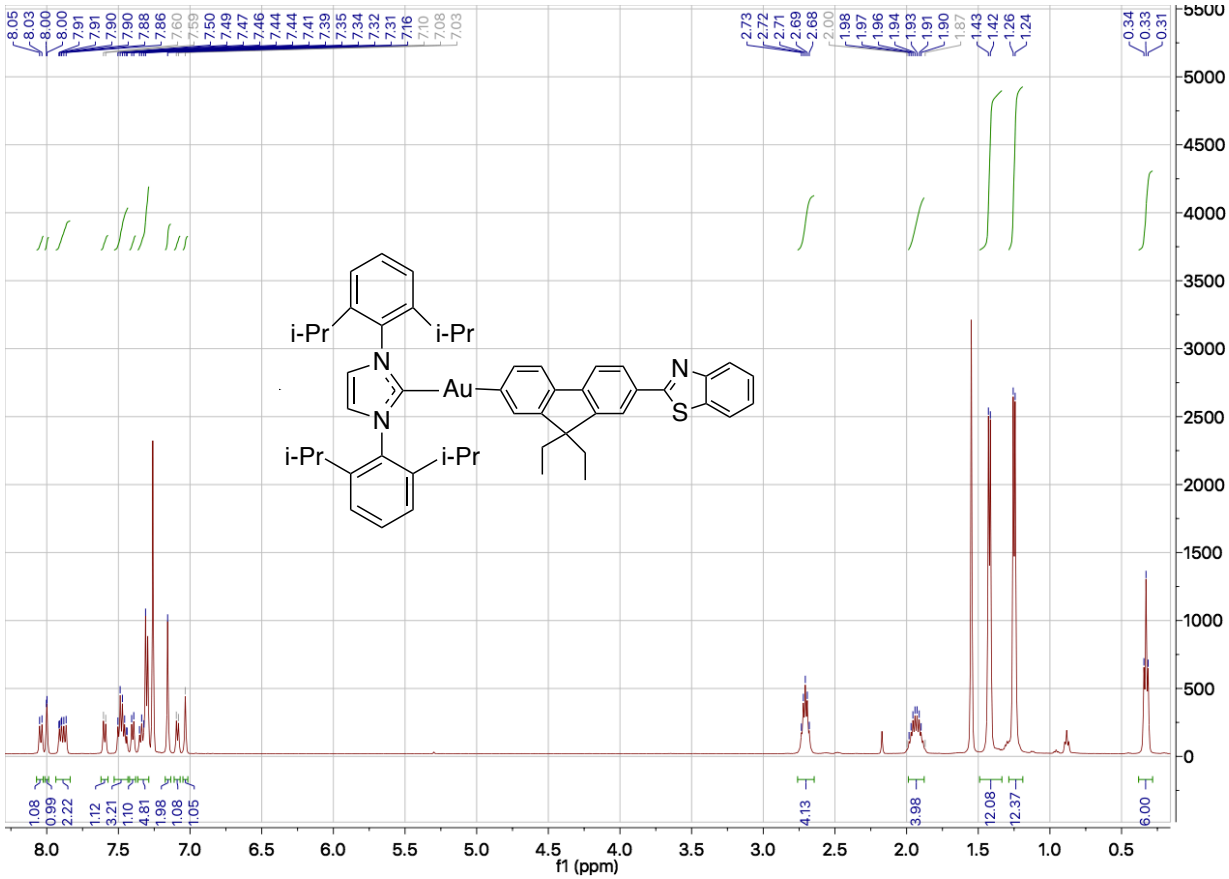


**Figure 2.17.**[1]H NMR Spectrum of **AuBTF2**

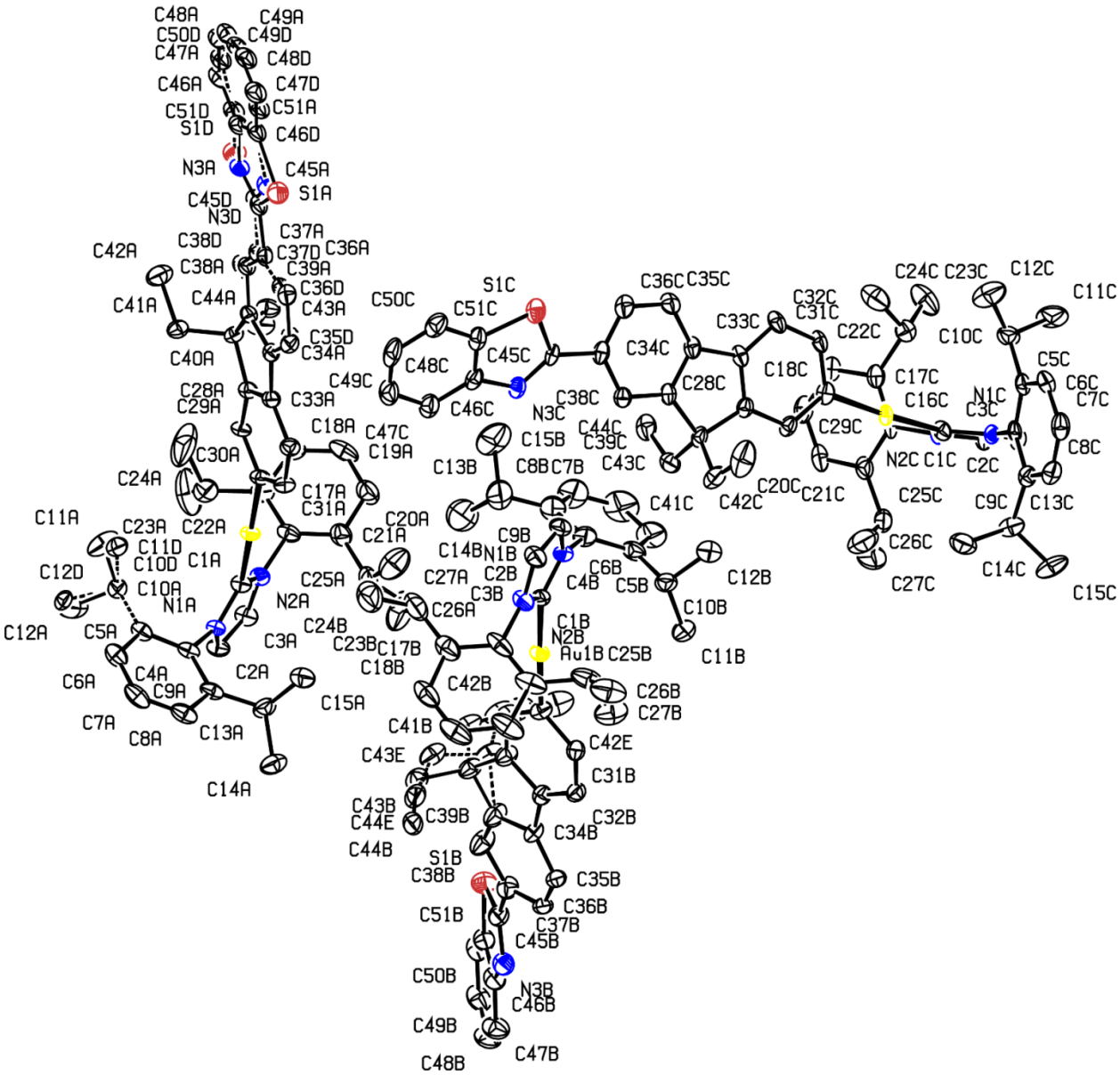


**Figure 2.18.** The three crystallographically independent molecules in the crystal structure of **AuBTF2** (50% probability level, 100 K). Hydrogen atoms are omitted for clarity.

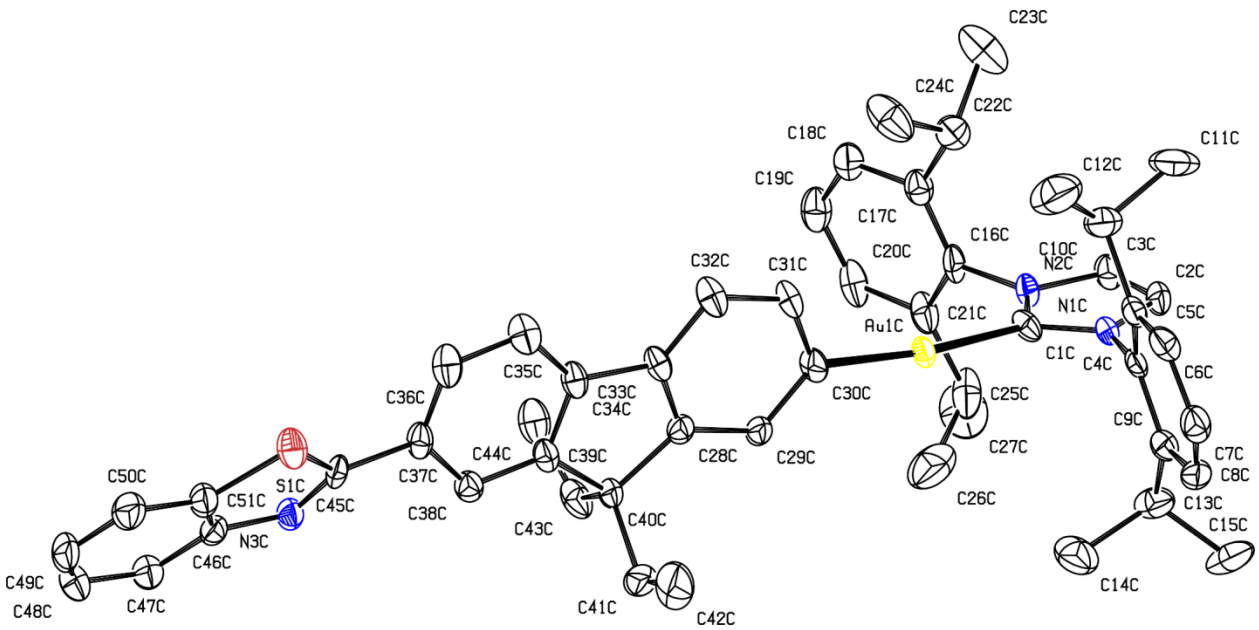


**Figure 2.19.** One of the three crystallographically independent molecules in the crystal structure of **AuBTF2** (50% probability level, 100 K). Hydrogen atoms are omitted for clarity.

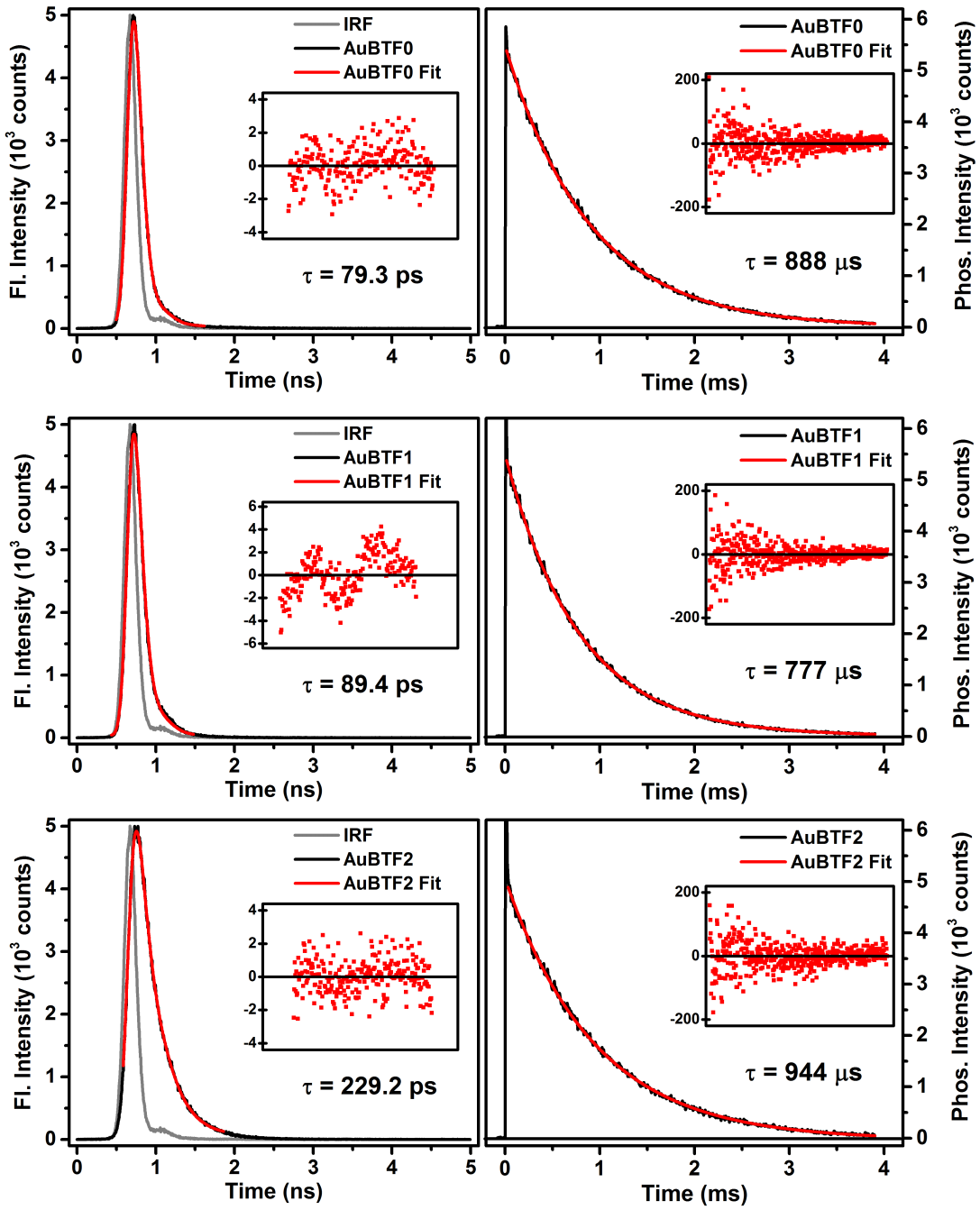


**Figure 2.20.** (Left) Fluorescence and (Right) phosphorescence lifetimes of (Top) **AuBTF0**, (Middle) **AuBTF1**, and (Bottom) **AuBTF2** collected in toluene solution. The residuals obtained from the fits are shown in the inset. These experiments were repeated a second time. The values given in Table 2.1 represent the average of the two trials.

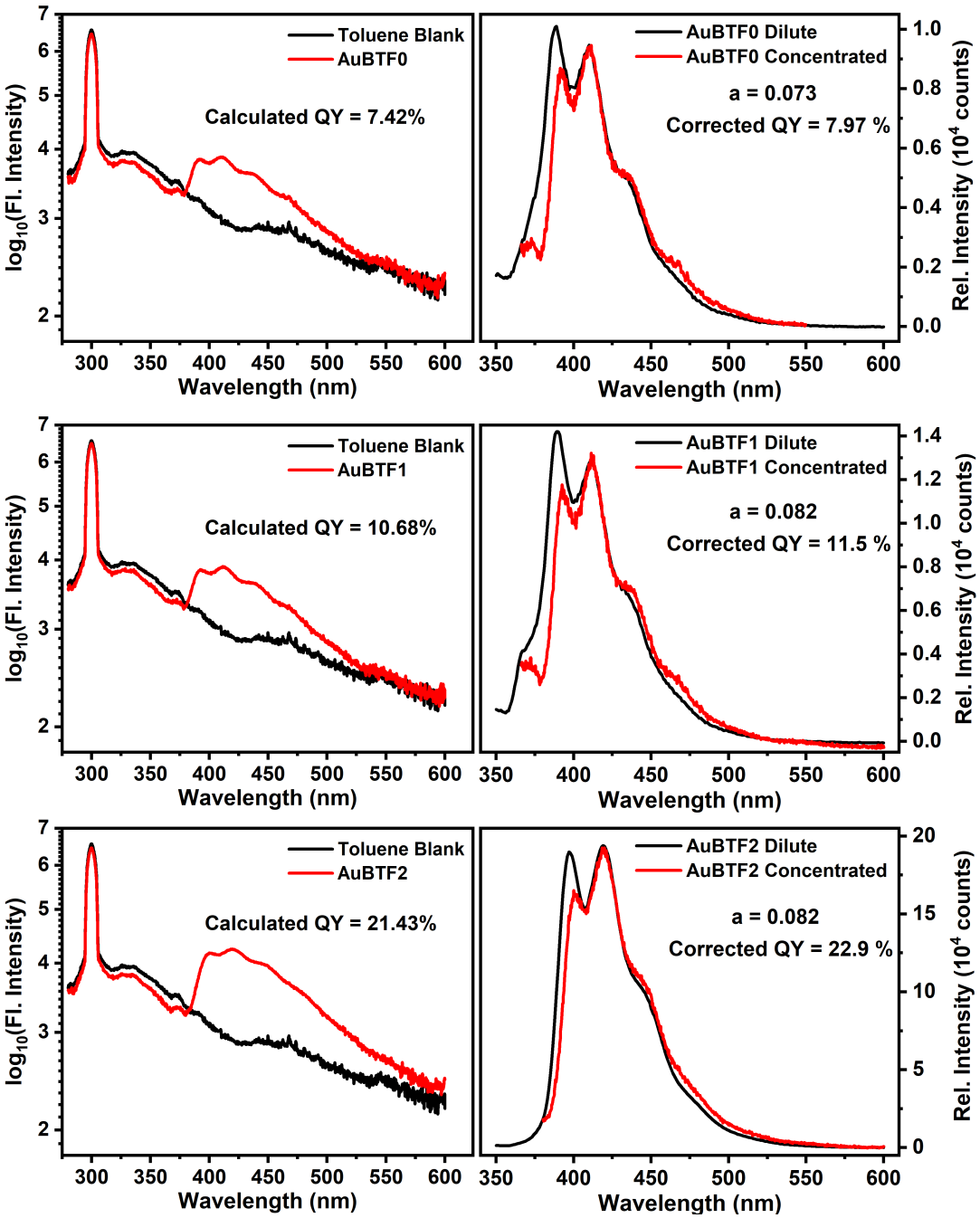


**Figure 2.21.** (Left) Raw and (Right) corrected fluorescence spectra in toluene solution of (Top) **AuBTF0**, (Middle) **AuBTF1**, and (Bottom) **AuBTF2** used to determine fluorescence quantum yield values. The experiments were repeated a second time. The values given in Table 2.1 represent the average of the two trials.

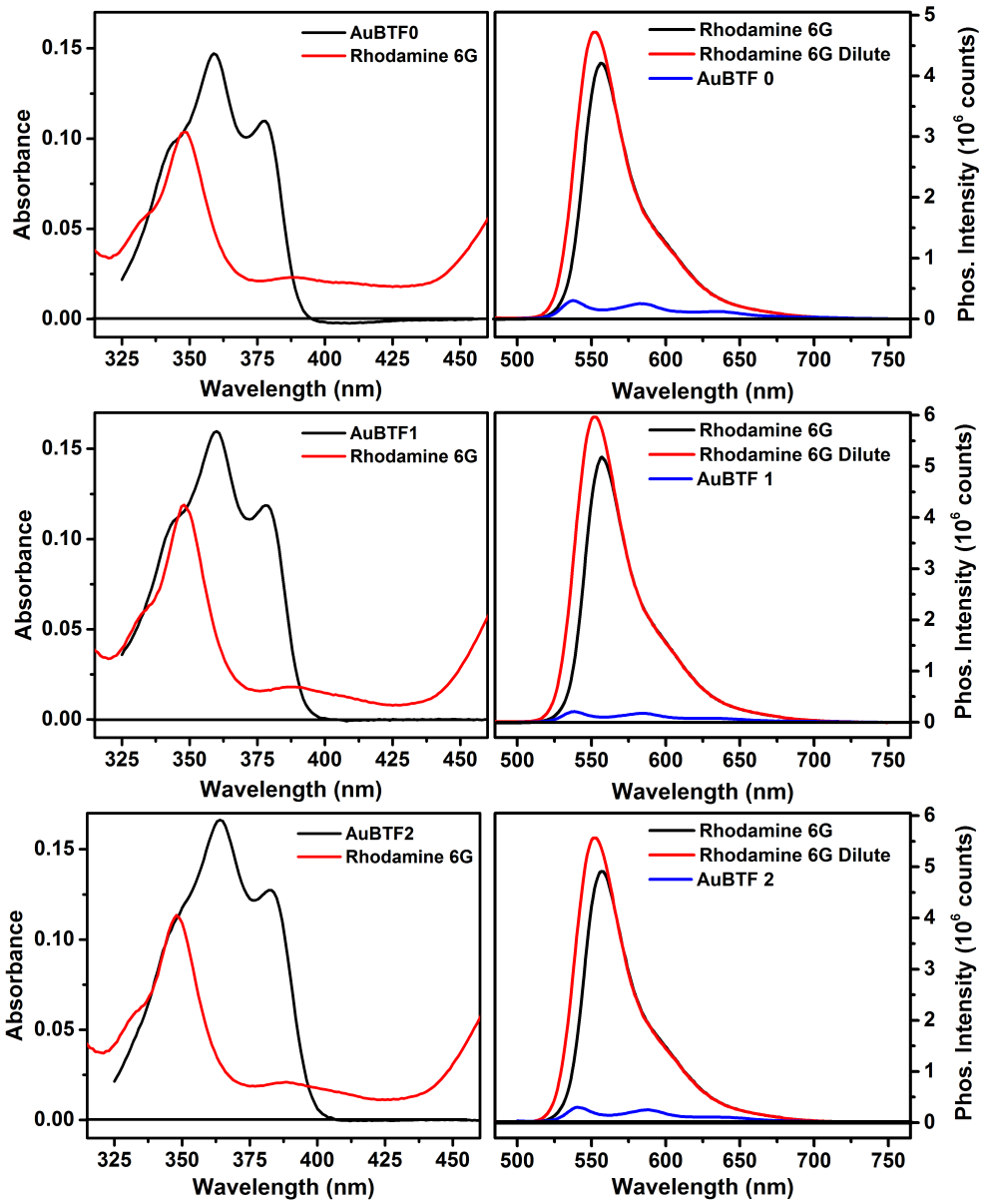


**Figure 2.22.** (Left) Absorption and (Right) luminescence spectra of the Rhodamine 6G reference along with (Top) **AuBTF0**, (Middle) **AuBTF1**, and (Bottom) **AuBTF2** used to determine phosphorescence quantum yield values. AuBTF spectra were collected in toluene and the Rhodamine 6G spectra were collected in absolute ethanol. The experiments were repeated in duplicated for **AuBTF0** and **AuBTF1** and in triplicate for **AuBTF2**. The values given in Table 2.1 represent the average of these trials.

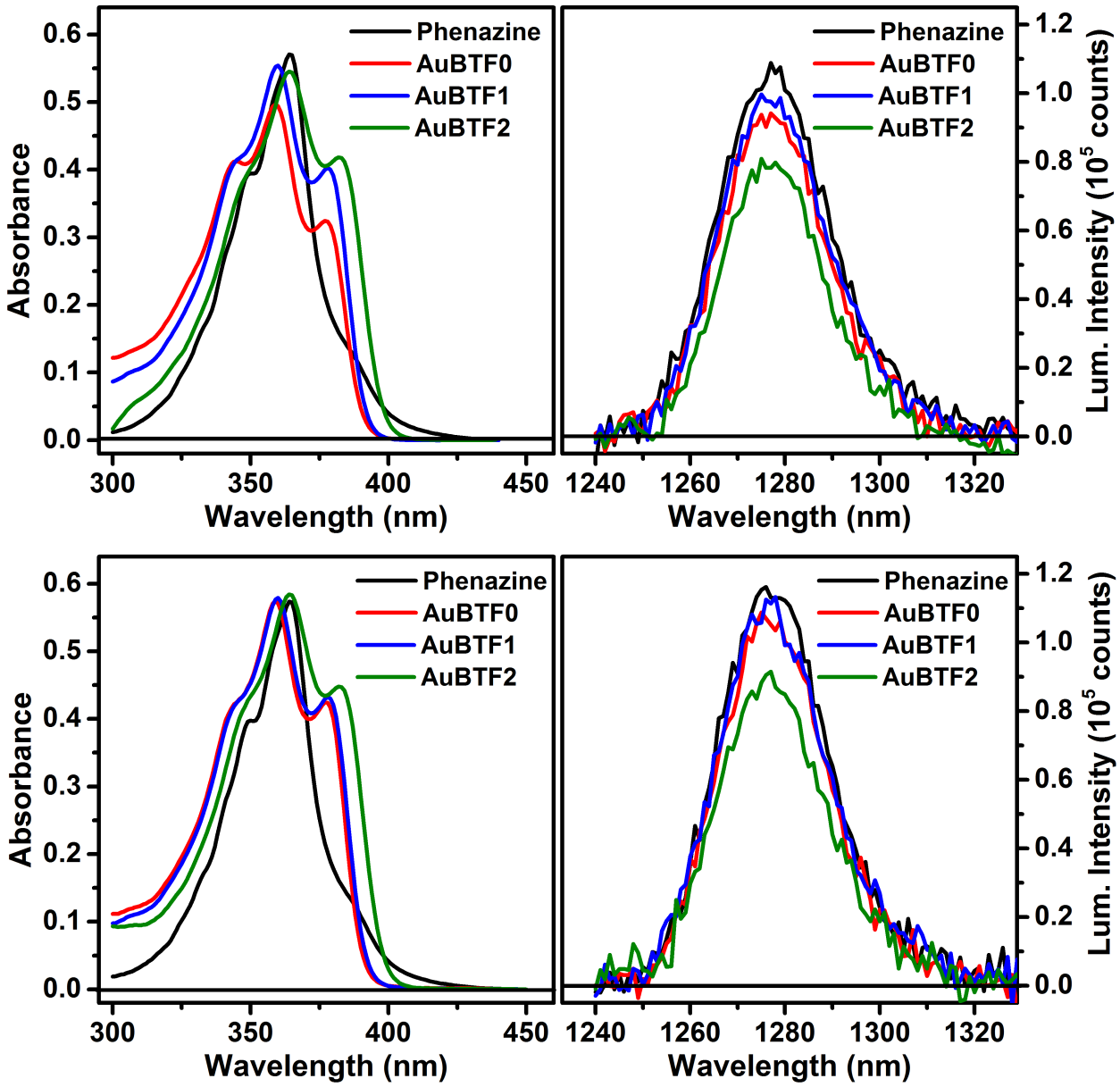


**Figure 2.23.** (Left) Absorption and (Right) singlet oxygen phosphorescence spectra collected from the phenazine reference and **AuBTF0**, **AuBTF1**, and **AuBTF2** used to determine photosensitized singlet oxygen phosphorescence quantum yield values. All spectra were collected in benzene. Both trials of this experiment are shown above. The value reported in Table 2.1 represents the average value obtained from these trials.

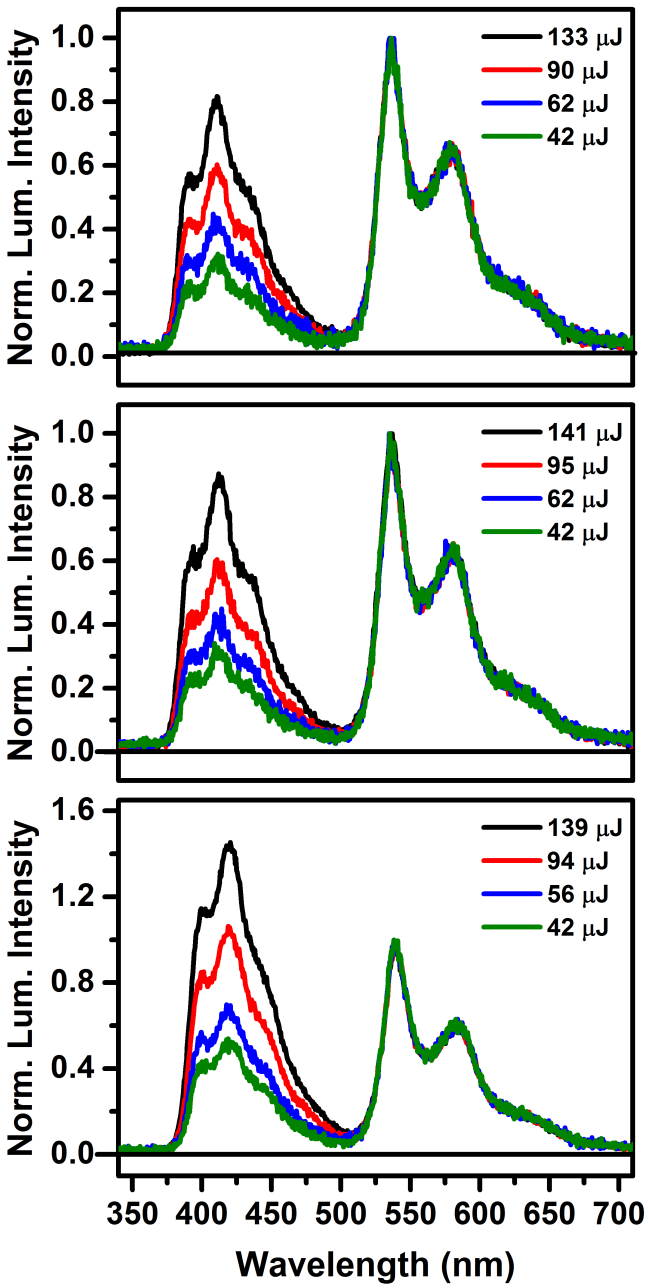


**Figure 2.24.** Delayed fluorescence observed in samples of (Top) **AuBTF0**, (Middle) **AuBTF1**, and (Bottom) **AuBTF2**. The data were collected in freeze-pump-thaw degassed toluene solution. The spectra were collected on the Andor iStar ICCD camera with a gate delay of 50 microseconds and a gate width of 90 microseconds. The signal is normalized to the phosphorescence maximum to demonstrate the influence of laser pulse energy on the magnitude of the delayed fluorescence signal.

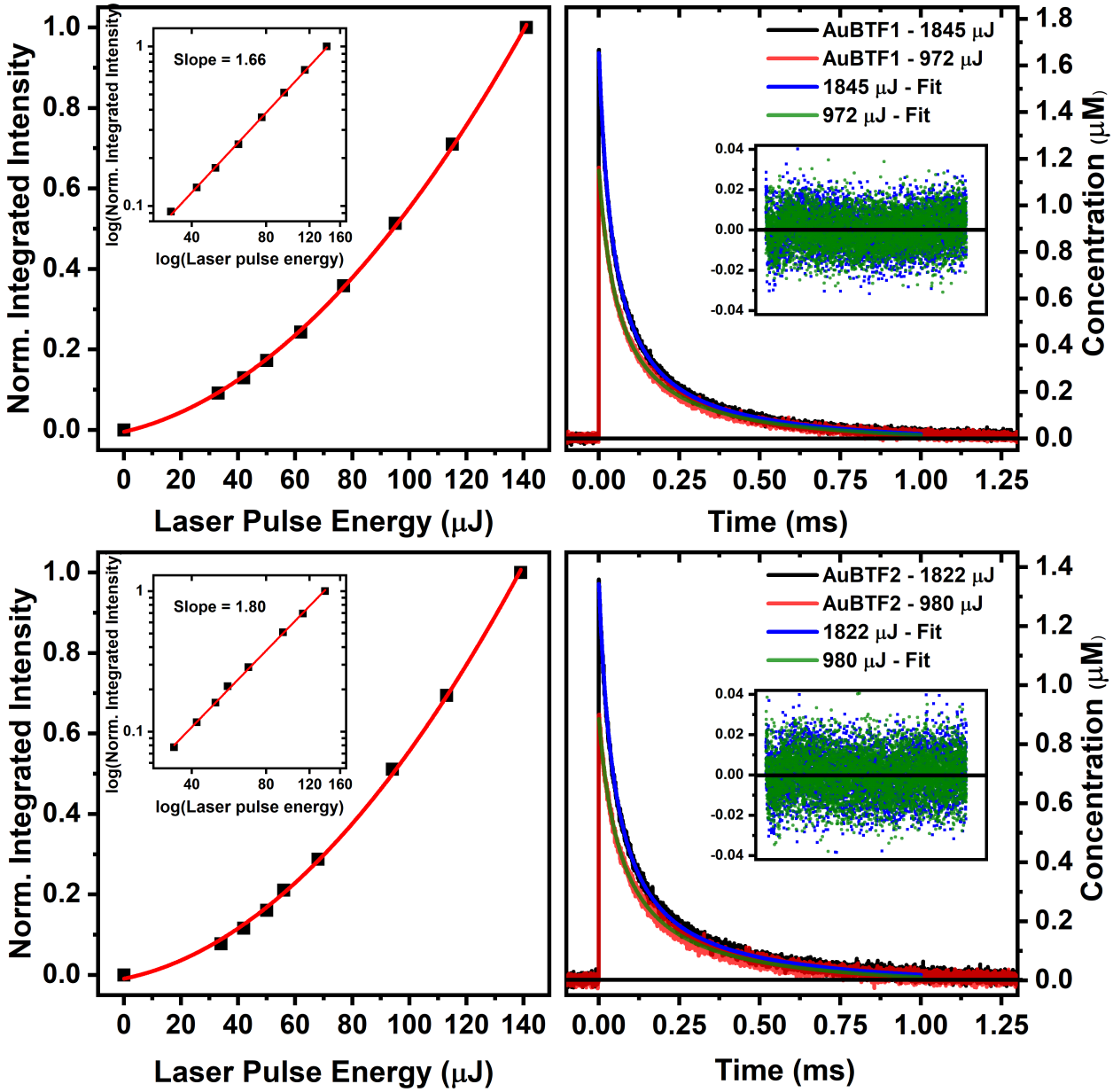


**Figure 2.25.** (Left) Fits of the normalized, integrated fluorescence intensity vs. laser pulse energy and (Right) triplet-triplet annihilation fitting of excited-state decay traces in freeze-pump-thaw deaerated toluene solution of (Top) **AuBTF1** and (Bottom) **AuBTF2**. The insets represent the double logarithm plot (Left) and residuals of the data fit (Right).

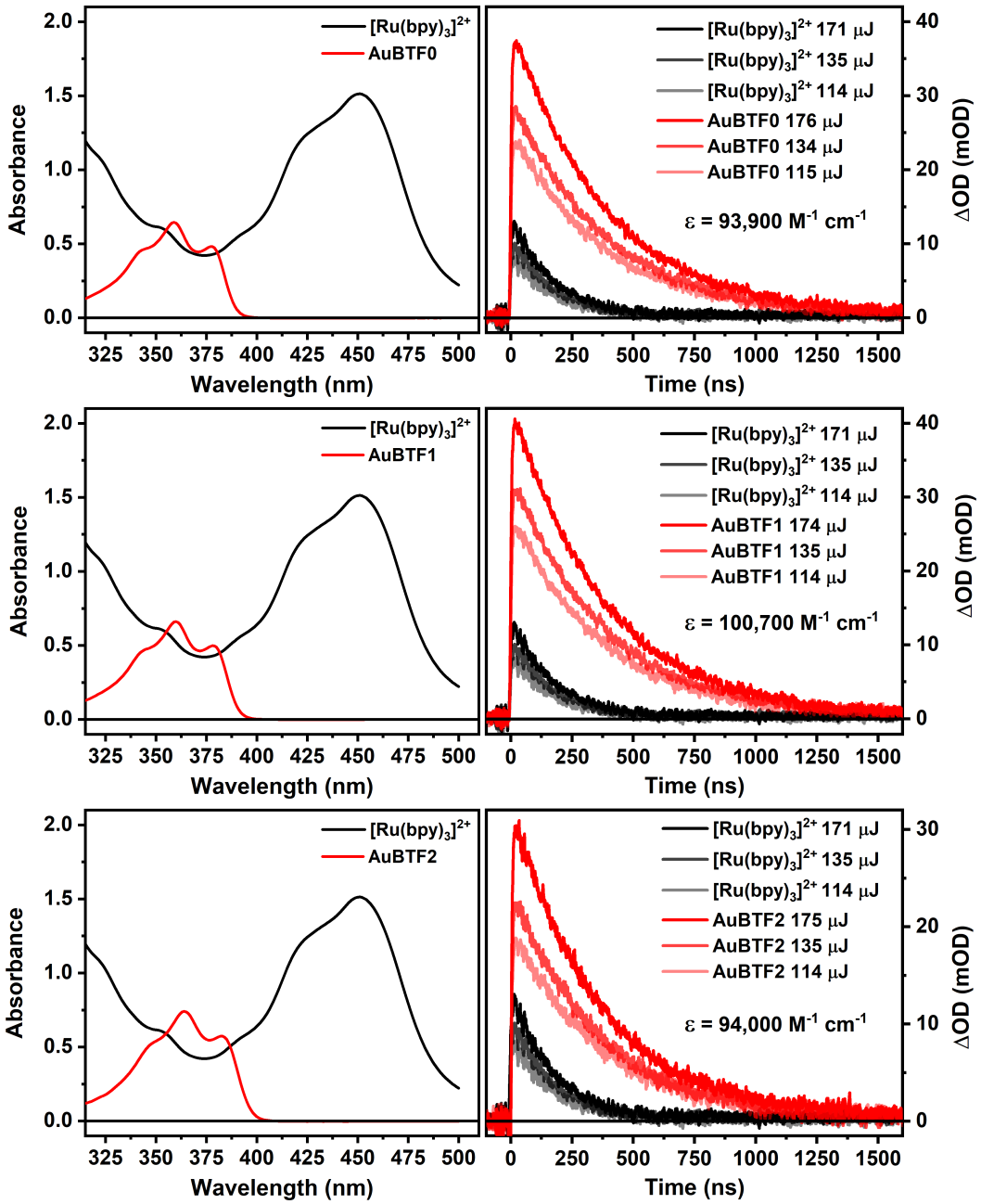


**Figure 2.26.** (Right) Absorbance and (Left) excited-state absorption decay traces at three laser excitation energies in samples of (Top) **AuBTF0** (547 nm), (Middle) **AuBTF1** (550 nm), and (Bottom) **AuBTF2** (562 nm) along with $[Ru(bpy)_3]^{2+}$ (370 nm). The AuBTF data was collected in aerated toluene solution and the $[Ru(bpy)_3]^{2+}$ was collected in aerated acetonitrile solution. All samples were excited at 355 nm.

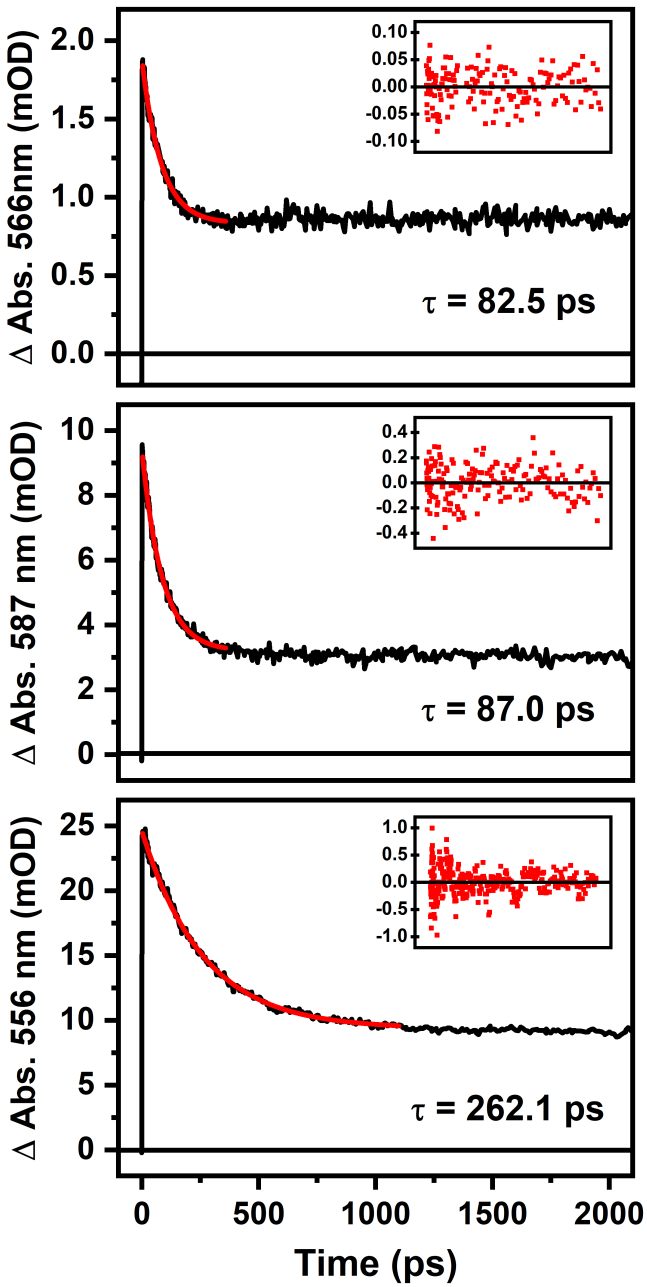


**Figure 2.27.** Ultrafast transient absorption decay trace collected at a single wavelength for (Top) **AuBTF0**, (Middle) **AuBTF1**, and (Bottom) **AuBTF2** in aerated toluene solution. The residual values obtained from monoexponential decay fits of the data are shown in the inset. The lifetime value represented in Table 2.1 is the average of the lifetime value obtained at 10 unique wavelengths in transient absorption spectrum.

**Calculations.**

Spin-restricted and time-dependent density-functional theory computations proceeded in Gaussian16 rev. A.03.[4] Geometries were optimized with the 6-31G(d) basis set for nonmetal atoms and the Stuttgard-Dresden effective core potential and basis set for Au.[5] Optimizations proceeded without constraints, and harmonic frequency calculations found all real vibrational frequencies, confirming that converged structures are local energy minima. Final single-point calculations employed the exchange and correlation functionals of Perdew, Burke, and Ernzerhof (PBE0),[6] and the TZVP basis set of Godbelt, Andzelm, and co-workers for nonmetals.[7] For metal atoms, the Stuttgart-Dresden effective core potential and basis set were used; scalar relativistic effects are included implicitly. Continuum solvation in toluene was imposed using the integral equation formalism of the polarizable continuum model.[8-11] Population analyses were performed with the AOMix-CDA program of Gorelsky.[12,13]

**Table 2.2. AuBTF1:** Summary of calculated electronic transitions to Franck-Condon singlet states. MO 181: HOMO; MO 182: LUMO.

| # | nm | 1000 $cm^{-1}$ | eV | *f* | Assignment |
|---|---|---|---|---|---|
| 1 | 372.9 | 26.82 | 3.325 | 1.6354 | 181→182(98.3%) (HOMO→LUMO) |
| 2 | 303.6 | 32.94 | 4.084 | 0.0030 | 180→182(94.2%) |
| 3 | 292.5 | 34.19 | 4.239 | 0.0149 | 178→182(45.3%) 181→183(18.2%) |
| | | | | | 177→182(11.5%) |
| 4 | 291.8 | 34.26 | 4.248 | 0.0123 | 179→182(82.2%) |
| 5 | 285.2 | 35.07 | 4.348 | 0.0421 | 181→183(24.5%) 176→182(23.4%) |
| | | | | | 177→182(16.6%) 178→182(13.1%) |
| 6 | 279.0 | 35.84 | 4.443 | 0.0931 | 177→182(63.0%) 178→182(29.7%) |
| 7 | 264.4 | 37.83 | 4.690 | 0.1960 | 181→183(41.5%) 181→184(20.5%) |
| | | | | | 181→185(15.7%) 176→182(12.1%) |
| 8 | 259.7 | 38.50 | 4.774 | 0.0210 | 181→184(49.2%) 176→182(31.3%) |
| 9 | 257.0 | 38.91 | 4.825 | 0.0021 | 181→186(64.4%) 181→185(30.0%) |
| 10 | 253.7 | 39.41 | 4.886 | 0.0008 | 173→182(92.5%) |
| 11 | 253.6 | 39.43 | 4.889 | 0.0258 | 181→185(36.1%) 181→186(20.0%) |
| | | | | | 181→184(13.4%) 176→182(12.5%) |
| 12 | 245.0 | 40.81 | 5.060 | 0.0064 | 175→182(94.7%) |
| 13 | 241.9 | 41.35 | 5.126 | 0.0184 | 180→183(53.0%) 180→185(18.5%) |

| | | | | | |
|---|---|---|---|---|---|
| 14 | 240.6 | 41.56 | 5.153 | 0.0024 | 181→187(60.1%) 180→183(11.8%) |
| 15 | 240.6 | 41.57 | 5.154 | 0.0102 | 180→186(35.1%) 181→187(27.7%) 180→185(12.2%) |
| 16 | 238.2 | 41.97 | 5.204 | 0.0060 | 180→185(31.1%) 180→189(19.8%) 180→184(19.5%) 180→186(16.4%) |
| 17 | 237.2 | 42.16 | 5.227 | 0.0560 | 181→189(37.5%) 179→183(17.0%) 180→186(16.4%) |
| 18 | 235.5 | 42.46 | 5.264 | 0.0258 | 181→188(80.2%) |
| 19 | 233.5 | 42.83 | 5.311 | 0.0001 | 181→190(88.2%) 177→190(10.3%) |
| 20 | 227.7 | 43.93 | 5.446 | 0.1100 | 174→182(32.8%) 178→184(15.7%) |
| 21 | 224.7 | 44.51 | 5.518 | 0.0164 | 179→183(54.9%) |
| 22 | 222.9 | 44.86 | 5.562 | 0.0482 | 178→183(32.9%) 174→182(32.3%) 177→184(15.0%) |
| 23 | 221.6 | 45.13 | 5.595 | 0.0022 | 177→183(24.4%) 178→183(12.7%) 178→184(10.9%) 180→187(10.6%) |
| 24 | 218.7 | 45.73 | 5.670 | 0.0816 | 180→187(67.7%) 177→183(13.0%) |
| 25 | 217.6 | 45.95 | 5.697 | 0.0038 | 179→186(51.1%) 179→185(36.7%) |
| 26 | 217.1 | 46.06 | 5.710 | 0.0477 | 178→184(27.1%) 177→183(22.9%) |
| 27 | 216.3 | 46.23 | 5.731 | 0.0001 | 172→182(61.8%) 168→182(27.8%) |
| 28 | 215.3 | 46.44 | 5.758 | 0.0329 | 180→188(50.6%) 180→189(16.8%) |
| 29 | 214.7 | 46.57 | 5.774 | 0.4645 | 177→184(41.9%) 178→183(23.4%) |
| 30 | 214.3 | 46.65 | 5.785 | 0.1260 | 179→184(17.0%) 177→183(16.0%) 181→189(13.9%) 179→186(11.2%) |
| 31 | 214.2 | 46.68 | 5.787 | 0.0014 | 180→184(62.1%) 180→189(18.4%) |
| 32 | 213.2 | 46.90 | 5.814 | 0.0365 | 170→182(55.4%) 171→182(16.0%) |
| 33 | 212.6 | 47.04 | 5.833 | 0.0010 | 178→190(73.4%) 177→190(16.9%) |
| 34 | 212.5 | 47.05 | 5.834 | 0.0093 | 169→182(72.6%) |
| 35 | 211.5 | 47.28 | 5.862 | 0.0073 | 181→191(49.8%) 178→184(11.9%) |
| 36 | 208.7 | 47.92 | 5.941 | 0.1667 | 176→183(35.8%) 178→185(21.9%) |
| 37 | 208.0 | 48.08 | 5.961 | 0.0051 | 180→189(34.6%) 180→185(20.8%) 180→188(12.3%) |
| 38 | 207.6 | 48.16 | 5.971 | 0.0018 | 181→192(68.3%) |
| 39 | 207.3 | 48.23 | 5.980 | 0.0384 | 175→186(32.1%) 175→185(27.2%) |
| 40 | 207.0 | 48.31 | 5.989 | 0.0004 | 167→182(36.9%) 168→182(20.6%) 164→182(15.9%) |

**Table 2.3. AuBTF1:** Summary of calculated electronic transitions to Franck-Condon triplet states. MO 181: HOMO; MO 182: LUMO.

| # | nm | 1000 $cm^{-1}$ | eV | Assignment |
|---|---|---|---|---|
| 1 | 526.5 | 18.99 | 2.355 | 181→182(81.6%) (HOMO→LUMO) |
| 2 | 394.6 | 25.34 | 3.142 | 178→182(35.4%) 181→183(15.0%) 177→182(13.1%) |
| 3 | 346.2 | 28.88 | 3.581 | 177→182(28.3%) 178→182(19.9%) |
| 4 | 327.0 | 30.59 | 3.792 | 176→182(16.6%) 179→182(14.5%) 178→182(13.5%) |

| | | | | |
|---|---|---|---|---|
| 5 | 322.1 | 31.04 | 3.849 | 179→182(40.5%) 181→183(12.4%) 176→182(10.9%) |
| 6 | 318.3 | 31.42 | 3.895 | 180→182(81.7%) |
| 7 | 317.6 | 31.48 | 3.903 | No transition contributes more than 10%. |
| 8 | 316.0 | 31.65 | 3.924 | 176→182(32.0%) 177→182(16.4%) 179→182(12.5%) |
| 9 | 304.2 | 32.87 | 4.076 | 178→184(13.7%) 177→184(12.5%) 176→183(10.6%) |
| 10 | 298.5 | 33.50 | 4.153 | 176→182(29.3%) 181→183(20.0%) 177→182(16.0%) |
| 11 | 287.1 | 34.84 | 4.319 | 181→184(32.9%) 178→184(18.9%) 181→185(11.7%) |
| 12 | 280.3 | 35.68 | 4.424 | 181→189(20.6%) 174→182(12.0%) 179→189(10.9%) |
| 13 | 278.8 | 35.86 | 4.446 | 173→182(86.2%) |
| 14 | 276.7 | 36.14 | 4.480 | 181→189(31.4%) 179→189(12.2%) |
| 15 | 268.4 | 37.26 | 4.620 | 181→189(20.0%) |
| 16 | 264.2 | 37.84 | 4.692 | 180→186(49.4%) 180→185(30.7%) |
| 17 | 259.9 | 38.48 | 4.771 | 180→183(22.1%) 180→186(13.1%) 180→188(10.9%) 175→182(10.5%) 180→184(10.2%) 180→182(10.1%) |
| 18 | 257.9 | 38.77 | 4.807 | 181→186(62.9%) 181→185(30.2%) |

**Optimized Cartesian Coordinates (Å)**
**Au-BTF0**

81

| | | | |
|---|---|---|---|
| P | 3.418635 | -1.374176 | -0.099802 |
| C | 1.891369 | -1.474997 | -1.097266 |
| C | 1.119911 | -0.314175 | -1.237322 |
| C | 1.469241 | -2.660170 | -1.708202 |
| C | -0.064531 | -0.344323 | -1.966271 |
| H | 1.453252 | 0.614357 | -0.778955 |
| C | 0.285587 | -2.683767 | -2.442559 |
| H | 2.067195 | -3.562817 | -1.617071 |
| C | -0.482364 | -1.528981 | -2.570257 |
| H | -0.656348 | 0.560684 | -2.070845 |
| H | -0.034101 | -3.606997 | -2.917909 |
| H | -1.403362 | -1.549778 | -3.146314 |
| C | 4.400529 | -2.840762 | -0.570972 |
| C | 4.276189 | -4.069751 | 0.085810 |
| C | 5.297816 | -2.717434 | -1.639415 |
| C | 5.033548 | -5.162609 | -0.328966 |
| H | 3.594389 | -4.171994 | 0.925731 |
| C | 6.047954 | -3.813687 | -2.053749 |

| | | | |
|---|---|---|---|
| H | 5.412482 | -1.758359 | -2.139741 |
| C | 5.916824 | -5.036734 | -1.398777 |
| H | 4.934960 | -6.112985 | 0.188323 |
| H | 6.742789 | -3.708856 | -2.882239 |
| H | 6.508909 | -5.890147 | -1.717641 |
| C | 2.884977 | -1.682713 | 1.619783 |
| C | 1.698368 | -2.357911 | 1.925711 |
| C | 3.709455 | -1.231786 | 2.658083 |
| C | 1.348456 | -2.587231 | 3.254171 |
| H | 1.043705 | -2.697297 | 1.127447 |
| C | 3.358260 | -1.467984 | 3.983604 |
| H | 4.621605 | -0.687012 | 2.424762 |
| C | 2.177778 | -2.145509 | 4.282635 |
| H | 0.423654 | -3.108833 | 3.484814 |
| H | 4.002159 | -1.112623 | 4.783149 |
| H | 1.900148 | -2.322262 | 5.318115 |
| Au | 4.578690 | 0.645452 | -0.380384 |
| C | 5.595077 | 2.400597 | -0.629550 |
| C | 6.962056 | 2.509552 | -0.292718 |
| C | 4.963782 | 3.550849 | -1.147370 |
| C | 7.680578 | 3.692194 | -0.455297 |
| H | 7.481920 | 1.642236 | 0.108926 |
| C | 5.666991 | 4.736440 | -1.315527 |
| H | 3.910347 | 3.511247 | -1.420984 |
| C | 7.026420 | 4.810217 | -0.969796 |
| H | 8.733571 | 3.736328 | -0.183941 |
| C | 5.168390 | 6.067955 | -1.854300 |
| C | 7.501330 | 6.161742 | -1.249475 |
| C | 6.428221 | 6.913206 | -1.768066 |
| C | 8.755701 | 6.748421 | -1.086184 |
| C | 6.603157 | 8.237006 | -2.120755 |
| C | 8.929220 | 8.080477 | -1.441485 |
| H | 9.591389 | 6.179550 | -0.687361 |
| C | 7.866388 | 8.836737 | -1.958702 |
| H | 5.791064 | 8.836448 | -2.522736 |
| H | 9.908244 | 8.536481 | -1.313567 |
| C | 4.030000 | 6.650407 | -0.985997 |
| H | 3.160291 | 5.986457 | -1.086003 |
| H | 3.731165 | 7.614196 | -1.421175 |
| C | 4.661791 | 5.945907 | -3.309582 |
| H | 3.761031 | 5.316856 | -3.298288 |
| H | 4.335648 | 6.942119 | -3.639344 |
| C | 5.665671 | 5.379912 | -4.305491 |
| H | 5.223882 | 5.327705 | -5.306663 |
| H | 6.562496 | 6.005775 | -4.367871 |
| H | 5.978883 | 4.369097 | -4.022769 |

| | | | |
|---|---|---|---|
| C | 4.362596 | 6.835559 | 0.488823 |
| H | 5.203698 | 7.523901 | 0.625158 |
| H | 3.501990 | 7.248407 | 1.026567 |
| H | 4.627612 | 5.882468 | 0.959080 |
| C | 8.031000 | 10.238348 | -2.337447 |
| N | 7.077384 | 10.974368 | -2.822407 |
| S | 9.590659 | 11.062301 | -2.157361 |
| C | 7.509118 | 12.251789 | -3.090120 |
| C | 8.867196 | 12.507634 | -2.793801 |
| C | 6.716023 | 13.278291 | -3.619034 |
| C | 9.440406 | 13.758697 | -3.014548 |
| C | 7.285330 | 14.522766 | -3.838982 |
| H | 5.672941 | 13.080652 | -3.846306 |
| C | 8.635061 | 14.761770 | -3.539774 |
| H | 10.484609 | 13.946734 | -2.784000 |
| H | 6.679103 | 15.325643 | -4.248848 |
| H | 9.059495 | 15.745274 | -3.720545 |

**Au-BTF1**

99

| | | | |
|---|---|---|---|
| P | 3.200936 | -1.676677 | -0.142914 |
| C | 1.491800 | -1.737413 | -0.891077 |
| C | 0.600967 | -2.927745 | -0.508780 |
| C | 0.731906 | -0.417504 | -0.679560 |
| H | 1.713331 | -1.812345 | -1.969363 |
| C | -0.702256 | -2.912835 | -1.311164 |
| H | 0.356286 | -2.865773 | 0.560224 |
| H | 1.121911 | -3.879025 | -0.659233 |
| C | -0.578122 | -0.404551 | -1.467714 |
| H | 0.516583 | -0.286135 | 0.390299 |
| H | 1.362141 | 0.429997 | -0.974422 |
| C | -1.459845 | -1.601530 | -1.120816 |
| H | -1.326858 | -3.764367 | -1.013843 |
| H | -0.471011 | -3.050410 | -2.377881 |
| H | -1.112661 | 0.534238 | -1.278008 |
| H | -0.348511 | -0.422689 | -2.543551 |
| H | -2.370544 | -1.595059 | -1.732172 |
| H | -1.784129 | -1.521214 | -0.072769 |
| C | 4.267456 | -2.750960 | -1.231034 |
| C | 5.659833 | -2.930045 | -0.608070 |
| C | 3.698018 | -4.087946 | -1.722342 |
| H | 4.393781 | -2.108403 | -2.117712 |
| C | 6.616029 | -3.614740 | -1.584951 |
| H | 5.581461 | -3.541956 | 0.301955 |
| H | 6.062342 | -1.954896 | -0.303790 |
| C | 4.670121 | -4.761770 | -2.694557 |
| H | 3.514321 | -4.759859 | -0.874158 |
| H | 2.734046 | -3.934803 | -2.221293 |
| C | 6.052987 | -4.946623 | -2.074842 |
| H | 7.591087 | -3.762128 | -1.104770 |
| H | 6.786204 | -2.951578 | -2.445471 |
| H | 4.259452 | -5.727379 | -3.014636 |
| H | 4.758660 | -4.142778 | -3.599476 |
| H | 6.735796 | -5.405553 | -2.800259 |
| H | 5.980290 | -5.644003 | -1.226986 |
| C | 3.235239 | -2.341265 | 1.597310 |
| C | 2.351425 | -1.478573 | 2.513335 |
| C | 2.982086 | -3.835666 | 1.836502 |
| H | 4.280204 | -2.136699 | 1.882620 |
| C | 2.558875 | -1.846049 | 3.982507 |
| H | 1.294329 | -1.629399 | 2.252817 |
| H | 2.569831 | -0.414901 | 2.353768 |

| | | | |
|---|---|---|---|
| C | 3.192373 | -4.187180 | 3.311852 |
| H | 1.957398 | -4.096807 | 1.547268 |
| H | 3.651146 | -4.444200 | 1.219020 |
| C | 2.317691 | -3.333691 | 4.226551 |
| H | 1.895282 | -1.240100 | 4.611477 |
| H | 3.588136 | -1.590585 | 4.274081 |
| H | 2.986050 | -5.253311 | 3.467968 |
| H | 4.249745 | -4.030977 | 3.571892 |
| H | 2.508893 | -3.583815 | 5.277275 |
| H | 1.259298 | -3.565611 | 4.035839 |
| Au | 4.121895 | 0.497683 | -0.131635 |
| C | 4.968448 | 2.362101 | -0.118055 |
| C | 5.696412 | 2.828684 | 0.999186 |
| C | 4.850330 | 3.238318 | -1.217818 |
| C | 6.280731 | 4.092872 | 1.040372 |
| H | 5.810173 | 2.181667 | 1.866821 |
| C | 5.427119 | 4.501511 | -1.192765 |
| H | 4.298068 | 2.921912 | -2.101930 |
| C | 6.143371 | 4.932262 | -0.063868 |
| H | 6.833326 | 4.414359 | 1.921228 |
| C | 5.408677 | 5.575887 | -2.268783 |
| C | 6.631333 | 6.284598 | -0.314457 |
| C | 6.211096 | 6.679643 | -1.600139 |
| C | 7.385495 | 7.151990 | 0.475091 |
| C | 6.538978 | 7.926857 | -2.094214 |
| C | 7.714083 | 8.406353 | -0.024198 |
| H | 7.715857 | 6.859336 | 1.468226 |
| C | 7.299919 | 8.808547 | -1.303195 |
| H | 6.226372 | 8.253210 | -3.082161 |
| H | 8.302135 | 9.081494 | 0.593222 |
| C | 3.970338 | 6.035300 | -2.598923 |
| H | 3.448735 | 5.189388 | -3.067544 |
| H | 4.032383 | 6.819850 | -3.365895 |
| C | 6.080934 | 5.093722 | -3.574462 |
| H | 5.457987 | 4.292109 | -3.994652 |
| H | 6.046941 | 5.919768 | -4.298436 |
| C | 7.514477 | 4.600516 | -3.427237 |
| H | 7.910150 | 4.277985 | -4.396643 |
| H | 8.170694 | 5.389388 | -3.043903 |
| H | 7.572943 | 3.749851 | -2.739710 |
| C | 3.158130 | 6.540774 | -1.413748 |
| H | 3.633647 | 7.409141 | -0.945046 |
| H | 2.155653 | 6.842284 | -1.736941 |
| H | 3.046221 | 5.764277 | -0.649405 |
| C | 7.635728 | 10.123894 | -1.843301 |
| N | 7.272549 | 10.539061 | -3.018962 |

| | | | |
|---|---|---|---|
| S | 8.592112 | 11.285800 | -0.905149 |
| C | 7.724258 | 11.813155 | -3.268758 |
| C | 8.474303 | 12.405911 | -2.227720 |
| C | 7.495484 | 12.534514 | -4.447626 |
| C | 8.994192 | 13.693835 | -2.343385 |
| C | 8.012225 | 13.815445 | -4.563465 |
| H | 6.919012 | 12.078084 | -5.246460 |
| C | 8.754889 | 14.390720 | -3.521427 |
| H | 9.569264 | 14.141912 | -1.538776 |
| H | 7.840525 | 14.383416 | -5.473437 |
| H | 9.150034 | 15.396269 | -3.634673 |

**Au-BTF2**

112

| | | | |
|---|---|---|---|
| C | 3.305882 | -1.170272 | 0.014226 |
| N | 2.954458 | -1.949348 | -1.040156 |
| N | 3.064584 | -1.950622 | 1.098232 |
| C | 2.503311 | -3.188201 | -0.623838 |
| C | 2.573015 | -3.188913 | 0.729335 |
| H | 2.179521 | -3.943169 | -1.323340 |
| H | 2.321830 | -3.944245 | 1.457731 |
| C | 3.287861 | -1.543480 | 2.456707 |
| C | 4.545053 | -1.786453 | 3.032066 |
| C | 2.236485 | -0.925784 | 3.152258 |
| C | 4.734137 | -1.380935 | 4.355140 |
| C | 2.479637 | -0.540242 | 4.472445 |
| C | 3.714384 | -0.763857 | 5.069104 |
| H | 5.697059 | -1.547513 | 4.830612 |
| H | 1.690590 | -0.053098 | 5.039106 |
| H | 3.883370 | -0.454088 | 6.096937 |
| C | 5.680839 | -2.443583 | 2.270946 |
| C | 6.154962 | -3.725033 | 2.962841 |
| C | 6.838763 | -1.462580 | 2.061944 |
| H | 5.309682 | -2.725074 | 1.279346 |
| H | 5.334350 | -4.440061 | 3.088882 |
| H | 6.939852 | -4.207317 | 2.369176 |
| H | 6.572172 | -3.515745 | 3.954573 |
| H | 6.501683 | -0.565735 | 1.530450 |
| H | 7.271437 | -1.148698 | 3.019220 |
| H | 7.634405 | -1.933758 | 1.472921 |
| C | 0.884953 | -0.654400 | 2.518987 |
| C | 0.643833 | 0.851295 | 2.371546 |
| C | -0.248558 | -1.326161 | 3.299597 |
| H | 0.887433 | -1.084014 | 1.511178 |
| H | 1.437289 | 1.319116 | 1.778292 |

| | | | |
|---|---|---|---|
| H | -0.314581 | 1.035934 | 1.872184 |
| H | 0.613172 | 1.346112 | 3.349493 |
| H | -0.088990 | -2.406730 | 3.386870 |
| H | -0.336862 | -0.917522 | 4.312765 |
| H | -1.206200 | -1.162018 | 2.792610 |
| C | 3.037932 | -1.541496 | -2.414177 |
| C | 1.925209 | -0.913918 | -2.996163 |
| C | 4.225705 | -1.795404 | -3.118259 |
| C | 2.032139 | -0.530338 | -4.334905 |
| C | 4.278805 | -1.390968 | -4.454031 |
| C | 3.195358 | -0.764634 | -5.057666 |
| H | 1.192011 | -0.036720 | -4.816095 |
| H | 5.185061 | -1.565588 | -5.027748 |
| H | 3.258301 | -0.456411 | -6.097850 |
| C | 5.430196 | -2.459868 | -2.478693 |
| C | 6.600590 | -1.477217 | -2.370082 |
| C | 5.838808 | -3.731615 | -3.227564 |
| H | 5.156656 | -2.754410 | -1.459491 |
| H | 6.314020 | -0.588424 | -1.796967 |
| H | 7.450981 | -1.952466 | -1.867081 |
| H | 6.937037 | -1.149787 | -3.360956 |
| H | 5.010164 | -4.445942 | -3.287123 |
| H | 6.164328 | -3.509880 | -4.250383 |
| H | 6.674619 | -4.220292 | -2.714085 |
| C | 0.648492 | -0.631670 | -2.226978 |
| C | -0.561763 | -1.308092 | -2.877662 |
| C | 0.425954 | 0.875953 | -2.070795 |
| H | 0.755967 | -1.050907 | -1.220510 |
| H | -0.415971 | -2.390282 | -2.968126 |
| H | -1.461283 | -1.133866 | -2.276334 |
| H | -0.752996 | -0.910708 | -3.881112 |
| H | 1.277127 | 1.348131 | -1.567917 |
| H | 0.293915 | 1.361150 | -3.045114 |
| H | -0.475035 | 1.067542 | -1.476257 |
| Au | 4.036988 | 0.745827 | -0.017290 |
| C | 4.769805 | 2.649747 | -0.040151 |
| C | 5.073198 | 3.337728 | 1.157770 |
| C | 5.006099 | 3.342316 | -1.248225 |
| C | 5.582898 | 4.634103 | 1.174948 |
| H | 4.904846 | 2.838525 | 2.110276 |
| C | 5.513511 | 4.634954 | -1.249308 |
| H | 4.787738 | 2.853577 | -2.197196 |
| C | 5.804348 | 5.284531 | -0.038185 |
| H | 5.803496 | 5.125959 | 2.120654 |
| C | 5.831642 | 5.529962 | -2.436920 |
| C | 6.322232 | 6.614563 | -0.339550 |

| | | | |
|---|---|---|---|
| C | 6.347966 | 6.777615 | -1.739417 |
| C | 6.755141 | 7.645125 | 0.494612 |
| C | 6.801411 | 7.954378 | -2.301810 |
| C | 7.210694 | 8.828319 | -0.073748 |
| H | 6.740840 | 7.532190 | 1.575433 |
| C | 7.240884 | 8.999203 | -1.466256 |
| H | 6.831007 | 8.102066 | -3.377800 |
| H | 7.549681 | 9.629678 | 0.578847 |
| C | 4.573860 | 5.829750 | -3.283866 |
| H | 4.251005 | 4.887073 | -3.746814 |
| H | 4.870070 | 6.491942 | -4.109490 |
| C | 6.904688 | 4.905703 | -3.357368 |
| H | 6.467988 | 4.009813 | -3.819822 |
| H | 7.100430 | 5.610343 | -4.177758 |
| C | 8.214982 | 4.537736 | -2.673613 |
| H | 8.916302 | 4.104734 | -3.395502 |
| H | 8.693219 | 5.416828 | -2.228137 |
| H | 8.052808 | 3.802524 | -1.878134 |
| C | 3.407751 | 6.448320 | -2.523878 |
| H | 3.686151 | 7.409712 | -2.078735 |
| H | 2.561345 | 6.623935 | -3.197109 |
| H | 3.066372 | 5.789798 | -1.717931 |
| C | 7.718996 | 10.235416 | -2.079739 |
| N | 7.786511 | 10.431131 | -3.361927 |
| S | 8.258074 | 11.603706 | -1.087919 |
| C | 8.272711 | 11.682201 | -3.659139 |
| C | 8.594559 | 12.489067 | -2.544157 |
| C | 8.462968 | 12.188911 | -4.951201 |
| C | 9.097218 | 13.779963 | -2.696663 |
| C | 8.963007 | 13.472718 | -5.103815 |
| H | 8.215937 | 11.568238 | -5.807055 |
| C | 9.277260 | 14.262027 | -3.987431 |
| H | 9.341760 | 14.393144 | -1.834589 |
| H | 9.114113 | 13.874899 | -6.101610 |
| H | 9.667776 | 15.265472 | -4.131398 |

**Single Crystal Structure Determinations:**

Single crystal data for Au-BTF0, Au-BTF1 and Au-BTF2 were collected using a Bruker Quest diffractometer with a fixed chi angle, a sealed tube fine focus X-ray tube, single crystal curved graphite incident beam monochromator, a Photon100 CMOS area detector and an Oxford

Cryosystems low temperature device. Examination and data collection were performed with Mo Kα radiation (λ = 0.71073 Å) at 150 K. Data were collected, reflections were indexed and processed, and the files scaled and corrected for absorption using APEX3 [1]. The space groups were assigned and the structures were solved by direct methods using XPREP within the SHELXTL suite of programs [2] and refined by full matrix least squares against $F^2$ with all reflections using Shelxl2018 [3] using the graphical interface Shelxle [4]. If not specified otherwise H atoms attached to carbon, boron and nitrogen atoms as well as hydroxyl hydrogens were positioned geometrically and constrained to ride on their parent atoms. C-H bond distances were constrained to 0.95 Å for aromatic and alkene C-H moieties, and to 1.00, 0.99 and 0.98 Å for aliphatic C-H, $CH_2$ and $CH_3$ moieties, respectively. $U_{iso}(H)$ values were set to a multiple of $U_{eq}(C)$ with 1.5 for $CH_3$ and 1.2 for C-H and $CH_2$ units, respectively.

For Au-BTF2 disorder is observed for solvate molecules. One benzene ring was refined as disordered over two orientations. A pentane molecule was refined as disordered with a minor benzene molecule. The two minor benzene molecules were constrained to resemble ideal hexagons with C-C bond distances of 1.39 Å. The major moieties were refined freely. $U^{ij}$ components of ADPs for disordered atoms closer to each other than 2.0 Å were restrained to be similar. Subject to these conditions the occupancy ratios refined to 0.702(5) to 0.298(5) and 0.780(6) to 0.220(6), respectively.

Complete crystallographic data, in CIF format, have been deposited with the Cambridge Crystallographic Data Centre. CCDC 1917590-1917592 contains the supplementary crystallographic data for this paper. These data can be obtained free of charge from The Cambridge Crystallographic Data Centre via www.ccdc.cam.ac.uk/data_request/cif.

[1] Bruker (2016). Apex3 v2016.9-0, Saint V8.34A, SAINT V8.37A, Bruker AXS Inc.: Madison (WI), USA, 2013/2014.

[2] a) SHELXTL suite of programs, Version 6.14, 2000-2003, Bruker Advanced X-ray Solutions, Bruker AXS Inc., Madison, Wisconsin: USA b) Sheldrick GM. A short history of SHELX. *Acta Crystallogr A*. **2008**, *64(1)*, 112–122.

[3] a) Sheldrick GM. University of Göttingen, Germany, **2018**. b) Sheldrick GM. Crystal structure refinement with SHELXL. *Acta Crystallogr Sect C Struct Chem*. **2015**, *71(1)*, 3–8.

[4] Hübschle CB, Sheldrick GM, Dittrich B. ShelXle: a Qt graphical user interface for SHELXL. *J. Appl. Crystallogr*. **2011**, *44(6)*, 1281–1284.

**Crystal Tables:**

**Table 2.4.** Crystal data: JJM-1-122(AuBTF0)

| | |
|---|---|
| Chemical formula | $C_{42}H_{35}AuNPS$ |
| $M_r$ | 813.70 |
| Crystal system, space group | Triclinic, $P\bar{1}$ |
| Temperature (K) | 150 |
| $a$, $b$, $c$ (Å) | 11.8146 (5), 12.7494 (6), 12.7733 (6) |
| α, β, γ (°) | 74.285 (2), 63.823 (2), 83.926 (2) |
| $V$ (Å$^3$) | 1661.94 (13) |
| $Z$ | 2 |
| Radiation type | Mo $K\alpha$ |
| μ (mm$^{-1}$) | 4.57 |
| Crystal size (mm) | 0.32 × 0.26 × 0.11 |
| Data collection | |
| Diffractometer | Bruker AXS D8 Quest CMOS diffractometer |
| Absorption correction | Multi-scan, *SADABS* 2016/2: Krause, L., Herbst-Irmer, R., Sheldrick G.M. & Stalke D., J. Appl. Cryst. 48 (2015) 3-10 |
| $T_{min}$, $T_{max}$ | 0.200, 0.269 |
| No. of measured, independent and observed [$I > 2\sigma(I)$] reflections | 51512, 12572, 10593 |
| $R_{int}$ | 0.039 |
| $(\sin \theta/\lambda)_{max}$ (Å$^{-1}$) | 0.771 |

| | |
|---|---|
| Refinement | |
| $R[F^2 > 2\sigma(F^2)]$, $wR(F^2)$, $S$ | 0.026, 0.050, 1.02 |
| No. of reflections | 12572 |
| No. of parameters | 418 |
| H-atom treatment | H-atom parameters constrained |
| $\Delta\rho_{max}$, $\Delta\rho_{min}$ (e Å$^{-3}$) | 2.51, −1.16 |

**Table 2.5.** Crystal data: JJM-1-200(AuBTF1)

| | |
|---|---|
| Chemical formula | $C_{42}H_{53}AuNPS$ |
| $M_r$ | 831.85 |
| Crystal system, space group | Triclinic, $P\bar{1}$ |
| Temperature (K) | 150 |
| $a$, $b$, $c$ (Å) | 12.5710 (8), 12.7256 (8), 13.7715 (9) |
| α, β, γ (°) | 104.775 (2), 104.891 (2), 111.277 (2) |
| $V$ (Å$^3$) | 1829.6 (2) |
| $Z$ | 2 |
| Radiation type | Mo $K\alpha$ |
| μ (mm$^{-1}$) | 4.15 |
| Crystal size (mm) | 0.51 × 0.46 × 0.36 |
| Data collection | |
| Diffractometer | Bruker AXS D8 Quest CMOS diffractometer |
| Absorption correction | Multi-scan, *SADABS* 2016/2: Krause, L., Herbst-Irmer, R., Sheldrick G.M. & Stalke D. (2015). J. Appl. Cryst. 48 3-10. |
| $T_{min}$, $T_{max}$ | 0.558, 0.747 |
| No. of measured, independent and observed $[I > 2\sigma(I)]$ reflections | 90033, 14030, 12735 |
| $R_{int}$ | 0.031 |
| $(\sin \theta/\lambda)_{max}$ (Å$^{-1}$) | 0.772 |
| Refinement | |
| $R[F^2 > 2\sigma(F^2)]$, $wR(F^2)$, $S$ | 0.022, 0.046, 1.14 |
| No. of reflections | 14030 |
| No. of parameters | 418 |
| H-atom treatment | H-atom parameters constrained |
| $\Delta\rho_{max}$, $\Delta\rho_{min}$ (e Å$^{-3}$) | 4.22, −1.17 |

**Table 2.6.** Crystal data: JJM-1-282(AuBTF2)

| | |
|---|---|
| Chemical formula | $C_{51}H_{56}AuN_3S \cdot 1.11(C_6H_6) \cdot 0.39(C_5H_{12})$ |
| $M_r$ | 1054.85 |
| Crystal system, space group | Triclinic, $P\bar{1}$ |
| Temperature (K) | 150 |
| $a$, $b$, $c$ (Å) | 14.8591 (8), 15.9180 (8), 24.8004 (14) |
| α, β, γ (°) | 91.478 (2), 98.399 (2), 114.388 (2) |
| $V$ (Å$^3$) | 5261.1 (5) |
| $Z$ | 4 |
| Radiation type | Mo $K\alpha$ |
| μ (mm$^{-1}$) | 2.88 |
| Crystal size (mm) | 0.48 × 0.46 × 0.22 |
| Data collection | |
| Diffractometer | Bruker AXS D8 Quest CMOS diffractometer |
| Absorption correction | Multi-scan, *SADABS* 2016/2: Krause, L., Herbst-Irmer, R., Sheldrick G.M. & Stalke D., J. Appl. Cryst. 48 (2015) 3-10 |
| $T_{min}$, $T_{max}$ | 0.532, 0.747 |
| No. of measured, independent and observed [$I > 2\sigma(I)$] reflections | 127152, 39788, 30231 |
| $R_{int}$ | 0.041 |
| $(\sin \theta/\lambda)_{max}$ (Å$^{-1}$) | 0.772 |
| Refinement | |
| $R[F^2 > 2\sigma(F^2)]$, $wR(F^2)$, $S$ | 0.035, 0.095, 1.04 |
| No. of reflections | 39788 |
| No. of parameters | 1270 |
| No. of restraints | 294 |
| H-atom treatment | H-atom parameters constrained |
| $\Delta\rho_{max}$, $\Delta\rho_{min}$ (e Å$^{-3}$) | 2.80, −2.00 |

## References


1 (a) J. E. Rogers, J. E. Slagle, D. M. Krein, A. R. Burke, B. C. Hall, A. Fratini, D. G. McLean, P. A. Fleitz, T. M. Cooper, M. Drobizhev, N. S. Makarov, A. Rebane, K. Y. Kim, R. Farley and K. S. Schanze, Platinum acetylide two-photon chromophores, *Inorg. Chem.*, 2007, **46**, 6483–6494.(b) J. E. Rogers, J. E. Slagle, D. G. McLean, R. L. Sutherland, M. C. Brant, J. Heinrichs, R. Jakubiak, R. Kannan, L. S. Tan and P. A. Fleitz, Insight into the nonlinear absorbance of two related series of two-photon absorbing chromophores, *J. Phys. Chem. A*, 2007, **111**, 1899–1906.

2 D. V Partyka, T. J. Robilotto, M. Zeller, A. D. Hunter and T. G. Gray, Dialkylbiarylphosphine Complexes of Gold(I) Halides. Gold−Aryl π-Interactions in the Solid State, *Organometallics*, 2008, **27**, 28–32.;

3 J. J. Mihaly, D. J. Stewart, T. A. Grusenmeyer, A. T. Phillips, J. E. Haley, M. Zeller and T. G. Gray, Photophysical properties of organogold(i) complexes bearing a benzothiazole-2,7-fluorenyl moiety: Selection of ancillary ligand influences white light emission, *Dalt. Trans.*, 2019, **48**, 15917–15927.

4 Gaussian 16, Revision A.03, M. J. Frisch, G. W. Trucks, H. B. Schlegel, G. E. Scuseria, M. A. Robb, J. R. Cheeseman, G. Scalmani, V. Barone, G. A. Petersson, H. Nakatsuji, X. Li, M. Caricato, A. V Marenich, J. Bloino, B. G. Janesko, R. Gomperts, B. Mennucci, H. P. Hratchian, J. V Ortiz, A. F. Izmaylov, J. L. Sonnenberg, D. Williams-Young, F. Ding, F. Lipparini, F. Egidi, J. Goings, B. Peng, A. Petrone, T. Henderson, D. Ranasinghe, V. G. Zakrzewski, J. Gao, N. Rega, G. Zheng, W. Liang, M. Hada, M. Ehara, K. Toyota, R. Fukuda, J. Hasegawa, M. Ishida, T. Nakajima, Y. Honda, O. Kitao, H. Nakai, T. Vreven, K. Throssell, J. A. Montgomery Jr., J. E. Peralta, F. Ogliaro, M. J. Bearpark, J. J. Heyd, E. N. Brothers, K. N. Kudin, V. N. Staroverov, T. A. Keith, R. Kobayashi, J. Normand, K. Raghavachari, A. P. Rendell, J. C. Burant, S. S. Iyengar, J. Tomasi, M. Cossi, J. M. Millam, M. Klene, C. Adamo, R. Cammi, J. W. Ochterski, R. L. Martin, K. Morokuma, O. Farkas, J. B. Foresman and D. J. Fox, Gaussian, Inc., Wallingford CT, 2016.

5 M. Dolg, U. Wedig, H. Stoll and H. Preuss, Energy-adjusted ab initio pseudopotentials for the first row transition elements, *J. Chem. Phys.*, 1987, **86**, 866–872.

6 J. P. Perdew, K. Burke and M. Ernzerhof, Generalized Gradient Approximation Made Simple, *Phys. Rev. Lett.*, 1996, **77**, 3865–3868.

7 N. Godbout, D. R. Salahub, J. Andzelm and E. Wimmer, Optimization of Gaussian-type basis sets for local spin density functional calculations. Part I. Boron through neon, optimization technique and validation, *Can. J. Chem.*, 1992, **70**, 560–571.

8 S. Miertuš, E. Scrocco and J. Tomasi, Electrostatic interaction of a solute with a continuum. A direct utilizaion of AB initio molecular potentials for the prevision of solvent effects, *Chem. Phys.*, 1981, **55**, 117–129.

9 J. Tomasi, B. Mennucci and R. Cammi, Quantum Mechanical Continuum Solvation Models, *Chem. Rev.*, 2005, **105**, 2999–3094.

10 E. Cancès, B. Mennucci and J. Tomasi, A new integral equation formalism for the polarizable continuum model: Theoretical background and applications to isotropic and anisotropic dielectrics, *J. Chem. Phys.*, 1997, **107**, 3032–3041.

11 B. Mennucci, E. Cancès and J. Tomasi, Evaluation of Solvent Effects in Isotropic and Anisotropic Dielectrics and in Ionic Solutions with a Unified Integral Equation Method: Theoretical Bases, Computational Implementation, and Numerical Applications, *J. Phys. Chem. B*, 1997, **101**, 10506–10517.

12 S. I. Gorelsky and A. B. P. Lever, Electronic structure and spectra of ruthenium diimine complexes by density functional theory and INDO/S. Comparison of the two methods, *J. Organomet. Chem.*, 2001, **635**, 187–196.

13 S. I. Gorelsky, AOMix: Program for Molecular Orbital Analysis, http://www.sg-chem.net.

## Chapter 3: Synthesis, Photophysics, and Computations for a Series of Gold(I) BTF Alkynyl Complexes (Au-ABTF(0-2).

In the previous chapter, a study on the synthesis, photophysics, and computations for a series of gold(I) BTF aryl (**Au-BTF(0-2)**) complexes was reported.[1] That study demonstrated the effect variation in ancillary ligand had on the excited-state dynamics for a series of gold(I) aryls bearing a benzothiazole-2,7-fluorenyl moiety. **Au-BTF2** (carbene ancillary ligand) displays an increased flourescene lifetime and quantum yield as well as a decreased triplet state quantum yield in comparison to **Au-BTF(0,1)** (phosphine ancillary ligand); **Au-BTF2** also displays a decreased rate of radiative and nonradiative decay as well as intersytem crossing rate contant (by a factor of 4) (Figure 3.1).

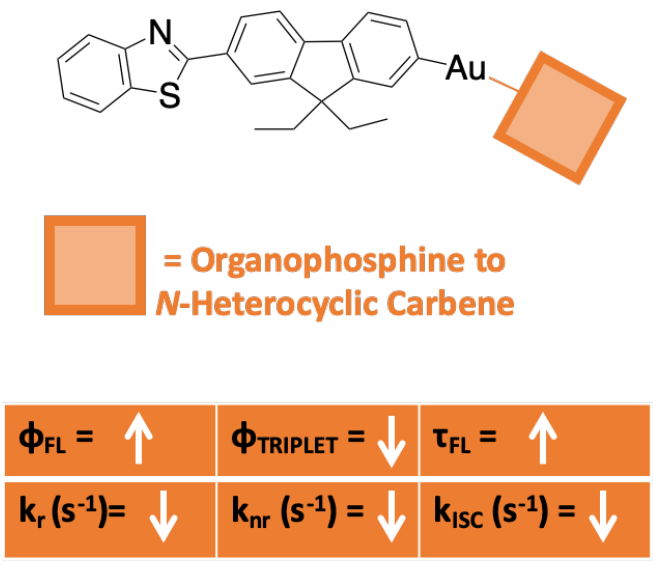


**Figure 3.1.** Photophysical trends in **Au-BTF** series when changing ancillary ligand from and organophosphine to an *N*-heterocyclic carbene.[1]

To broaden the scope of understanding for gold(I) chromophores as triplet photoactive materials, a series of gold(I) BTF alkynyl complexes (**Au-ABTF(0-2)**) were synthesized and photophysically characterized with computational support. Of specific interest is the effect

changing the nature of the gold-chromophore bond as well as the ancillary ligand have on excited-state dynmaics and to add to an expanding library of structre-property relationships. First, the previously reported BTF alkyne ligand was synthesized according to Scheme 3.1.[2]

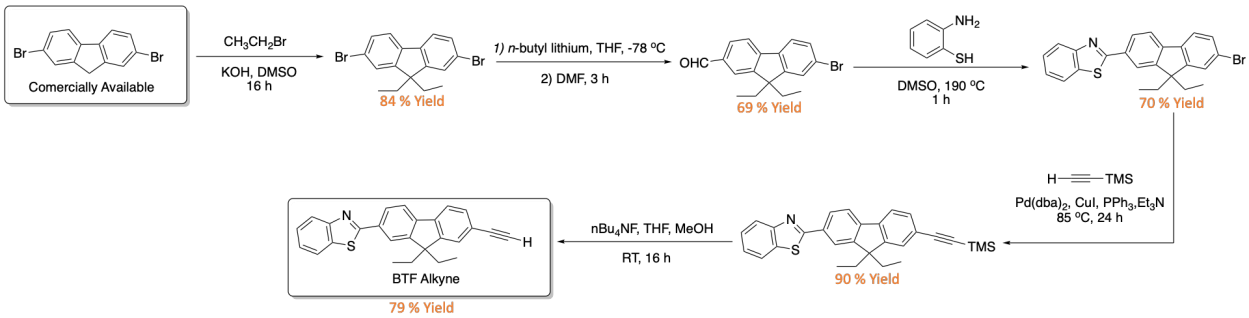


**Scheme 3.1.** Synthesis of BTF alkyne ligand.

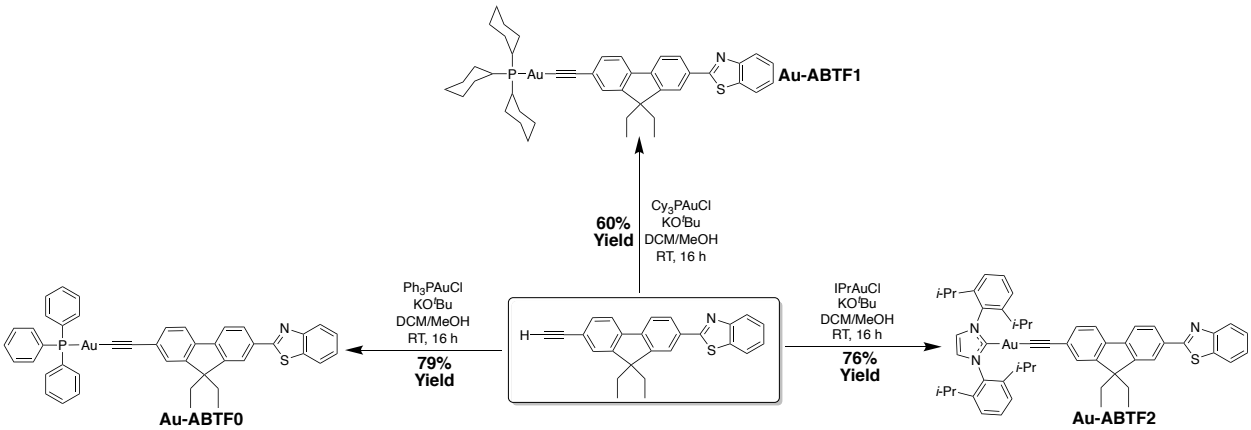


**Scheme 3.2.** Synthesis of new **Au-ABTF(0-2)**.

The BTF alkyne was then reacted with choice gold(I) chloride starting materials[3] by *in situ* deprotonation of the alkyne and subsequent of addition to a suspension of gold starting material (Scheme 3.2).[2] Purification by vapor diffusion of pentane into concentrated dichloromethane solutions yielded the new complexes **Au-ABTF0** (79% isolated yield), **Au-ABTF1** (60% isolated yield), and **Au-ABTF2** (76% isolated yield), repectively.

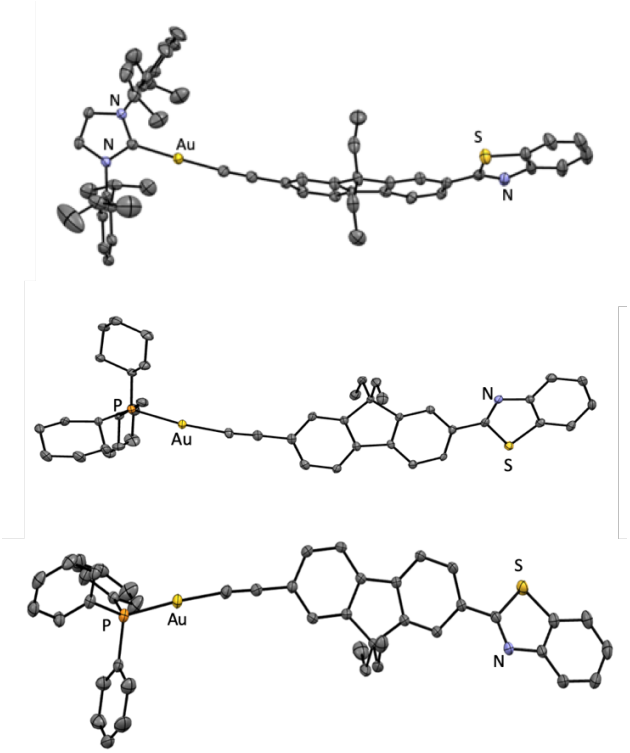


**Figure 3.2.** Crystal structures of **Au-ABTF2** (top), **Au-ABTF1** (middle), **Au-ABTF0** (bottom). (50% probability level, 150 K). Hydrogen atoms are omitted for clarity. A partial atom labeling scheme appears; unlabeled atoms are carbon.

Thermal ellipsoid representations of all three complexes appear in Figure 3.2. All three structures show linear two-coordination at gold; packing diagrams show no evidence of aurophilic interactions or π-π stacking. **Au-ABTF0** has an Au-C bond length 1.996(2) Å and an Au-P length of 2.268(6) Å and **Au-ABTF1** has an Au-C bond length of 2.007(4) Å and an Au-P length of 2.288 Å demonstrating little variation in these bond lengths between the two phosphine complexes. **Au-ABTF2** has an Au-$C_{carbene}$ length of 2.018 Å and an Au-$C_{alkyne}$ length of 1.981 Å.

**Photophysical Characterization of Au-BTF(0-2) vs Au-ABTF(0-2):**

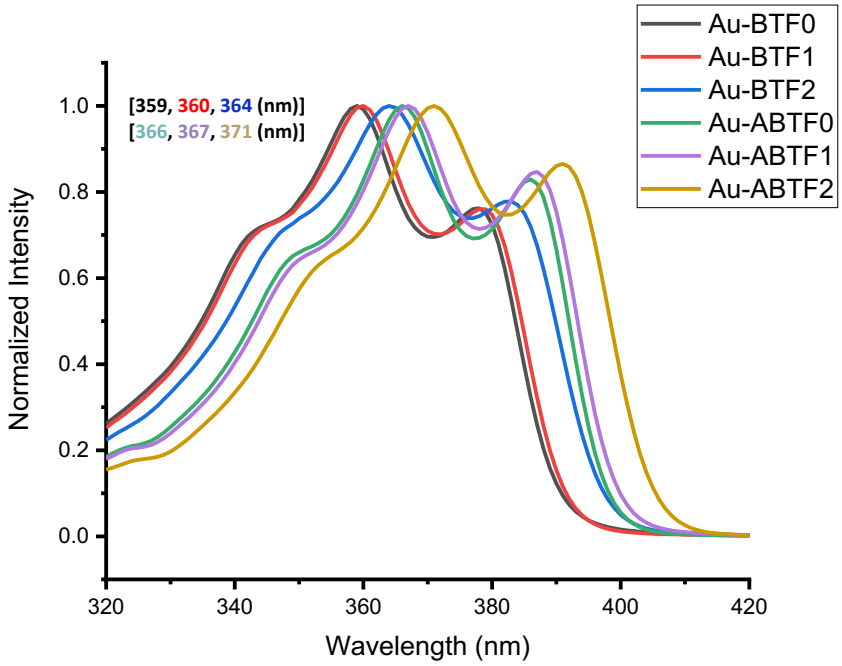


**Figure 3.3.** Ground-state absorption spectra of **Au-BTF** and **Au-ABTF** series in toluene.

Normalized ground-state absorption spectra appear in Figure 3.3, which collects spectra of the series of complexes, **Au-BTF0-2** and **Au-ABTF0-2**. The spectra for all six complexes are similar in band shape and highly strucutred, with two pronounced lower energy peaks and a high energy shoulder. In both the aryl and alkynyl series, the phosphine complexes have maxima at nearly identical energies, with the carbene complexes red-shifted in comparison (Figure 3.3). Absorption spectra of alkynyls are red-shifted compared to those of the aryls. **Au-ABTF0–2** have molar absorptivity values of (7-9 x $10^4$ $M^{-1}$ $cm^{-1}$) that are larger than those of aryls **Au-BTF0–2** (5-6 x $10^4$ $M^{-1}$ $cm^{-1}$) (Tables 3.1/2.1).

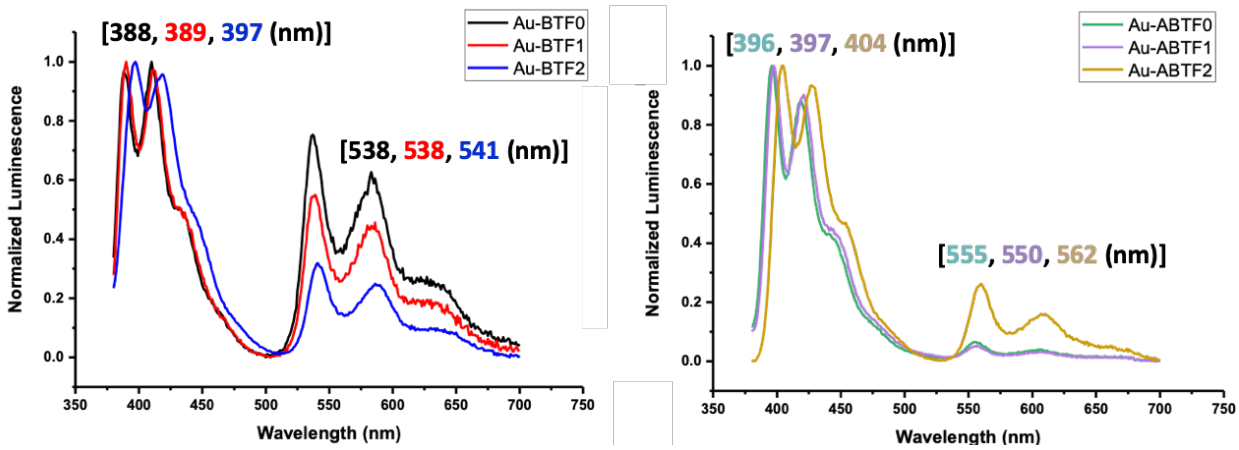


**Figure 3.4.** Room-temperature, luminescence spectra of aryl complexes **Au-BTF0–2** and alkynyl complexes **Au-ABTF0–2** series collected in freeze-pump-thaw degassed toluene.

Luminescence spectra collected in freeze-pump-thaw degassed toluene for gold(I) aryl and alkyl complexes are shown in Figure 3.4. All complexes are characterized by dual-luminescence; highly structured fluorescence and phosphorescence. In both series (**Au-BTF** and **Au-ABTF**), the complexes containing the carbene ancillary ligand are the most red-shifted. Interestingly, in the aryl series, the phosphine complexes **AuBTF0** and **AuBTF1** have higher phosphorescence intensities than carbene complex **AuBTF2**. For the corresponding alkynyls; the converse is true, and the carbene complex displays the highest phosphorescence intensity of the three alkynyls.

| Experimental Results: | Complex: | | |
|---|---|---|---|
| | Au-ABTF0 | Au-ABTF1 | Au-ABTF2 |
| $\lambda_{ABS}$/nm ($10^4$ $M^{-1}cm^{-1}$) | 366 (7.79) | 367 (8.77) | 371 (6.89) |
| $\lambda_{FL}$ (nm) | 396 | 396 | 404 |
| $\phi_{FL}$ | 0.41 ± 0.03 | 0.44 ± 0.007 | 0.23 ± 0.02 |
| $\tau_{FL}$ – TCSPC (ps) | 312 ± 6 | 339 ± 1 | 206 ± 13 |
| $\tau_{FL}$ – TA (ps) | 288 ± 7 | 301 ± 7 | 192 ± 4 |
| $k_r$ ($s^{-1}$) | 1.3 x $10^9$ | 1.3 x $10^9$ | 1.1 x $10^9$ |
| $k_{nr}$ ($s^{-1}$) | 3.7 x $10^8$ | 9.8 x $10^7$ | 7.8 x $10^8$ |
| $k_{ISC}$ ($s^{-1}$) | 1.5 x $10^9$ | 1.6 x $10^9$ | 3.0 x $10^9$ |
| $\lambda_{PHOS}$ (nm) | 420 | 420 | 427 |
| $\phi_{TRIPLET}$ | 0.47 ± 0.04 | 0.53 ± 0.007 | 0.61 ± 0.02 |
| $\phi_{PHOS}$ | 0.02 ± 0.0004 | 0.06 ± 0.009 | 0.04 ± 0.005 |
| $\tau_{PHOS}$ (μs) | 715 | 492 | 609 |
| $k_T$ ($s^{-1}$) | 3,000 | 2,030 | 1,630 |
| $k_{TT}$ ($M^{-1}$ $s^{-1}$) | 9.2 ± 0.3 x $10^9$ | 1.4 ± 0.2 x $10^{10}$ | 2.5 ± 0.7 x $10^{10}$ |
| $\Delta\varepsilon_{T_1-T_n}/\lambda$ nm ($10^4$ $M^{-1}$ $cm^{-1}$) | 592 (14.0 ± 2.0) | 595 (13.8 ± 3.0) | 610 (9.0 ± 4.0) |
| $\Delta\varepsilon_{S_1-S_n}/\lambda$ nm ($10^4$ $M^{-1}$ $cm^{-1}$) | 620 (21.1) | 634 (36.5) | 624 (18.9) |

**Table 3.1.** Photophysical data for **Au-ABTF(0-2)**.

All data collected in room temperature toluene. Legend: $\lambda_{FL}$ = wavelength of fluorescence; $\varphi_{FL}$ = emission quantum yield of fluorescence; $\tau_{FL}$ =lifetime of fluorescence; TCSPC = time-correlated single-photon counting; TA = transient absorption; $k_r$ = radiative decay rate constant; $k_{nr}$ = non-radiative decay rate constant; $k_{ISC}$ = rate constant of intersystem crossing; $\lambda_{PHOS}$ = wavelength of phosphorescence; $\varphi_{TRIPLET}$ = quantum yield of triplet state formation; $\varphi_{PHOS}$ = emission quantum yield of phosphorescence; $\tau_{PHOS}$ = lifetime of phosphorescence; $k_T$ = rate constant for formation of triplet excited state; $k_{TT}$ = rate constant of triplet–triplet annihilation; $\Delta\varepsilon_{T1-Tn}$ = molar absorptivity of triplet–triplet absorption; $\Delta\varepsilon_{S1-Sn}$=molar absorptivity of excited-singlet–singlet absorption. a Estimated from the peak maximum of the dilute luminescence spectrum used for the reabsorption correction in fluorescence quantum yield experiments. b Estimated from the peak maximum of the phosphorescence signal.

Static and transient photophysical measurements were performed on alkynyls **Au-ABTF(0-2)** to gain an understanding of their excited-state dynamics and in order to compare to

the aryl series **Au-BTF(0-2)**. In the alkynyl series, the phosphine complexes (**Au-ABTF(0,1)** display larger fluorescence quantum yields, longer fluorescnce lifetimes and smaller triplet-state quantum yields in comparision to the carbene complex **Au-ABTF2** (Table 3.1); the converse of what is seen in the aryl series. For the alkynyl series, the carbene complex **Au-ABTF2** displays a rate of intersytem crossing twice that of the phosphine complexes, the converse of the Au-BTF series. **Au-ABTF2** also shows a smaller $k_r$ and a larger $k_{nr}$ in comparison to the two phosphine alkynyl complexes.

When comparing the effect the nature of the gold-chromophore linkage has on excited-state dynamics in the two series, we see a noticable difference when the ancillary ligand is a phosphine and the linkage is an aryl or alkynyl and almost identical dynamics when the anciallry ligand is a carbene and the linkage is an aryl or alkynyl (Figure 3.5). **Au-ABTF0** displays an increased fluorescene quantum yield and lifetime and a decreased triplet state quantum yield compared to **Au-BTF0** as well as an increased rate of $k_r$ and a decreased rate of $k_{nr}$ and $k_{isc}$ suggesting that the alkynyl linkage slows down intersytem crossing to some degree.

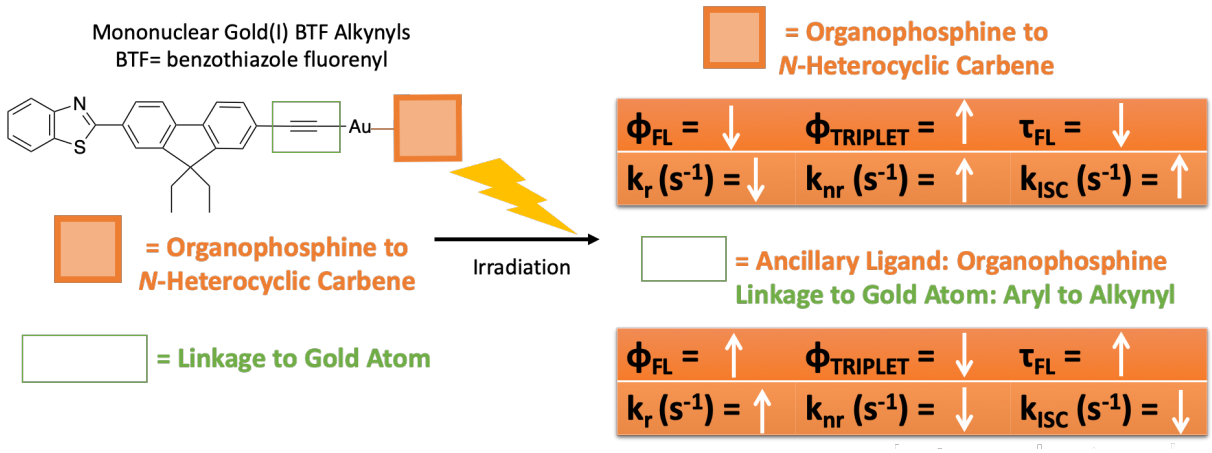


**Figure 3.5.** Demonstation of the effects changing ancillary ligand or gold-chromophore linkage has on excited-state dynamics in the **Au-ABTF** series.

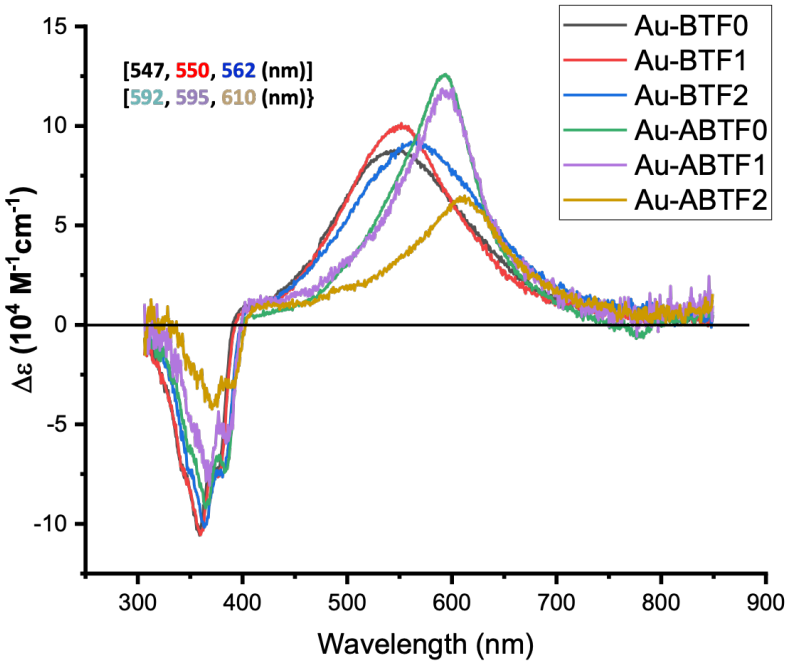


**Figures 3.6.** Nanosecond transient absorption spectra of the **Au-BTF** and **Au-ABTF** series in molar absorptivity units following three freeze-pump-thaw cycles in toluene (left). All samples were excited at 355 nm. The spectra were collected 100 ns after the laser pulse. Spectra were converted to units of Δε using relative actinometry measurements with a $[Ru(bpy)_3]^{2+}$ standard (left).

Nanosecond transient absorption spectra in molar absorptivity units for both series of compounds can be found in Figure 3.6. All six compounds have excited-state extinction coefficients ($\Delta\varepsilon_{T_1-T_n}$) ~1 x $10^5$ $M^{-1}$ $cm^{-1}$, and are characterized by a bleach of the ground-state and strong positive absorption throughout the visible region. The energy trends are identical to those of the ground-state absorption spectra; in each series the carbene complex is the most red-shifted and the **Au-ABTF** series is red-shifted in comparison to the **Au-BTF** series.

Delayed fluoresce was observed in all three complexes. Figure 3.7b shows the normalized luminescence intensity vs. wavelength where the signal is normalized to the phosphorescence

maximum to demonstrate the effect laser pulse energy has on the fluorescence intensity. As laser pulse energy is increased, we observe a clear increase in fluorescence intensity. Figure 3.7a displays the normalized integrated fluorescence intensity vs. laser pulse energy and the inset is the logarithmic plot. A slope of nearly two is observed demonstrating that the delayed fluorescence is a result of a bimolecular process (triplet-triplet annihilation). Dependence of delayed fluorescence on laser pulse energy is also indicative of a triplet-triplet annihilation decay pathway. It is believed that the slope is not exactly two in any of the complexes due to the fast rate of intersystem crossing, which efficiently depopulates the triplet excited state.

Triplet-triplet annihilation rate constants ($k_{TT}$) can be obtained by fitting the nanosecond decay traces after conversion from ΔOD to concentration by Beer's law Figure 3.7a (right). A discussion of the process as well as the fit equation used can be found in the experimental section of this chapter. The fits were done at two different pulse energies with the parameter of $k_T$ being held constant; the values were then averaged, which appear in Table 3.1. All three complexes exhibit triplet-triplet annihilation rate constants ($k_{TT}$) ~1 x $10^{10}$ $M^{-1}$ $s^{-1}$. This value indicates that triplet-triplet annihilation is diffusion controlled in the solvent of toluene.

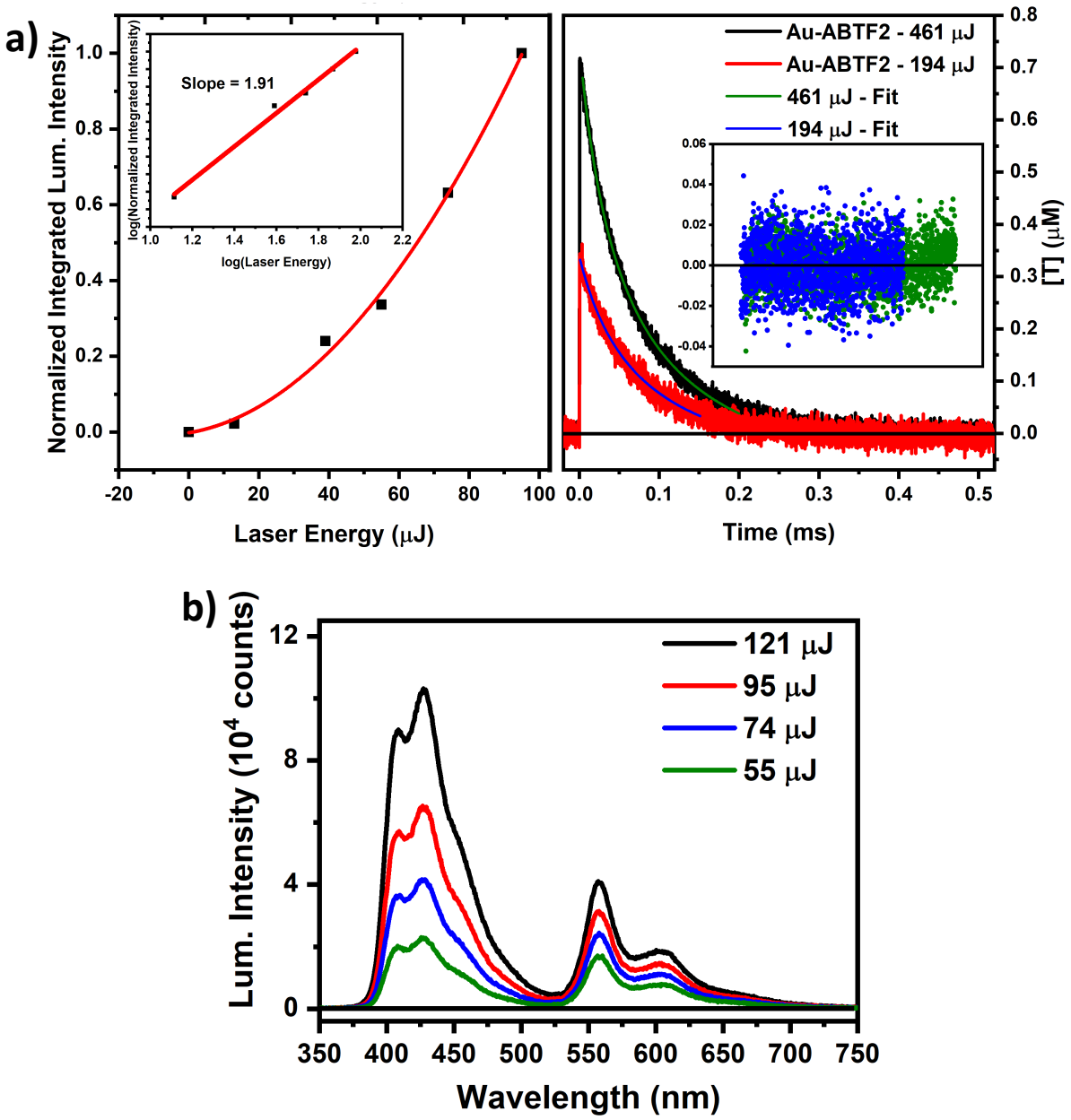


**Figure 3.7.** a) Fits of the normalized, integrated fluorescence intensity vs. laser pulse energy (left) and triplet-triplet annihilation fitting of excited-state decay traces in freeze-pump-thaw degassed toluene of **Au-ABTF2** (right). b) Delayed fluorescence observed in **Au-ABTF2**, the signal is normalized to the phosphorescence maximum. Data are representative of all complexes.

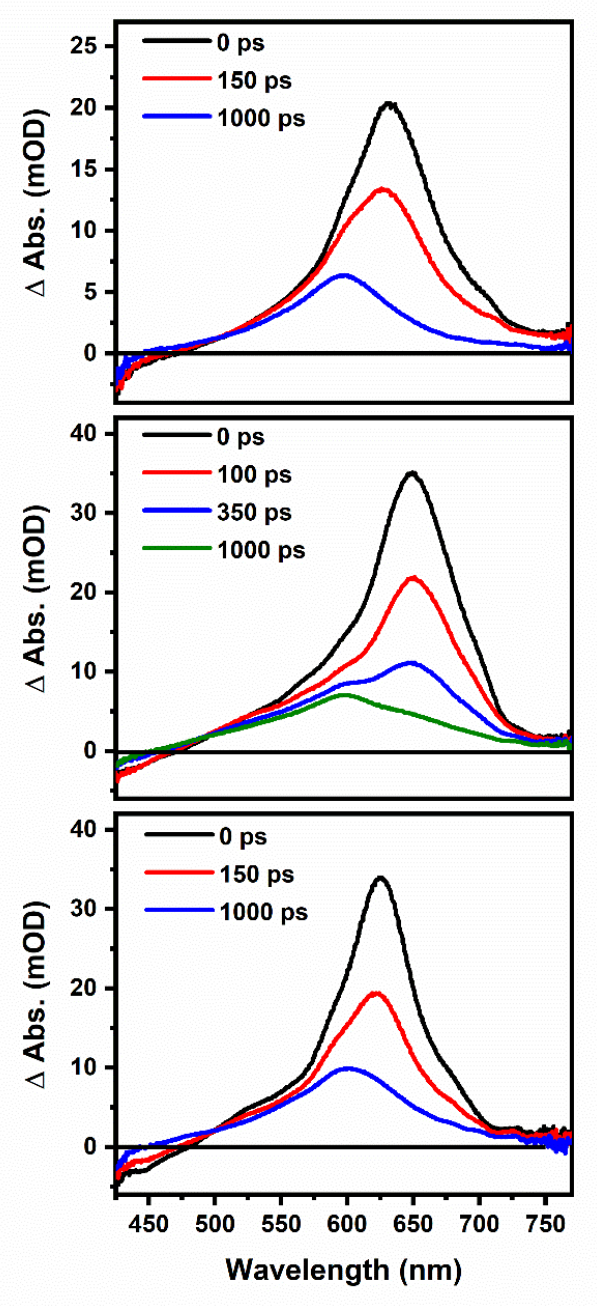


**Figure 3.8.** Picosecond Transient Absorption Spectra for **Au-ABTF0** (top), **Au-ABTF1** (center), and **Au-ABTF2** (bottom) in toluene. All samples were excited at 400 nm using the frequency doubled output of Ti:sapphire.

Picosecond transient absorption measurements were performed in order to quantify the excited-state dynamics in alkynyl **Au-ABTF** series (Figure 3.8). All three complexes exhibit both

singlet and triplet excited-state absorption. The transient progression from singlet state to the triplet state is seen at different time delays (Figure 3.8). Values for the singlet lifetimes were obtained from decay traces. The $S_1 - S_n$ absorption transitions are represented by shortest time delay spectra and the $T_1 - T_n$ absorption transitions are represented by the longest time delay spectra for each complex. All three complexes have $\Delta\varepsilon_{S_1-S_n}$ ~1.8 x $10^5$ $M^{-1}$ $cm^{-1}$ and exhibit a single isosbestic point at ~ 510 nm.

**Computations**

Density-functional theory calculations were undertaken to gain insight into the origin of the photophysical behavior of the alkynyl **Au-ABTF** series. Details for the calculations appear in the experimental section of this chapter. Figure 3.9 displays a frontier orbital energy level diagram with Kohn-Sham orbital plots for both the HOMO and LUMO in electron density. The HOMO consists of 3% Au, 28% carbon-carbon triple bond, 58% fluorene, and 10% benzothiazole; the LUMO consists 54% fluorene and 41 %, and 4% carbon-carbon triple bond; percentages are of electron density.

The $S_1$ state again derives primarily from a (98%) LUMO ← HOMO excitation; these results, in conjunction with structured absorption spectra, indicate that the absorption transitions are π-π* in nature. These results occur across all three complexes. Figure 3.10 displays a time-dependent density-functional theory state plot for **Au-ABTF(0-2)**. These results accord with the photophysical data obtained for the three complexes, particularly in regards to the rate of intersystem crossing. In the **Au-ABTF** series, the carbene complex, **Au-ABTF2**, displays the fastest intersystem crossing and also has the smallest $S_1$-to-$T_2$ energy gap of the series (Figure 3.10).

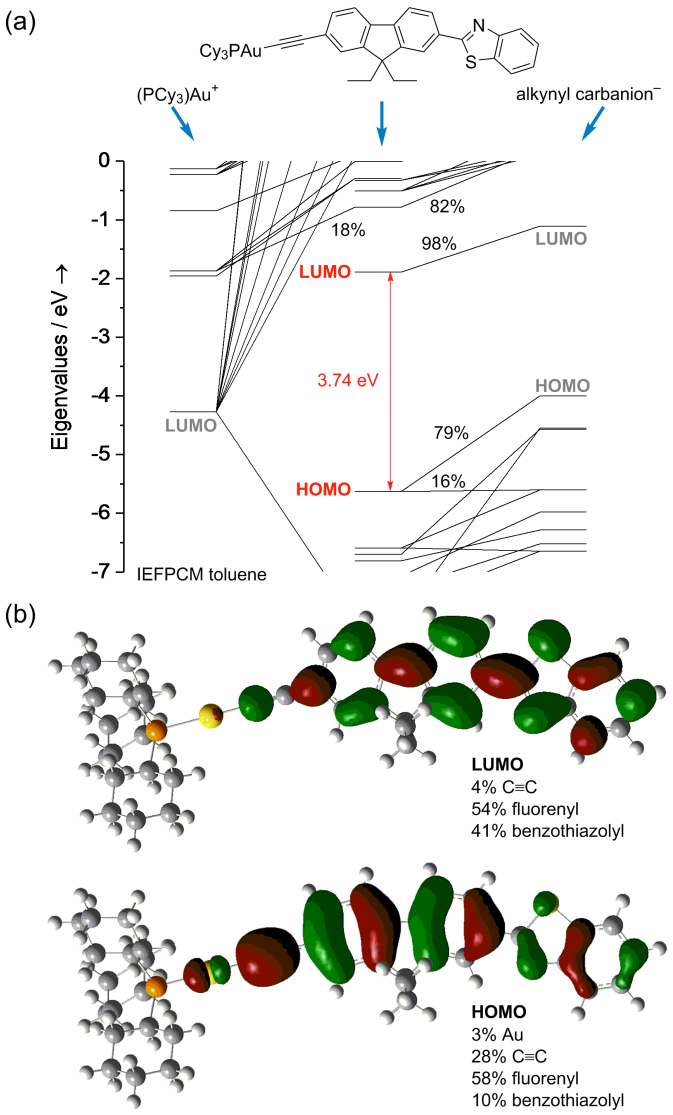


**Figure 3.9.** (a) Frontier orbital energy diagram of **Au-ABTF1**. (b) Kohn-Sham orbital plots (HOMO and LUMO) for **Au-ABTF1**. Percentages are of electron density.

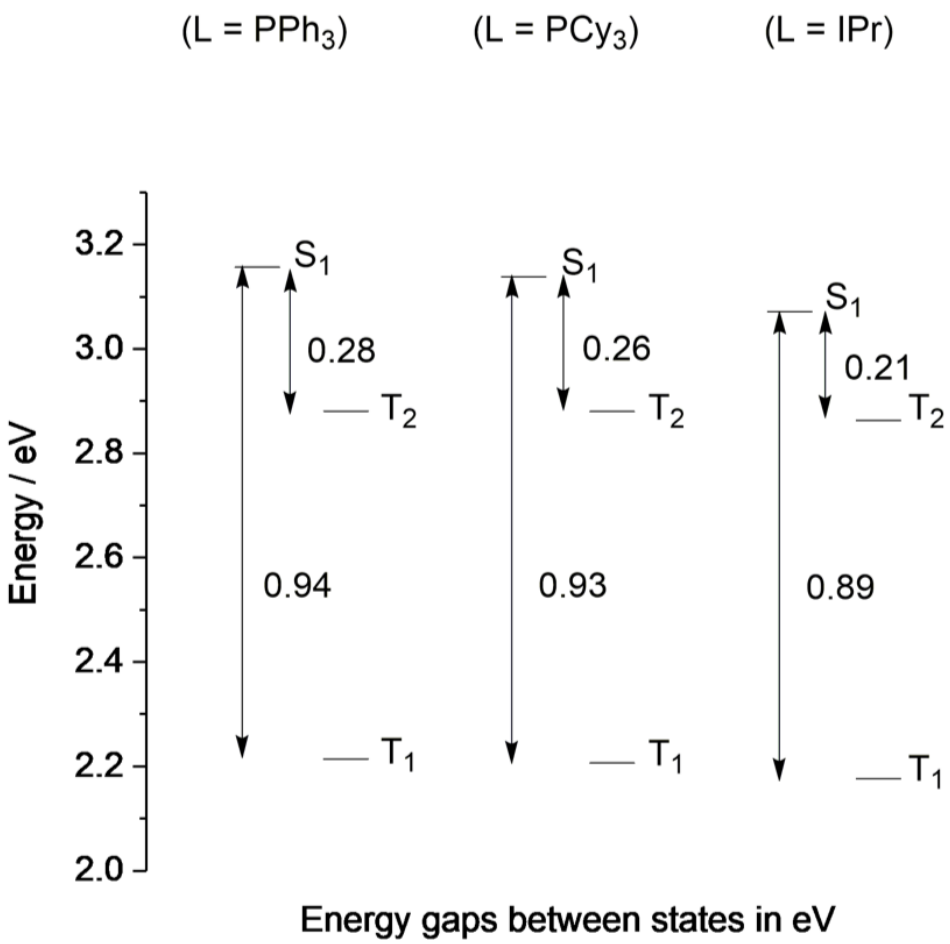


**Figure 3.10** Time-dependent density-functional theory (TD-DFT) state plot showing $S_1$, $T_1$, and $T_2$ states and their corresponding energies in electron volts (eV) for the three **Au-ABTF** complexes.

**Conclusions.**

Three new gold(I) BTF alkynyl complexes, **Au-ABTF(0-2)**, were synthesized and photophysically characterized. The complexes were synthesized by *in situ* deprotonation on the alkyne ligand precursor and addition to a gold(I) chloride starting material in good yields (60-79%). Crystal structures were obtained for each complex, all show linear gold(I). No evidence of aurophilic or π-π* stacking interactions is found in crystallographic packing diagrams. The three complexes are characterized by structured ground-state absorption and emission spectra following

the energy trends **Au-ABTF0** ≈ **Au-ABTF1** > **AuA-BTF2**. These complexes exhibit dual fluorescence and phosphorescence emission. General trends in the photophysical data are as follows: The two phosphine complexes (**Au-ABTF 0,1**) exhibit longer fluorescence lifetimes, smaller triplet state quantum yields, and larger fluorescence quantum yields compared to the carbene complex, **Au-ABTF2**. **Au-ABTF 0** and **1** also display rates of intersystem crossing half that of **Au-ABTF2** with a higher rate of nonradiative decay and lower rate of radiate decay. This is the converse of what is observed in the **Au-BTF** series.

Strong and broad triplet-excited state absorption was established via nanosecond transient absorption measurements. Delayed fluorescence via triplet-triplet annihilation was also observed by way of laser pulse energy dependence studies. All three complexes exhibit triplet-triplet annihilation rate constants ($k_{TT}$) ~1 x $10^{10}$ $M^{-1}$ $s^{-1}$, indicating that triplet-triplet annihilation is diffusion-controlled in toluene. Picosecond transient spectra show that both the singlet and triplet states strongly absorb with $\Delta\varepsilon_{S_1-S_n}$ ~1.8 x $10^5$ $M^{-1}$ $cm^{-1}$ and $\Delta\varepsilon_{T_1-T_n}$ on the order of 1 x $10^5$ $M^{-1}$ $cm^{-1}$. A progression from the singlet to the triplet state is also visible and an isosbestic point around 510 nm is evident. Density-functional theory calculations show that both the HOMO and LUMO for all three complexes are localized on the BTF ligand and that the $S_1$ state derives from a (98%) LUMO ← HOMO excitation. This leads us to believe that the absorption transitions are π-π* in nature. TD-DFT computations agree with the photophysical data. (**Au-ABTF 0,1**) have computed $S_1$-to-$T_2$ energy gaps that are larger than that of the carbene complex **Au-ABTF2**, which is believed to contribute to the lesser rates of intersystem crossing and smaller triplet-state quantum yields of the alkynyls **Au-ABTF0** and **Au-ABTF1**

**Experimental Details.**

**General Considerations.** All experimental procedures were carried out under an inert atmosphere of argon using standard Schlenk line techniques. Microanalyses (C, H, and N) were undertaken by Atlantic Microlab. Mass spectrometry was performed at the University of Cincinnati Mass Spectrometry facility. (Phosphine)gold(I) chlorides and (i-$Pr_2$NHC)AuCl were prepared according to literature procedures.[3] Benzathiazole Ligand was synthesized according to literature procedure.[2] Dry 2-propanol, benzene, dichloromethane, pentane, and cesium carbonate were purchased from Sigma Aldrich and used as received. $^1$H NMR experiments were performed on a Bruker-500 Ascend Advanced III HD NMR spectrometer operating at 500.24 MHz. $^1$H chemical shifts are reported in parts per million ($\delta$) with integration and multiplicity (s = singlet, d = doublet, t = triplet, q = quartet, dd = doublet of doublets, dt = doublet of triplets, td = triplet of doublets, ddd = doublet of doublet of doublets, and m = multiplet), measured from tetramethylsilane (0 ppm) and are referenced to residual solvent in $CDCl_3$ (7.26 ppm). $^{31}P\{^1H\}$ NMR, chemical shifts were determined relative to concentrated $H_3PO_4$. Thermogravimetric analysis (TGA) of the Au(I) complexes were carried out using a TA Q500. Samples were heated at a ramp rate of 10 °C min$^{-1}$ to a final temperature of 600 °C or 800°C. TGA experiments were run in air.

**Instrumentation and photophysical measurements.**

Details regarding instrumentation and photophysical measurements can be found here:

http://www.rsc.org/suppdata/d0/cp/d0cp01539c/d0cp01539c1.pdf

Synthesis, NMR, Mass Spectrometry and Elemental Analysis

**Au-ABTF2:**

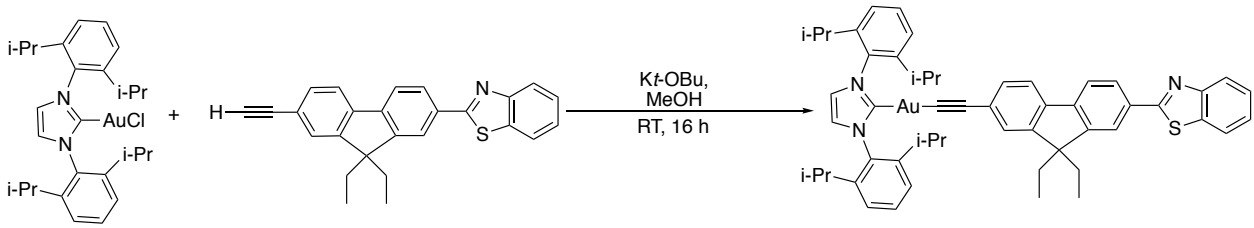


To a 20 mL scintillation vial equipped with a stir bar was added (23.5 mg, 0.322 mmol) of potassium *tert*-butoxide along with 4 mL of MeOH via syringe. The suspension was stirred until a solution was observed, after which (79.4 mg, 0.209 mmol) of BTF alkyne was added. Most didn't dissolve, so 3 mL of DCM was added creating a yellow solution. This solution was stirred at RT for 45 min and then transferred to another 20 mL scintillation vial containing 2 mL of MeOH and (100 mg, 0.161 mmol) IPrAuCl, creating a yellow solution. This solution was stirred in the absence of light for 16 h and then concentrated *in vacuo*. The yellow solid was dissolved in dichloromethane, filtered over Celite, concentrated, and washed with (4 x 25 mL) of pentanes. The yellow solid was allowed to dry and then dissolved in hot ethanol and allowed to crystallize in a freezer at -10 $^{o}$C. After two crops, 119 mg of yellow crystals were obtained. (76 % yield). $^{1}$H NMR (500 MHz, Chloroform-*d*) δ 8.06 (d, *J* = 8.2 Hz, 1H), 8.03 (s, 1H), 7.96 (d, *J* = 9.3 Hz, 1H), 7.89 (d, 7.8 Hz, 1H), 7.66 (d, *J* = 8.0 Hz, 1H), 7.54-7.44 (m, 4H), 7.40-7.30 (m, 7H), 7.13 (s, 2H), 2.62 (sept, *J* = 6.8 Hz), 2.03 (m, *J* = 35.6, 13.6, 6.7 Hz, 4H), 1.41 (d, *J* = 6.8 Hz, 12H), 1.23 (d, *J* = 6.9 Hz, 12H), 0.21 (t, *J* = 7.3 Hz, 6H). HRMS (FT-ICR, $[M+H]^{+}$) m/z calcd for $MH^{+}$ $C_{53}H_{57}AuN_3S^{+}$964.39339, found 964.39332 . Anal. Calcd for: $C_{53}H_{56}AuN_3S$: C, (66.03); H, (5.86); N, (4.36). Found: C, (65.80); H, (5.69); N, (4.37).

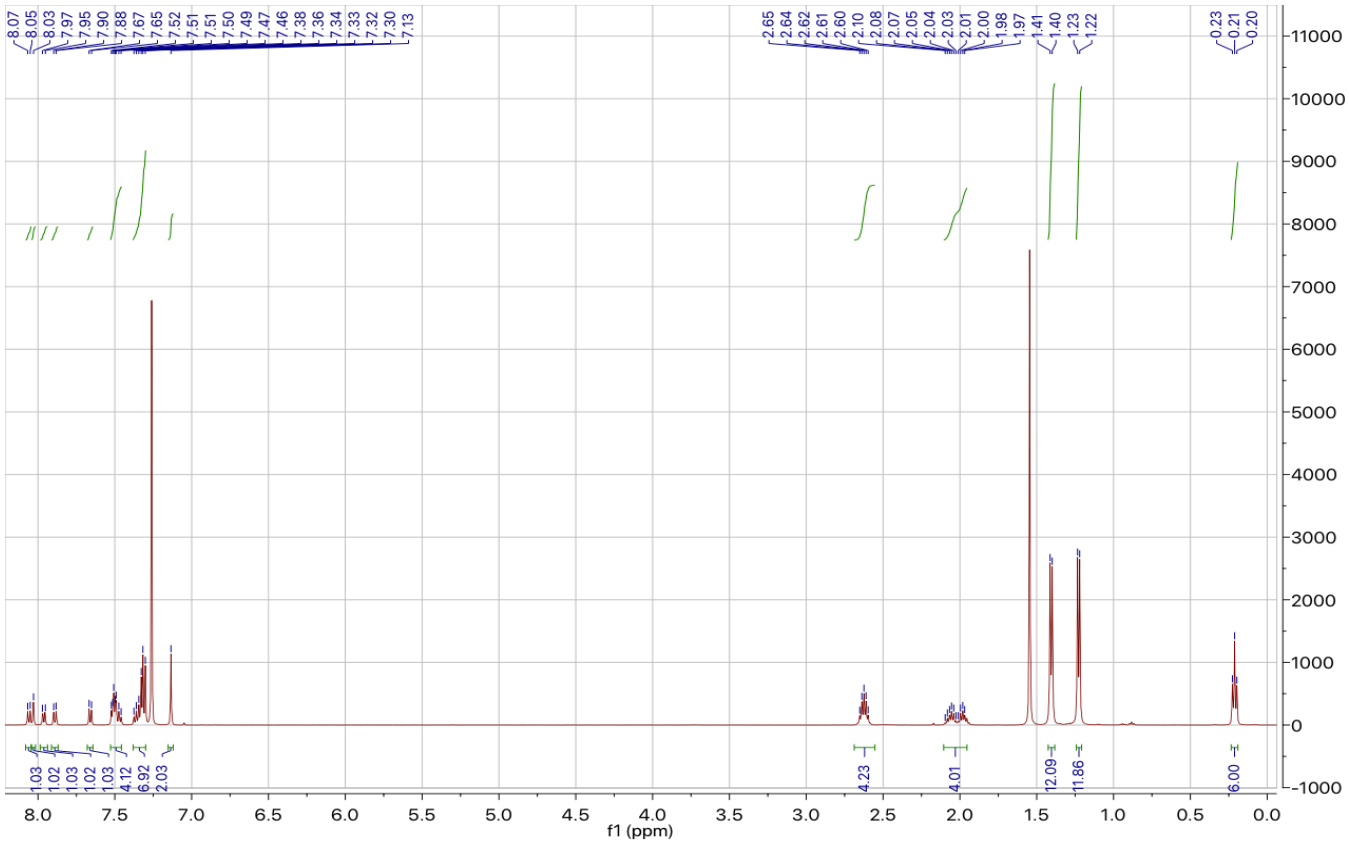


**Figure 3.11**: $^{1}$H NMR Spectrum of **Au-ABTF2**

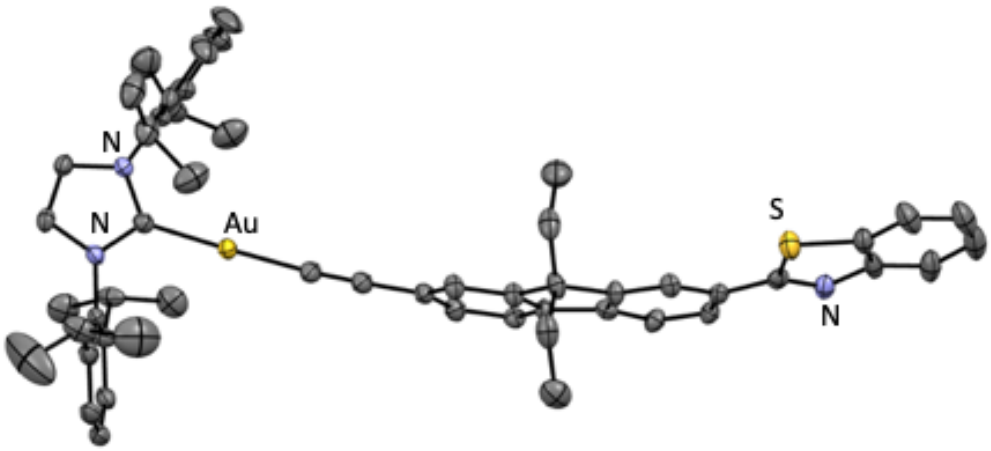


**Figure 3.12.** Thermal ellipsoid representation of **Au-ABTF2** (50% probability level, 150 K). Hydrogen atoms are omitted for clarity. Unlabeled atoms are carbon.

**ABTF1:**

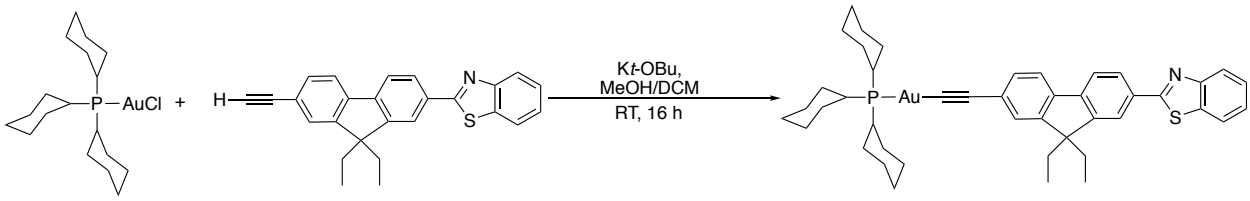


To a 20 mL scintillation vial equipped with a stir bar was added (24.1 mg, 0.215 mmol) of potassium *tert*-butoxide along with 4 mL of MeOH via syringe. The suspension was stirred until a solution was observed, after which (81.5 mg, 0.215 mmol) of BTF alkyne was added. Most didn't dissolve, so 3 mL of DCM was added creating a yellow solution. This solution was stirred at RT for 45 min and then transferred to another 20 mL scintillation vial containing 2 mL of MeOH and (100 mg, 0.195 mmol) $Cy_3PAuCl$, creating a yellow/brown solution. This solution was stirred in the absence of light for 16 h and then concentrated *in vacuo*. The brown/yellow solid was dissolved in dichloromethane, filtered over Celite, concentrated, and washed with (4 x 25 mL) of pentanes. The brown solid was allowed to dry and then subjected to crystallization via slow diffusion of pentanes into a concentrated dichloromethane solution yielding 100 mg of analytically pure material. (Yield 60 %). $^1$H NMR (500 MHz, Chloroform-*d*) δ 8.10 – 8.05 (m, 2H), 8.00 (dd, *J* = 7.9, 1.7 Hz, 1H), 7.91 (d, *J* = 8.0 Hz, 1H), 7.73 (d, *J* = 7.9 Hz, 1H), 7.62 (d, *J* = 7.8 Hz, 1H), 7.55 – 7.45 (m, 3H), 7.40 – 7.35 (m, 1H), 2.18 – 1.96 (m, 13H), 1.86 (d, *J* = 11.0 Hz, 7H), 1.75 (s, 2H), 1.50 (d, *J* = 12.7 Hz, 7H), 1.29 (t, *J* = 11.7 Hz, 9H), 0.30 (t, *J* = 7.3 Hz, 6H).$^{31}$P NMR (121 MHz, $CDCl_3$) δ (ppm): 56.41. HRMS (FT-ICR, $[M+H]^+$) m/z calcd for $MH^+C_{44}H_{54}AuNPS^+$856.33746, found 856.33733. Anal. Calcd for: $C_{44}H_{53}AuNPS$: C, (61.74); H, (6.24); N, (1.64). Found: C, (61.48); H, (6.07); N, (1.79).

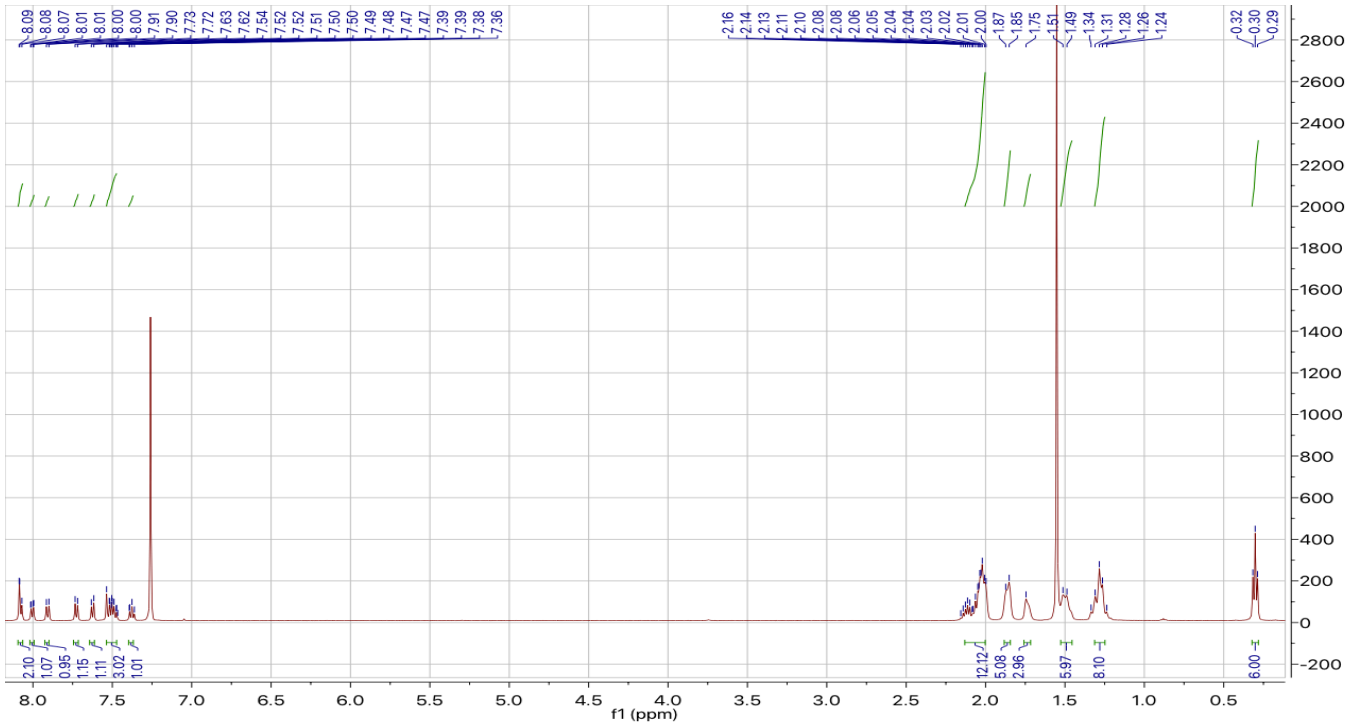


**Figure 3.13.** $^{1}$H NMR Spectrum of **Au-ABTF1**

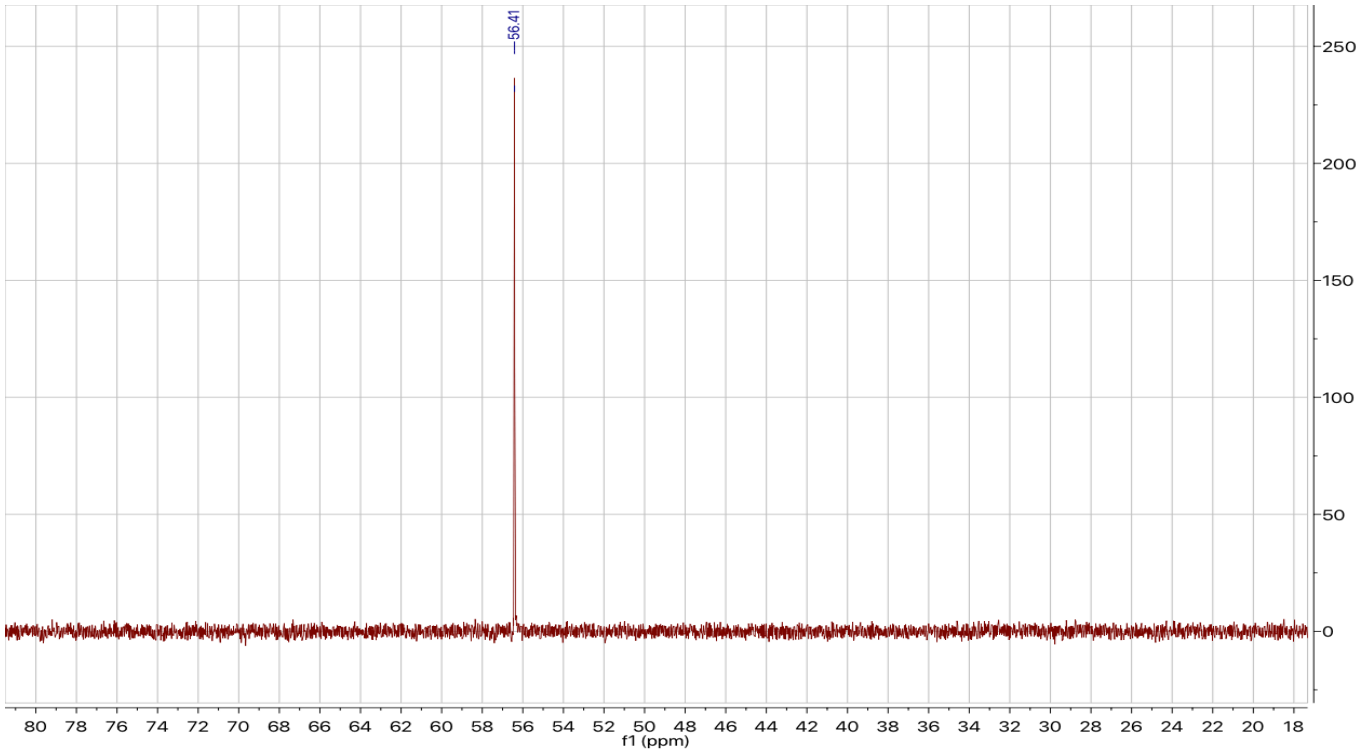


**Figure 3.14.** $^{31}$P{$^{1}$H} NMR Spectrum of **Au-ABTF1**

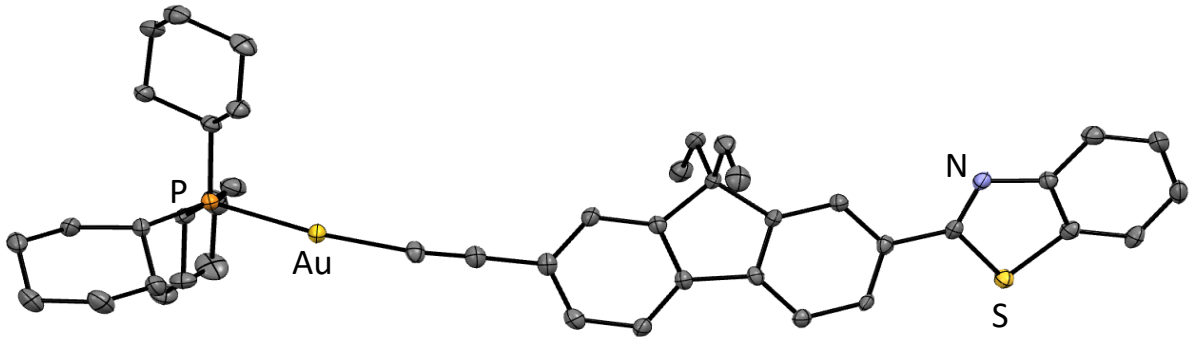


**Figure 3.15.** Thermal ellipsoid representation of **Au-ABTF1** (50% probability level, 150 K). Hydrogen atoms are omitted for clarity. Unlabeled atoms are carbon.

**Au-ABTF0:**

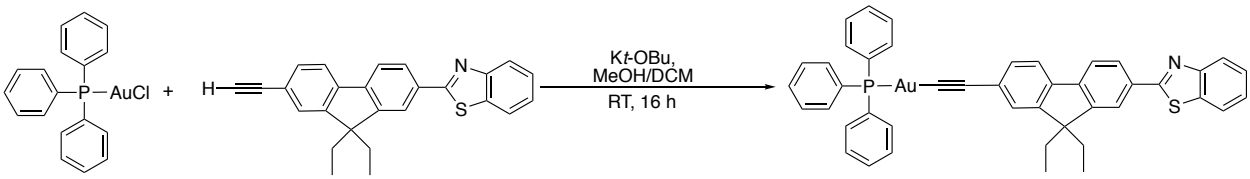


To a 20 mL scintillation vial equipped with a stir bar was added (29.5 mg, 0.263 mmol) of potassium *tert*-butoxide along with 4 mL of MeOH via syringe. The suspension was stirred until a solution was observed, after which (99.6 mg, 0.263 mmol) of BTF alkyne was added. Most didn't dissolve, so 3 mL of DCM was added creating a yellow solution. This solution was stirred at RT for 45 min and then transferred to another 20 mL scintillation vial containing 2 mL of MeOH and (100 mg, 0.202 mmol) $Ph_3AuCl$, creating a yellow/brown solution. This solution was stirred in the absence of light for 16 h and then concentrated *in vacuo*. The brown/yellow solid was dissolved in dichloromethane, filtered over Celite, concentrated, and washed with (4 x 25 mL) of pentanes. The brown solid was allowed to dry and then subjected to crystallization via slow diffusion of pentanes into a concentrated dichloromethane solution yielding 135 mg of analytically pure material. (Yield

79 %). $^{1}$H NMR (500 MHz, Chloroform-*d*) δ 8.11 – 8.06 (m, 2H), 8.01 (dd, *J* = 7.9, 1.7 Hz, 1H), 7.91 (d, *J* = 7.8 Hz, 1H), 7.74 (d, *J* = 7.9 Hz, 1H), 7.65 (d, *J* = 7.8 Hz, 1H), 7.62 – 7.43 (m, 18H), 7.42 – 7.35 (m, 1H), 2.09 (m, *J* = 28.5, 7.0 Hz, 4H), 0.32 (t, *J* = 7.3 Hz, 6H). $^{31}$P NMR (121 MHz, $CDCl_3$) δ (ppm): 42.35. HRMS (FT-ICR, $[M+H]^+$) m/z calcd for $MH^+C_{44}H_{36}AuNPS^+$, 838.19661 found 838.19670. Anal. Calcd for: $C_{44}H_{35}AuNPS$: C, (63.08); H, (4.21); N, (1.67). Found: C, (62.97); H, (4.25); N, (1.72).

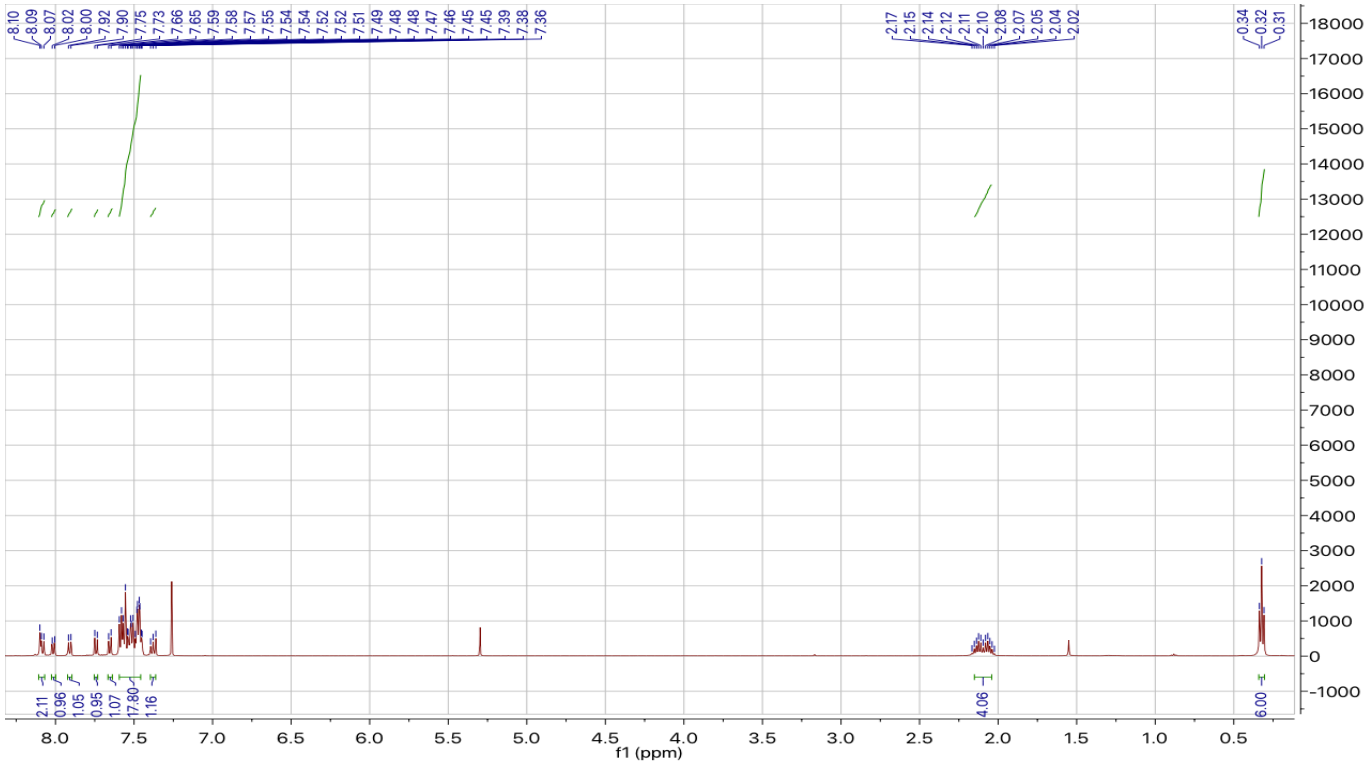


**Figure 3.16.** $^{1}$H NMR Spectrum of **Au-ABTF0**

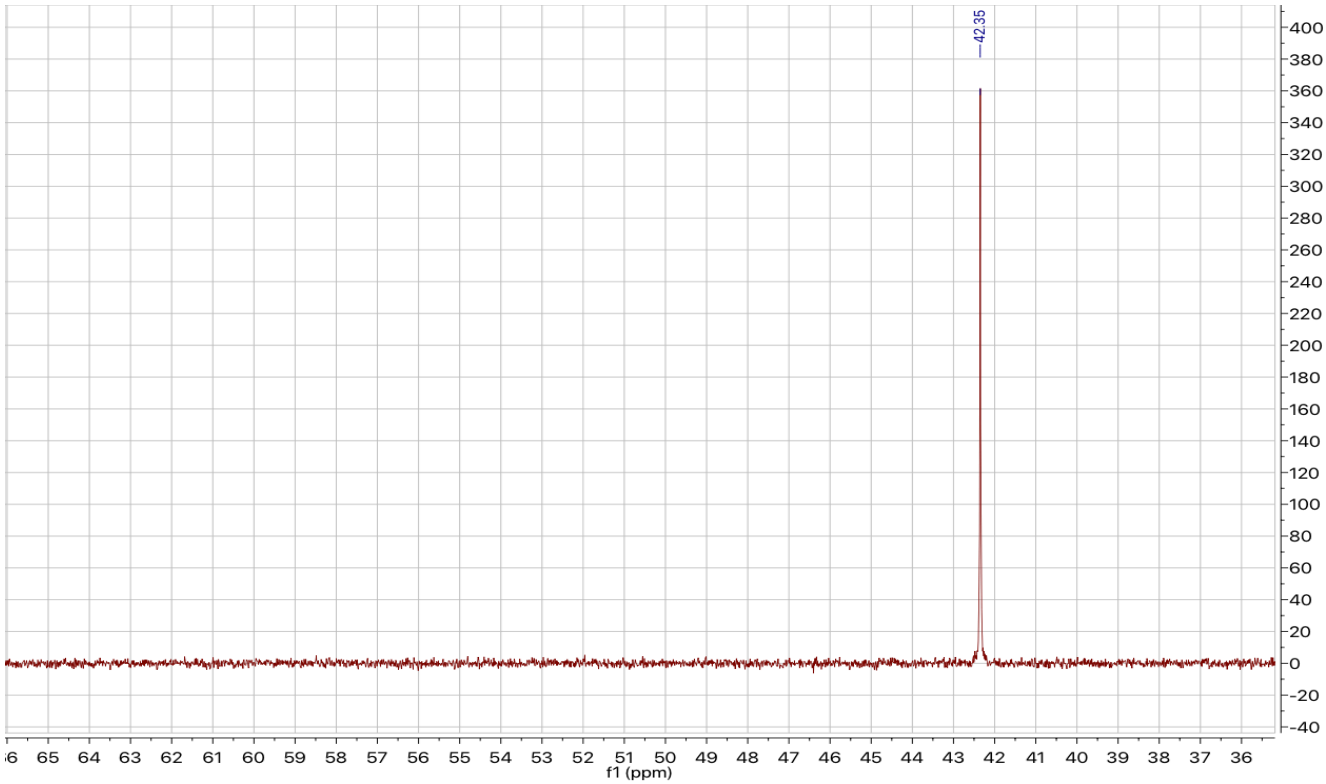


**Figure 3.17.** $^{31}P\{^{1}H\}$ NMR of **Au-ABTF0**

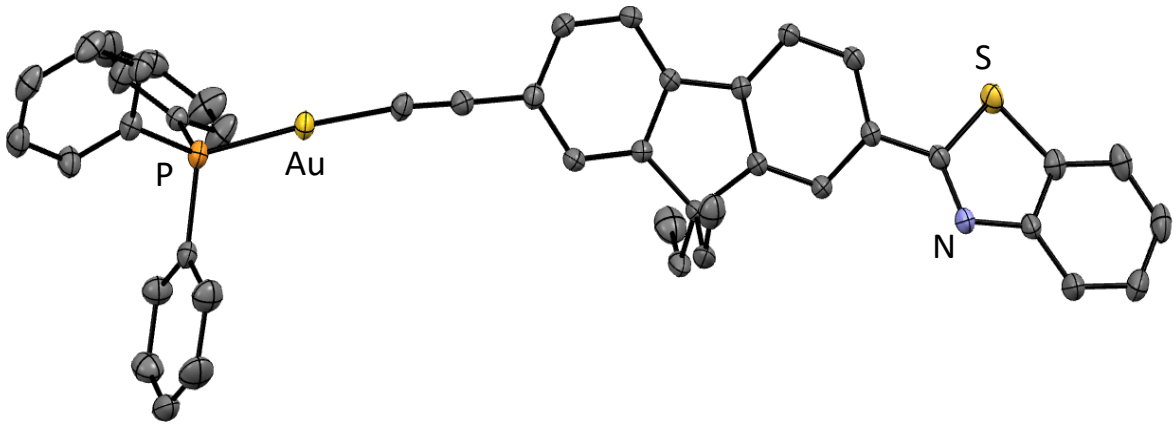


**Figure 3.18.** Thermal ellipsoid representation of **Au-ABTF0** (50% probability level, 150 K). Hydrogen atoms are omitted for clarity. Unlabeled atoms are carbon.

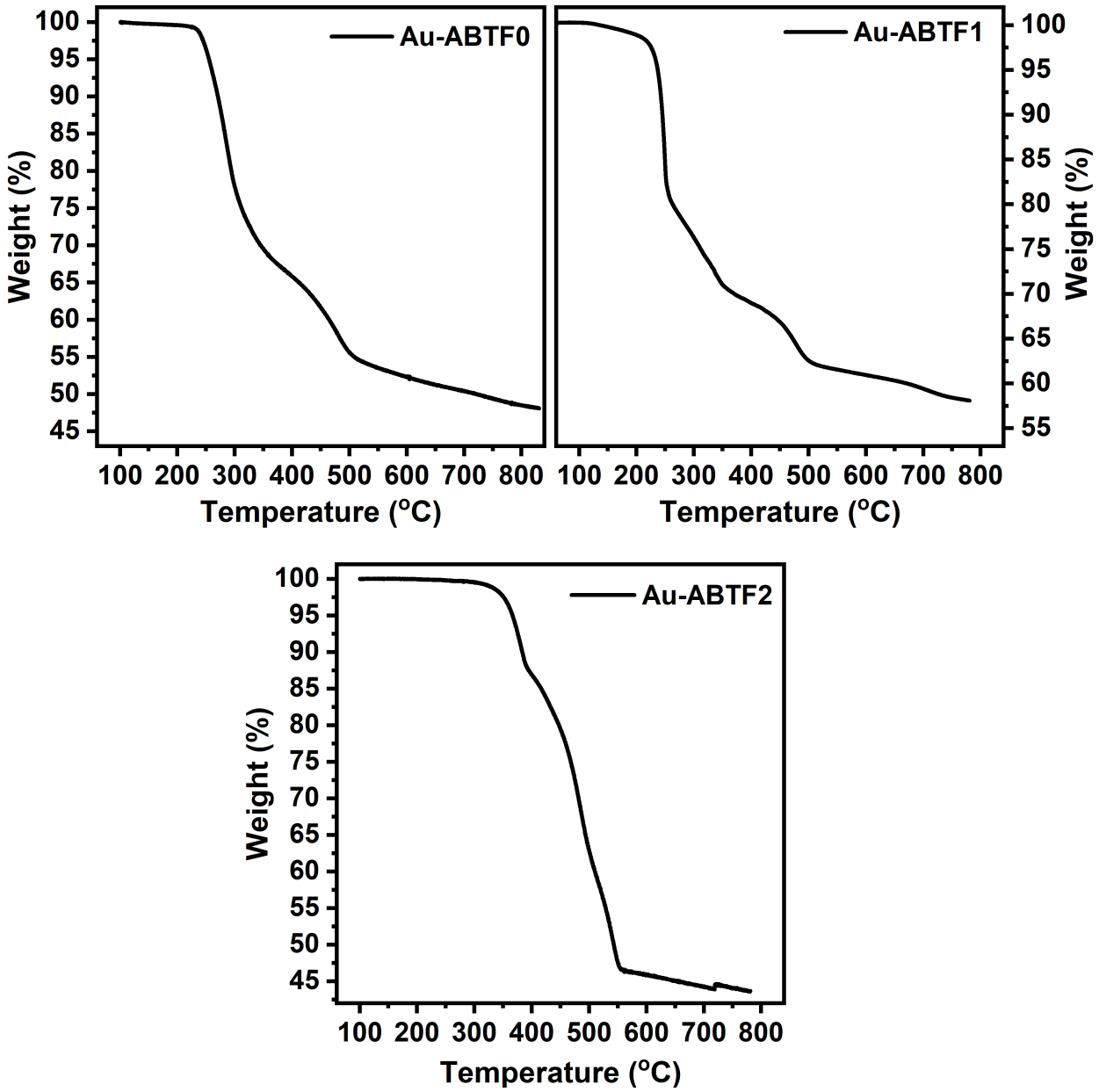


**Figure 3.19.** Thermogravimetric Analysis of **Au-ABTF0** (top left), **Au-ABTF1** (top right), **Au-ABTF2** (bottom center).

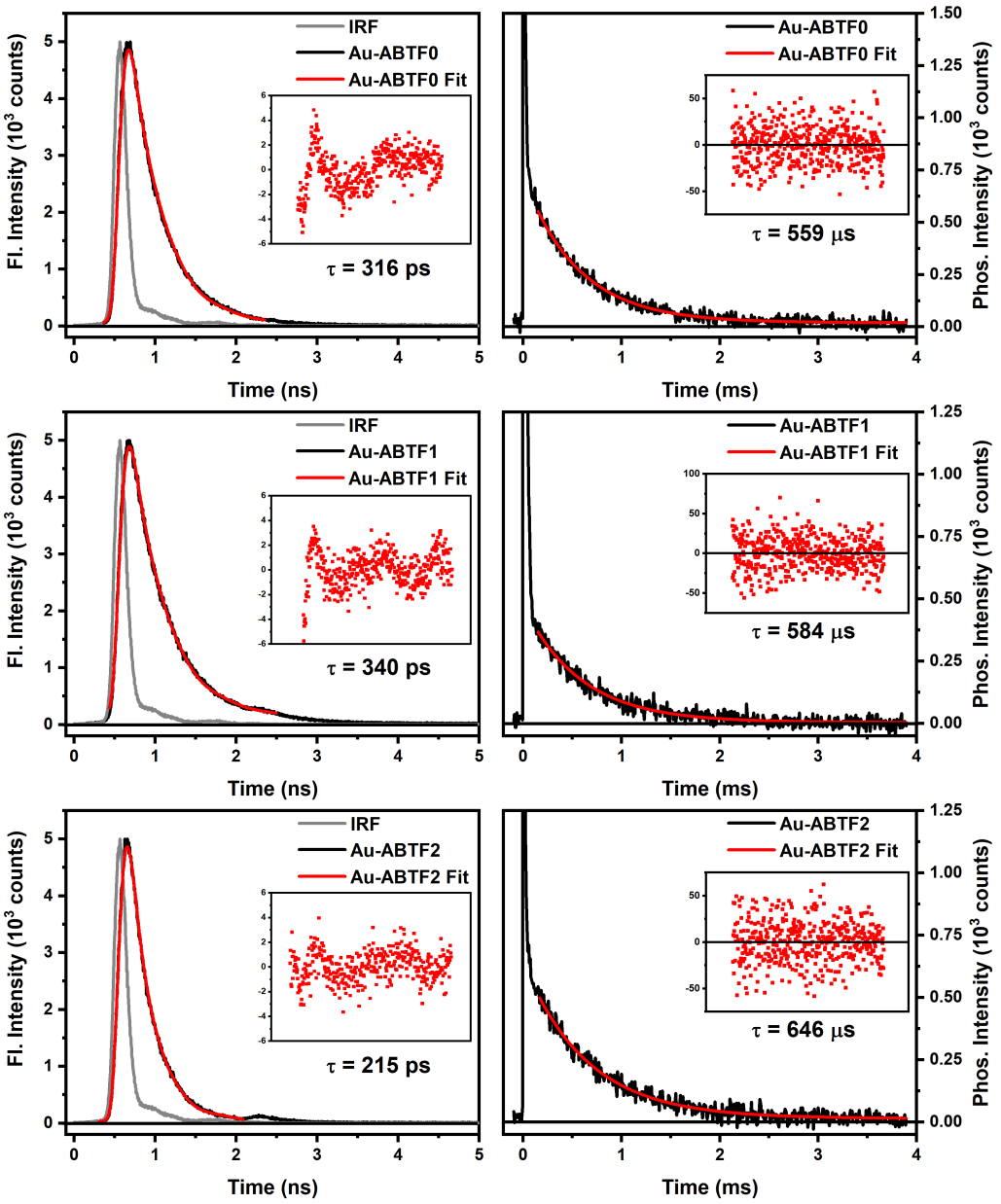


**Figure 3.20.** Fluorescence Lifetimes with IRF (Left) and Phosphorescence Lifetimes (Right) of **Au-ABTF0** (Top), **Au-ABTF1** (Middle), and **Au-ABTF2** (Bottom). All lifetime values were collected in toluene. The fluorescence lifetimes were fit using the reconvolution fit provided by Edinburgh Instruments. The phosphorescence lifetimes were obtained following three freeze-pump-thaw degas cycles and fit using a monoexponential decay equation in Origin. Residuals for all fits are provided in the inset. Table 3.1 summarizes the lifetime averages of duplicate trials.

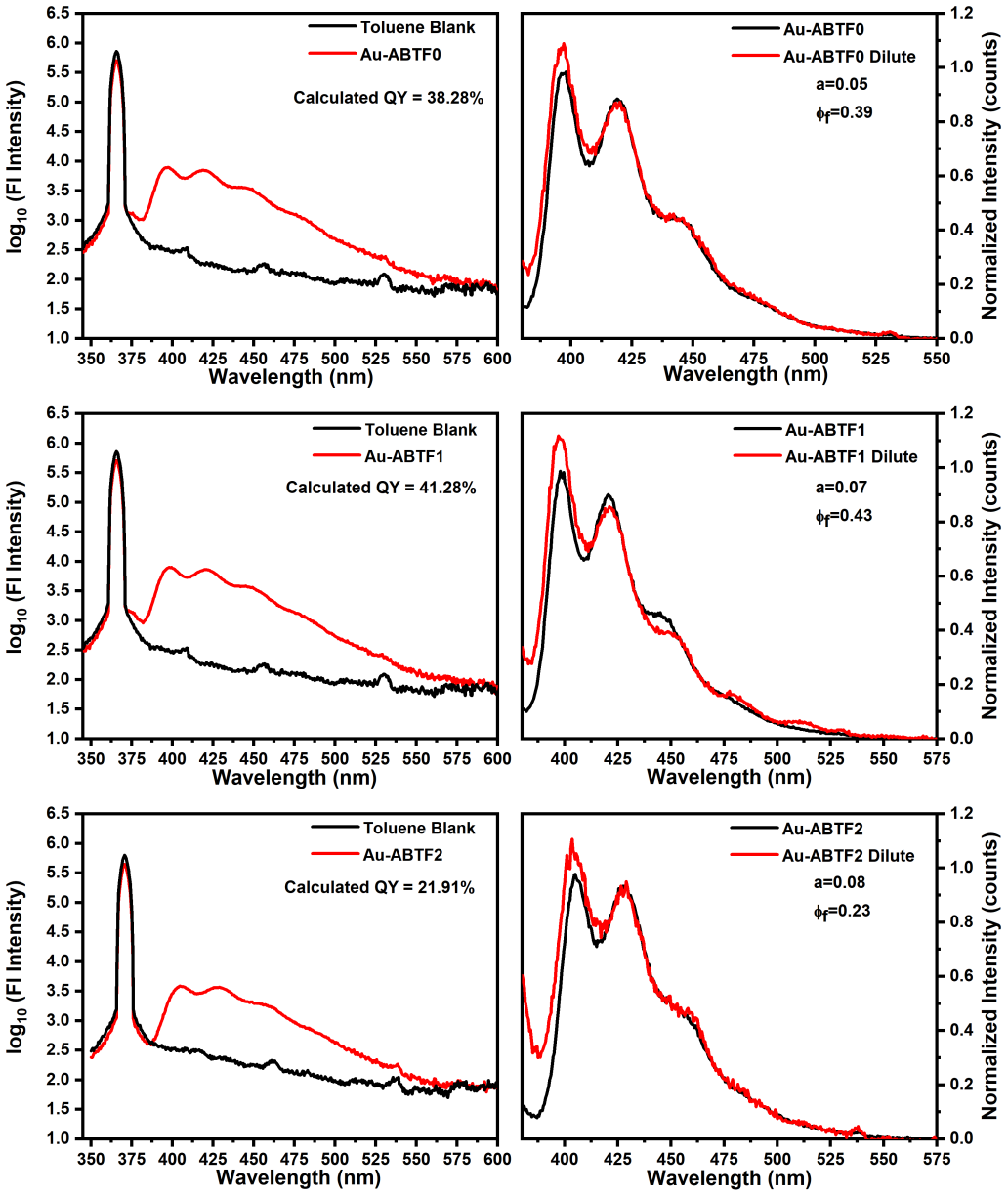


**Figure 3.21.** Raw (Left) and Corrected (Right) Fluorescence Quantum Yields of **Au-ABTF0** (Top), **Au-ABTF1** (Middle), and **Au-ABTF2** (Bottom). Fluorescence quantum yield values were collected in toluene. The dilute samples used for the reabsorption correction were a one tenth serial dilution of the concentrated samples. The experiments were performed in duplicate with the average value reported in Table 3.1.

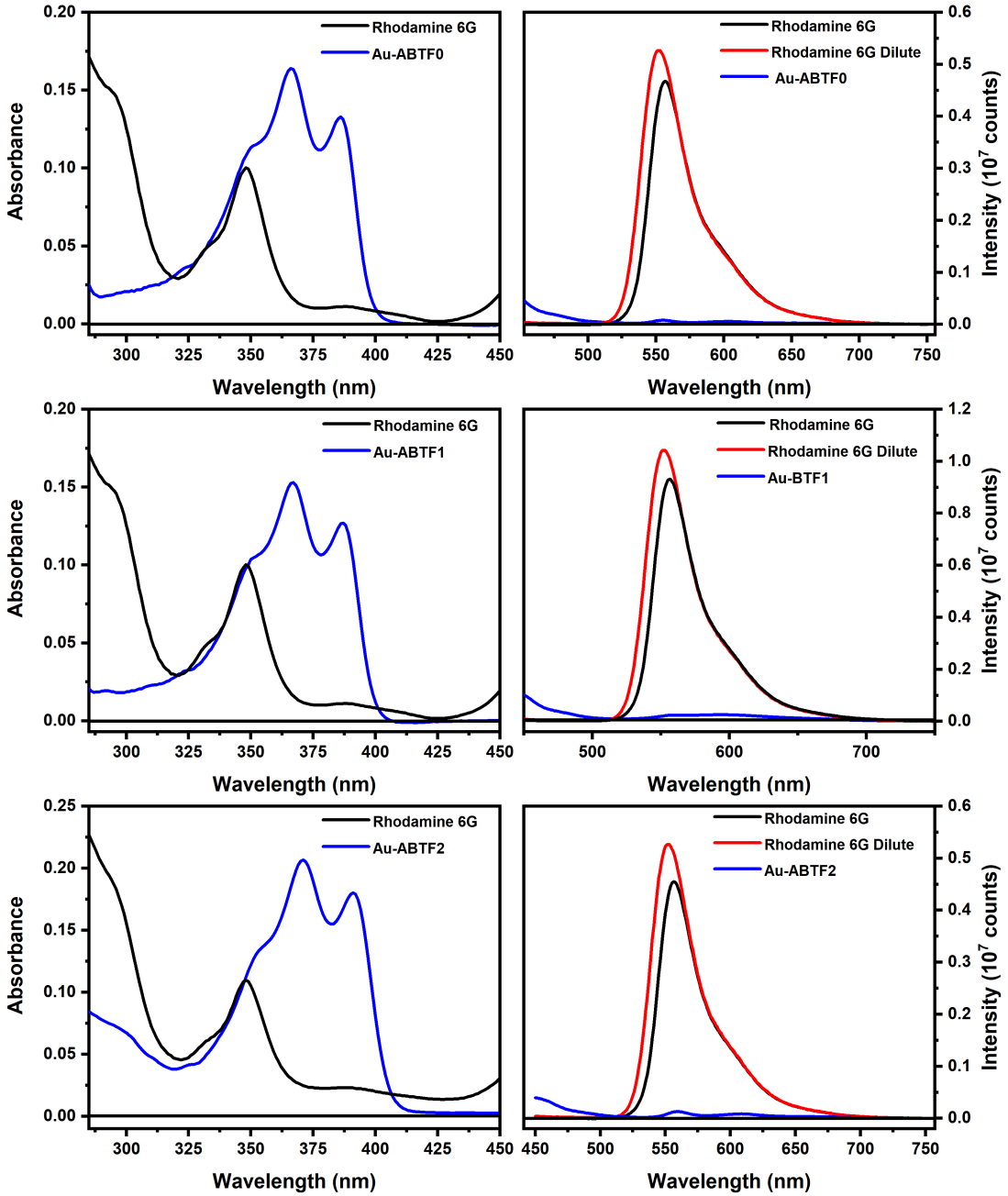


**Figure 3.22.** Ground State Absorption (Left) and Luminescence Emission (Right) of reference Rhodamine 6G and **Au-ABTF0** (Top), **Au-ABTF1** (Middle), and **Au-ABTF2** (Bottom) for Phosphorescence Quantum Yields. Au-ABTF samples were collected in toluene and Rhodamine 6G was collected in ethanol. All experiments were performed in duplicate with average values reported in Table 3.1.

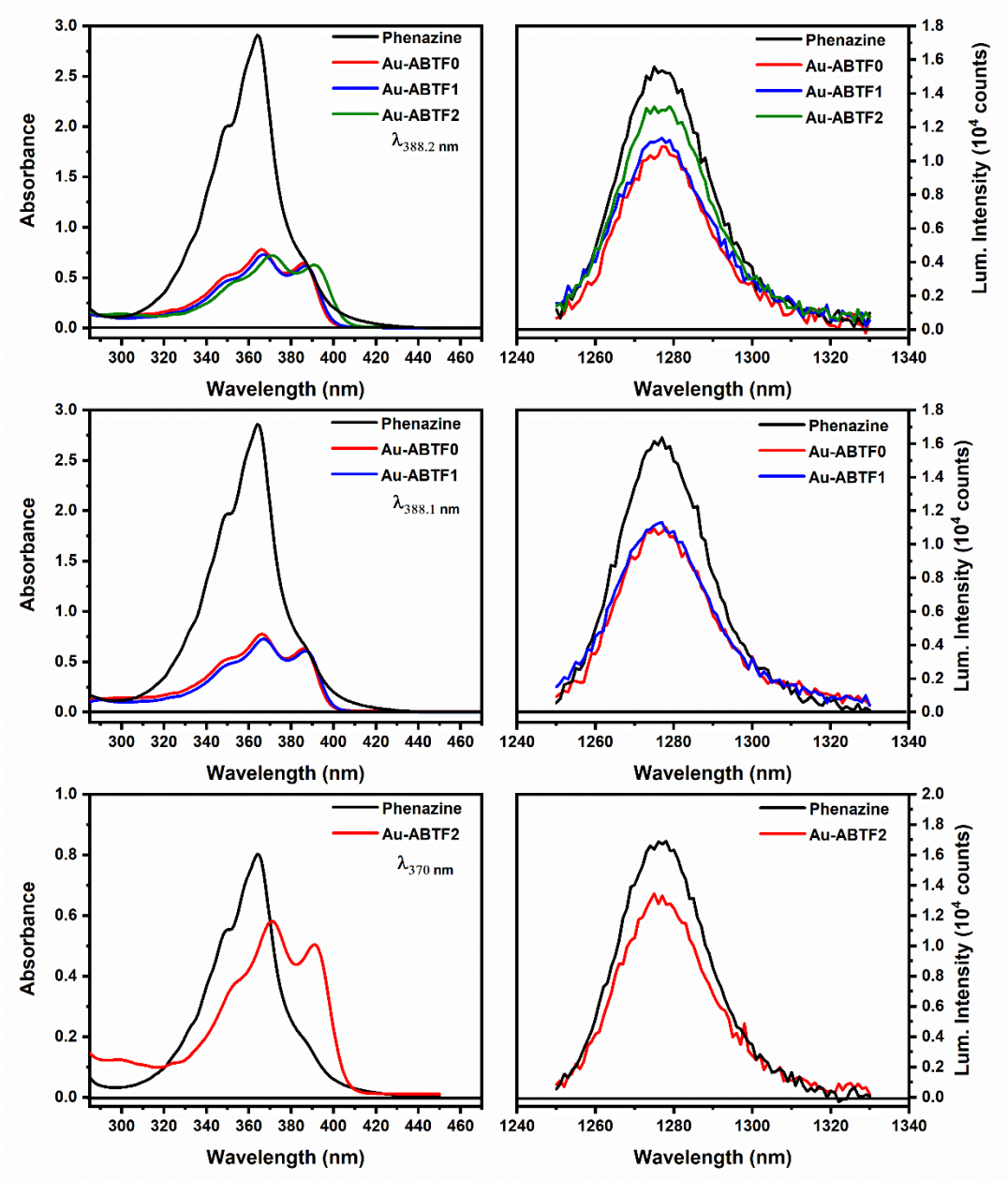


**Figure 3.23.** Ground State Absorption (Left) and Singlet Oxygen Emission (Right). The top figures portray trial one of all samples, the middle figures portray trial two of **Au-ABTF0** and **Au-ABTF1**, and the bottom figures portray trial two of **Au-ABTF2**. All experiments were performed in toluene using phenazine as a reference. The average triplet quantum yield is reported in Table 3.1.

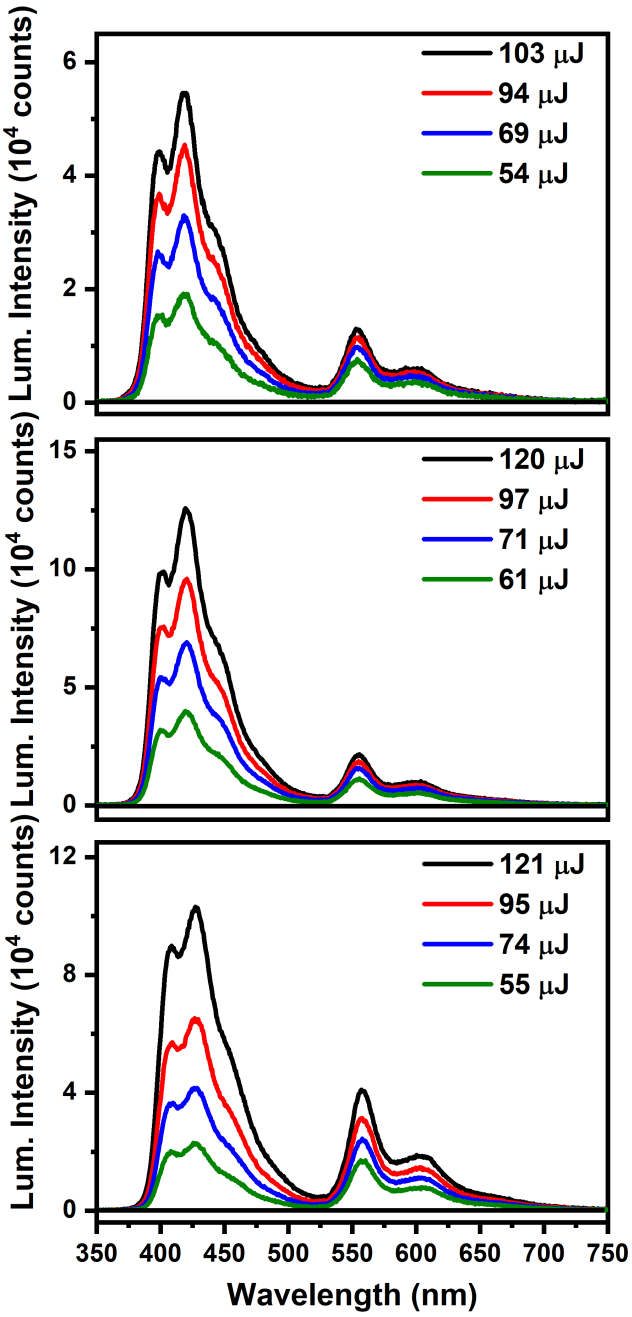


**Figure 3.24.** Delayed Fluorescence of **Au-ABTF0** (Top), **Au-ABTF1** (Middle), and **Au-ABTF2** (Bottom). The experiments were performed in freeze-pump-thaw degassed toluene solutions. Spectra were collected using 355 nm excitation, a 50 μs bandwidth, and a 99 μs gate width on the Andor iStar ICCD camera.

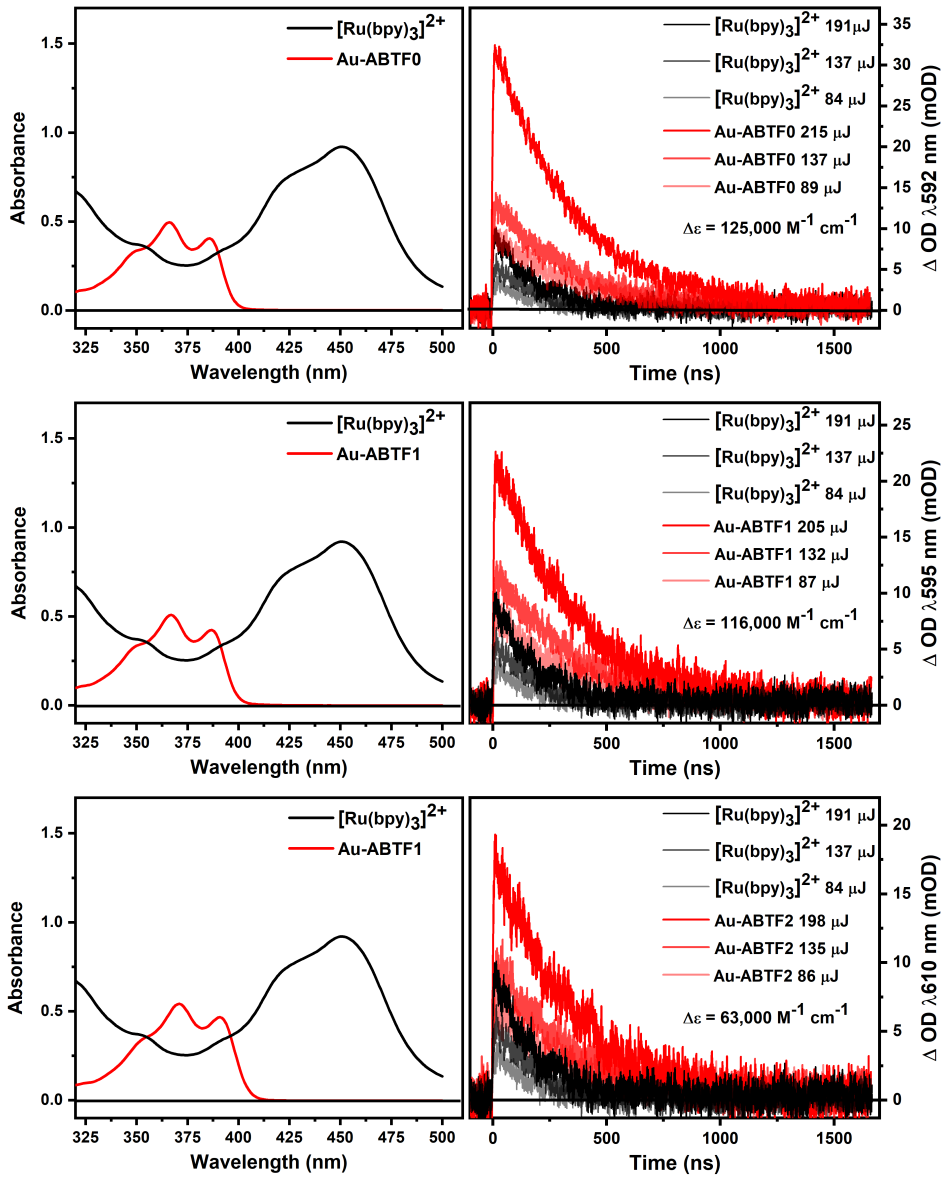


**Figure 3.25.** Ground State Absorption (Left) and Excited State Decay Traces at Three Laser Excitation Energies of **Au-ABTF0** (Top), **Au-ABTF1** (Middle), and **Au-ABTF2** (Bottom) in Toluene. $[Ru(bpy)_3]^{2+}$ dissolved in acetonitrile was used as the actinometer. 370 nm was used as the detection wavelength for $[Ru(bpy)_3]^{2+}$ samples. Au-ABTF data was collected in toluene and the transient absorption signal was monitored at the maximum of the triplet-triplet absorption in each sample. All experiments were performed in aerated solutions with 355 nm excitation and fit to monoexponential fits in Origin. The average of two trials is reported in Table 3.1.

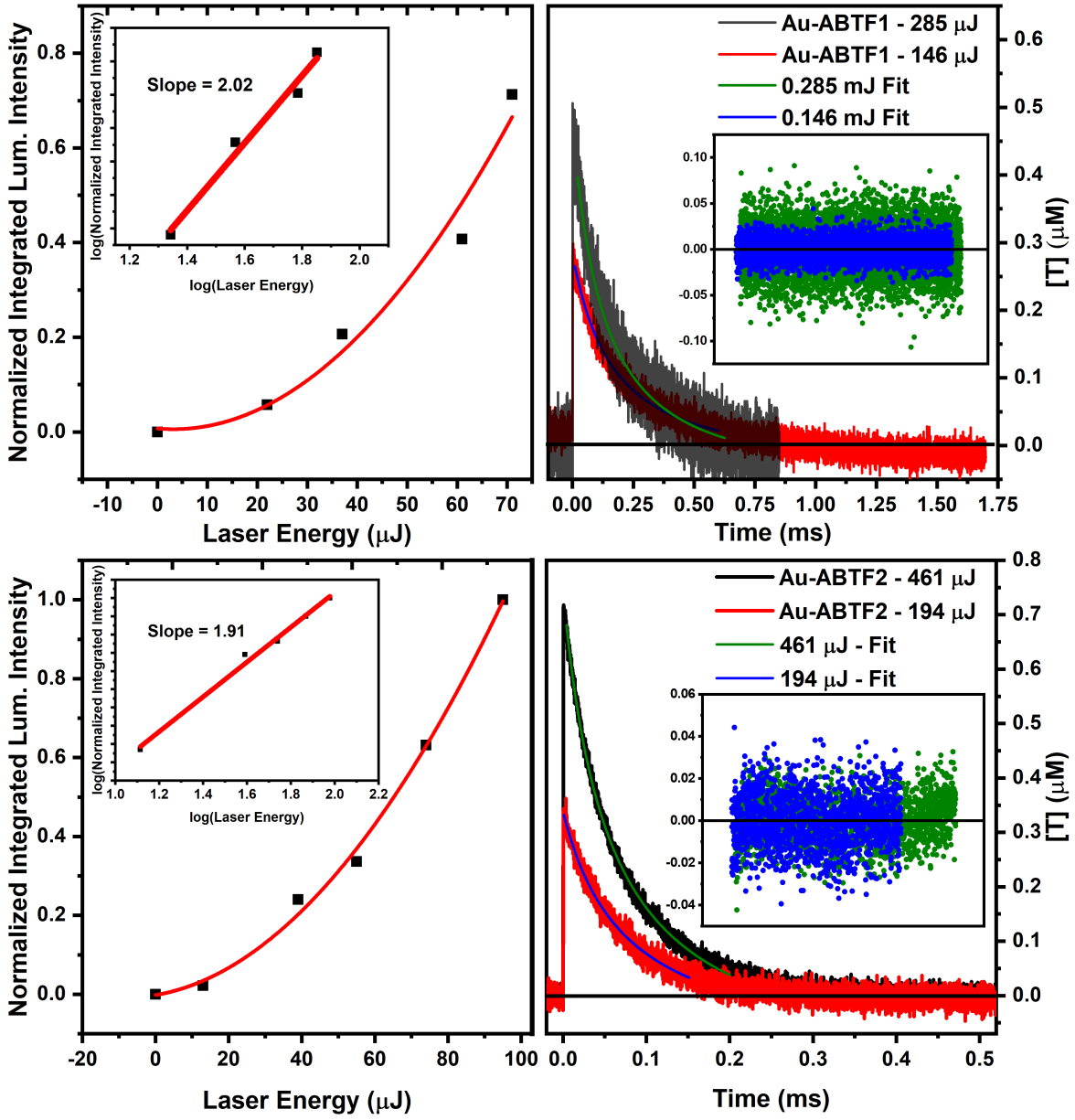


**Figure 3.26.** Fits of the Normalized Integrated Fluorescence Intensity vs. Laser Pulse Energy (Left) and Triplet Triplet Annihilation Fitting of Excited-State Decay Traces of **Au-ABTF1** (Top) and **Au-ABTF2** (Bottom). Experiments were performed in freeze-pump-thaw deaerated solutions. The insets represent the double logarithm plot (Left) and residuals of the fit data (Right). Au-ABTF1 285 μJ kinetic data is shown at 25% transparency for clarity.

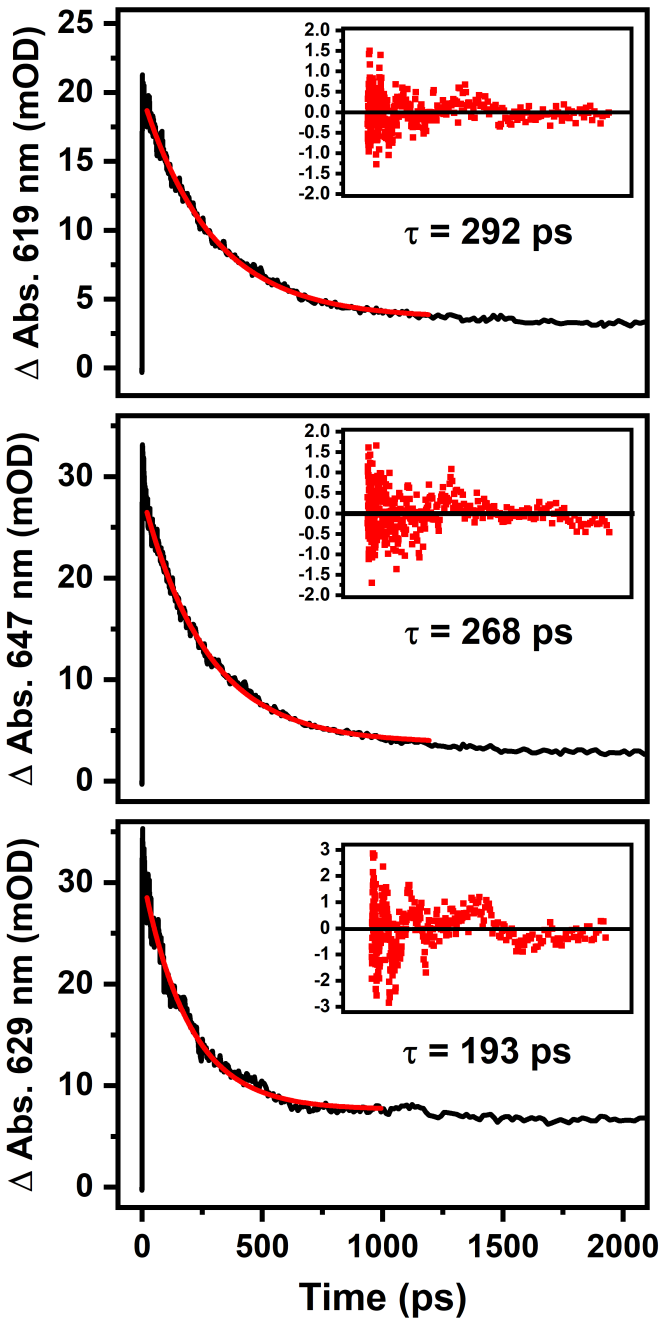


**Figure 3.27.** Ultrafast Transient Absorption Decay Trace for **Au-ABTF0** (Top), **Au-ABTF1** (Middle), and **Au-ABTF2** (Bottom) in Aerated Toluene. Lifetime values were collected in aerated toluene. Residuals of the fits are portrayed in the insets. Lifetimes reported in the figure represent the fit obtained from a single wavelength. The average lifetime value obtained from fits at ten wavelengths in the TA spectra is reported in Table 3.1.

**X-Ray Crystallography**

Single crystals of **Au-ABTF0**, **Au-ABTF1** and **Au-ABTF2** were selected under a stereomicroscope with polarizing filter and mounted with the aid of a trace of Fomblin oil on the goniometer head of a Bruker Quest diffractometer with a fixed chi angle, a sealed tube fine focus X-ray tube, single crystal curved graphite incident beam monochromator, a Photon100 CMOS area detector and an Oxford Cryosystems low temperature device. Examination and data collection were performed with Mo Kα radiation (λ = 0.71073 Å) at 150 K. Data were collected, reflections were indexed and processed, and the files scaled and corrected for absorption using APEX3. The space groups were assigned and the structures were solved by direct methods using XPREP within the SHELXTL suite of programs[4] and refined by full matrix least squares against $F^2$ with all reflections using Shelxl2018[5] using the graphical interface Shelxle.[6] If not specified otherwise H atoms attached to carbon atoms were positioned geometrically and constrained to ride on their parent atoms. C-H bond distances were constrained to 0.95 Å for aromatic moieties, and to 1.00, 0.99 and 0.98 Å for aliphatic C-H, $CH_2$ and $CH_3$ moieties, respectively. Methyl $CH_3$ H atoms were allowed to rotate but not to tip to best fit the experimental electron density. $U_{iso}$(H) values were set to a multiple of $U_{eq}$(C) with 1.5 for $CH_3$, $NH_3^+$ and OH, and 1.2 for C-H, $CH_2$, B-H, N-H and $NH_2$ units, respectively.

In Au-ABTF2, a solvate methylene chloride molecule was refined as partially occupied. The occupancy rate refined to 0.784(5).

Additional refinement details are given in the table, below.

Complete crystallographic data, in CIF format, have been deposited with the Cambridge Crystallographic Data Centre. CCDC 1953520-1953522 contains the supplementary crystallographic data for this paper. These data can be obtained free of charge from The Cambridge Crystallographic Data Centre via www.ccdc.cam.ac.uk/data_request/cif.

**Table 3.2.** Crystallography Experimental details

| | jjm_1_141_0m | jjm_1_145_0m | jjm_1_139_0m |
|---|---|---|---|
| Crystal data | | | |
| Chemical formula | $C_{44}H_{35}AuNPS$ | $C_{44}H_{53}AuNPS$ | $C_{53}H_{56}AuN_3S\cdot0.784(CH_2Cl_2)$ |
| $M_r$ | 837.72 | 855.87 | 1030.59 |
| Temperature (K) | 150 | 150 | 150 |
| Crystal system, space group | Triclinic, $P\bar{1}$ | Triclinic, $P\bar{1}$ | Orthorhombic, $P2_12_12_1$ |
| $a$, $b$, $c$ (Å) | 8.7524 (4), 13.6920 (6), 16.4993 (8) | 10.5754 (5), 14.0285 (7), 14.1291 (9) | 15.0586 (5), 17.6860 (7), 19.2675 (8) |
| α, β, γ (°) | 114.3972 (15), 90.4473 (18), 103.7777 (16) | 106.091 (2), 98.004 (2), 106.3596 (17) | 90, 90, 90 |
| $V$ (Å$^3$) | 1736.22 (14) | 1878.03 (18) | 5131.4 (3) |
| $Z$ | 2 | 2 | 4 |
| Radiation type | Mo $K\alpha$ | Mo $K\alpha$ | Mo $K\alpha$ |
| $F(000)$ | 832 | 868 | 2092 |
| $D_x$ (Mg m$^{-3}$) | 1.602 | 1.514 | 1.334 |
| No. of reflections for cell measurement | 9797 | 7259 | 9988 |
| θ range (°) for cell measurement | 3.1–30.6 | 2.9–28.3 | 2.9–32.0 |
| μ (mm$^{-1}$) | 4.38 | 4.05 | 3.03 |
| Crystal shape | Block | Plate | Block |
| Colour | Colourless | Colourless | Colourless |
| Crystal size (mm) | 0.24 × 0.17 × 0.16 | 0.09 × 0.08 × 0.02 | 0.21 × 0.17 × 0.11 |
| | | | |

| | | | |
|---|---|---|---|
| Data collection | | | |
| Diffractometer | Bruker AXS D8 Quest CMOS diffractometer | | |
| Radiation source | sealed tube X-ray source | | |
| Monochromator | Triumph curved graphite crystal | | |
| Scan method | ω and phi scans | | |
| Absorption correction | Multi-scan, SADABS 2016/2[7] | | |
| Radiation source | sealed tube X-ray source | | |
| $T_{min}$, $T_{max}$ | 0.650, 0.747 | 0.632, 0.746 | 0.647, 0.747 |
| No. of measured, independent and observed [$I > 2\sigma(I)$] reflections | 51677, 13091, 10286 | 26102, 8750, 7004 | 54147, 15987, 11944 |
| $R_{int}$ | 0.040 | 0.079 | 0.044 |
| θ values (°) | $\theta_{max}$ = 33.2, $\theta_{min}$ = 3.3 | $\theta_{max}$ = 28.3, $\theta_{min}$ = 3.0 | $\theta_{max}$ = 33.2, $\theta_{min}$ = 2.9 |
| $(\sin \theta/\lambda)_{max}$ (Å$^{-1}$) | 0.771 | 0.667 | 0.770 |
| Range of $h$, $k$, $l$ | $h$ = -13→13, $k$ = -20→20, $l$ = -25→25 | $h$ = -14→14, $k$ = -18→18, $l$ = -18→18 | $h$ = -18→20, $k$ = -20→25, $l$ = -24→29 |
| | | | |
| Refinement | | | |
| Refinement on | $F^2$ | | |
| $R[F^2 > 2\sigma(F^2)]$, $wR(F^2)$, $S$ | 0.032, 0.058, 1.01 | 0.034, 0.074, 1.04 | 0.032, 0.057, 0.95 |
| No. of reflections | 13091 | 8750 | 15987 |
| No. of parameters | 435 | 435 | 561 |
| No. of restraints | 0 | | |
| H-atom treatment | H-atom parameters constrained | | |
| Weighting scheme | $w = 1/[\sigma^2(F_o^2) + (0.0192P)^2 + 1.2299P]$ where $P = (F_o^2 + 2F_c^2)/3$ | $w = 1/[\sigma^2(F_o^2) + (0.0242P)^2 + 0.4044P]$ where $P = (F_o^2 + 2F_c^2)/3$ | $w = 1/[\sigma^2(F_o^2) + (0.0111P)^2]$ where $P = (F_o^2 + 2F_c^2)/3$ |
| $(\Delta/\sigma)_{max}$ | 0.003 | 0.001 | 0.003 |
| $\Delta\rho_{max}$, $\Delta\rho_{min}$ (e Å$^{-3}$) | 2.40, -1.58 | 1.95, -0.99 | 2.05, -0.93 |
| Absolute structure | – | – | Flack x determined using 4436 quotients [(I+)-(I-)]/[(I+)+(I-)][8] |

| | | | |
|---|---|---|---|
| Absolute structure parameter | – | – | -0.013 (3) |

Computer programs: Apex3 v2016.9-0 (Bruker, 2016), *SAINT* V8.37A (Bruker, 2016), *SHELXS97*[4], *SHELXL2018*/3[5], SHELXLE Rev900[6].

**Calculations**

Spin-restricted and time-dependent density-functional theory computations proceeded in Gaussian16 rev. A.03.[9] Geometries were optimized with the 6-31G(d) basis set for nonmetal atoms and the Stuttgard-Dresden effective core potential and basis set for Au.[10] Optimizations proceeded without constraints, and harmonic frequency calculations found all real vibrational frequencies, confirming that converged structures are local energy minima. Final single-point calculations employed the exchange and correlation functionals of Perdew, Burke, and Ernzerhof (PBE0),[11] and the TZVP basis set of Godbelt, Andzelm, and co-workers for nonmetals.[12] For metal atoms, the Stuttgart-Dresden effective core potential and basis set were used; scalar relativistic effects are included implicitly. Continuum solvation in toluene was imposed using the integral equation formalism of the polarizable continuum model.[13-16] Population analyses were performed with the AOMix-CDA program of Gorelsky.[17,18]

**Table 3.3. AuABTF0:** Summary of calculated electronic transitions to Franck-Condon <u>singlet</u> states.

HOMO = 178; LUMO = 179

| # | nm | 1000 cm-1 | eV | f | Assignment |
|---|---|---|---|---|---|
| 1 | 392.8 | 25.46 | 3.156 | 1.9462 | 178->179(97.5%) |
| 2 | 316.5 | 31.59 | 3.917 | 0.0003 | 178->181(94.2%) |
| 3 | 315.6 | 31.68 | 3.928 | 0.0287 | 178->180(93.5%) |
| 4 | 302.4 | 33.07 | 4.100 | 0.0001 | 176->179(81.8%) 176->183(11.3%) |
| 5 | 301.1 | 33.21 | 4.118 | 0.0840 | 177->179(80.8%) 175->179(12.3%) |
| 6 | 297.6 | 33.60 | 4.166 | 0.0256 | 175->179(37.2%) 178->186(14.3%) 177->179(13.1%) 178->183(11.3%) |
| 7 | 294.1 | 34.00 | 4.216 | 0.0435 | 175->179(38.7%) 178->183(21.8%) 178->186(11.8%) |
| 8 | 290.7 | 34.40 | 4.265 | 0.0001 | 178->182(97.3%) |
| 9 | 287.5 | 34.78 | 4.313 | 0.1121 | 178->183(46.3%) 174->179(21.0%) 178->187(11.0%) |

| | | | | | |
|---|---|---|---|---|---|
| 10 | 281.4 | 35.54 | 4.406 | 0.0813 | 174->179(45.4%) 172->179(17.9%) 178->183(11.2%) |
| 11 | 276.9 | 36.11 | 4.478 | 0.0002 | 178->184(97.2%) |
| 12 | 275.4 | 36.31 | 4.502 | 0.0001 | 178->185(74.7%) 178->189(15.3%) |
| 13 | 264.1 | 37.87 | 4.695 | 0.0470 | 172->179(46.4%) 178->186(36.9%) |
| 14 | 262.0 | 38.17 | 4.732 | 0.0134 | 178->187(66.4%) 178->186(18.1%) |
| 15 | 256.7 | 38.95 | 4.829 | 0.0024 | 176->180(44.6%) 164->179(42.8%) |
| 16 | 256.4 | 39.00 | 4.835 | 0.0014 | 164->179(47.9%) 176->180(39.7%) |
| 17 | 256.0 | 39.06 | 4.843 | 0.0102 | 178->188(64.2%) |
| 18 | 255.5 | 39.13 | 4.852 | 0.0722 | 176->181(63.8%) 178->188(11.1%) |
| 19 | 253.6 | 39.43 | 4.888 | 0.0647 | 173->179(72.2%) 173->180(19.8%) |
| 20 | 253.5 | 39.44 | 4.891 | 0.0001 | 178->189(56.6%) 178->185(20.6%) 177->181(14.0%) |
| 21 | 249.5 | 40.08 | 4.969 | 0.0811 | 177->180(75.0%) 176->181(14.2%) |
| 22 | 247.6 | 40.38 | 5.006 | 0.0181 | 177->181(71.9%) 178->189(14.6%) |
| 23 | 246.8 | 40.53 | 5.025 | 0.1286 | 173->181(83.5%) |
| 24 | 245.0 | 40.81 | 5.060 | 0.0227 | 171->179(81.9%) |
| 25 | 244.3 | 40.93 | 5.074 | 0.0404 | 178->190(30.1%) 178->191(25.7%) 173->180(12.6%) |
| 26 | 244.1 | 40.97 | 5.079 | 0.1327 | 173->180(57.8%) 173->179(14.3%) |
| 27 | 241.4 | 41.42 | 5.135 | 0.0096 | 173->182(30.6%) 169->180(15.8%) 168->181(15.1%) |
| 28 | 240.9 | 41.51 | 5.147 | 0.0166 | 178->190(25.1%) 178->191(24.7%) 177->183(12.7%) |
| 29 | 239.8 | 41.70 | 5.170 | 0.0001 | 176->183(67.2%) |
| 30 | 238.3 | 41.96 | 5.202 | 0.0006 | 176->182(91.8%) |
| 31 | 235.6 | 42.44 | 5.262 | 0.0158 | 175->180(65.7%) 175->183(11.8%) |
| 32 | 235.5 | 42.46 | 5.264 | 0.0086 | 170->179(69.4%) 170->180(11.4%) |
| 33 | 234.7 | 42.61 | 5.282 | 0.0023 | 177->182(23.4%) 168->181(10.2%) |
| 34 | 234.6 | 42.62 | 5.284 | 0.0418 | 177->183(57.0%) 178->190(13.1%) |
| 35 | 234.2 | 42.70 | 5.294 | 0.0130 | 168->180(12.7%) 173->185(12.5%) 169->181(12.1%) 167->181(11.5%) |
| 36 | 233.5 | 42.83 | 5.310 | 0.0015 | 177->182(68.7%) |
| 37 | 233.2 | 42.88 | 5.317 | 0.0000 | 175->181(98.9%) |
| 38 | 232.2 | 43.07 | 5.340 | 0.0002 | 178->193(72.7%) 177->193(12.1%) |
| 39 | 231.5 | 43.21 | 5.357 | 0.0045 | 178->192(77.6%) |
| 40 | 230.1 | 43.46 | 5.388 | 0.0116 | 175->180(19.5%) 177->187(16.9%) 175->183(16.0%) 177->186(12.3%) |

**Table 3.4. AuABTF0:** Summary of calculated electronic transitions to Franck-Condon triplet states.

HOMO = 178; LUMO = 179

| # | nm | 1000 cm-1 | eV | f | Assignment |
|---|---|---|---|---|---|
| 1 | 559.9 | 17.86 | 2.214 | 0.0000 | 178->179(78.6%) |
| 2 | 430.4 | 23.24 | 2.881 | 0.0000 | 177->179(46.0%) 178->183(23.0%) |
| 3 | 363.8 | 27.49 | 3.408 | 0.0000 | 175->179(38.3%) |
| 4 | 353.4 | 28.30 | 3.509 | 0.0000 | 173->180(18.4%) 169->182(11.3%) |
| 5 | 353.3 | 28.30 | 3.509 | 0.0000 | 173->181(19.2%) 168->182(11.1%) |
| 6 | 352.1 | 28.40 | 3.522 | 0.0000 | 166->181(13.3%) 165->180(11.3%) 167->182(10.4%) |
| 7 | 332.5 | 30.08 | 3.729 | 0.0000 | 175->179(25.8%) 178->186(16.4%) 171->179(10.1%) |

| | | | | | |
|---|---|---|---|---|---|
| 8 | 327.5 | 30.54 | 3.786 | 0.0000 | 178->187(19.5%) 178->186(13.0%) |
| 9 | 325.8 | 30.70 | 3.806 | 0.0000 | 172->179(28.7%) 177->179(13.2%) 178->180(12.3%) |
| 10 | 320.1 | 31.24 | 3.873 | 0.0000 | 178->181(62.9%) 176->179(17.4%) |

**Table 3.5. AuABTF1:** Summary of calculated electronic transitions to Franck-Condon singlet states.

HOMO = 187; LUMO = 188

| # | nm | 1000 cm-1 | eV | f | Assignment |
|---|---|---|---|---|---|
| 1 | 395.1 | 25.31 | 3.138 | 1.8708 | 187->188(97.5%) |
| 2 | 306.8 | 32.59 | 4.041 | 0.0000 | 185->188(83.4%) 185->189(13.4%) |
| 3 | 302.3 | 33.08 | 4.102 | 0.1135 | 186->188(86.2%) |
| 4 | 298.9 | 33.46 | 4.149 | 0.0260 | 187->189(41.6%) 187->190(23.3%) 184->188(12.1%) 181->188(10.4%) |
| 5 | 294.9 | 33.91 | 4.205 | 0.1009 | 184->188(65.1%) 187->189(20.5%) |
| 6 | 290.4 | 34.43 | 4.269 | 0.1285 | 187->190(37.5%) 187->189(26.9%) 183->188(16.5%) |
| 7 | 281.7 | 35.49 | 4.401 | 0.0713 | 183->188(50.7%) 181->188(18.5%) 187->195(11.7%) |
| 8 | 275.8 | 36.26 | 4.496 | 0.0039 | 187->192(82.8%) |
| 9 | 264.6 | 37.79 | 4.685 | 0.0317 | 181->188(51.6%) 187->190(26.1%) 183->188(13.5%) |
| 10 | 257.8 | 38.80 | 4.810 | 0.0040 | 187->191(70.8%) |
| 11 | 256.3 | 39.01 | 4.837 | 0.0004 | 178->188(91.8%) |
| 12 | 253.0 | 39.52 | 4.900 | 0.0140 | 182->188(92.9%) |
| 13 | 248.9 | 40.17 | 4.981 | 0.0221 | 187->193(67.3%) |
| 14 | 248.1 | 40.31 | 4.998 | 0.0021 | 185->189(63.5%) 185->188(14.2%) |
| 15 | 246.2 | 40.63 | 5.037 | 0.0194 | 180->188(85.1%) |
| 16 | 244.9 | 40.83 | 5.062 | 0.0849 | 187->195(64.0%) |
| 17 | 239.6 | 41.74 | 5.175 | 0.0056 | 187->194(85.4%) |
| 18 | 237.1 | 42.18 | 5.230 | 0.0364 | 186->189(65.4%) 187->193(11.6%) |
| 19 | 233.2 | 42.89 | 5.318 | 0.0001 | 187->196(82.5%) 186->196(13.5%) |
| 20 | 232.3 | 43.06 | 5.338 | 0.0465 | 184->189(34.5%) 186->190(24.2%) 186->191(12.5%) |
| 21 | 228.9 | 43.68 | 5.415 | 0.0061 | 186->190(39.6%) 185->192(14.5%) |
| 22 | 228.6 | 43.75 | 5.425 | 0.0008 | 185->190(62.7%) 185->195(10.8%) |
| 23 | 226.0 | 44.24 | 5.485 | 0.3480 | 185->192(26.2%) 184->189(17.5%) 186->190(17.3%) 187->197(10.2%) |
| 24 | 225.4 | 44.37 | 5.501 | 0.0009 | 179->188(92.6%) |
| 25 | 223.3 | 44.77 | 5.551 | 0.3159 | 187->197(39.5%) 185->192(26.3%) |
| 26 | 219.0 | 45.66 | 5.662 | 0.2439 | 183->189(38.1%) 187->197(11.2%) 184->191(10.7%) |
| 27 | 218.8 | 45.70 | 5.666 | 0.1466 | 184->190(27.9%) 186->191(25.5%) |
| 28 | 217.8 | 45.91 | 5.693 | 0.3156 | 183->189(31.4%) 184->190(28.0%) 187->197(13.8%) |
| 29 | 216.9 | 46.11 | 5.717 | 0.0744 | 182->189(58.3%) |
| 30 | 215.8 | 46.34 | 5.746 | 0.0045 | 186->192(71.0%) |
| 31 | 214.1 | 46.70 | 5.790 | 0.0789 | 181->189(53.3%) |
| 32 | 213.9 | 46.75 | 5.797 | 0.0023 | 187->198(70.6%) |
| 33 | 213.8 | 46.77 | 5.799 | 0.0059 | 185->193(59.8%) |
| 34 | 213.6 | 46.82 | 5.805 | 0.0110 | 182->192(25.4%) 183->190(20.3%) 181->189(12.0%) |

| | | | | | |
|---|---|---|---|---|---|
| 35 | 213.3 | 46.87 | 5.812 | 0.1888 | 182->192(37.0%) 183->190(17.6%) |
| 36 | 212.7 | 47.01 | 5.829 | 0.0001 | 184->196(92.1%) |
| 37 | 211.1 | 47.36 | 5.872 | 0.0139 | 184->191(28.3%) 183->190(16.9%) 184->190(13.8%) |
| 38 | 209.5 | 47.74 | 5.918 | 0.0044 | 177->188(81.3%) |
| 39 | 208.6 | 47.93 | 5.943 | 0.0030 | 169->188(59.1%) 167->188(16.1%) |
| 40 | 208.4 | 47.99 | 5.950 | 0.0181 | 175->188(50.4%) 176->188(16.5%) |

**Table 3.6. AuABTF1:** Summary of calculated electronic transitions to Franck-Condon triplet states.

HOMO = 187; LUMO = 188

| # | nm | 1000 cm-1 | eV | f | Assignment |
|---|---|---|---|---|---|
| 1 | 561.9 | 17.80 | 2.206 | 0.0000 | 187->188(77.6%) |
| 2 | 430.5 | 23.23 | 2.880 | 0.0000 | 186->188(46.2%) 187->189(28.4%) |
| 3 | 363.3 | 27.53 | 3.413 | 0.0000 | 184->188(39.0%) 184->191(10.2%) |
| 4 | 332.6 | 30.07 | 3.728 | 0.0000 | 187->190(38.5%) 184->188(18.9%) |
| 5 | 329.0 | 30.40 | 3.769 | 0.0000 | 187->190(20.1%) 181->190(10.7%) |
| 6 | 325.9 | 30.68 | 3.804 | 0.0000 | 181->188(19.1%) 187->189(17.2%) 184->188(15.6%) 186->188(13.3%) |
| 7 | 319.0 | 31.35 | 3.887 | 0.0000 | 185->188(70.1%) 185->189(19.4%) |
| 8 | 317.3 | 31.51 | 3.907 | 0.0000 | 183->188(40.3%) 181->188(23.0%) |
| 9 | 307.3 | 32.55 | 4.035 | 0.0000 | 181->188(32.2%) 183->188(21.9%) 187->189(13.8%) |
| 10 | 305.5 | 32.73 | 4.058 | 0.0000 | 184->191(24.7%) |

**Table 3.7. AuABTF2:** Summary of calculated electronic transitions to Franck-Condon singlet states.

HOMO = 215; LUMO = 216

| # | nm | 1000 cm-1 | eV | f | Assignment |
|---|---|---|---|---|---|
| 1 | 403.7 | 24.77 | 3.071 | 1.8963 | 215->216(97.1%) |
| 2 | 316.6 | 31.59 | 3.917 | 0.0000 | 213->216(81.6%) 213->217(11.6%) |
| 3 | 310.8 | 32.18 | 3.990 | 0.1193 | 215->217(89.3%) |
| 4 | 305.8 | 32.70 | 4.054 | 0.2069 | 214->216(87.0%) |
| 5 | 299.4 | 33.40 | 4.141 | 0.0030 | 215->220(33.8%) 212->216(26.2%) 215->221(17.6%) |
| 6 | 293.7 | 34.04 | 4.221 | 0.0278 | 212->216(58.4%) |
| 7 | 283.5 | 35.27 | 4.373 | 0.0355 | 210->216(59.4%) 215->226(13.9%) 207->216(12.8%) |
| 8 | 277.5 | 36.03 | 4.468 | 0.0006 | 215->218(96.7%) |
| 9 | 277.3 | 36.06 | 4.471 | 0.0000 | 215->219(96.4%) |
| 10 | 273.0 | 36.63 | 4.542 | 0.0467 | 215->221(53.1%) 215->220(39.2%) |
| 11 | 269.6 | 37.10 | 4.599 | 0.0004 | 215->222(93.6%) |
| 12 | 269.3 | 37.13 | 4.603 | 0.0129 | 211->216(84.7%) 211->217(13.8%) |
| 13 | 266.0 | 37.60 | 4.662 | 0.0184 | 207->216(51.6%) 215->221(17.8%) 210->216(12.3%) |
| 14 | 263.3 | 37.97 | 4.708 | 0.0012 | 213->217(80.4%) 213->216(11.9%) |
| 15 | 260.9 | 38.33 | 4.752 | 0.0365 | 215->223(72.0%) |
| 16 | 258.6 | 38.67 | 4.794 | 0.0004 | 215->224(88.7%) |
| 17 | 256.0 | 39.06 | 4.843 | 0.0002 | 202->216(91.5%) |

| | | | | | |
|---|---|---|---|---|---|
| 18 | 251.1 | 39.83 | 4.938 | 0.0034 | 209->216(38.8%) 206->216(26.5%) 208->216(14.5%) |
| 19 | 250.7 | 39.88 | 4.945 | 0.0075 | 215->228(75.7%) |
| 20 | 250.2 | 39.97 | 4.956 | 0.0025 | 208->216(73.1%) 209->216(23.3%) |
| 21 | 249.6 | 40.07 | 4.968 | 0.0128 | 209->216(32.7%) 206->216(28.1%) |
| 22 | 247.8 | 40.35 | 5.003 | 0.1116 | 215->226(54.8%) 206->216(13.1%) |
| 23 | 246.0 | 40.64 | 5.039 | 0.0167 | 211->217(71.4%) 211->216(13.1%) |
| 24 | 244.3 | 40.93 | 5.075 | 0.0764 | 214->217(72.1%) |
| 25 | 241.1 | 41.48 | 5.143 | 0.0045 | 215->225(89.1%) |
| 26 | 236.6 | 42.26 | 5.239 | 0.0004 | 205->216(24.7%) 208->219(14.5%) 205->217(10.4%) |
| 27 | 235.5 | 42.46 | 5.265 | 0.0001 | 215->229(83.9%) 214->229(12.4%) |
| 28 | 235.1 | 42.53 | 5.273 | 0.0061 | 209->219(19.0%) 213->218(18.7%) 205->218(14.0%) 208->222(12.8%) |
| 29 | 234.1 | 42.72 | 5.297 | 0.0445 | 214->220(37.8%) 212->217(10.0%) |
| 30 | 233.7 | 42.78 | 5.304 | 0.0014 | 213->220(63.9%) |
| 31 | 233.6 | 42.81 | 5.307 | 0.0001 | 205->216(68.3%) |
| 32 | 232.7 | 42.97 | 5.327 | 0.0011 | 213->219(96.5%) |
| 33 | 232.4 | 43.03 | 5.335 | 0.0060 | 215->227(97.7%) |
| 34 | 232.3 | 43.05 | 5.338 | 0.0052 | 213->221(51.7%) 213->226(14.4%) |
| 35 | 232.1 | 43.08 | 5.342 | 0.0051 | 213->218(71.5%) |
| 36 | 231.4 | 43.22 | 5.359 | 0.0208 | 203->216(52.9%) 206->216(14.0%) |
| 37 | 229.2 | 43.63 | 5.409 | 0.0253 | 212->217(23.7%) 214->223(21.0%) 214->220(15.3%) 203->216(13.2%) |
| 38 | 228.8 | 43.71 | 5.420 | 0.0112 | 204->216(85.9%) |
| 39 | 228.3 | 43.80 | 5.430 | 0.0383 | 215->230(51.2%) |
| 40 | 227.0 | 44.05 | 5.462 | 0.0359 | 213->222(84.0%) |

**Table 3.8. AuABTF2:** Summary of calculated electronic transitions to Franck-Condon triplet states.

HOMO = 215; LUMO = 216

| # | nm | 1000 cm-1 | eV | f | Assignment |
|---|---|---|---|---|---|
| 1 | 569.7 | 17.55 | 2.176 | 0.0000 | 215->216(76.7%) |
| 2 | 433.0 | 23.09 | 2.863 | 0.0000 | 214->216(44.6%) 215->217(20.1%) |
| 3 | 363.8 | 27.49 | 3.408 | 0.0000 | 212->216(33.7%) 212->223(11.0%) |
| 4 | 353.6 | 28.28 | 3.506 | 0.0000 | 208->218(21.6%) 205->222(17.8%) 204->219(14.9%) |
| 5 | 336.8 | 29.69 | 3.681 | 0.0000 | 215->221(23.9%) 215->220(15.4%) 215->217(10.5%) 214->216(10.0%) |
| 6 | 334.3 | 29.91 | 3.708 | 0.0000 | 212->216(35.0%) 207->216(19.0%) |
| 7 | 328.2 | 30.47 | 3.778 | 0.0000 | 213->216(70.9%) 213->217(16.1%) |
| 8 | 324.6 | 30.80 | 3.819 | 0.0000 | 215->220(22.5%) |
| 9 | 318.3 | 31.41 | 3.895 | 0.0000 | 210->216(39.3%) 207->216(26.0%) |
| 10 | 313.7 | 31.88 | 3.953 | 0.0000 | 215->217(23.2%) |

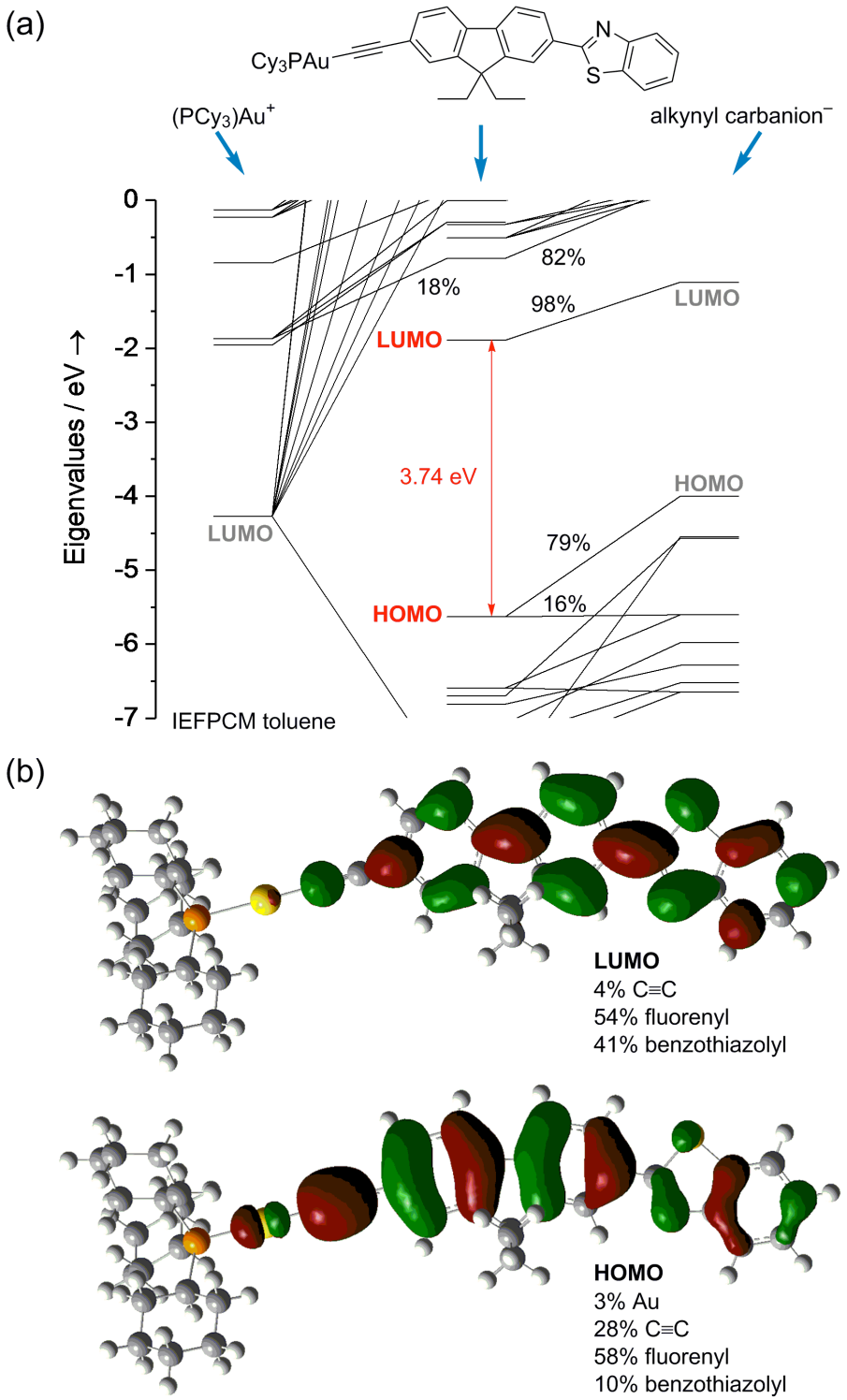


**Figure 3.28.** (a) Frontier orbital energy diagram of **Au-ABTF1**. (b) Kohn-Sham orbital plots (HOMO and LUMO) for **Au-ABTF1**. (Percentages are of electron density)

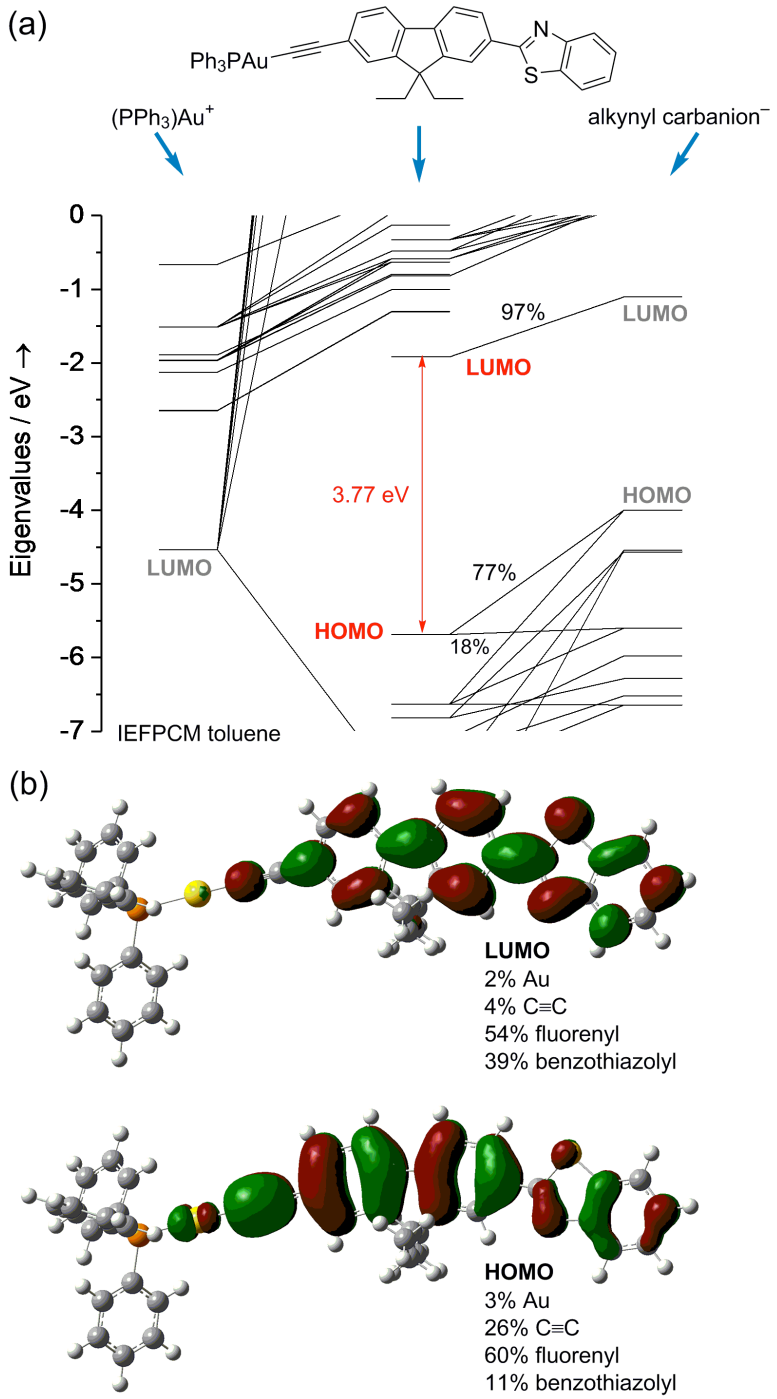


**Figure 3.29.** (a) Frontier orbital energy diagram of **Au-ABT0**. (b) Kohn-Sham orbital plots (HOMO and LUMO) for **Au-ABTF0**. (Percentages are of electron density)

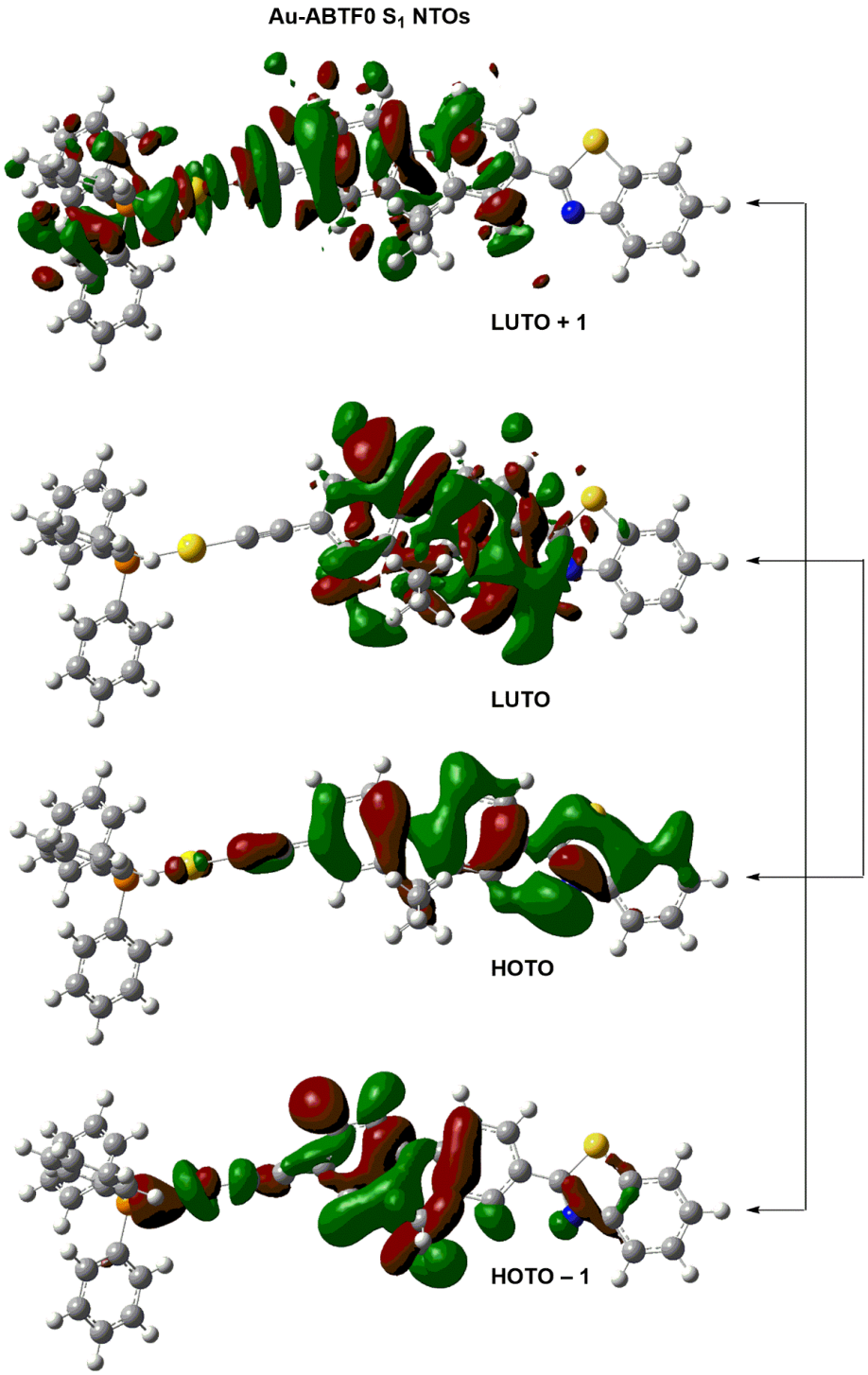


**Figure 3.30** Natural transition orbitals of the Franck-Condon $S_1$ state of **Au-ABTF0**. Contour levels are 0.02 a.u.

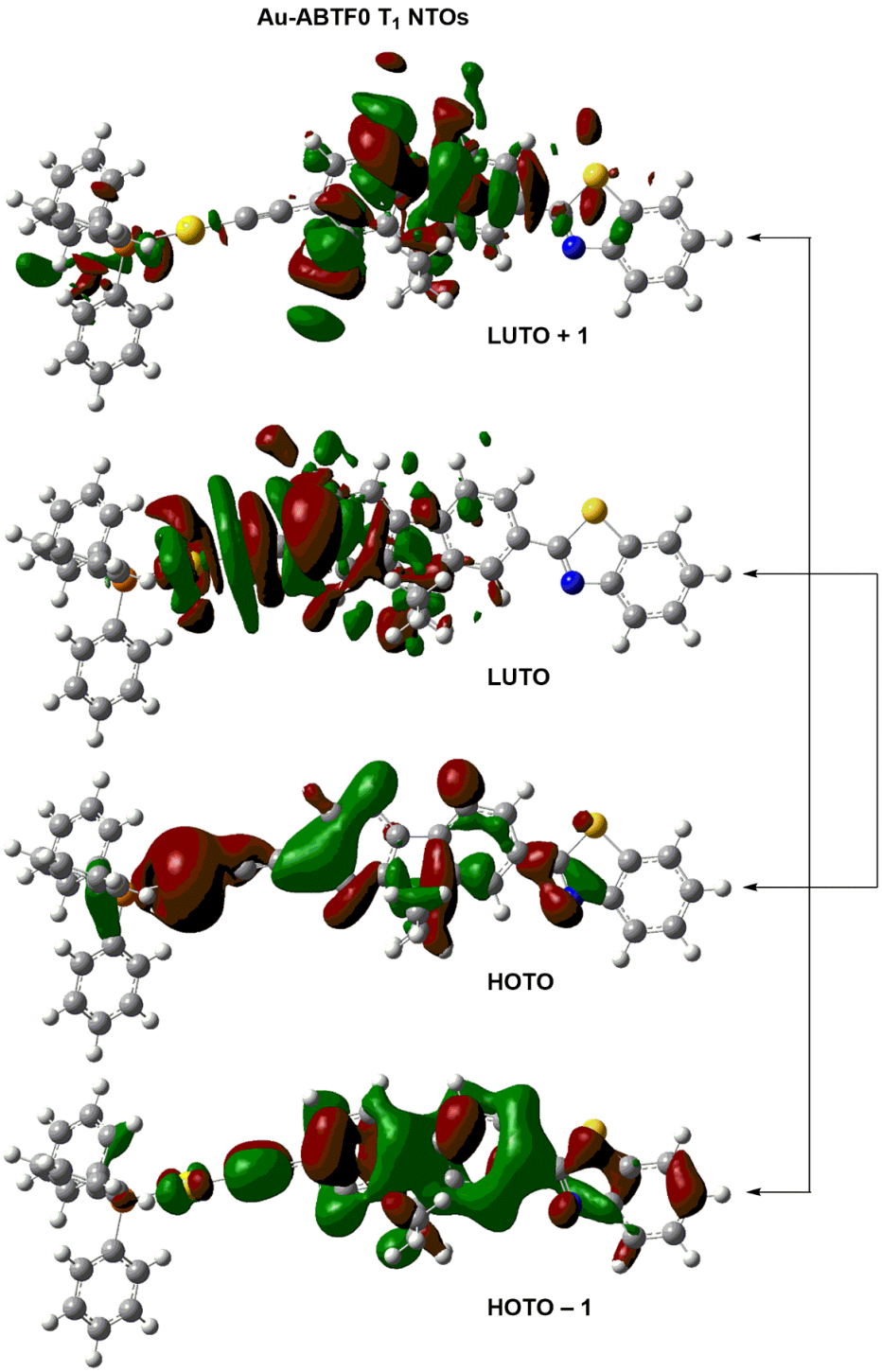


**Figure 3.31** Natural transition orbitals of the Franck-Condon $T_1$ state of **Au-ABTF0**. Contour levels are 0.02 a.u.

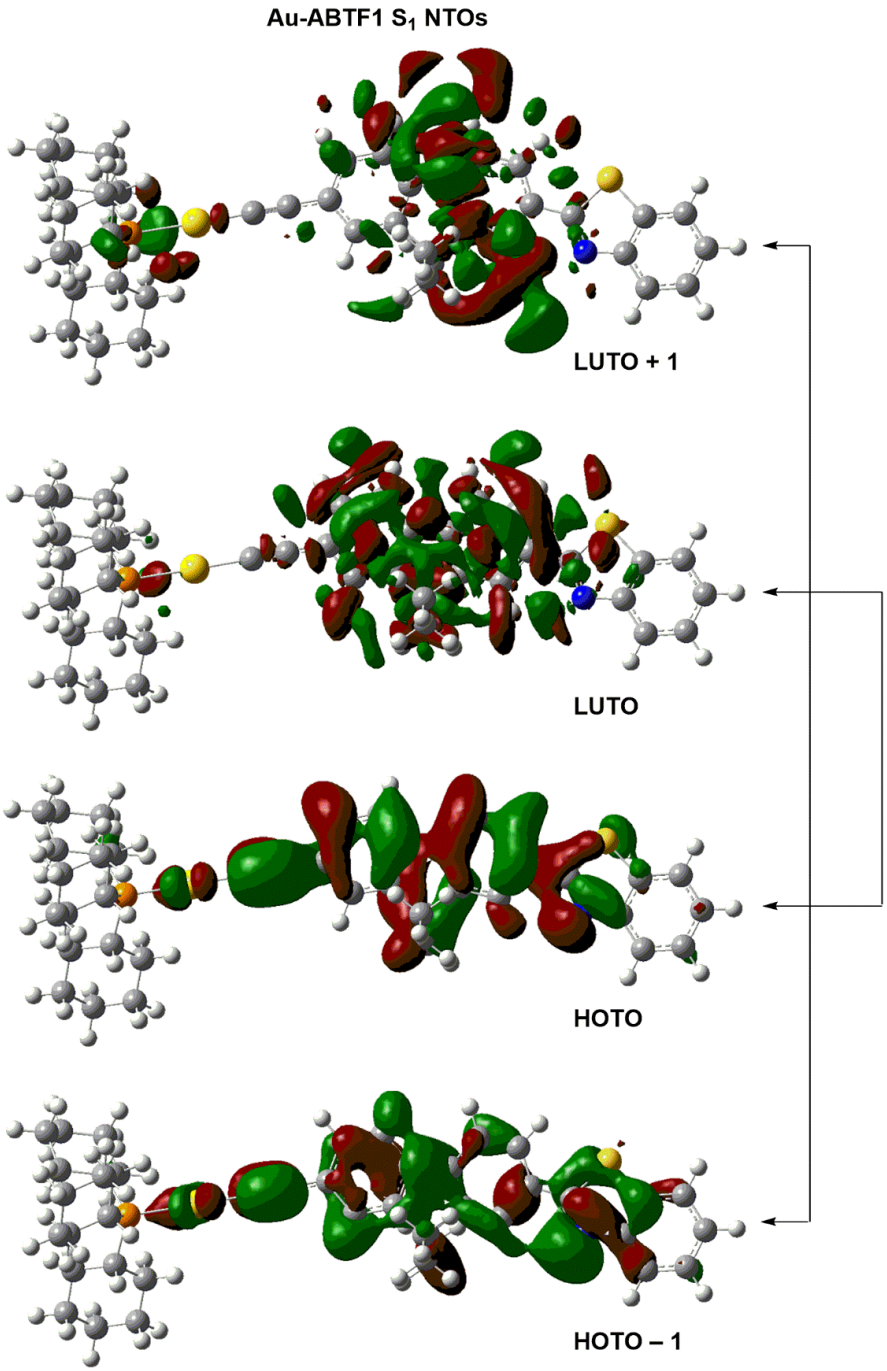


**Figure 3.32.** Natural transition orbitals of the Franck-Condon $S_1$ state of **Au-ABTF1**. Contour levels are 0.02 a.u.

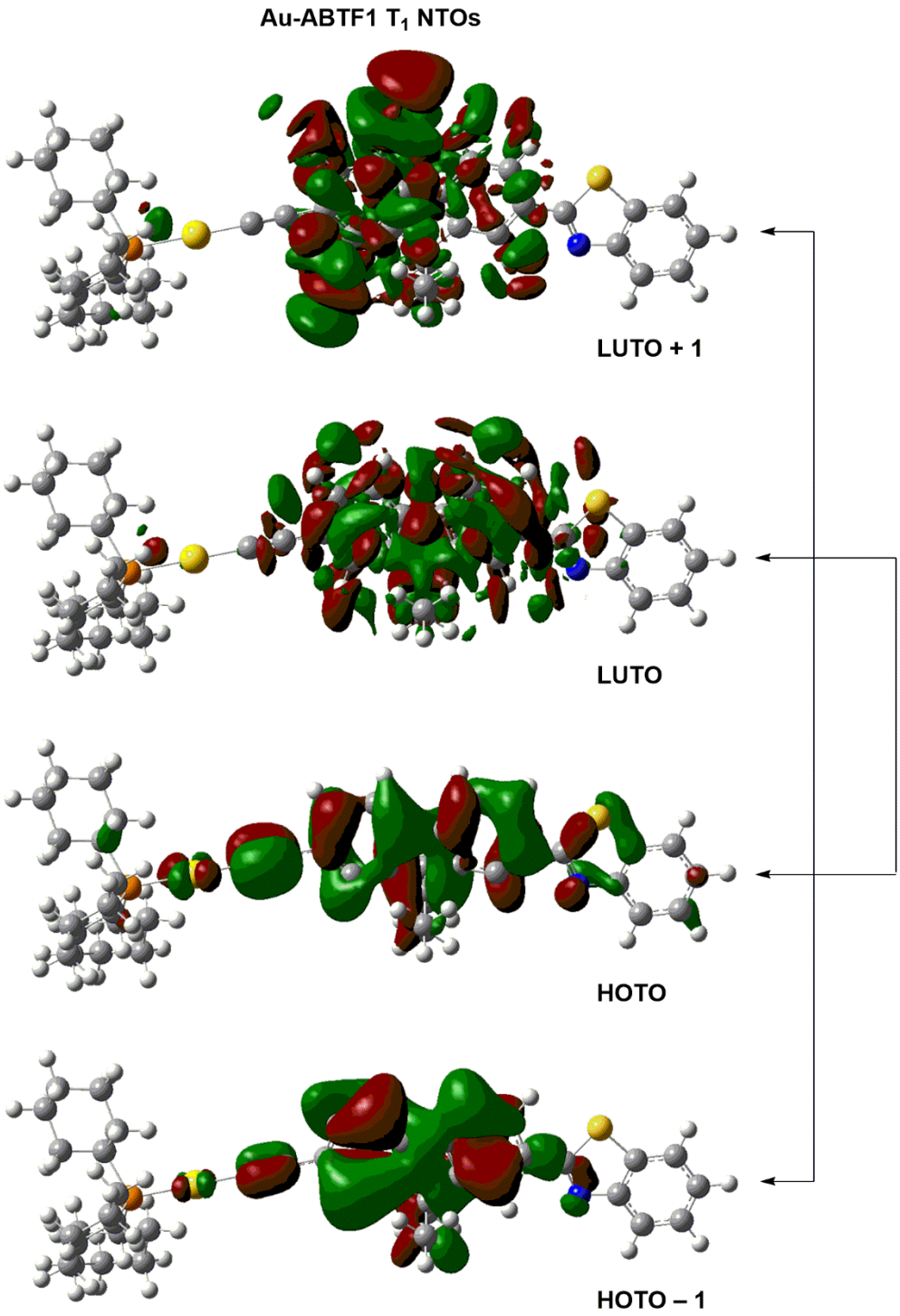


**Figure 3.33.** Natural transition orbitals of the Franck-Condon $T_1$ state of **Au-ABTF1**. Contour levels are 0.02 a.u.

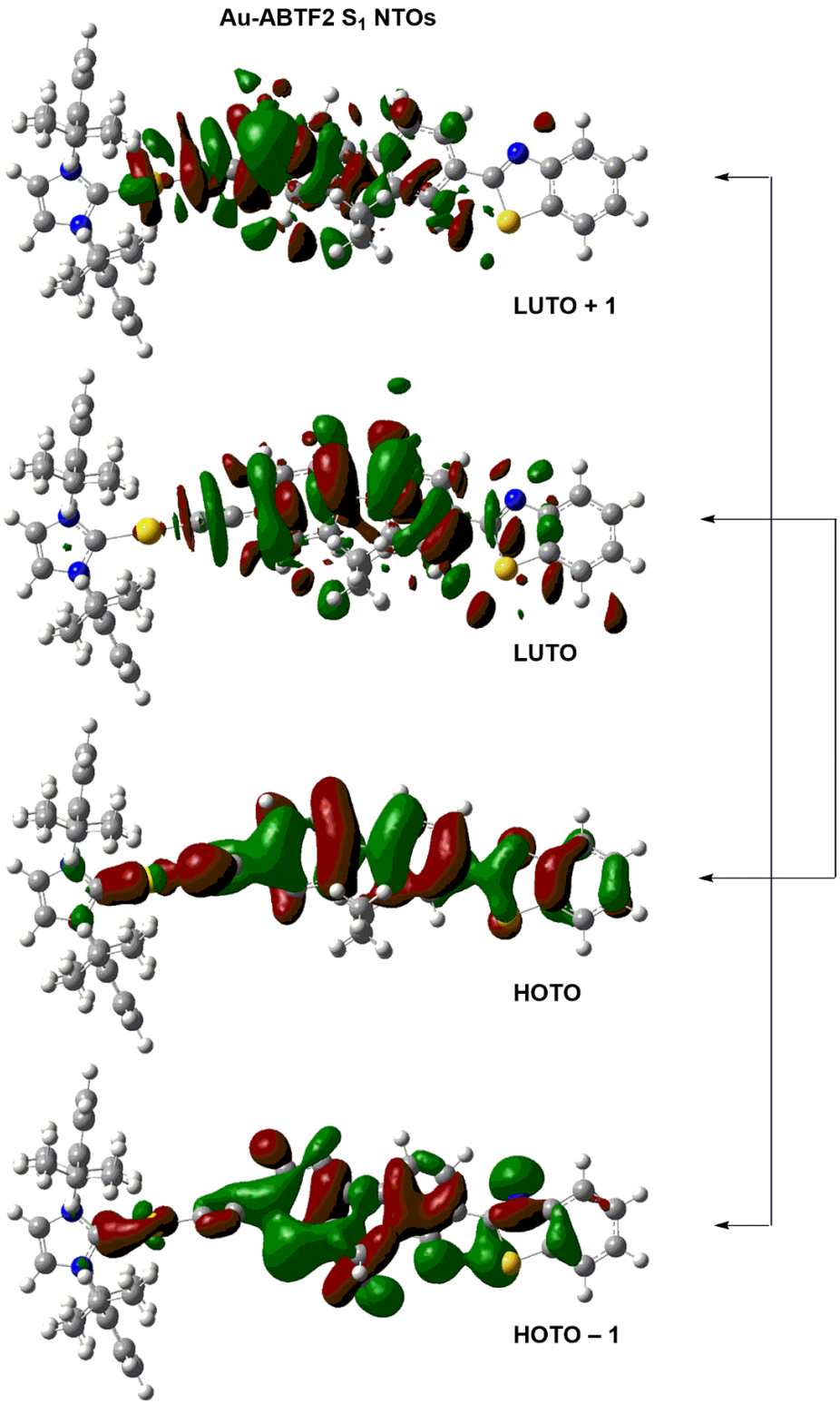


**Figure 3.34** Natural transition orbitals of the Franck-Condon $S_1$ state of **Au-ABTF2**. Contour levels are 0.02 a.u.

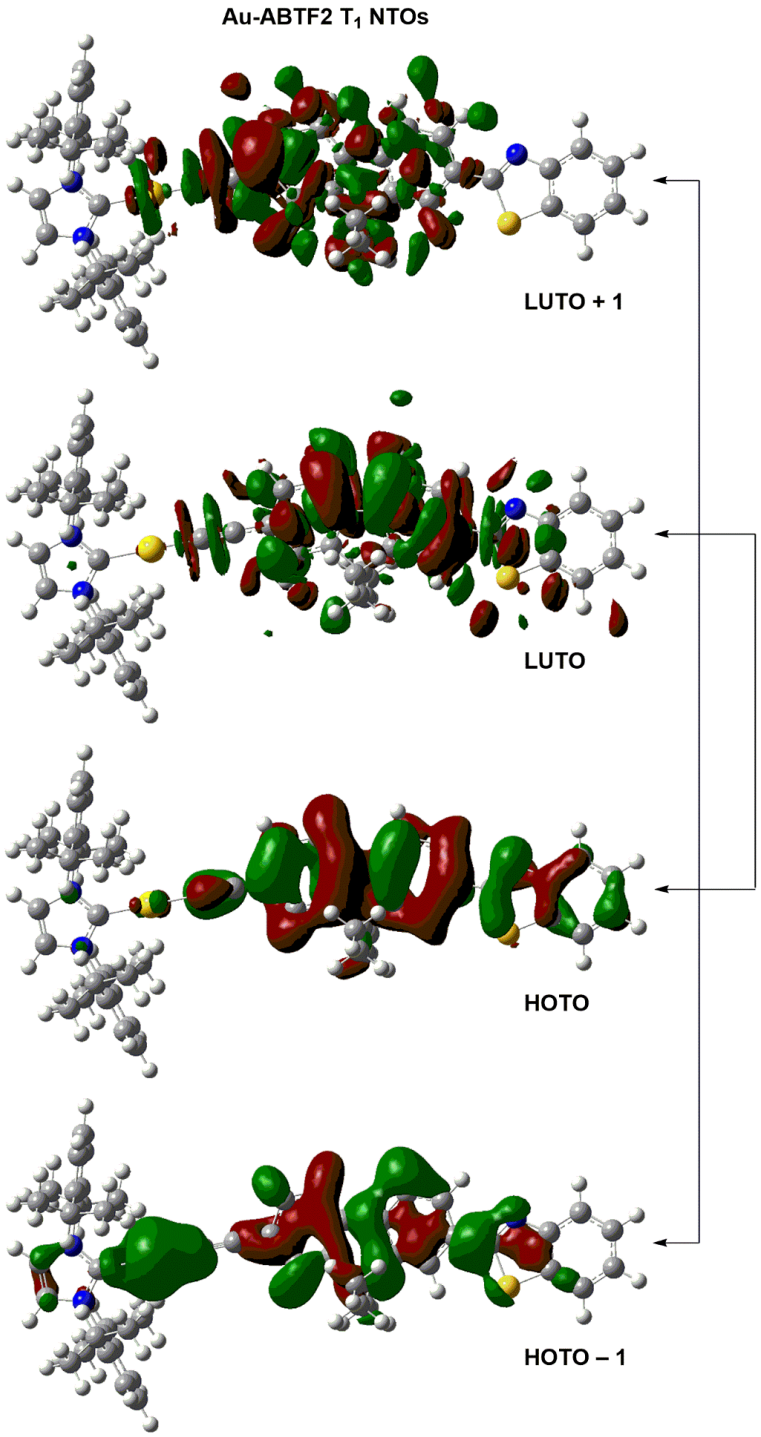


**Figure 3.35** Natural transition orbitals of the Franck-Condon $T_1$ state of **Au-ABTF2**. Contour levels are 0.02 a.u.

**References.**


1 J. J. Mihaly, D. J. Stewart, T. A. Grusenmeyer, A. T. Phillips, J. E. Haley, M. Zeller and T. G. Gray, Photophysical properties of organogold(i) complexes bearing a benzothiazole-2,7-fluorenyl moiety: Selection of ancillary ligand influences white light emission, *Dalt. Trans.*, 2019, **48**, 15917–15927.

2 J. E. Rogers, J. E. Slagle, D. M. Krein, A. R. Burke, B. C. Hall, A. Fratini, D. G. McLean, P. A. Fleitz, T. M. Cooper, M. Drobizhev, N. S. Makarov, A. Rebane, K. Y. Kim, R. Farley and K. S. Schanze, Platinum acetylide two-photon chromophores, *Inorg. Chem.*, 2007, **46**, 6483–6494. ; L. Gao, D. V. Partyka, J. B. Updegraff, N. Deligonul and T. G. Gray, Synthesis, structures, and excited-state geometries of alkynylgold(I) complexes, *Eur. J. Inorg. Chem.*, 2009, **2009**, 2711–2719.

3 D. V Partyka, T. J. Robilotto, M. Zeller, A. D. Hunter and T. G. Gray, Dialkylbiarylphosphine Complexes of Gold(I) Halides. Gold−Aryl π-Interactions in the Solid State, *Organometallics*, 2008, **27**, 28–32.

4 G. M. Sheldrick, A short history of SHELX, *Acta Crystallogr. Sect. A*, 2008, **64**, 112–122.

5 G. M. Sheldrick, Crystal structure refinement with SHELXL, *Acta Crystallogr. Sect. C*, 2015, **71**, 3–8.

6 C. B. Hübschle, G. M. Sheldrick and B. Dittrich, ShelXle: a Qt graphical user interface for SHELXL, *J. Appl. Crystallogr.*, 2011, **44**, 1281–1284.

7 L. Krause, R. Herbst-Irmer, G. M. Sheldrick and D. Stalke, Comparison of silver and molybdenum microfocus X-ray sources for single-crystal structure determination, *J. Appl. Crystallogr.*, 2015, **48**, 3–10.

8 S. Parsons, H. D. Flack and T. Wagner, Use of intensity quotients and differences in absolute structure refinement, *Acta Crystallogr. Sect. B*, 2013, **69**, 249–259.

9 Gaussian 16, Revision A.03, M. J. Frisch, G. W. Trucks, H. B. Schlegel, G. E. Scuseria, M. A. Robb, J. R. Cheeseman, G. Scalmani, V. Barone, G. A. Petersson, H. Nakatsuji, X. Li, M. Caricato, A. V Marenich, J. Bloino, B. G. Janesko, R. Gomperts, B. Mennucci, H. P. Hratchian, J. V Ortiz, A. F. Izmaylov, J. L. Sonnenberg, D. Williams-Young, F. Ding, F. Lipparini, F. Egidi, J. Goings, B. Peng, A. Petrone, T. Henderson, D. Ranasinghe, V. G. Zakrzewski, J. Gao, N. Rega, G. Zheng, W. Liang, M. Hada, M. Ehara, K. Toyota, R. Fukuda, J. Hasegawa, M. Ishida, T. Nakajima, Y. Honda, O. Kitao, H. Nakai, T. Vreven,

K. Throssell, J. A. Montgomery Jr., J. E. Peralta, F. Ogliaro, M. J. Bearpark, J. J. Heyd, E. N. Brothers, K. N. Kudin, V. N. Staroverov, T. A. Keith, R. Kobayashi, J. Normand, K. Raghavachari, A. P. Rendell, J. C. Burant, S. S. Iyengar, J. Tomasi, M. Cossi, J. M. Millam, M. Klene, C. Adamo, R. Cammi, J. W. Ochterski, R. L. Martin, K. Morokuma, O. Farkas, J. B. Foresman and D. J. Fox, Gaussian, Inc., Wallingford CT, 2016.

10 M. Dolg, U. Wedig, H. Stoll and H. Preuss, Energy-adjusted ab initio pseudopotentials for the first row transition elements, *J. Chem. Phys.*, 1987, **86**, 866–872.

11 J. P. Perdew, K. Burke and M. Ernzerhof, Generalized Gradient Approximation Made Simple, *Phys. Rev. Lett.*, 1996, **77**, 3865–3868.

12 N. Godbout, D. R. Salahub, J. Andzelm and E. Wimmer, Optimization of Gaussian-type basis sets for local spin density functional calculations. Part I. Boron through neon, optimization technique and validation, *Can. J. Chem.*, 1992, **70**, 560–571.

13 S. Miertuš, E. Scrocco and J. Tomasi, Electrostatic interaction of a solute with a continuum. A direct utilizaion of AB initio molecular potentials for the prevision of solvent effects, *Chem. Phys.*, 1981, **55**, 117–129.

14 J. Tomasi, B. Mennucci and R. Cammi, Quantum Mechanical Continuum Solvation Models, *Chem. Rev.*, 2005, **105**, 2999–3094.

15 E. Cancès, B. Mennucci and J. Tomasi, A new integral equation formalism for the polarizable continuum model: Theoretical background and applications to isotropic and anisotropic dielectrics, *J. Chem. Phys.*, 1997, **107**, 3032–3041.

16 B. Mennucci, E. Cancès and J. Tomasi, Evaluation of Solvent Effects in Isotropic and Anisotropic Dielectrics and in Ionic Solutions with a Unified Integral Equation Method: Theoretical Bases, Computational Implementation, and Numerical Applications, *J. Phys. Chem. B*, 1997, **101**, 10506–10517.

17 S. I. Gorelsky and A. B. P. Lever, Electronic structure and spectra of ruthenium diimine complexes by density functional theory and INDO/S. Comparison of the two methods, *J. Organomet. Chem.*, 2001, **635**, 187–196.

18 S. I. Gorelsky, AOMix: Program for Molecular Orbital Analysis, http://www.sg-chem.net.

## Chapter 4: Synthesis, Photophysics, and Computations for a Series of Digold(I) BTF Alkynyls and Triazolyl (Au-DiBTF(0-3).

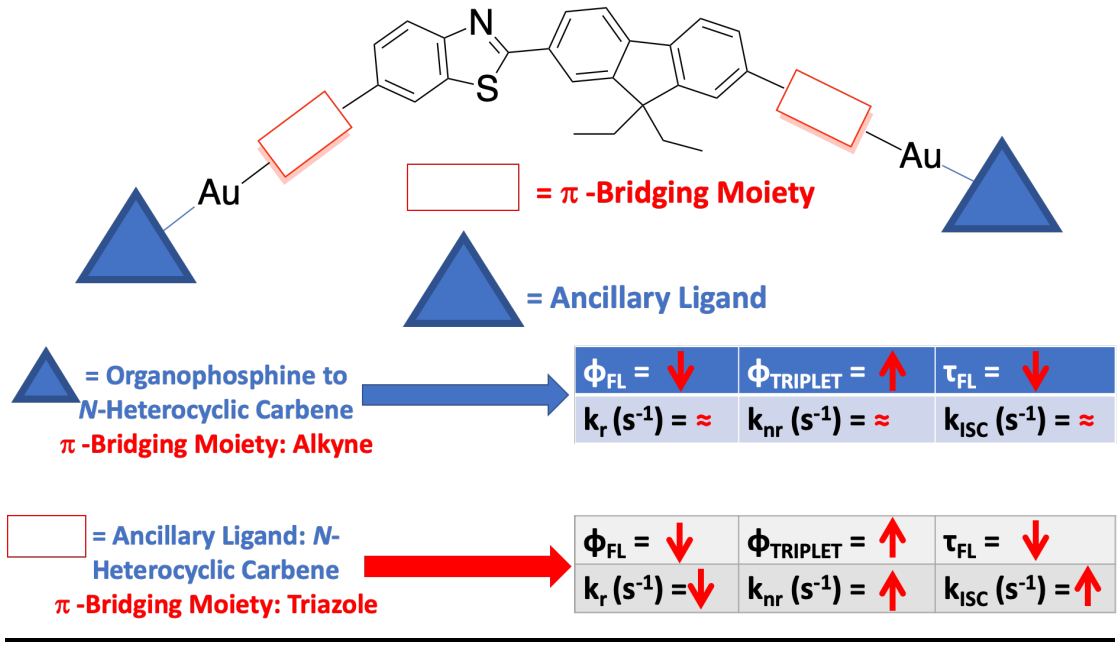


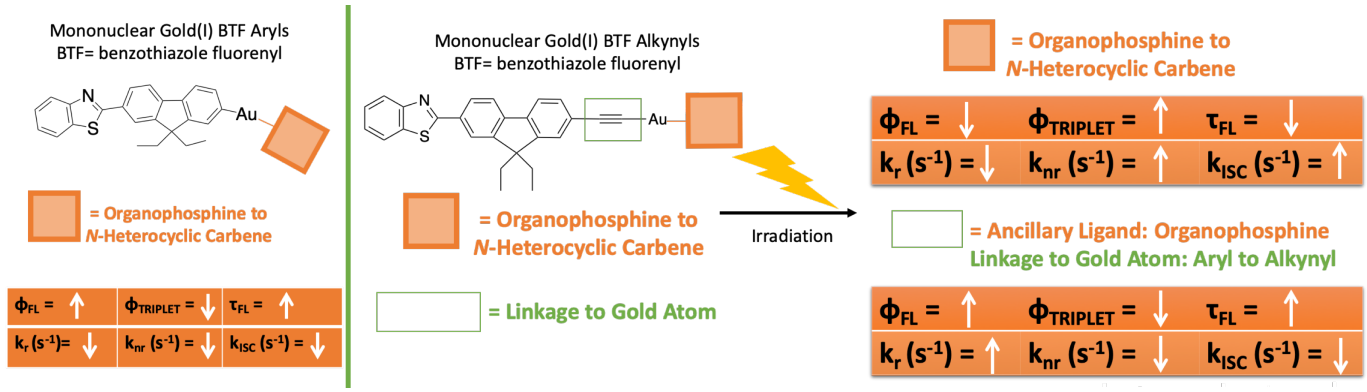


**Figure 4.1.** Summary of photophysics results **Au-BTF** series (left). Summary of photophysics results **Au-ABTF** series (right).[1,2]

The experimental results of Chapters 2 and 3 demonstrate that phosphorescence and fluorescence coexist upon excitation of mono-gold(I) chromophores in hydrocarbon solution at room temperature (Figure 4.1).[1,2] While the spin-orbit coupling of a single gold center suffices to populate triplet states, quantum yields of triplet formation are limited. A series of asymmetric, di-

gold(I) complexes, metalated at opposite ends of the fluorenyl-benzothiazolyl chromophore has been prepared to test two hypotheses: (i) That a second gold(I) center will facilitate intersystem crossing, leading to higher triplet quantum yields, and (ii) the gold-carbon interface (σ-bond, alkynyl linkage, or triazolyl) will materially affect the excited-state dynamics.

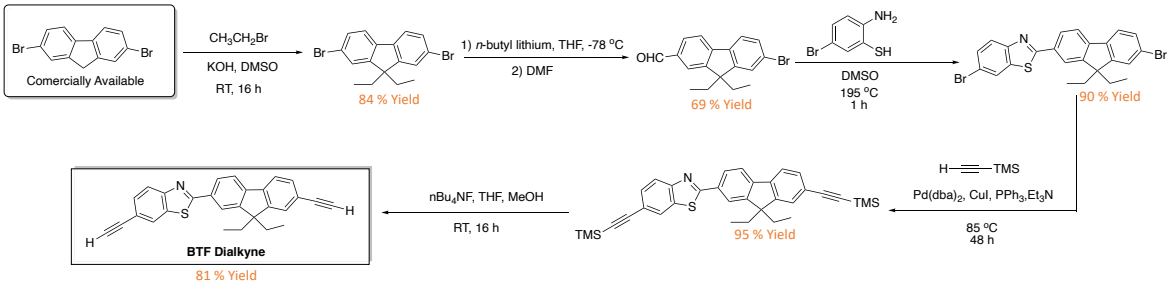


**Scheme 4.1.** Synthesis of new asymmetric BTF Dialkyne ligand.

Synthesis of the new BTF dialkyne ligand appears in Scheme 4.1. The BTF dialkyne ligand precursor was then reacted with choice gold(I) chloride starting[3] materials by *in situ* deprotonation of the alkyne and subsequent of addition to a suspention of gold starting material.[4] Vapor diffusion of pentane into concentrated dichloromethane solutions or washing with copious amounts of pentane yielded the new complexes **Au-DiBTF0** (52% isolated yield), **Au-DiBTF1** (60% isolated yield), and **Au-DiBTF2** (80% isolated yield), repectively (Scheme 4.2). Further functionalization of **Au-DiBTF2** via a copper catalyzed click reaction yielded the triazolyl, **Au-DiBTF3** in 73% yield (Scheme 4.3).[4] A crystal structure of **Au-DiBTF3** appears in Figure 4.2. The gold(I) center is nearly linear in geometry and crystallographic packing diagrams show no evidence of aurophilic interactions or π-π stacking.

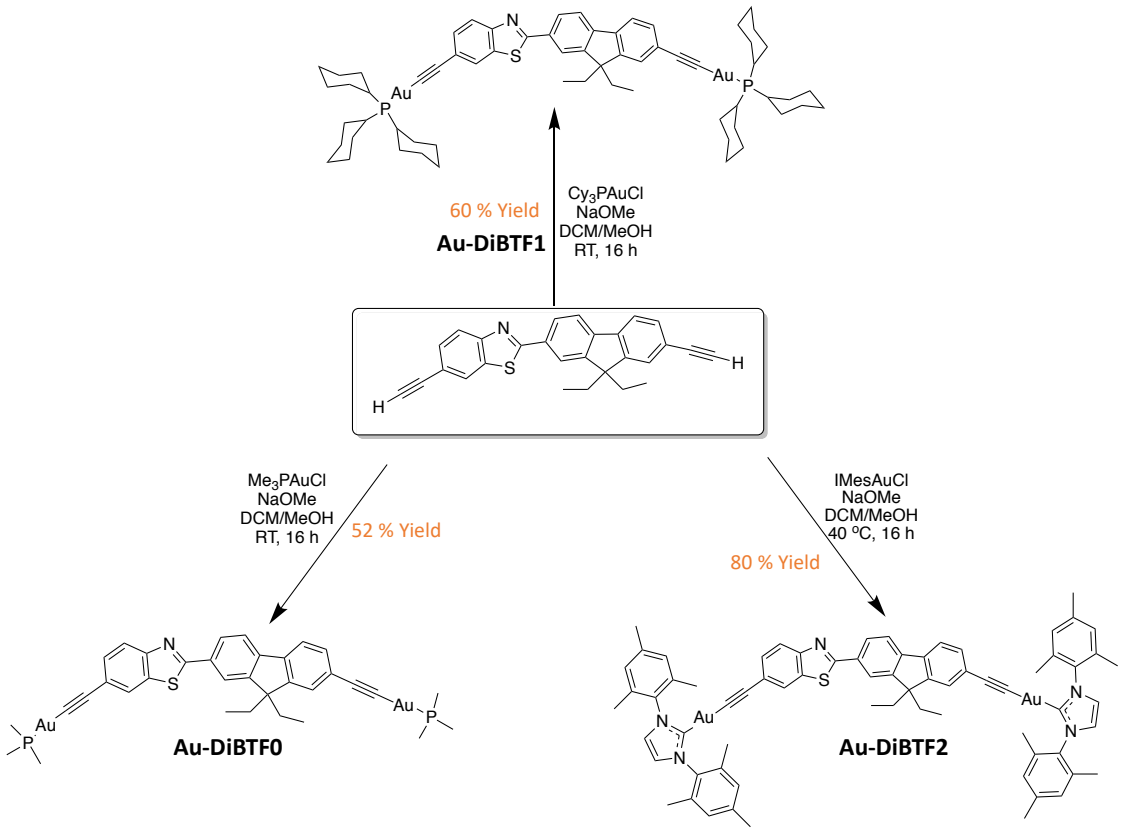


**Scheme 4.2.** Synthesis of new **Au-DiBTF(0-2)**.

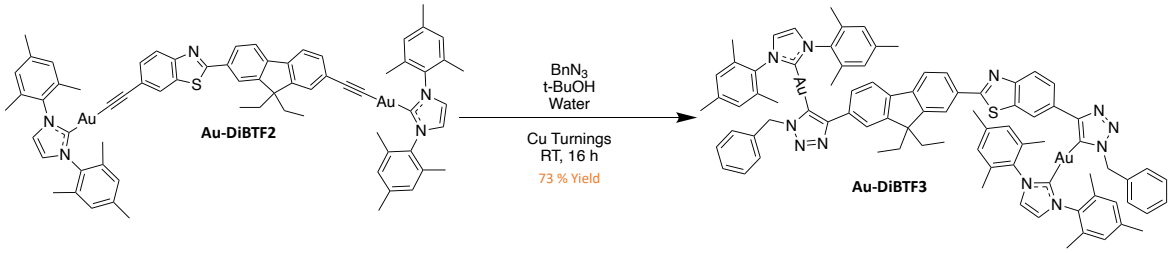


**Scheme 4.3.** Synthesis of new **Au-DiBTF3**.

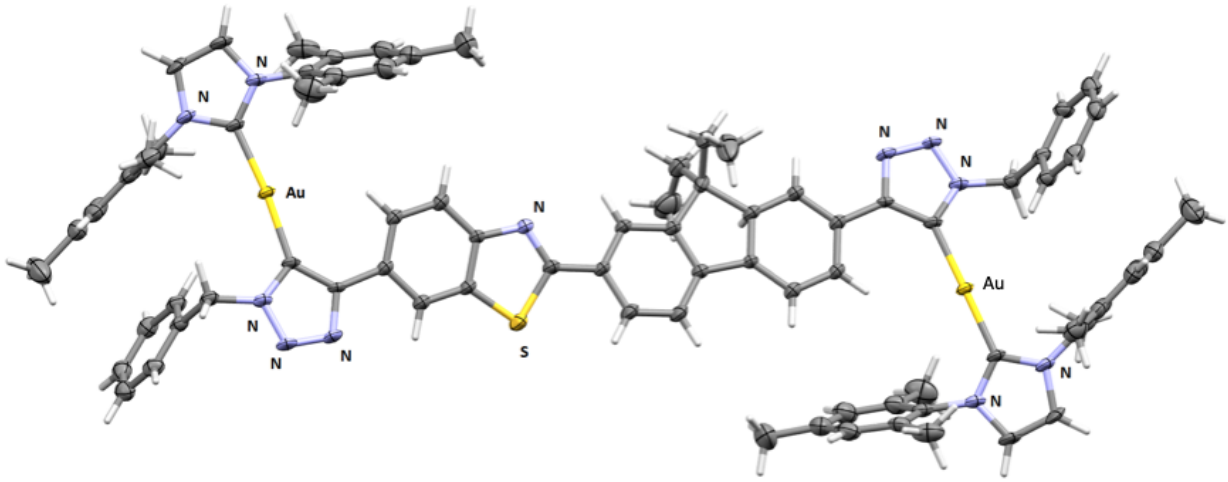


**Figure 4.2.** Thermal ellipsoid representation of **Au-DiBTF3** (50% probability level, 150 K). A partial atom labeling scheme is indicated. The structure is disordered across an inversion center; disordered equivalent atoms omitted for clarity.

**Photophysical Characterization of Au-DiBTF(0-3).**

Normalized ground-state absorption spectra are shown appear in Figure 4.3 (a, left). All four complexes exhibit structured absorption profiles with molar absorptivity values between 5-7 x $10^4$ $M^{-1}$ $cm^{-1}$(Table 4.1). The two phosphine complexes **Au-DiBTF(0,1)** have absorption maxima at 383 and 384 nm. Changing the ancillary ligand from an organophosphine to an *N*-heterocyclic carbene (**Au-DiBTF2**) leads to a red-shift in the absorption maximum to 387 nm. Modification of the alkynyl linkage in **Au-DiBTF2** to a triazolyl, as in **Au-DiBTF3**, leads to a further red-shift in the absorption maximum to 390 nm. Emission spectra in freeze-pump-thaw degassed toluene appear in Figure 4.3 (a, right). All complexes are characterized by structured fluorescence and weak phosphorescence. Fluorescence maxima energy trends follow that of the ground-state absorption spectra.

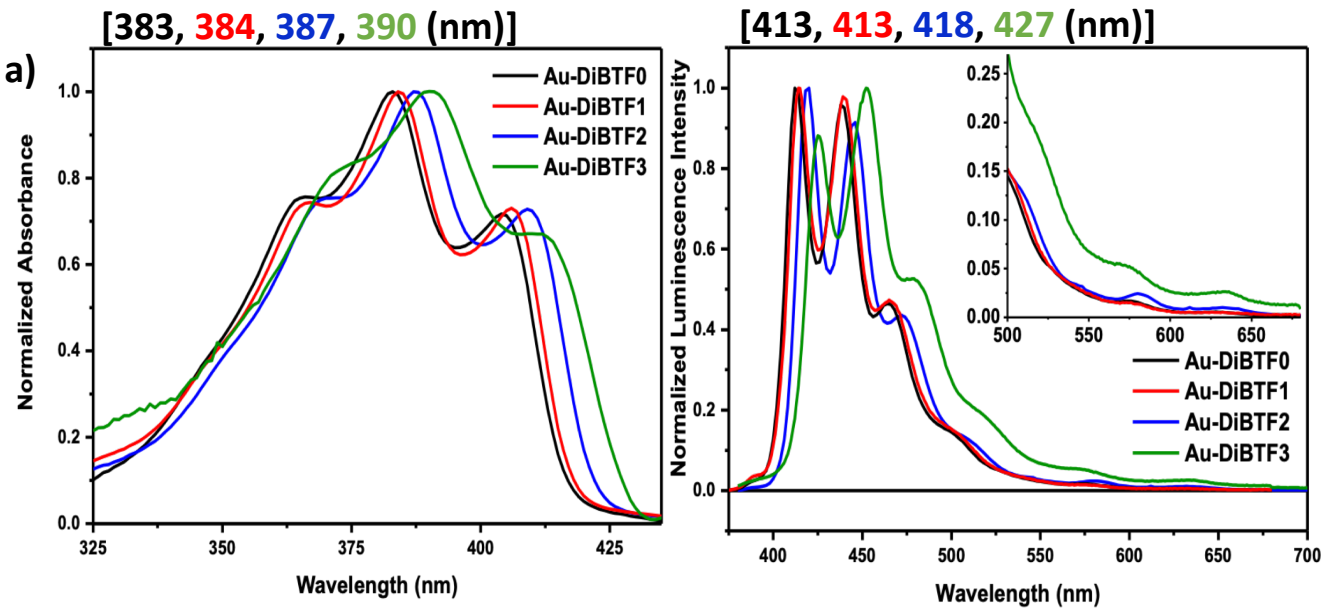


**Figure 4.3.** (a, left) Ground-state absorption spectra of **Au-DiBTF(0-3)** in toluene at room temperature with absorption wavelength maxima. (a, right) Emission spectra of **Au-DiBTF(0-3)** in freeze-pump-thaw deaerated toluene at room temperature with fluorescence wavelength maxima.

The two phosphine complexes display identical luminescence maxima, both being at 413 nm. Changing the ancillary ligand to an *N*-heterocyclic carbene (**Au-DiBTF2**) leads to a red-shift of the fluorescence maximum to 418 nm. Altering the alkynyl bridge of **Au-DiBTF2** to a triazolyl leads to a further red-shift to 427 nm. Table 4.1 summarizes the static photophysical data for **Au-DiBTF(0-3)**.

| Experimental Results: | Complex: | | | |
|---|---|---|---|---|
| | Au-DiBTF0 | Au-DiBTF1 | Au-DiBTF2 | Au-DiBTF3 |
| Ground-State Absorption Maximum $\lambda_{ABS}$/nm | 383 | 384 | 387 | 390 |
| [A]Extinction Coefficient in Dichloromethane ($10^4$ $M^{-1}cm^{-1}$) *(Estimated error ± 5%) | 6.00 | 5.10 | 6.76 | 6.99 |
| Flourescence Maximum $\lambda_{FL}$ (nm) | 413 | 413 | 418 | 427 |
| Fluorescence Quantum Yield ($\phi_{FL}$) | 0.55 ± 0.02 | 0.55 ± 0.02 | 0.44 ± 0.01 | 0.28 ± 0.02 |
| Intersystem Crossing Quantum Yield ($\phi_{TRIPLET}$) | 0.51 ± 0.01 | 0.43 ± 0.02 | 0.57 ± 0.02 | 0.68 ± 0.01 |
| Fluorescence Lifetime ($\tau_{FL}$ – TCSPC (ps)) | 438 ± 5 | 442 ± 1 | 380 ± 1 | 369 ± 1 |
| $k_r$ ($s^{-1}$) | $1.3 \times 10^9$ | $1.2 \times 10^9$ | $1.2 \times 10^9$ | $7.6 \times 10^8$ |
| $k_{nr}$ ($s^{-1}$) | $\leq 2.3 \times 10^7$ | $\leq 4.5 \times 10^7$ | $\leq 2.6 \times 10^7$ | $1.08 \times 10^8$ |
| $k_{ISC}$ ($s^{-1}$) | $1.2 \times 10^9$ | $9.7 \times 10^8$ | $1.5 \times 10^9$ | $2.4 \times 10^9$ |

**Table 4.1.** Summary of Photophysical Data for **Au-DiBTF(0-3)**.

All data collected in room temperature toluene. Legend: $\lambda_{FL}$ = wavelength of fluorescence; $\varphi_{FL}$ = emission quantum yield of fluorescence; $\tau_{FL}$ =lifetime of fluorescence; TCSPC = time-correlated single-photon counting; $k_r$ = radiative decay rate constant; $k_{nr}$ = non-radiative decay rate constant; $k_{ISC}$ = rate constant of intersystem crossing; $\lambda_{PHOS}$ = wavelength of phosphorescence; $\varphi_{TRIPLET}$ = quantum yield of triplet state formation.

Fluorescence lifetime, fluorescence quantum yield, and triplet state quantum yield data appear in Table 4.1. Changing the ancillary ligand from an organophosphine (**Au-DiBTF(0,1)**) to an *N*-heterocyclic carbene (**Au-DiBTF2**) affords small decreases in fluorescence quantum yield and lifetime, and a small increase in triplet-state quantum yield. Modifying the alkynyl linkage in **Au-DiBTF2** to a triazolyl in **Au-DiBTF3**, leads to a further increase in triplet state quantum yield and further decreases in fluorescence lifetime and quantum yield. Obtainment of lifetimes and quantum yields allows for calculation of excited-state rate constants for radiative decay ($k_r$), nonradiative decay ($k_{nr}$) and intersystem crossing ($k_{isc}$). With only subtle changes in lifetime and quantum yield data for **Au-DiBTF(0,1,** and **2)**, we find similar rates of radiative and non-radiative as well as rate of intersystem crossing. **Au-DiBTF3**; which has a triazole linkage, displays a slower

rate of radiative decay and faster rates of non-radiative decay and rate of intersystem crossing compared to the alkynyl complexes.

**Computations**

Density-functional theory calculations were undertaken on model complexes to gain insight into the origin of the photophysical behavior for the **Au-DiBTF** series. In all model complexes, designated **Au-DiBTF(0′–3′)** fluorenyl methyl groups and carbene 2,6-diisopropyl groups were replaced with methyls for computational tractability. Details for the calculations can be found in the experimental section of this chapter. Figure 4.4 displays a frontier orbital energy level diagram with Kohn-Sham orbital plots for both the HOMO and LUMO in electron density. A standard Mulliken population analysis finds that HOMO consists of 2% Au, 37% triazole, 39% fluorene, and 22% benzothiazole; the LUMO consists 2% Au, 7% triazole, 54% fluorene, and 36% benzothiazole, where percentages are of orbital density.

The $S_1$ state is again derived primarily (98%) from a LUMO ← HOMO excitation. These results, in conjunction with highly structured absorption spectra, support the assignment that the absorption transitions are π-π* in nature. The results are representative for all four structures. Figure 4.5 displays a time-dependent density-functional theory (TD-DFT) state plot for **Au-DiBTF(0-3)'**. The results accord the photophysical data obtained for the four complexes, particularly in regards to the rate of intersystem crossing. Generally, the alkynyl complexes **(Au-DiBTF(0-2')** display similar rates of intersystem crossing. TD-DFT computations accord with this result demonstrating that regardless of ancillary ligand, the $S_1$-to-$T_2$ energy gap for the alkynyl complexes are similar (0.43 and 0.44) (Figure 4.5). The triazolyl complex, **Au-DiBTF3'**, displays a rate of intersystem crossing nearly twice that of the alkynyl complexes, and also exhibits an $S_1$-to-$T_2$ energy gap nearly half that of the alkynyl analogues (0.27).

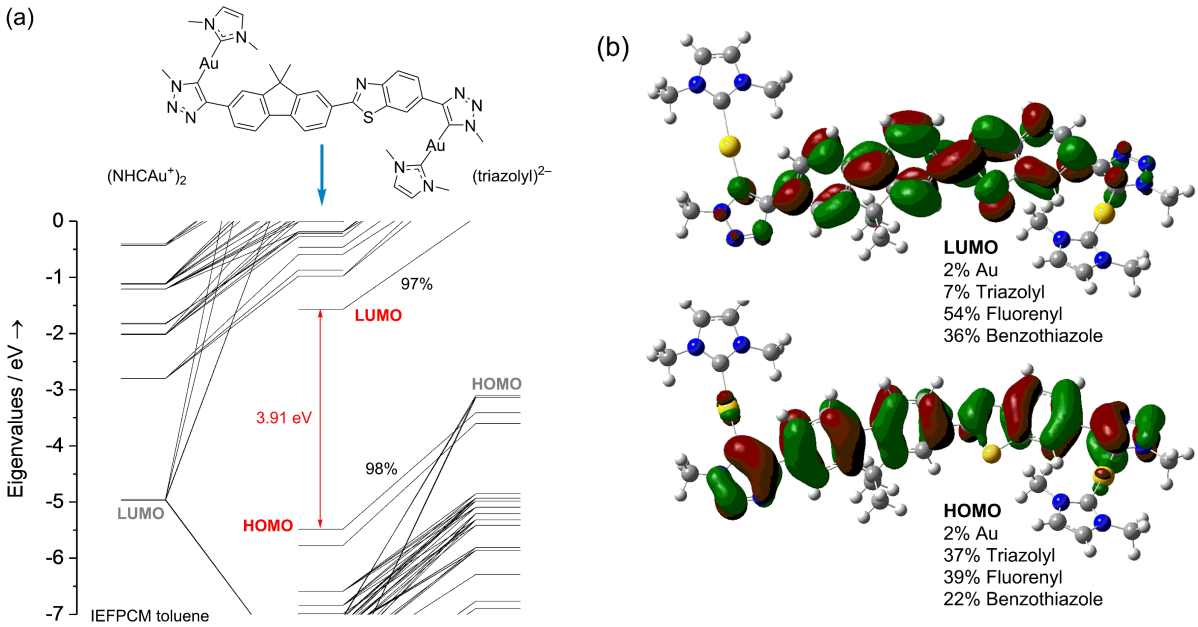


**Figure 4.4.** (Left) Partial Kohn-Sham orbital energy level diagram of model complex **Au-DiBTF3′**. Fluorenyl ethyl groups and carbene 2,6-diisopropylphenyl groups have been replaced with methyl groups for computational tractability. (Right) Plots of selected orbitals, with fragment compositions indicated. Percentages are of orbital density (contour level 0.02 a.u.).

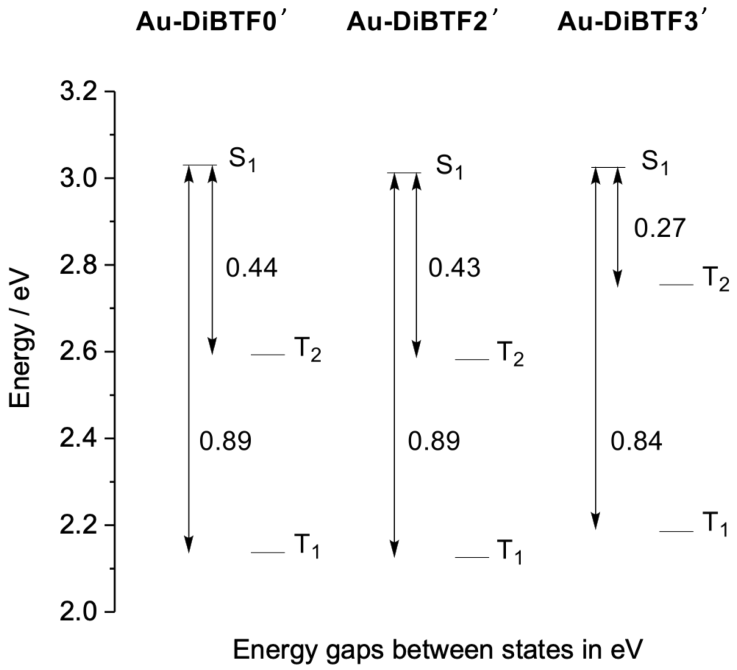


**Figure 4.5.** Calculated excited-state energies of **Au-DiBTF(0–3)'.**

**Conclusions.**

Four new digold(I) BTF complexes, **Au-DiBTF(0-3)** were synthesized and photophysically characterized in yields of 52-80%. The four complexes are characterized by highly structured ground-state absorption and emission spectra following the energy trends **Au-DiBTF0** ≈ **Au-DiBTF1** > **Au-DiBTF2** > **Au-DiBTF3**. These complexes emit via dual-luminescence; highly structured fluorescence and phosphorescence. General trends in the photophysical data: The three alkynyl complexes (**Au-DiBTF (0-2)**) exhibit similar fluorescence lifetimes, triplet state quantum yields, and fluorescence quantum yields leading to similar excited-state rate constants. **Au-DiBTF3** exhibits an increased triplet state quantum yield and a decreased fluorescence lifetime fluorescence quantum yield leading to the fastest rate of intersystem crossing

Density-functional theory calculations show that both the HOMO and LUMO for all four complexes is localized on the BTF ligand and that the $S_1$ state derives from a (98%) LUMO ←

HOMO excitation. This leads us to believe that the absorption transitions are π-π* in nature. TD-DFT computations agree with the photophysical data. **Au-DiBTF** (**0-2**) have computed similar $S_1$-to-$T_2$ energy gaps while **Au-DiBTF3** exhibits an $S_1$-to-$T_2$ energy gap nearly half that of the alkynyl complexes. This is believed to contribute to the greater rate of intersystem crossing and larger triplet-state quantum yield of **Au-DiBTF3**.

**Experimental Details.**

**General Considerations.** All experimental procedures were carried out under an inert atmosphere of argon using standard Schlenk line techniques. All purchased chemicals were used as received without any further manipulation. Microanalyses (C, H, and N) were undertaken by Atlantic Microlab. Mass spectrometry was performed at the University of Cincinnati Mass Spectrometry facility. (Phosphine)gold(I) chlorides and (IMesNHC)AuCl were prepared according to literature procedures.[3] BTF Dialkyne was synthesized according to a modified literature procedure that was referenced in the manuscript.[2] Dry MeOH, dichloromethane, pentanes, diethyl ether, THF, DMF, 1.6 M n-butyl lithium in hexanes, KOH, diethyl bromide, $Pd(dba)_2$, CuI, $PPh_3$, Copper turnings were purchased from Sigma Aldrich. DMSO, *tert*-butanol, and sodium hydroxide were purchased from Fisher Scientific. Dibromofluorene was purchased from Accela. TMS-acetylene, triethylamine, and benzyl azide were purchased from Alfa Aesar. Tetrabutylammonium fluoride was purchased from TCI. 2-amino-5-bromobenzenethiol was purchased from AChemBlock. $^1$H NMR experiments were performed on a Bruker-500 Ascend Advanced III HD NMR spectrometer operating at 500.24 MHz. $^1$H chemical shifts are reported in parts per million ($\delta$) with integration and multiplicity (s = singlet, d = doublet, t = triplet, q = quartet, dd = doublet of doublets, dt = doublet of triplets, td = triplet of doublets, ddd = doublet of doublet of doublets, and m = multiplet), measured from tetramethylsilane (0 ppm) and are referenced to residual solvent in $CDCl_3$ (7.26 ppm). $^{31}P\{^1H\}$ NMR, chemical shifts were determined relative to concentrated $H_3PO_4$.

**Synthesis, NMR, Mass Spectrometry and Elemental Analysis**

Ligand Synthesis: All compounds not described in this SI have been reported previously. HRMS and EA are only reported for the organometallic complexes which are the last steps in the overall

syntheses.

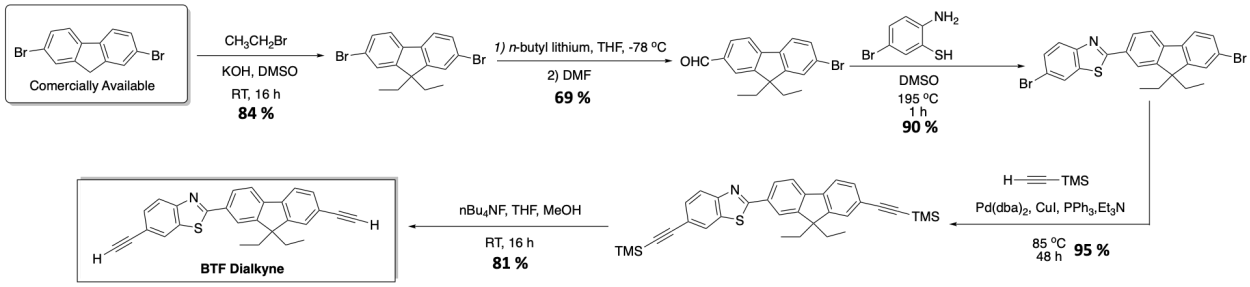


**Scheme 4.4.** Synthesis of BTF dialkyne ligand

**6-bromo-2-(7-bromo-9,9-diethyl-9*H*-fluoren-2-yl)benzo[*d*]thiazole:**

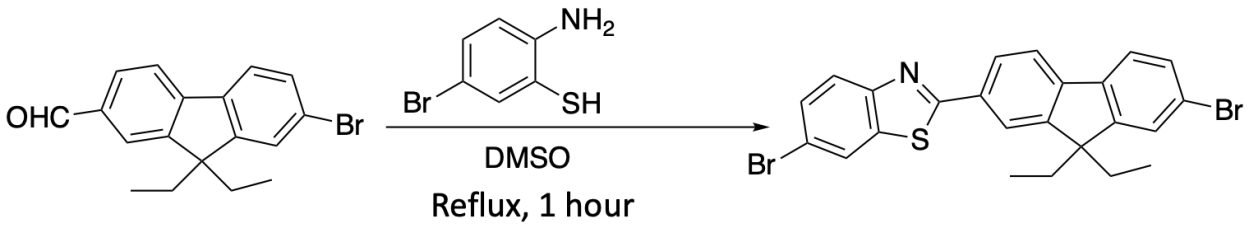


To a 100 mL flask equipped with a stir bar was added (2.00 g, 6.08 mmol) of aldehyde, and (1.54 g, 7.60 mmol) of 2-amino-5-bromobenzenethiol. DMSO (20 mL) was then added and a reflux condenser was attached. The vessel was allowed to heat at 195 °C for 1 hour (behind a blast shield). The mixture was then poured into DI water yielding a grey suspension. This suspension was then filtered under vacuum to yield the crude product as a dark gray solid. Purification via flash column chromatography was performed. Hexanes was used to elute the starting material and 7:3 DCM:Hexanes was used to elute the product as a white solid. (2.80 g, 90 % yield).$^1$H NMR (500 MHz, Chloroform-*d*) δ 8.09 – 8.04 (m, 2H), 8.03 – 7.99 (m, 1H), 7.93 (d, *J* = 8.6 Hz, 1H), 7.77 (d, *J* = 7.9 Hz, 1H), 7.64 – 7.58 (m, 2H), 7.52 – 7.48 (m, 2H), 2.19 – 2.14 (m, 2H), 2.07 (dd, *J* = 13.8, 7.2 Hz, 2H), 0.35 (t, *J* = 7.3 Hz, 6H).

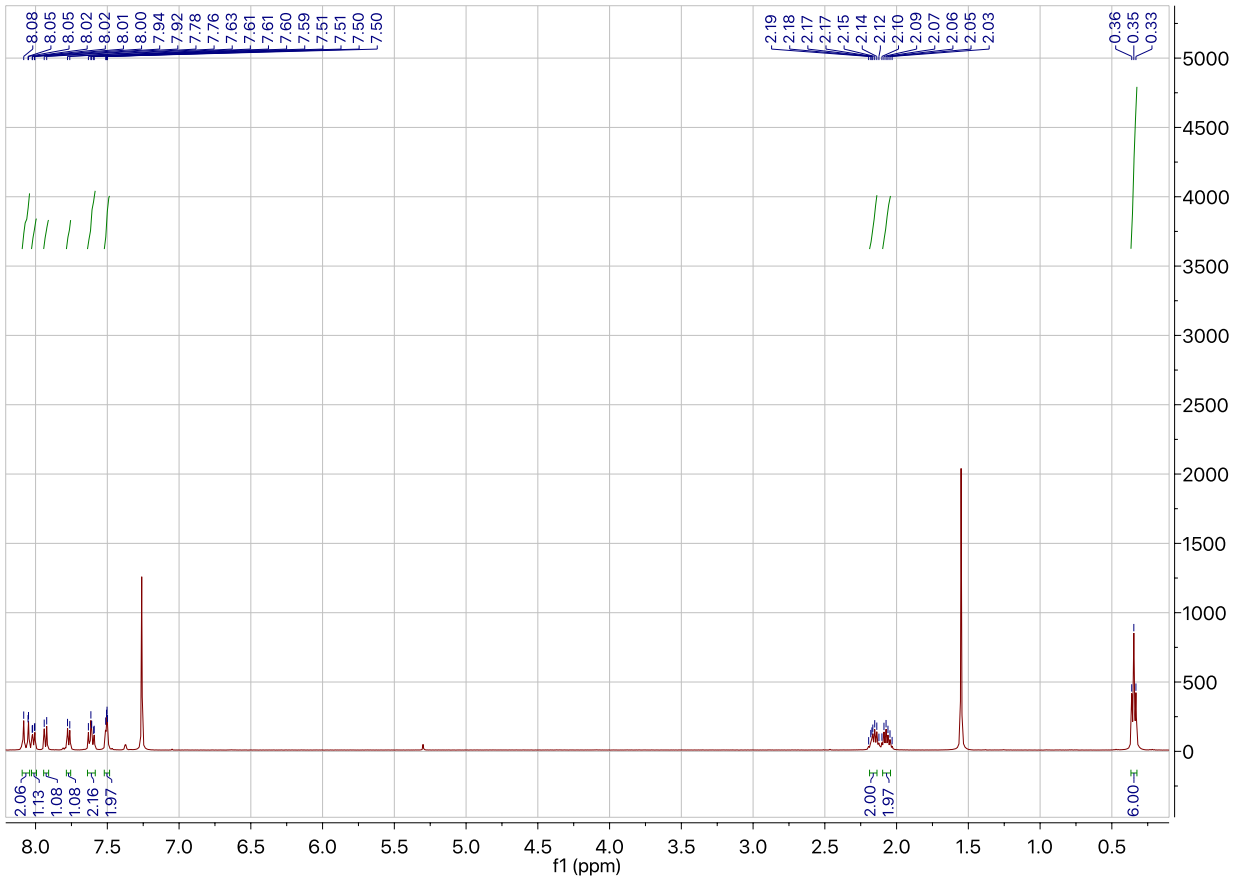


**Figure 4.6.** $^{1}$H NMR Spectrum of 6-bromo-2-(7-bromo-9,9-diethyl-9*H*-fluoren-2-yl)benzo[*d*]thiazole

**2-(9,9-diethyl-7-((trimethylsilyl)ethynyl)-9*H*-fluoren-2-yl) ((trimethylsilyl)ethynyl) benzo [*d*]thiazole:**

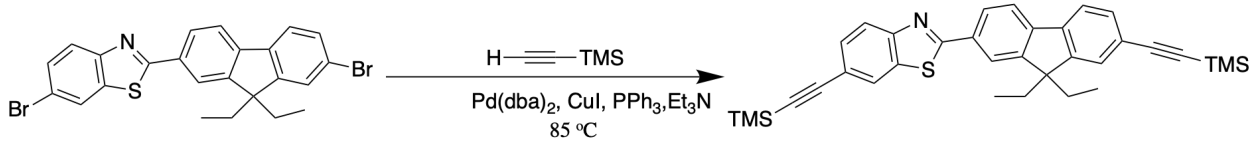


To a flame-dried 50 mL round bottom flask equipped with a stir bar was added (200 mg, 0.390 mmol) of dibromo species, (8.9 mg, 0.0156 mmol) of palladium source, (8.2 mg, 0.0312 mmol) of triphenylphosphine, and (3.0 mg, 0.0156 mmol) of copper(I) iodide. A reflux condenser was then added and the system was purged with argon for 20 min. 10 mL of triethyl amine (which was

deareated by three freeze-pump-thaw cycles) was then cannulated into the flask containing all other reactants. (0.162 mL, 1.17 mmol) of TMS acetylene was quickly added to the flask via syringe. The flask was then heated at 85 $^{o}$C for 48 h. The contents were then concentrated on the roto-evaporator. Dichloromethane was then added and the suspension was filtered over a silica plug to yield a red/orange solution. The crude mixture was purified by flash column chromatography using 7:3 DCM:Hexanes as an eluent to afford product as an off-white solid (202 mg, 95 % Yield). $^{1}$H NMR (500 MHz, Chloroform-*d*) δ 8.09 (s, 1H), 8.04 – 8.01 (m, 2H), 7.98 (d, *J* = 8.4 Hz, 1H), 7.77 (d, *J* = 7.9 Hz, 1H), 7.69 (d, *J* = 7.8 Hz, 1H), 7.58 (d, *J* = 9.6 Hz, 1H), 7.52 – 7.46 (m, 2H), 2.15 (dd, *J* = 13.8, 7.2 Hz, 2H), 2.08 (dd, *J* = 13.8, 7.2 Hz, 2H), 0.31 (t, *J* = 7.4 Hz, 6H), 0.29 (s, 9H), 0.28 (s, 9H).

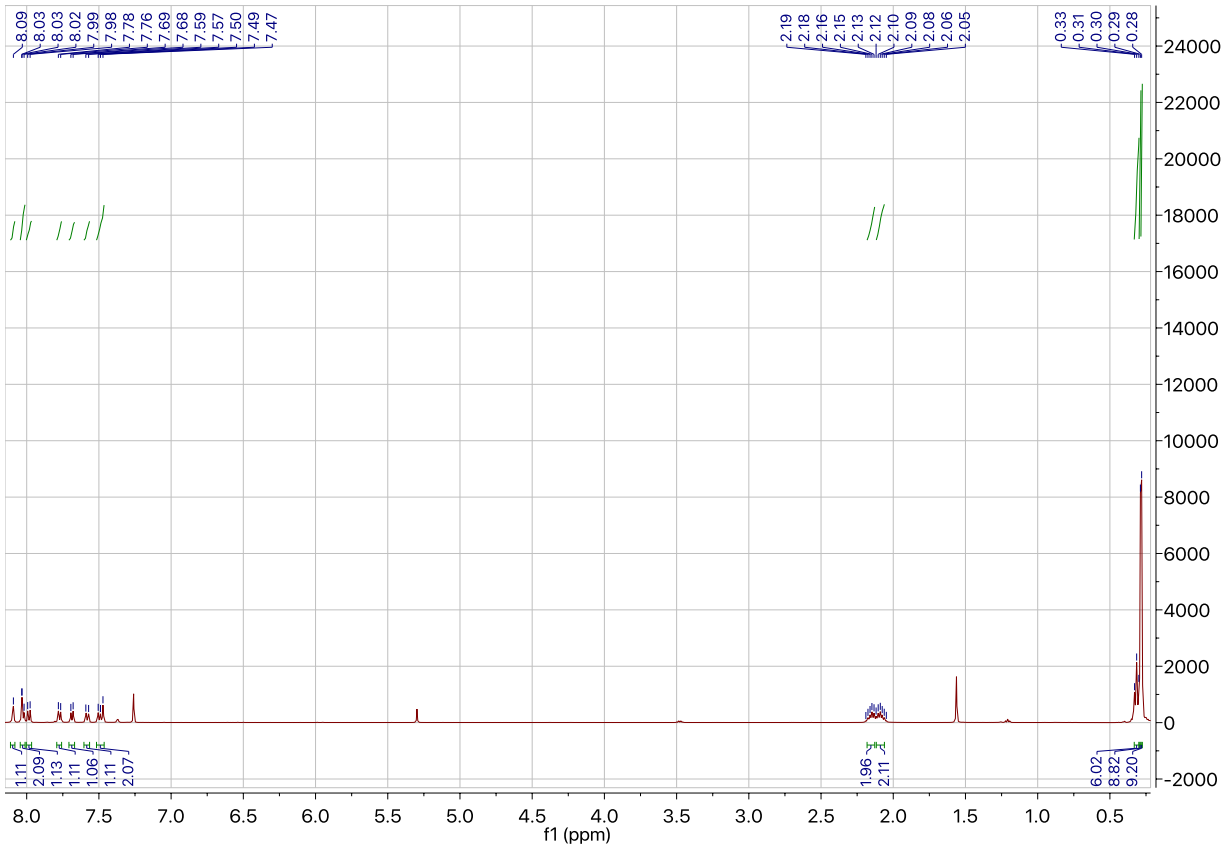


**Figure 4.7.** [1]H NMR Spectrum of 2-(9,9-diethyl-7-((trimethylsilyl)ethynyl)-9*H*-fluoren-2-yl) ((trimethylsilyl)ethynyl) benzo [*d*]thiazole

**2-(9,9-diethyl-7-ethynyl-9*H*-fluoren-2-yl)-6-ethynylbenzo[*d*]thiazole:**

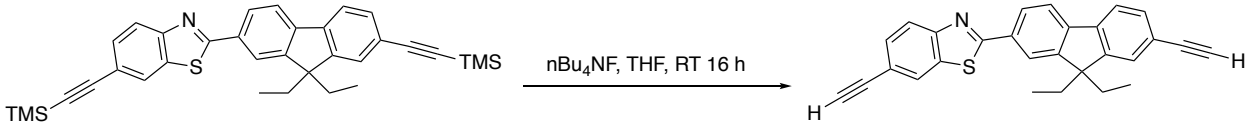


To a 25 mL round bottom flask equipped with a stir bar was added (174 mg, 0.318 mmol) of dialkyne. 10 mL of THF was then added creating an orange solution. (185 mg, 0.796 mmol) of tetrabutyl ammonium fluoride was then added and the solution turned wine red almost immediately. This solution was allowed to stir overnight. The solution was then concentrated on the roto-evaporator and purified by flash column chromatography using 9:1 DCM: Hexanes as an

eluent to yield an orange solid (129 mg, 81 % yield). $^{1}$H NMR (500 MHz, Chloroform-*d*) δ 8.11 (s, 1H), 8.07 – 8.04 (m, 1H), 8.04 – 7.99 (m, 2H), 7.80 (d, *J* = 7.9 Hz, 1H), 7.72 (d, *J* = 7.8 Hz, 1H), 7.63 – 7.59 (m, 1H), 7.54 – 7.49 (m, 2H), 3.17 (s, 2H), 2.19 – 2.08 (m, 4H), 0.34 (t, *J* = 7.3 Hz, 6H).

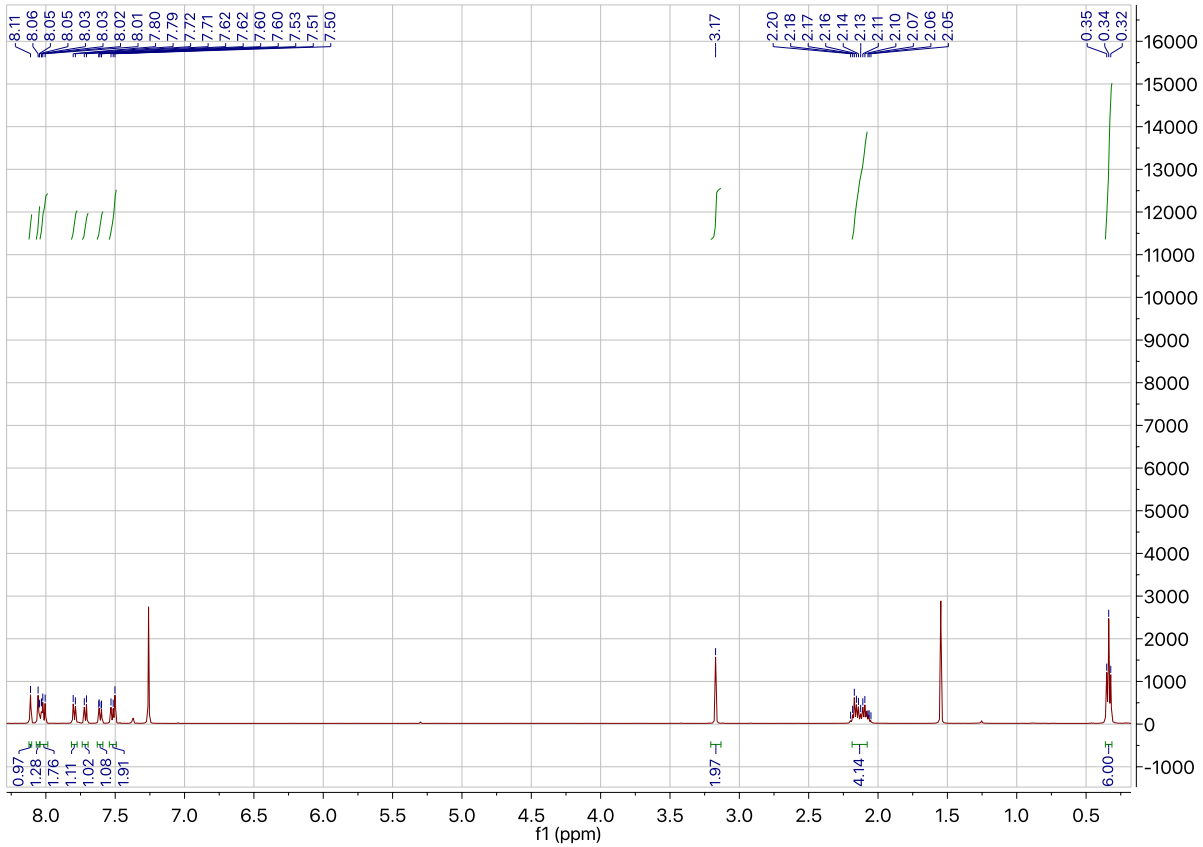


**Figure 4.8** $^{1}$H NMR Spectrum of 2-(9,9-diethyl-7-ethynyl-9*H*-fluoren-2-yl)-6-ethynylbenzo[*d*]thiazole

**Au-DiBTF0:**

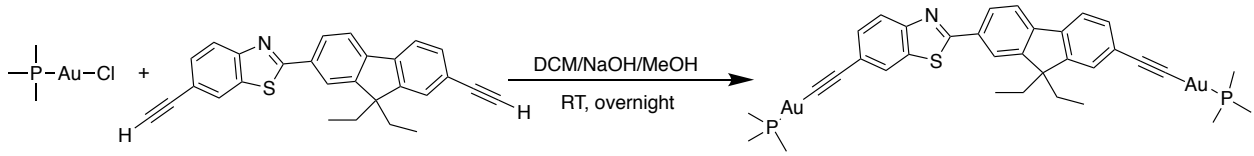


BTF Dialkyne ligand (65.8 mg, 0.163 mmol) was added to a flame-dried 25 mL round bottom flask equipped with a stir bar. After purging with argon for 20 minutes, 10 mL of dry dichloromethane was added. Then, NaOMe (6 mL, 1.63 mmol) (prepared from dissolving 42.7 mg of NaOH in 25 mL dry MeOH) was added and the solution was allowed to stir for 15 min. To a separate 50 mL flask that was flame-dried and equipped with a stir bar was added (100 mg, 0.326 mmol) of $PMe_3AuCl$, the flask was then purged with argon for 20 minutes. After 20 minutes, 2 mL of dry MeOH was added. The basic solution was then added dropwise to the suspension of $Me_3PAuCl$ while stirring. After complete addition, the contents were allowed to stir at RT for 16 h. The mixture was then concentrated on a roto-evaporator, dissolved in DCM and passed through a Celite plug. This orange-ish solution was then concentrated to dryness. Analytically pure material was obtained through either washing with copious amounts of pentanes/diethyl ether, or by vapor diffusion of diethyl ether into a concentrated dichloromethane solution (81.8 mg, 53 % Yield). $^1$H NMR (500 MHz, Chloroform-*d*) δ 8.05 (s, 1H), 8.00 – 7.95 (m, 2H), 7.91 (d, *J* = 8.5 Hz, 1H), 7.72 (d, *J* = 8.0 Hz, 1H), 7.63 (s, 1H), 7.57 (d, *J* = 8.5 Hz, 1H), 7.50 – 7.45 (m, 2H), 2.07 (ddt, *J* = 28.6, 13.6, 7.1 Hz, 4H), 1.55 (s, 9H), 1.53 (s, 9H), 0.31 (t, *J* = 7.3 Hz, 6H). $^{31}$P NMR (202 MHz, $CDCl_3$) δ 0.09, 0.00. HRMS (FT-ICR, $[M+H]^+$) m/z calcd for $MH^+$ $C_{34}H_{38}NP_2SAu_2^+$, 948.15257 found 948.15257. Anal. Calcd for: $C_{34}H_{37}Au_2NP_2S$: C, (43.09); H, (3.94); N, (1.48). Found: C, (43.34); H, (4.08); N, (1.37).


**Figure 4.9** $^{1}$H NMR Spectrum of **Au-DiBTF0**

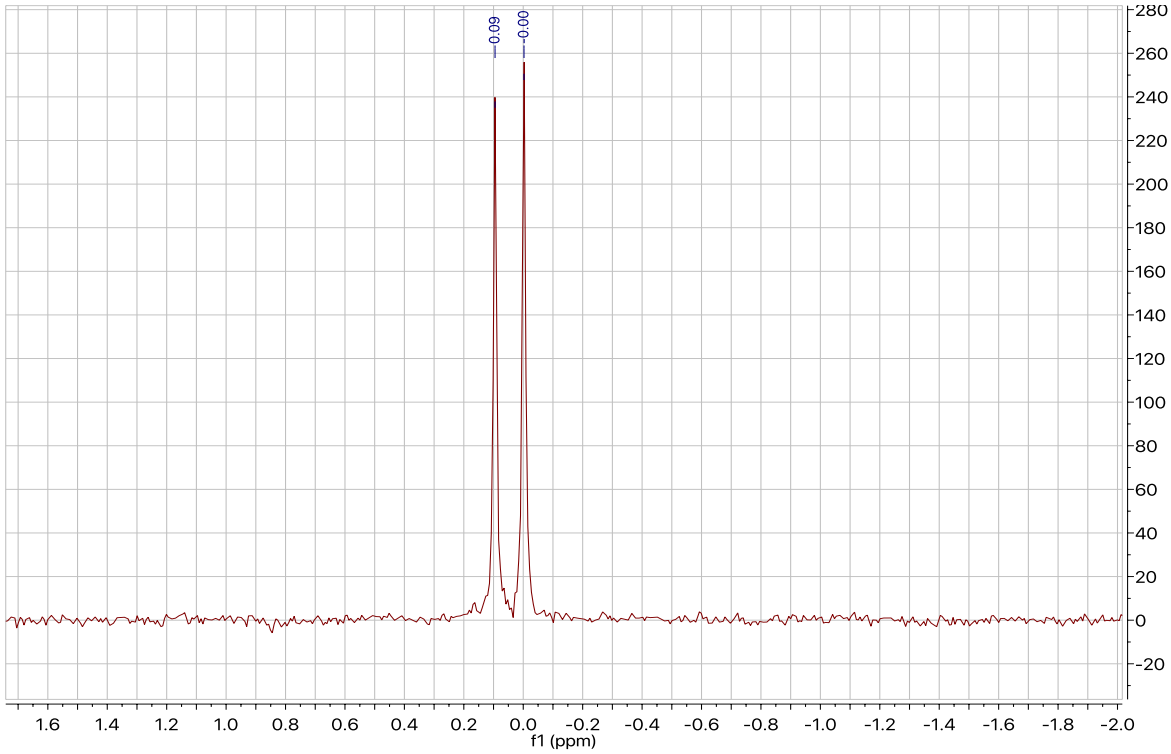


**Figure 4.10** $^{31}$P{$^{1}$H} NMR Spectrum of **Au-DiBTF0**

**Au-DiBTF1:**

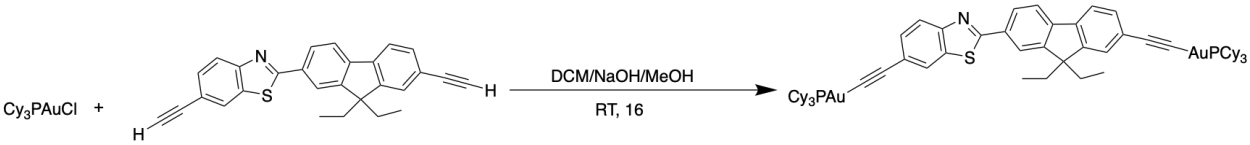


BTF Dialkyne ligand (49.36 mg, 0.122 mmol) was added to a flame-dried 25 mL round bottom flask equipped with a stir bar. After purging with argon for 20 minutes, 10 mL of dry dichloromethane was added. Then, NaOMe (6 mL, 1.63 mmol) (prepared from dissolving 42.7 mg of NaOH in 25 mL dry MeOH) was added and the solution was allowed to stir for 15 min. To a separate 50 mL flask that was flame-dried and equipped with a stir bar was added (83.59 mg, 0.163 mmol) of $Cy_3PAuCl$, the flask was then purged with argon for 20 minutes. After 20 minutes, 2 mL of dry MeOH was added. The basic solution was then added dropwise to the suspension of $Cy_3PAuCl$ while stirring. After complete addition, the contents were allowed to stir at RT for 16 h. The mixture was then concentrated on a roto-evaporator, dissolved in DCM and passed through a Celite plug. This orange-ish solution was then concentrated to dryness. Analytically pure material was obtained through either washing with copious amounts of pentanes/diethyl ether, or by vapor diffusion of diethyl ether into a concentration dichloromethane solution (100 mg, 60 % Yield). $^1$H NMR (500 MHz, Chloroform-*d*) δ 8.02 (d, *J* = 14.0 Hz, 2H), 7.99 – 7.95 (m, 1H), 7.90 (d, *J* = 8.5 Hz, 1H), 7.71 (d, *J* = 8.0 Hz, 1H), 7.63 – 7.58 (m, 2H), 7.53 – 7.48 (m, 2H), 2.10 – 1.97 (m, 22H), 1.86 (d, *J* = 7.9 Hz, 12H), 1.74 (s, 6H), 1.50 (d, *J* = 11.4 Hz, 11H), 1.28 (p, *J* = 13.9, 13.3 Hz, 19H), 0.29 (t, *J* = 7.3 Hz, 6H). $^{31}$P NMR (202 MHz, $CDCl_3$) δ 56.40, 56.32. HRMS (FT-ICR, $[M+H]^+$) m/z calcd for $MH^+$ $C_{64}H_{86}NP_2SAu_2^+$,1356.52818 found 1356.53847. Anal. Calcd for: $C_{64}H_{85}Au_2NP_2S$: C, (56.68); H, (6.32); N, (1.03). Found: C, (56.63); H, (6.34); N, (1.17).

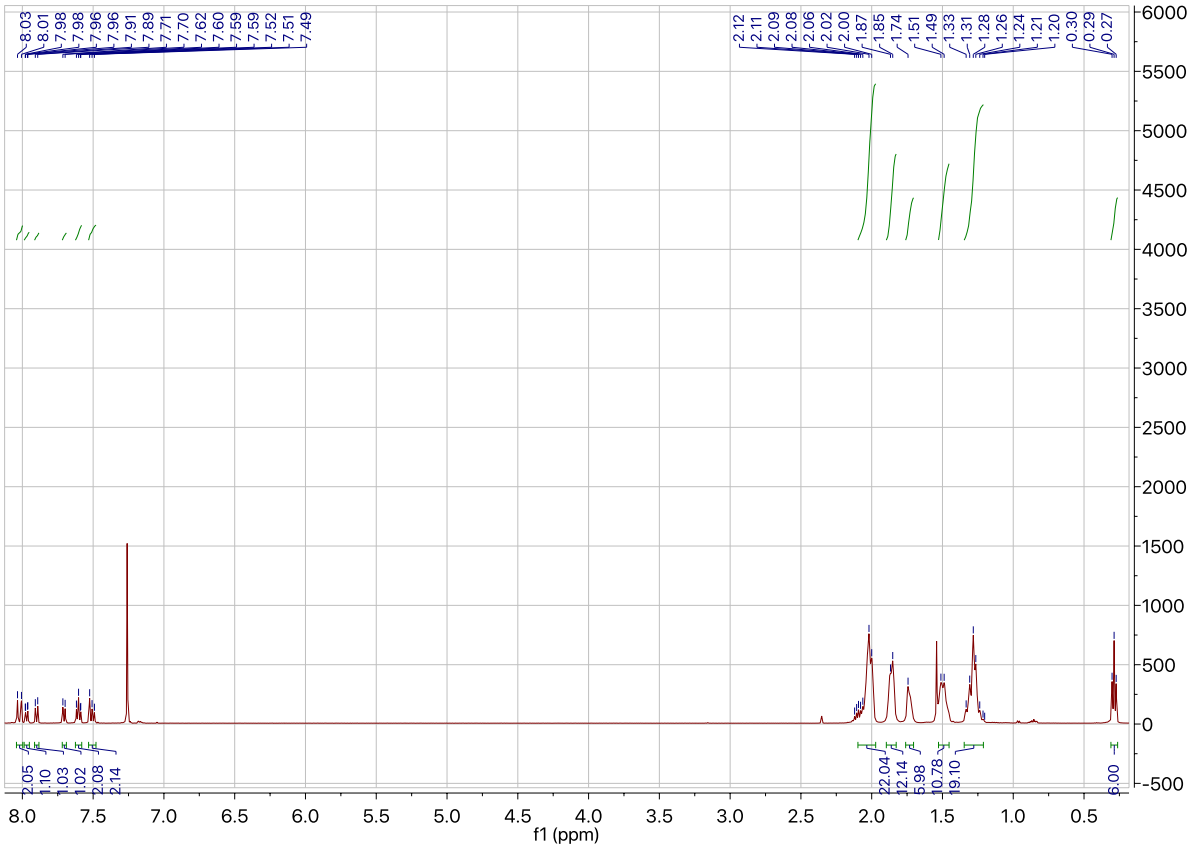


**Figure 4.11.** $^{1}$H NMR Spectrum of **Au-DiBTF1** (Disclaimer: Peak that overlaps with water was integrated with solvent peak function turned "off" in the MestReNova software in order to achieve maximum accuracy)

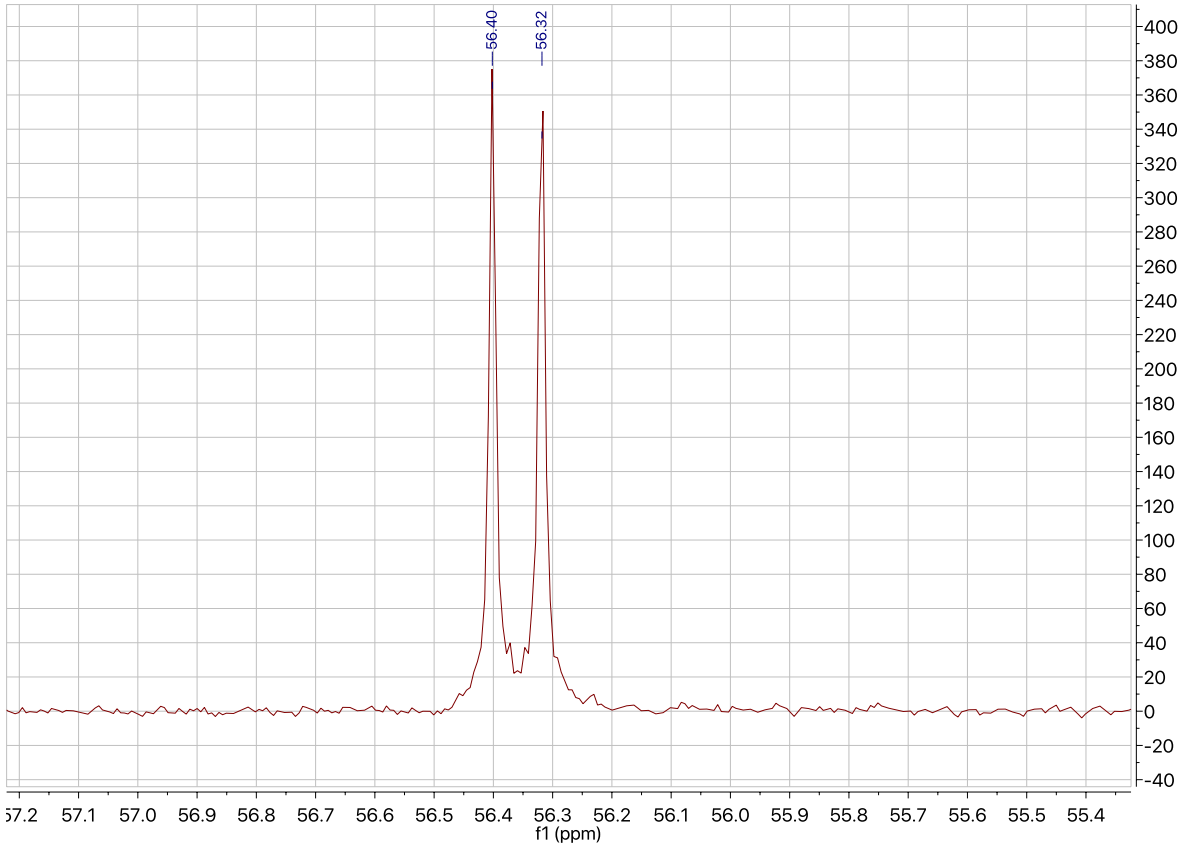


**Figure 4.12** $^{31}P\{^{1}H\}$ NMR Spectrum of **Au-DiBTF1**

**Au-DiBTF2:**

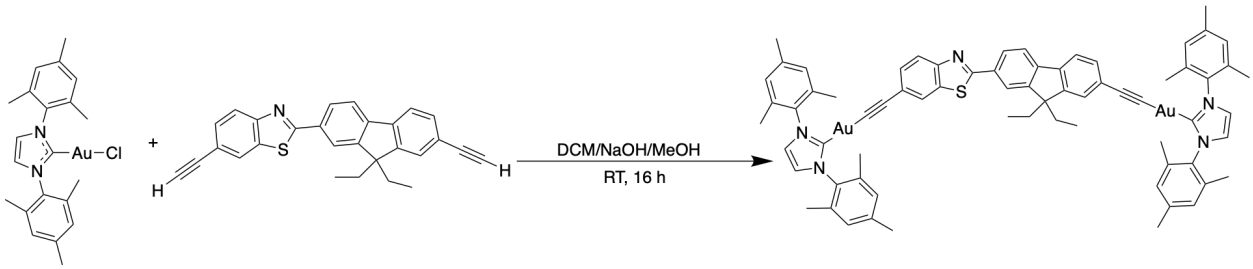


BTF Dialkyne ligand (65.8 mg, 0.163 mmol) was added to a flame-dried 25 mL round bottom flask equipped with a stir bar. After purging with argon for 20 minutes, 10 mL of dry dichloromethane was added. Then, NaOMe (6 mL, 1.63 mmol) (prepared from dissolving 42.7 mg of NaOH in 25 mL dry MeOH) was added and the solution was allowed to stir for 15 min. To a separate 50 mL flask that was flame-dried and equipped with a stir bar was added (176 mg, 0.326 mmol) of IMesAuCl, the flask was then purged with argon for 20 minutes. After 20 minutes, 2 mL

of dry MeOH was added. The basic solution was then added dropwise to the suspension of IMesAuCl while stirring. After complete addition, the contents were allowed to stir at RT for 16 h. The mixture was then concentrated on a roto-evaporator, dissolved in DCM and passed through a Celite plug. This yellow-ish solution was then concentrated to dryness. Analytically pure material was obtained through either washing with copious amounts of pentanes/diethyl ether, or by vapor diffusion of diethyl ether into a concentration dichloromethane solution (185 mg, 81% yield).$^{1}$H NMR (500 MHz, Chloroform-*d*) δ 7.95 (s, 1H), 7.90 (d, *J* = 8.0 Hz, 1H), 7.84 (s, 1H), 7.79 (d, *J* = 8.6 Hz, 1H), 7.62 (d, *J* = 8.0 Hz, 1H), 7.50 (d, *J* = 7.9 Hz, 1H), 7.43 (d, *J* = 10.0 Hz, 1H), 7.34 (d, *J* = 10.2 Hz, 2H), 7.07 (d, *J* = 1.7 Hz, 4H), 6.99 (s, 8H), 2.35 (s, 12H), 2.13 (s, 24H), 2.05 – 2.00 (m, 2H), 1.96 – 1.92 (m, 2H), 0.19 (t, *J* = 7.3 Hz, 6H). HRMS (FT-ICR, $[M+H]^+$) m/z calcd for $MH^+$ $C_{70}H_{68}N_5SAu_2^+$1404.45178 found 1404.45210. Anal. Calcd for:$C_{74}H_{67}Au_2N_5S$: C, (59.87); H, (4.81); N, (4.99). Found: C, (59.86); H, (4.98); N, (5.07).

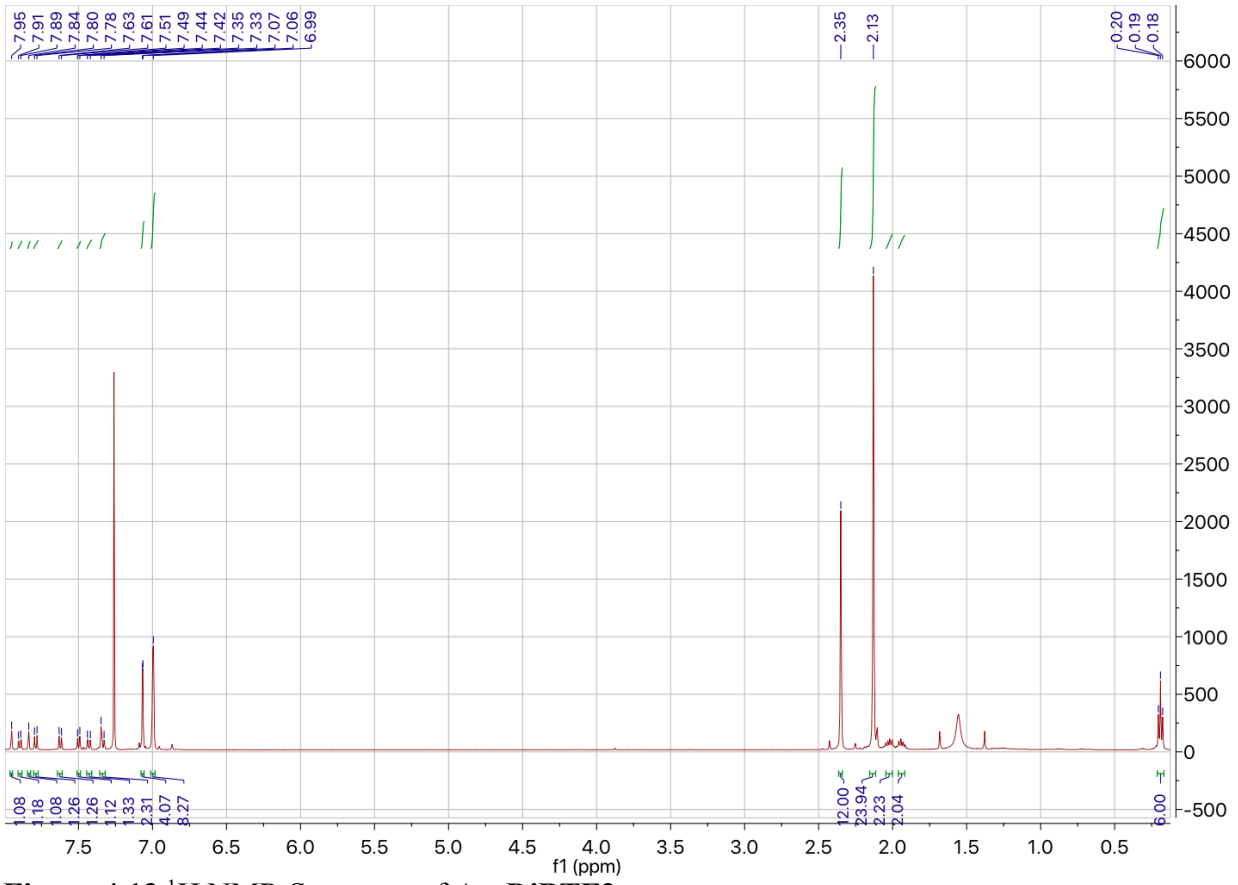


**Figure 4.13** $^{1}$H NMR Spectrum of **Au-DiBTF2**

**Au-DiBTF3:**

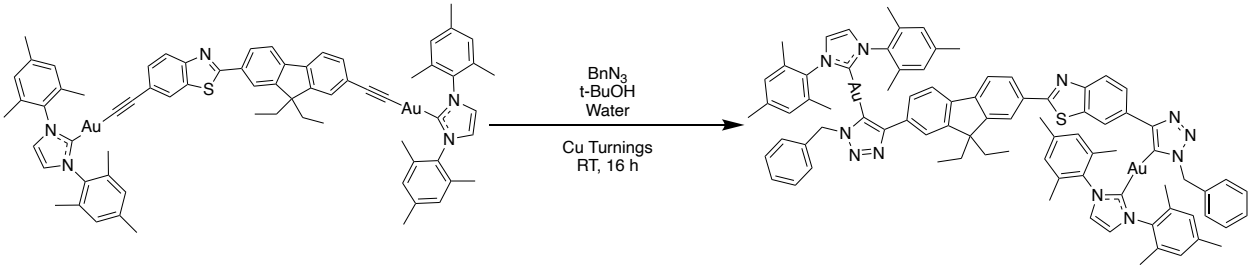


To a 50 mL flask equipped with a stir bar was added (88.9 mg, 0.064 mmol) of Au-DiBTF2. 10 mL of *tert*-butanol was then added along with 5.0 mL of DI water. (0.516 mL, 0.362 mmol) of benzyl azide was then added dropwise and allowed to stir for 5 min. An excess of copper turnings (around 4 times the stoichiometry of the starting material) was then added and the suspension was allowed to stir overnight. After 16 h, DCM was added and an extraction was performed twice. These extracts were dried over magnesium sulfate and filtered. Concentrated *in vacuo* to yield a

tan solid which was washed with pentanes and dried. The compound was purified by slow diffusion of pentanes into a concentrated solution of dichloromethane to yield tan crystals (78.3 mg, 73 % Yield). $^1$H NMR (500 MHz, Chloroform-*d*) δ 8.58 (s, 1H), 8.18 (s, 1H), 8.09 (s, 1H), 8.07 – 8.04 (m, 1H), 7.99 (d, $J$ = 8.5 Hz, 1H), 7.87 (d, $J$ = 8.0 Hz, 1H), 7.73 (dd, $J$ = 20.5, 8.2 Hz, 3H), 7.17 (dd, $J$ = 14.3, 4.5 Hz, 12H), 7.03 (s, 10H), 5.15 (s, 2H), 5.11 (s, 2H), 2.40 (s, 6H), 2.37 (s, 6H), 2.17 – 2.11 (m, 28H), 0.31 (t, $J$ = 7.3 Hz, 6H). HRMS (FT-ICR, $[M+H]^+$) m/z calcd for $MH^+$ $C_{84}H_{82}N_{11}SAu_2^+$,1671.58345 found 1671.58275. Anal. Calcd for:$C_{84}H_{81}N_{11}SAu_2$: C, (60.39); H, (4.89); N, (9.22). Found: C, (60.27); H, (4.88); N, (9.34).

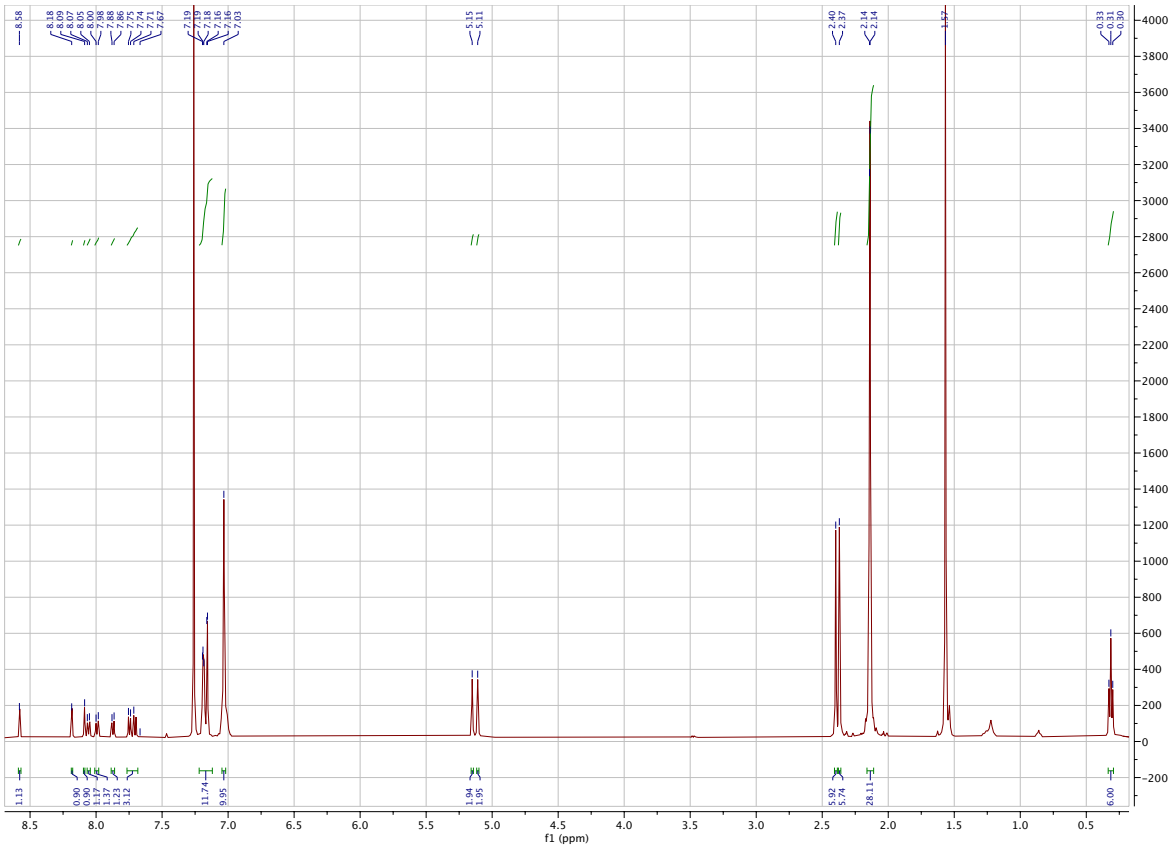


**Figure 4.14** $^1$H NMR Spectrum of **Au-DiBTF3**

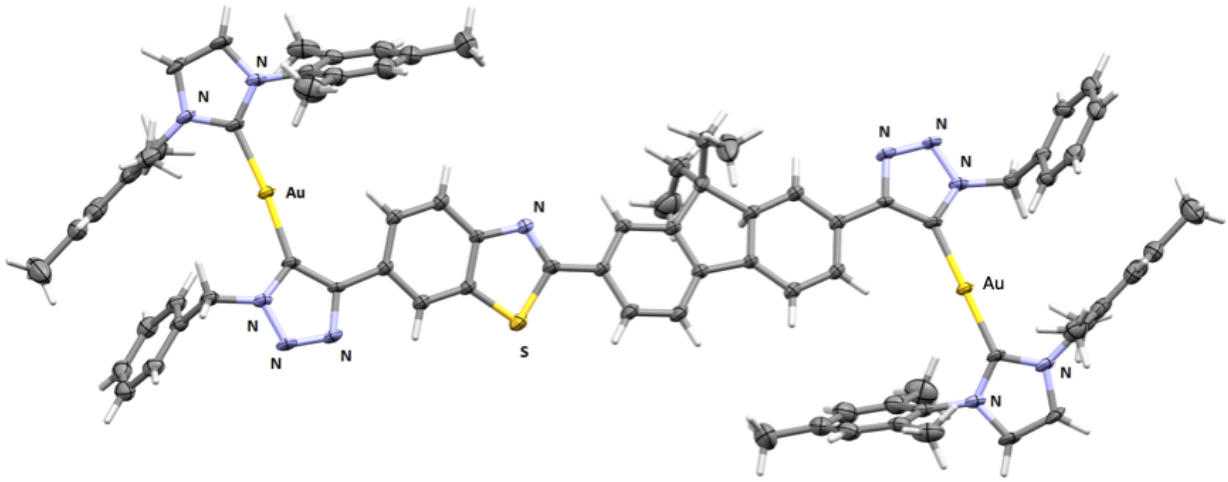


**Figure 4.15** Thermal ellipsoid representation of **Au-DiBTF3** (50% probability level, 150 K). A partial atom labeling scheme is indicated; unlabeled atoms are carbon and hydrogen. The structure is disordered across an inversion center. (disordered equivalent atoms omitted for clarity).

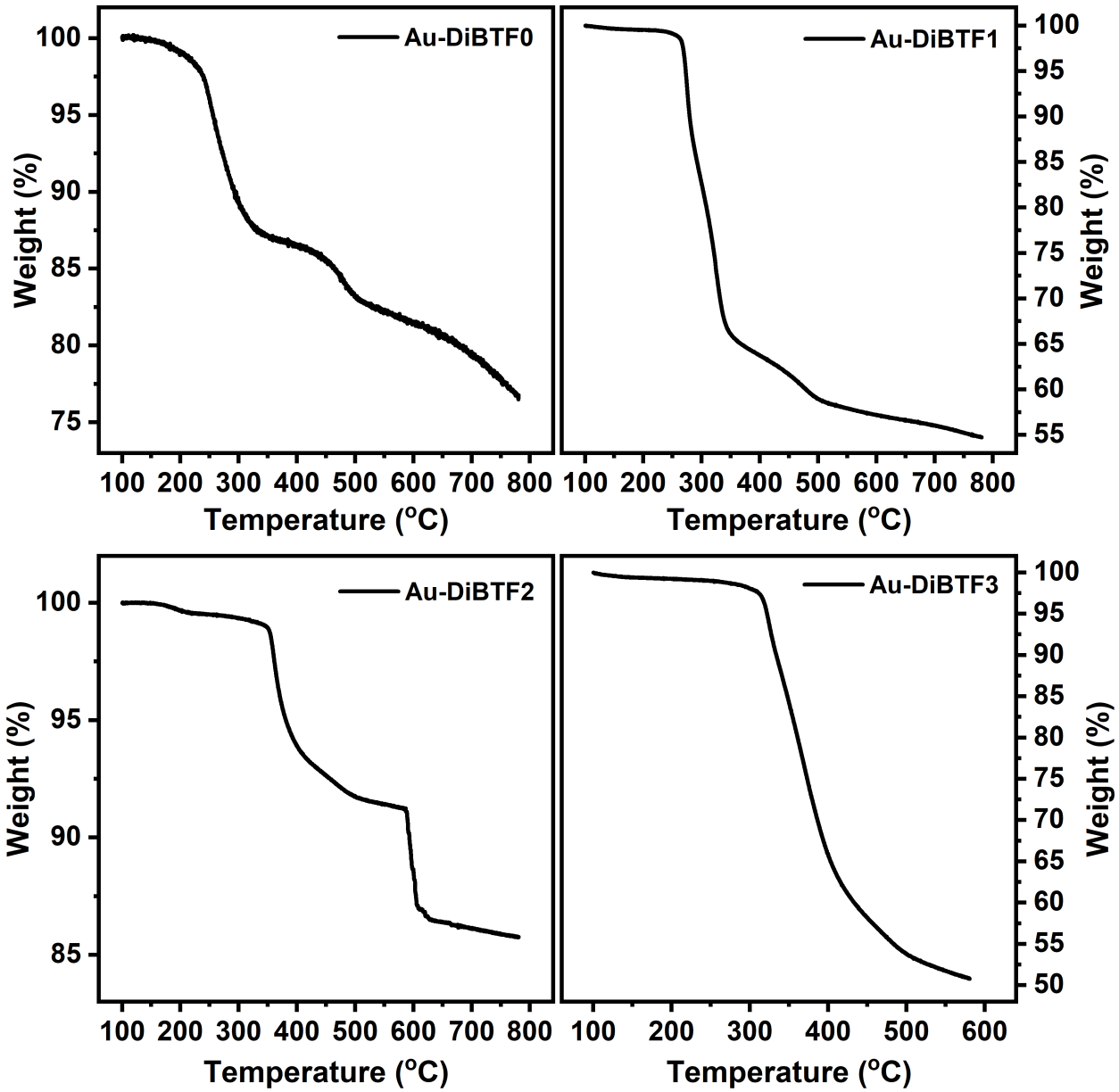


**Figure 4.16.** Thermogravimetric Analysis of **Au-DiBTF0** (top left), **Au-DiBTF1** (top right), **Au-DiBTF2** (bottom left), and **Au-DiBTF3** (bottom right).

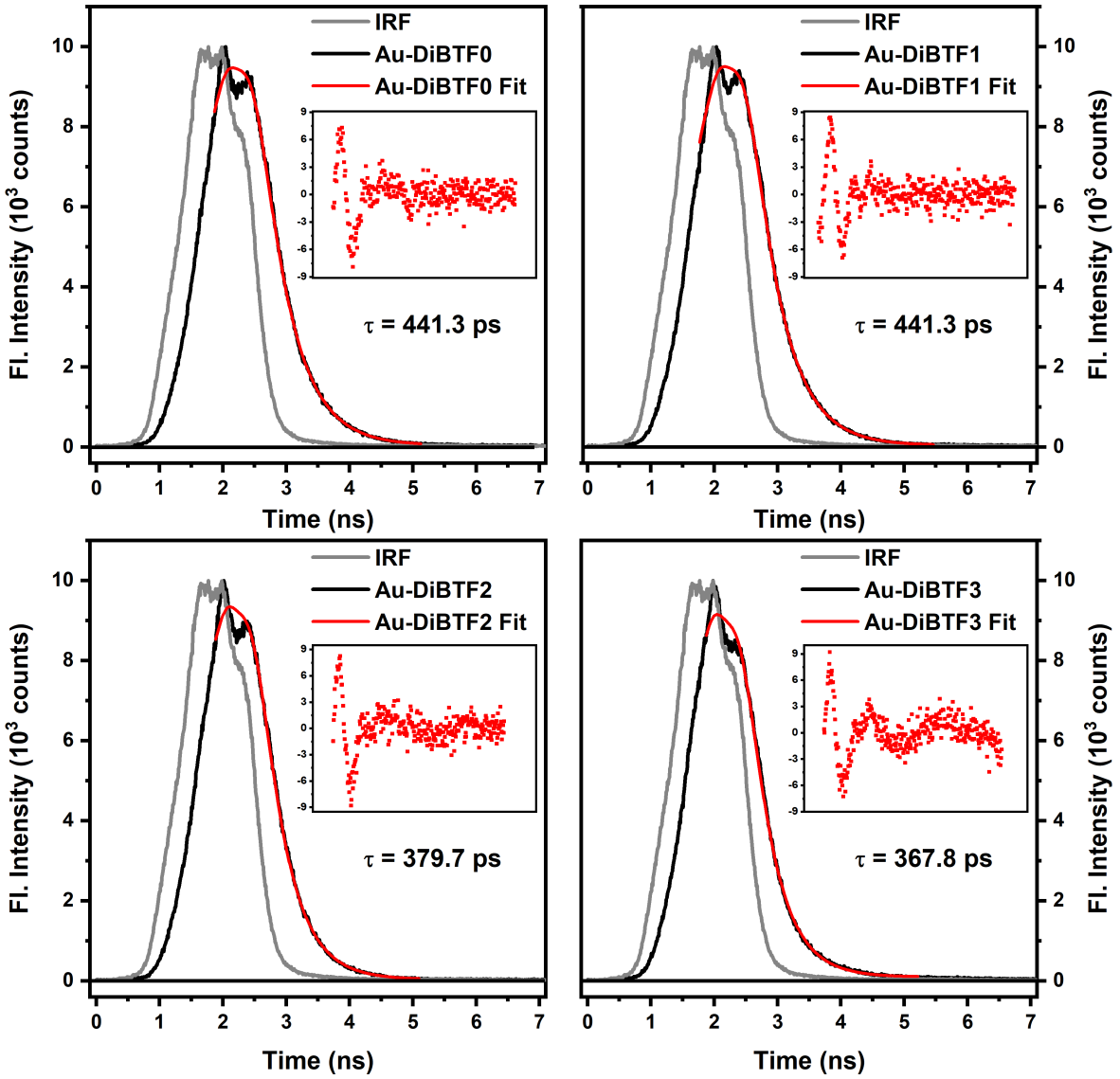


**Figure 4.17.** TCSPC Fluorescence Lifetimes of **Au-DiBTF0** (top left), **Au-DiBTF1** (top right), **Au-DiBTF2** (bottom left), and **Au-DiBTF3** (bottom right) collected in aerated toluene. Lifetimes were collected in duplicate, and the average values are reported in Table 4.1.

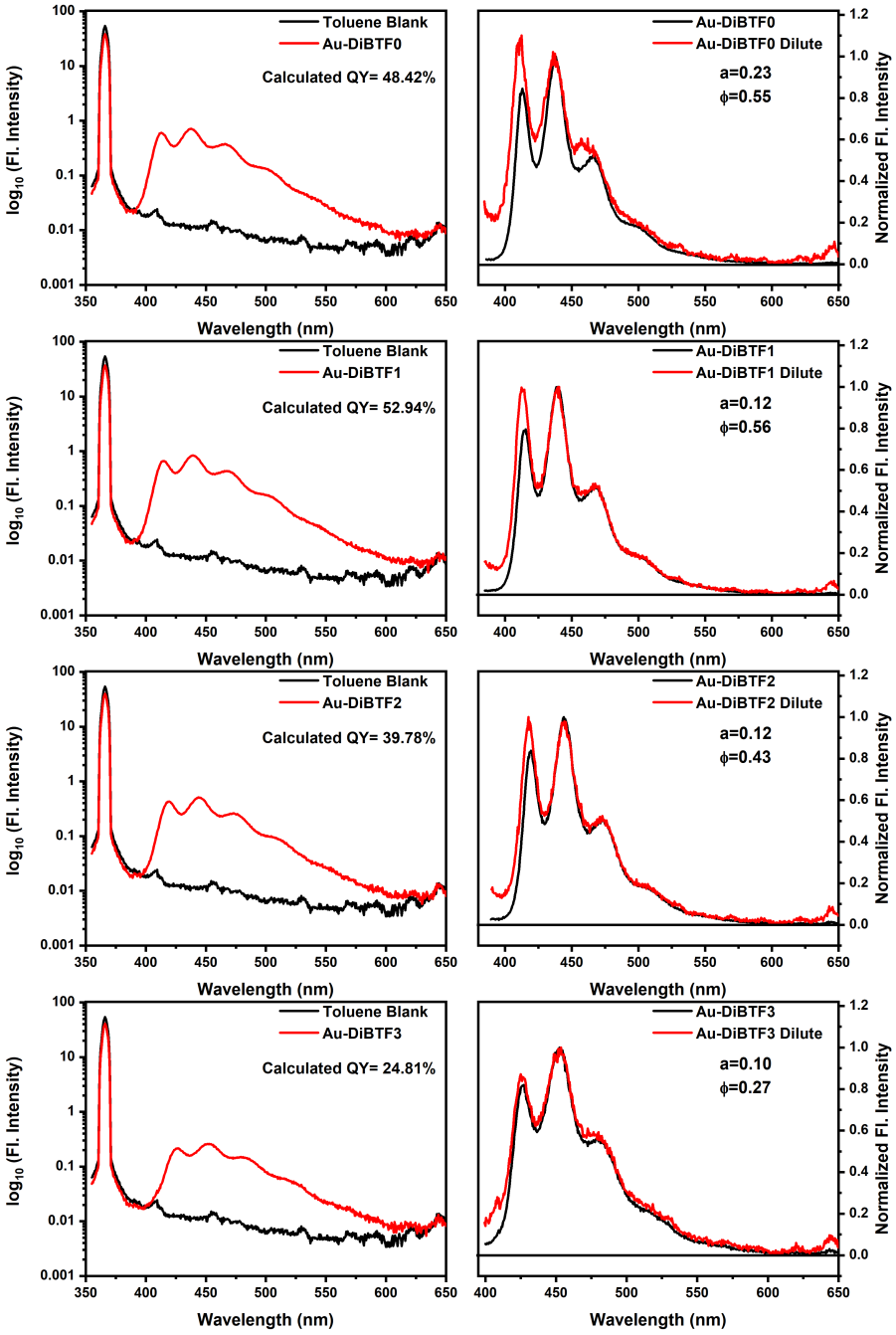


**Figure 4.18.** Fluorescence Quantum Yields of **Au-DiBTF0** (top), **Au-DiBTF1** (middle top), **Au-DiBTF2** (middle bottom), and **Au-DiBTF3** (bottom) collected in aerated toluene. The fluorescence quantum yields were collected in duplicate where the average value is reported in Table 4.1.

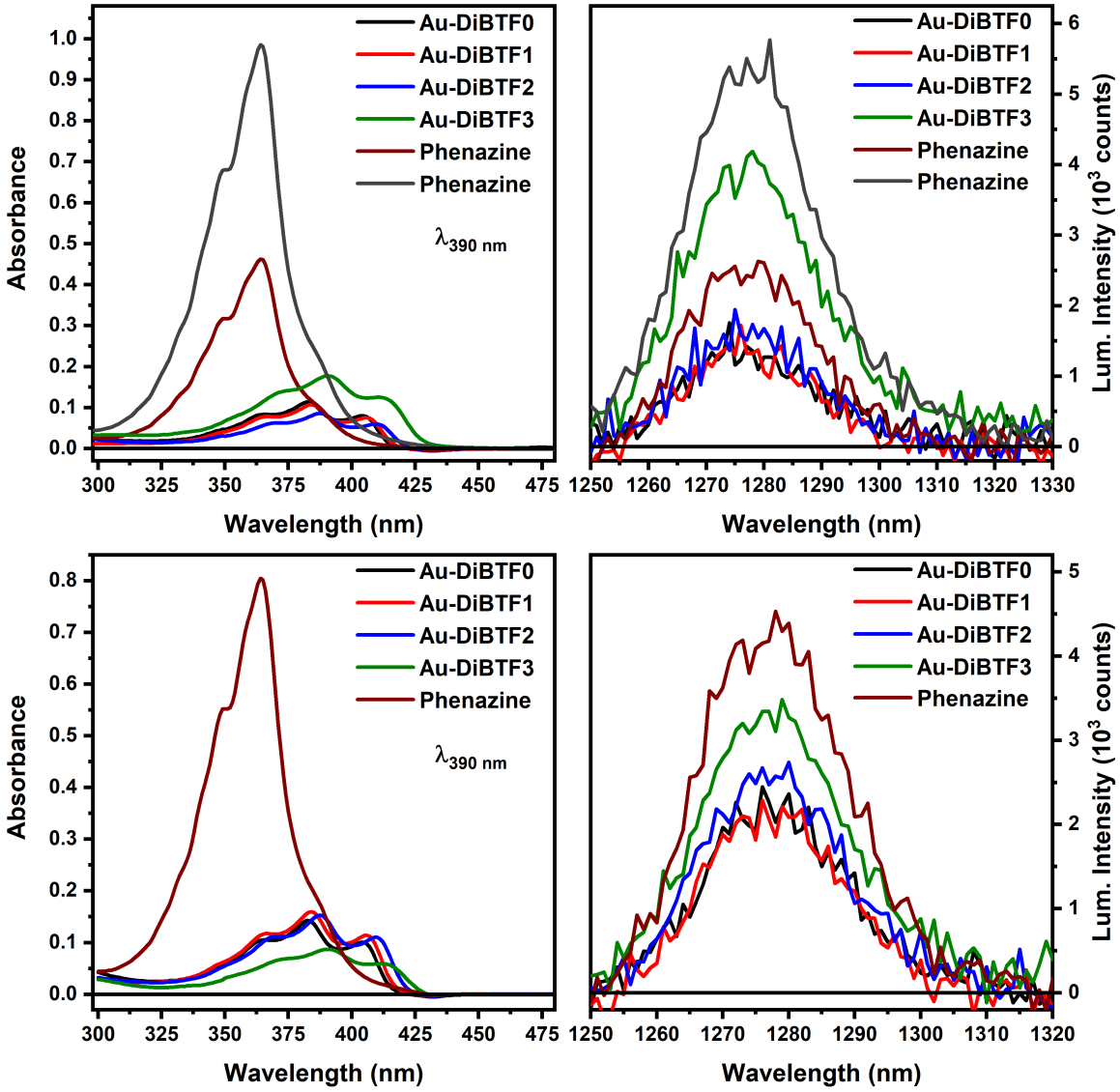


**Figure 4.19.** Singlet Oxygen Phosphorescence Triplet Quantum Yields collected in aerated toluene. Phenazine was used as the reference standard for both trials, and all complexes were excited at 390 nm. The average of trial 1 (top) and trial 2 (bottom) is reported in Table 4.1.

**X-Ray Crystallography**

A single crystal of **Au-DiBTF3** was selected under a stereomicroscope with polarizing filter and mounted with the aid of a trace of Fomblin oil on the goniometer head of a Bruker Quest diffractometer with a fixed chi angle, a sealed tube fine focus X-ray tube, single crystal curved graphite incident beam monochromator, a Photon100 CMOS area detector and an Oxford Cryosystems low temperature device. Examination and data collection were performed with Mo Kα radiation (λ = 0.71073 Å) at 150 K. Data were collected, reflections were indexed and processed, and the files scaled and corrected for absorption using APEX3. The space group was assigned and the structure was solved by direct methods using XPREP within the SHELXTL suite of programs[5] and refined by full matrix least squares against $F^2$ with all reflections using Shelxl2018[6] using the graphical interface Shelxl.[7] If not specified otherwise H atoms attached to carbon atoms were positioned geometrically and constrained to ride on their parent atoms. C-H bond distances were constrained to 0.95 Å for aromatic moieties, and to 1.00, 0.99 and 0.98 Å for aliphatic C-H, $CH_2$ and $CH_3$ moieties, respectively. Methyl $CH_3$ H atoms were allowed to rotate but not to tip to best fit the experimental electron density. $U_{iso}$(H) values were set to a multiple of $U_{eq}$(C) with 1.5 for $CH_3$, $NH_3^+$ and OH, and 1.2 for C-H, $CH_2$, B-H, N-H and $NH_2$ units, respectively.

The bridging ligand is disordered across an inversion center, with the S,N heterocycle being superimposed atop of the fluorene unit. The disorder causes a slight shift for the triazole and benzyl units at the ends of the bridging units, and induces disorder for a solvate occupied pocket beside partially occupied C atoms C34 and C35 of the fluorene unit (not present for the S,N heterocycle). All disordered six membered aromatic rings were constrained to resemble ideal hexagons with C-C bonds of 1.39 Å (AFIX 66). The two benzyl triazole units were restrained to have similar

geometries. Equivalent bond distances in the diethyl group of the fluorene unit were restrained to be similar in length. The C-C bonds connecting the triazole units were restrained to be similar in length. Overlapping pairs of atoms across the inversion center as well as C34 and C35 were constrained to have identical ADPs. C24 was restrained to be close to isotropic. C-Cl bond distances within the dichloromethane molecules were restrained to 1.79(2) Å and Cl...Cl distances to be similar in length. $U^{ij}$ components of ADPs for disordered atoms closer to each other than 2.0 Å were restrained to be similar. The occupancy sum for the DCM molecules was constrained to unity. Subject to these conditions the occupancy rates for the DCM molecules refined to 0.396(3), 0.386(3) and 0.218(3).

Additional refinement details are given in the table, below.

Complete crystallographic data, in CIF format, have been deposited with the Cambridge Crystallographic Data Centre. CCDC 1953525 contains the supplementary crystallographic data for this paper. These data can be obtained free of charge from The Cambridge Crystallographic Data Centre via www.ccdc.cam.ac.uk/data_request/cif.

**Table 4.2.** Crystallography Experimental details

| | Au-DiBTF3 (Internal code: JJM_2_11_0m) |
|---|---|
| Crystal data | |
| Chemical formula | $C_{84}H_{82}Au_2N_{11}S\cdot2(CH_2Cl_2)$ |
| $M_r$ | 1841.45 |
| Crystal system, space group | Triclinic, $P\bar{1}$ |
| Temperature (K) | 150 |
| *a*, *b*, *c* (Å) | 11.1777 (5), 11.4827 (5), 17.6403 (8) |
| □, □, □ (°) | 78.319 (2), 83.944 (2), 71.757 (2) |

| | |
|---|---|
| $V$ (Å$^3$) | 2103.64 (16) |
| $Z$ | 1 |
| $F$(000) | 921 |
| $D_x$ (Mg m$^{-3}$) | 1.454 |
| Radiation type | Mo $K$□ |
| No. of reflections for cell measurement | 9989 |
| □ range (°) for cell measurement | 2.3–32.0 |
| □ (mm$^{-1}$) | 3.68 |
| Crystal shape | Plate |
| Colour | Yellow |
| Crystal size (mm) | 0.22 × 0.18 × 0.06 |
| | |
| Data collection | |
| Diffractometer | Bruker AXS D8 Quest CMOS diffractometer |
| Radiation source | fine focus sealed tube X-ray source |
| Monochromator | Triumph curved graphite crystal |
| Detector resolution (pixels mm$^{-1}$) | 10.4167 |
| Scan method | □ and phi scans |
| Absorption correction | Multi-scan, SADABS 2016/2 (Krause et al. 2015)[8] |
| $T_{min}$, $T_{max}$ | 0.168, 0.268 |
| No. of measured, independent and observed [$I > 2$□($I$)] reflections | 41053, 13707, 10905 |
| $R_{int}$ | 0.040 |
| □ values (°) | □$_{max}$ = 32.1, □$_{min}$ = 2.2 |
| (sin □/□)$_{max}$ (Å$^{-1}$) | 0.748 |
| Range of $h$, $k$, $l$ | $h$ = -16□16, $k$ = -17□16, $l$ = -26□26 |
| | |
| Refinement | |
| Refinement on | $F^2$ |
| $R[F^2 > 2$□$(F^2)]$, $wR(F^2)$, $S$ | 0.043, 0.131, 1.03 |

| | |
|---|---|
| No. of reflections | 13707 |
| No. of parameters | 573 |
| No. of restraints | 403 |
| H-atom treatment | H-atom parameters constrained |
| Weighting scheme | $w = 1/[\square^2(F_o^2) + (0.0735P)^2 + 2.8068P]$ where $P = (F_o^2 + 2F_c^2)/3$ |
| $(\square/\square)_{max}$ | 0.001 |
| $\square\rho_{max}$, $\square\rho_{min}$ (e Å$^{-3}$) | 2.59, -2.01 |

Computer programs: Apex3 v2018.1-0 (Bruker, 2018), *SAINT* V8.38A (Bruker, 2016), *SHELXS97* (Sheldrick, 2008), *SHELXL2018*/3 (Sheldrick, 2015, 2018), SHELXLE Rev946 (Hübschle *et al.*, 2011)

**Calculations.** Spin-restricted static and time-dependent density-functional theory computations proceeded in Gaussian16 rev. A.03.[9] Model complexes were calculated for computational tractability. Fluorenyl ethyl groups and carbene mesityls were modeled as methyl, as were triazolyl benzyls. Geometries were optimized without constraint with the 6-31G(d) basis set for nonmetal atoms and the Stuttgart-Dresden effective core potential and basis set for Au.[10] Final single-point calculations employed the exchange and correlation functionals of Perdew, Burke, and Ernzerhof (PBE0),[11] and the TZVP basis set of Godbelt, Andzelm, and co-workers for nonmetals.[12] For metal atoms, the Stuttgart-Dresden effective core potential and basis set were used; scalar relativistic effects are included implicitly. Continuum solvation in toluene was imposed using the integral equation formalism of the polarizable continuum model.[13-16] Population analyses were performed with the AOMix-CDA program of Gorelsky.[17,18] Calculations of Franck-Condon triplet excited states proceeded at the optimized ground-state geometries, and are spin-unrestricted.

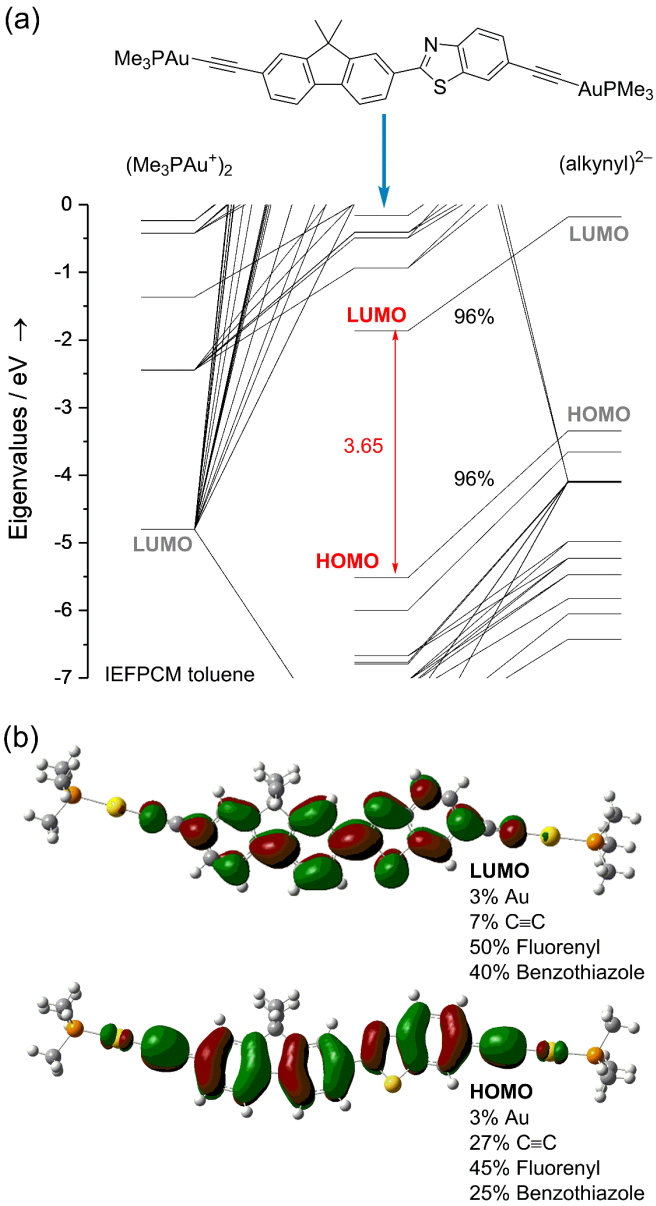


**Figure 4.20.** (a) Frontier orbital energy diagram of model complex **Au-DiBTF0′**. (b) Kohn-Sham orbital plots (HOMO and LUMO). (Percentages are of electron density).

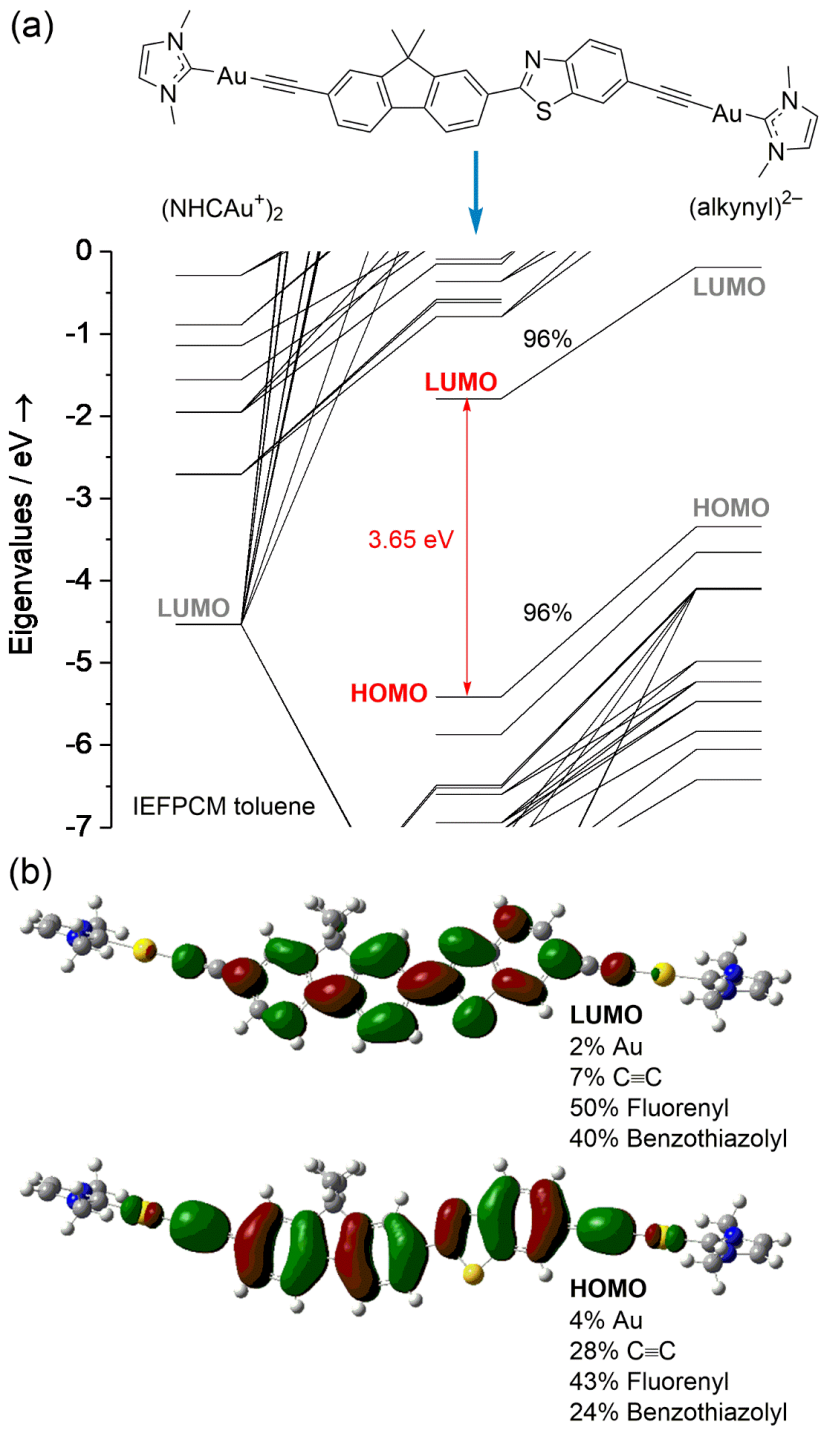


**Figure 4.21.** (a) Frontier orbital energy diagram of model complex **Au-DiBTF2′**. (b) Kohn-Sham orbital plots (HOMO and LUMO). (Percentages are of electron density).

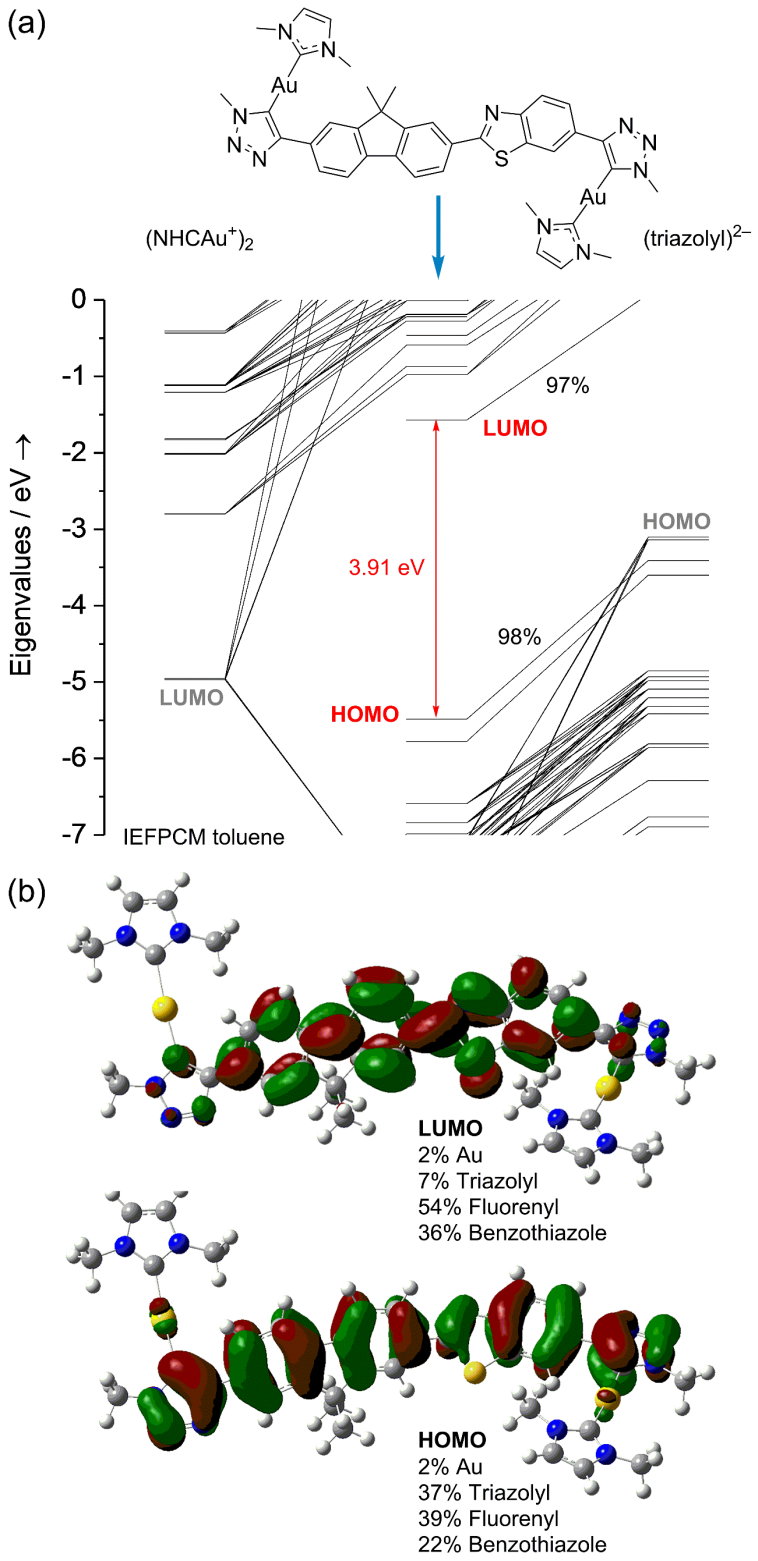


**Figure 4.22.** (a) Frontier orbital energy diagram of model complex **Au-DiBTF3′**. (b) Kohn-Sham orbital plots (HOMO and LUMO). (Percentages are of electron density).

**Table 4.3.** Composition of Franck-Condon singlet excited states.

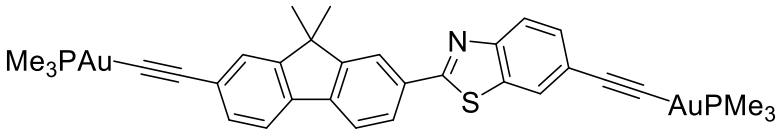


158 = HOMO; 159 = LUMO

| # | nm | 1000 cm-1 | eV | f | Assignment |
|---|---|---|---|---|---|
| 1 | 411.6 | 24.29 | 3.012 | 2.5048 | 168→169(97.4%) |
| 2 | 346.2 | 28.89 | 3.582 | 0.0163 | 167→169(97.5%) |
| 3 | 310.5 | 32.21 | 3.994 | 0.0001 | 166→169(81.9%) |
| | | | | | 166→170(10.7%) |
| 4 | 308.1 | 32.46 | 4.024 | 0.0004 | 165→169(82.9%) |
| | | | | | 165→170(10.3%) |
| 5 | 307.3 | 32.54 | 4.035 | 0.0109 | 168→170(57.3%) |
| | | | | | 164→169(24.8%) |
| 6 | 303.9 | 32.91 | 4.080 | 0.0015 | 164→169(54.2%) |
| | | | | | 168→170(27.2%) |
| 7 | 298.8 | 33.47 | 4.149 | 0.0104 | 168→171(64.1%) |
| 8 | 296.3 | 33.75 | 4.185 | 0.0213 | 168→172(47.3%) |
| | | | | | 168→173(11.7%) |
| 9 | 291.4 | 34.32 | 4.255 | 0.0228 | 168→173(48.7%) |
| | | | | | 168→172(15.5%) |
| 10 | 281.3 | 35.55 | 4.408 | 0.0226 | 162→169(29.2%) |
| | | | | | 163→169(28.9%) |
| | | | | | 168→180(14.0%) |
| | | | | | 159→169(12.2%) |
| 11 | 276.5 | 36.16 | 4.483 | 0.4729 | 167→170(49.6%) |
| | | | | | 168→174(22.1%) |
| 12 | 273.4 | 36.58 | 4.535 | 0.0028 | 163→169(25.5%) |
| | | | | | 168→175(18.5%) |
| | | | | | 162→169(17.7%) |
| 13 | 265.9 | 37.61 | 4.664 | 0.0248 | 168→175(32.9%) |
| | | | | | 163→169(26.4%) |
| | | | | | 162→169(10.8%) |
| 14 | 262.2 | 38.14 | 4.729 | 0.1281 | 167→170(23.0%) |
| | | | | | 168→174(22.6%) |
| | | | | | 159→169(11.8%) |
| | | | | | 162→169(10.6%) |
| 15 | 260.4 | 38.41 | 4.762 | 0.0216 | 159→169(44.4%) |
| 16 | 257.8 | 38.79 | 4.809 | 0.0004 | 155→169(92.5%) |
| 17 | 256.9 | 38.93 | 4.827 | 0.0102 | 167→171(33.4%) |
| | | | | | 167→172(11.9%) |
| | | | | | 168→172(10.4%) |
| 18 | 254.6 | 39.28 | 4.870 | 0.0897 | 166→171(24.2%) |
| | | | | | 166→170(21.5%) |

| | | | | | |
|---|---|---|---|---|---|
| | | | | | 167→172(12.0%) |
| 19 | 254.2 | 39.34 | 4.877 | 0.0444 | 167→171(32.3%) |
| | | | | | 167→172(17.8%) |
| | | | | | 165→170(13.8%) |
| | | | | | 168→171(10.6%) |
| 20 | 252.7 | 39.57 | 4.906 | 0.0964 | 165→170(25.3%) |
| | | | | | 166→170(14.6%) |
| | | | | | 167→172(14.3%) |
| 21 | 251.8 | 39.72 | 4.925 | 0.0130 | 160→169(93.1%) |
| 22 | 251.5 | 39.76 | 4.930 | 0.0141 | 161→169(92.6%) |
| 23 | 251.4 | 39.78 | 4.932 | 0.1052 | 166→170(17.4%) |
| | | | | | 166→172(13.5%) |
| 24 | 249.5 | 40.08 | 4.969 | 0.0422 | 167→173(50.6%) |
| | | | | | 168→180(10.5%) |
| 25 | 246.1 | 40.64 | 5.038 | 0.1075 | 168→180(34.9%) |
| | | | | | 167→173(16.0%) |
| 26 | 245.0 | 40.81 | 5.060 | 0.9165 | 165→172(27.5%) |
| | | | | | 166→171(15.6%) |
| | | | | | 167→173(10.1%) |
| 27 | 243.1 | 41.13 | 5.100 | 0.0051 | 168→182(41.9%) |
| | | | | | 168→179(32.9%) |
| 28 | 240.6 | 41.56 | 5.153 | 0.0037 | 168→178(69.4%) |
| | | | | | 168→179(14.7%) |
| 29 | 240.4 | 41.59 | 5.157 | 0.1000 | 167→174(18.4%) |
| | | | | | 164→170(13.0%) |
| | | | | | 167→175(12.3%) |
| 30 | 239.8 | 41.69 | 5.169 | 0.0002 | 168→176(92.8%) |
| 31 | 238.6 | 41.91 | 5.196 | 0.0004 | 168→177(90.5%) |
| 32 | 238.2 | 41.98 | 5.205 | 0.0043 | 167→175(21.4%) |
| | | | | | 168→181(16.5%) |
| | | | | | 167→174(10.4%) |
| 33 | 235.6 | 42.45 | 5.263 | 0.0031 | 168→182(42.0%) |
| | | | | | 168→179(33.6%) |
| 34 | 234.8 | 42.59 | 5.280 | 0.0070 | 167→175(25.7%) |
| | | | | | 158→169(18.9%) |
| | | | | | 168→181(17.9%) |
| | | | | | 164→170(12.9%) |
| 35 | 233.3 | 42.86 | 5.314 | 0.0530 | 164→170(43.6%) |
| | | | | | 158→169(16.7%) |
| 36 | 232.2 | 43.06 | 5.339 | 0.0135 | 158→169(42.1%) |
| | | | | | 168→181(22.8%) |
| | | | | | 167→174(18.6%) |
| 37 | 232.1 | 43.08 | 5.342 | 0.0717 | 161→171(68.1%) |
| | | | | | 161→172(21.7%) |
| 38 | 231.9 | 43.12 | 5.346 | 0.0903 | 160→172(50.0%) |
| | | | | | 160→171(26.6%) |

| | | | | | |
|---|---|---|---|---|---|
| | | | | | 160→170(17.4%) |
| 39 | 231.5 | 43.20 | 5.356 | 0.0061 | 157→169(64.4%) |
| | | | | | 166→173(21.3%) |
| 40 | 230.8 | 43.33 | 5.372 | 0.0003 | 166→173(48.9%) |
| | | | | | 157→169(24.8%) |
| 41 | 227.2 | 44.01 | 5.457 | 0.0136 | 156→169(60.8%) |
| 42 | 226.3 | 44.18 | 5.478 | 0.0006 | 165→175(68.5%) |
| | | | | | 165→173(12.9%) |
| 43 | 225.6 | 44.33 | 5.496 | 0.0084 | 168→183(42.4%) |
| | | | | | 167→180(17.9%) |
| 44 | 224.5 | 44.55 | 5.523 | 0.0592 | 167→180(37.6%) |
| | | | | | 164→173(12.0%) |
| | | | | | 167→181(11.5%) |
| 45 | 224.3 | 44.58 | 5.527 | 0.0013 | 164→172(45.9%) |
| | | | | | 164→171(27.3%) |
| 46 | 221.7 | 45.10 | 5.592 | 0.0387 | 163→170(38.4%) |
| | | | | | 162→170(10.2%) |
| 47 | 221.4 | 45.18 | 5.601 | 0.0204 | 167→182(19.4%) |
| | | | | | 164→182(15.4%) |
| | | | | | 167→179(14.1%) |
| 48 | 220.5 | 45.35 | 5.623 | 0.1889 | 164→173(30.9%) |
| | | | | | 164→171(25.1%) |
| 49 | 219.4 | 45.57 | 5.650 | 0.0602 | 165→174(26.7%) |
| | | | | | 165→170(13.3%) |
| | | | | | 165→171(11.8%) |
| 50 | 219.2 | 45.62 | 5 .656 | 0.0005 | 167→177(89.5%) |

**Table 4.4.** Composition of Franck-Condon triplet excited states.

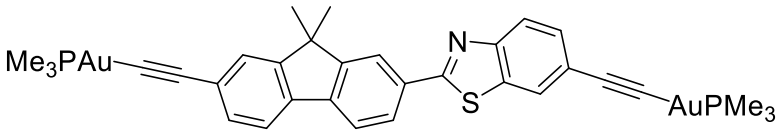


158 = HOMO; 159 = LUMO

| # | nm | 1000 cm-1 | eV | f | Assignment |
|---|---|---|---|---|---|
| 1 | 580.3 | 17.23 | 2.137 | 0.0000 | 158→159(80.7%) |
| 2 | 478.2 | 20.91 | 2.593 | 0.0000 | 157→159(51.3%) |
| | | | | | 158→160(28.7%) |
| 3 | 386.0 | 25.91 | 3.212 | 0.0000 | 157→160(23.1%) |
| | | | | | 156→159(18.5%) |
| | | | | | 158→161(12.8%) |
| 4 | 348.3 | 28.71 | 3.560 | 0.0000 | 156→159(45.8%) |
| | | | | | 158→160(10.8%) |
| 5 | 334.1 | 29.93 | 3.711 | 0.0000 | 157→159(30.3%) |
| | | | | | 158→160(23.4%) |

| | | | | | |
|---|---|---|---|---|---|
| | | | | | 156→159(14.0%) |
| 6 | 327.8 | 30.50 | 3.782 | 0.0000 | 158→162(45.5%) |
| | | | | | 158→161(15.0%) |
| 7 | 318.4 | 31.40 | 3.894 | 0.0000 | 151→159(33.4%) |
| | | | | | 153→159(15.3%) |
| 8 | 315.0 | 31.75 | 3.937 | 0.0000 | 152→159(30.5%) |
| 9 | 314.1 | 31.83 | 3.947 | 0.0000 | 155→159(61.9%) |
| | | | | | 155→160(20.7%) |
| 10 | 311.6 | 32.10 | 3.980 | 0.0000 | 154→159(62.0%) |
| | | | | | 154→160(19.0%) |
| 11 | 309.8 | 32.28 | 4.003 | 0.0000 | 158→165(22.6%) |
| 12 | 306.8 | 32.59 | 4.041 | 0.0000 | 156→165(29.4%) |
| | | | | | 157→165(12.9%) |
| | | | | | 158→165(10.5%) |
| 13 | 305.4 | 32.74 | 4.059 | 0.0000 | 151→159(25.7%) |
| | | | | | 158→165(18.8%) |
| | | | | | 158→160(10.5%) |
| | | | | | 153→159(10.4%) |
| 14 | 301.0 | 33.22 | 4.119 | 0.0000 | 151→169(12.6%) |
| | | | | | 152→162(12.0%) |
| 15 | 288.2 | 34.70 | 4.302 | 0.0000 | 158→164(62.8%) |
| | | | | | 157→164(19.8%) |
| 16 | 286.8 | 34.87 | 4.324 | 0.0000 | 158→163(51.9%) |
| | | | | | 157→163(29.6%) |
| 17 | 286.1 | 34.95 | 4.334 | 0.0000 | 153→159(11.6%) |
| | | | | | 157→160(10.9%) |
| 18 | 284.5 | 35.15 | 4.358 | 0.0000 | 158→169(40.4%) |
| | | | | | 152→159(13.9%) |
| 19 | 282.9 | 35.34 | 4.382 | 0.0000 | 148→159(83.5%) |
| 20 | 278.8 | 35.87 | 4.448 | 0.0000 | 151→162(13.0%) |
| | | | | | 153→159(12.0%) |
| 21 | 276.1 | 36.21 | 4.490 | 0.0000 | 154→163(27.5%) |
| | | | | | 155→164(24.6%) |
| 22 | 274.6 | 36.41 | 4.515 | 0.0000 | 155→164(29.0%) |
| | | | | | 154→163(28.9%) |
| 23 | 270.7 | 36.94 | 4.580 | 0.0000 | 158→161(23.5%) |
| | | | | | 157→160(21.6%) |
| | | | | | 158→162(14.0%) |
| 24 | 261.3 | 38.27 | 4.745 | 0.0000 | 156→160(15.8%) |
| | | | | | 158→168(15.6%) |
| 25 | 259.0 | 38.61 | 4.787 | 0.0000 | 158→170(17.0%) |

**Table 4.5.** Composition of Franck-Condon singlet excited states.

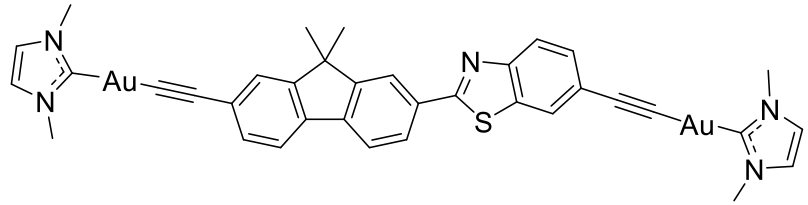

168 = HOMO; 169 = LUMO

| # | nm | 1000 cm-1 | eV | f | Assignment |
|---|---|---|---|---|---|
| 1 | 411.6 | 24.29 | 3.012 | 2.5048 | 168→169(97.4%) |
| 2 | 346.2 | 28.89 | 3.582 | 0.0163 | 167→169(97.5%) |
| 3 | 310.5 | 32.21 | 3.994 | 0.0001 | 166→169(81.9%) |
| | | | | | 166→170(10.7%) |
| 4 | 308.1 | 32.46 | 4.024 | 0.0004 | 165→169(82.9%) |
| | | | | | 165→170(10.3%) |
| 5 | 307.3 | 32.54 | 4.035 | 0.0109 | 168→170(57.3%) |
| | | | | | 164→169(24.8%) |
| 6 | 303.9 | 32.91 | 4.080 | 0.0015 | 164→169(54.2%) |
| | | | | | 168→170(27.2%) |
| 7 | 298.8 | 33.47 | 4.149 | 0.0104 | 168→171(64.1%) |
| 8 | 296.3 | 33.75 | 4.185 | 0.0213 | 168→172(47.3%) |
| | | | | | 168→173(11.7%) |
| 9 | 291.4 | 34.32 | 4.255 | 0.0228 | 168→173(48.7%) |
| | | | | | 168→172(15.5%) |
| 10 | 281.3 | 35.55 | 4.408 | 0.0226 | 162→169(29.2%) |
| | | | | | 163→169(28.9%) |
| | | | | | 168→180(14.0%) |
| | | | | | 159→169(12.2%) |
| 11 | 276.5 | 36.16 | 4.483 | 0.4729 | 167→170(49.6%) |
| | | | | | 168→174(22.1%) |
| 12 | 273.4 | 36.58 | 4.535 | 0.0028 | 163→169(25.5%) |
| | | | | | 168→175(18.5%) |
| | | | | | 162→169(17.7%) |
| 13 | 265.9 | 37.61 | 4.664 | 0.0248 | 168→175(32.9%) |
| | | | | | 163→169(26.4%) |
| | | | | | 162→169(10.8%) |
| 14 | 262.2 | 38.14 | 4.729 | 0.1281 | 167→170(23.0%) |
| | | | | | 168→174(22.6%) |
| | | | | | 159→169(11.8%) |
| | | | | | 162→169(10.6%) |
| 15 | 260.4 | 38.41 | 4.762 | 0.0216 | 159→169(44.4%) |
| 16 | 257.8 | 38.79 | 4.809 | 0.0004 | 155→169(92.5%) |
| 17 | 256.9 | 38.93 | 4.827 | 0.0102 | 167→171(33.4%) |
| | | | | | 167→172(11.9%) |
| | | | | | 168→172(10.4%) |
| 18 | 254.6 | 39.28 | 4.870 | 0.0897 | 166→171(24.2%) |

| | | | | | |
|---|---|---|---|---|---|
| | | | | | 166→170(21.5%) |
| | | | | | 167→172(12.0%) |
| 19 | 254.2 | 39.34 | 4.877 | 0.0444 | 167→171(32.3%) |
| | | | | | 167→172(17.8%) |
| | | | | | 165→170(13.8%) |
| | | | | | 168→171(10.6%) |
| 20 | 252.7 | 39.57 | 4.906 | 0.0964 | 165→170(25.3%) |
| | | | | | 166→170(14.6%) |
| | | | | | 167→172(14.3%) |
| 21 | 251.8 | 39.72 | 4.925 | 0.0130 | 160→169(93.1%) |
| 22 | 251.5 | 39.76 | 4.930 | 0.0141 | 161→169(92.6%) |
| 23 | 251.4 | 39.78 | 4.932 | 0.1052 | 166→170(17.4%) |
| | | | | | 166→172(13.5%) |
| 24 | 249.5 | 40.08 | 4.969 | 0.0422 | 167→173(50.6%) |
| | | | | | 168→180(10.5%) |
| 25 | 246.1 | 40.64 | 5.038 | 0.1075 | 168→180(34.9%) |
| | | | | | 167→173(16.0%) |
| 26 | 245.0 | 40.81 | 5.060 | 0.9165 | 165→172(27.5%) |
| | | | | | 166→171(15.6%) |
| | | | | | 167→173(10.1%) |
| 27 | 243.1 | 41.13 | 5.100 | 0.0051 | 168→182(41.9%) |
| | | | | | 168→179(32.9%) |
| 28 | 240.6 | 41.56 | 5.153 | 0.0037 | 168→178(69.4%) |
| | | | | | 168→179(14.7%) |
| 29 | 240.4 | 41.59 | 5.157 | 0.1000 | 167→174(18.4%) |
| | | | | | 164→170(13.0%) |
| | | | | | 167→175(12.3%) |
| 30 | 239.8 | 41.69 | 5.169 | 0.0002 | 168→176(92.8%) |
| 31 | 238.6 | 41.91 | 5.196 | 0.0004 | 168→177(90.5%) |
| 32 | 238.2 | 41.98 | 5.205 | 0.0043 | 167→175(21.4%) |
| | | | | | 168→181(16.5%) |
| | | | | | 167→174(10.4%) |
| 33 | 235.6 | 42.45 | 5.263 | 0.0031 | 168→182(42.0%) |
| | | | | | 168→179(33.6%) |
| 34 | 234.8 | 42.59 | 5.280 | 0.0070 | 167→175(25.7%) |
| | | | | | 158→169(18.9%) |
| | | | | | 168→181(17.9%) |
| | | | | | 164→170(12.9%) |
| 35 | 233.3 | 42.86 | 5.314 | 0.0530 | 164→170(43.6%) |
| | | | | | 158→169(16.7%) |
| 36 | 232.2 | 43.06 | 5.339 | 0.0135 | 158→169(42.1%) |
| | | | | | 168→181(22.8%) |
| | | | | | 167→174(18.6%) |
| 37 | 232.1 | 43.08 | 5.342 | 0.0717 | 161→171(68.1%) |
| | | | | | 161→172(21.7%) |
| 38 | 231.9 | 43.12 | 5.346 | 0.0903 | 160→172(50.0%) |

| | | | | | |
|---|---|---|---|---|---|
| | | | | | 160→171(26.6%) |
| | | | | | 160→170(17.4%) |
| 39 | 231.5 | 43.20 | 5.356 | 0.0061 | 157→169(64.4%) |
| | | | | | 166→173(21.3%) |
| 40 | 230.8 | 43.33 | 5.372 | 0.0003 | 166→173(48.9%) |
| | | | | | 157→169(24.8%) |
| 41 | 227.2 | 44.01 | 5.457 | 0.0136 | 156→169(60.8%) |
| 42 | 226.3 | 44.18 | 5.478 | 0.0006 | 165→175(68.5%) |
| | | | | | 165→173(12.9%) |
| 43 | 225.6 | 44.33 | 5.496 | 0.0084 | 168→183(42.4%) |
| | | | | | 167→180(17.9%) |
| 44 | 224.5 | 44.55 | 5.523 | 0.0592 | 167→180(37.6%) |
| | | | | | 164→173(12.0%) |
| | | | | | 167→181(11.5%) |
| 45 | 224.3 | 44.58 | 5.527 | 0.0013 | 164→172(45.9%) |
| | | | | | 164→171(27.3%) |
| 46 | 221.7 | 45.10 | 5.592 | 0.0387 | 163→170(38.4%) |
| | | | | | 162→170(10.2%) |
| 47 | 221.4 | 45.18 | 5.601 | 0.0204 | 167→182(19.4%) |
| | | | | | 164→182(15.4%) |
| | | | | | 167→179(14.1%) |
| 48 | 220.5 | 45.35 | 5.623 | 0.1889 | 164→173(30.9%) |
| | | | | | 164→171(25.1%) |
| 49 | 219.4 | 45.57 | 5.650 | 0.0602 | 165→174(26.7%) |
| | | | | | 165→170(13.3%) |
| | | | | | 165→171(11.8%) |
| 50 | 219.2 | 45.62 | 5.656 | 0.0005 | 167→177(89.5%) |

**Table 4.6.** Composition of Franck-Condon triplet excited states.

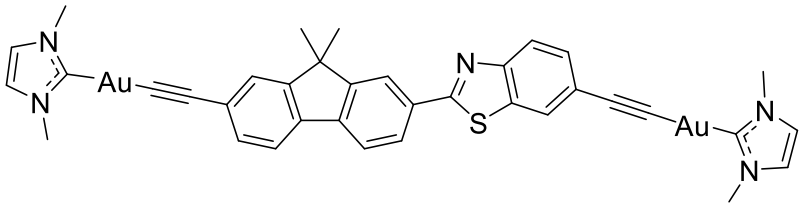


168 = HOMO; 169 = LUMO

| # | nm | 1000 cm-1 | eV | f | Assignment |
|---|---|---|---|---|---|
| 1 | 583.3 | 17.14 | 2.126 | 0.0000 | 168→169(80.5%) |
| 2 | 480.3 | 20.82 | 2.582 | 0.0000 | 167→169(52.1%) |
| | | | | | 168→170(26.0%) |
| 3 | 385.5 | 25.94 | 3.217 | 0.0000 | 167→170(21.0%) |
| | | | | | 164→169(19.7%) |
| | | | | | 168→174(14.0%) |
| 4 | 347.3 | 28.79 | 3.570 | 0.0000 | 164→169(42.0%) |
| | | | | | 168→170(12.6%) |

| | | | | | |
|---|---|---|---|---|---|
| 5 | 335.8 | 29.78 | 3.692 | 0.0000 | 167→169(30.3%) |
| | | | | | 168→170(20.7%) |
| | | | | | 164→169(15.6%) |
| 6 | 330.1 | 30.29 | 3.756 | 0.0000 | 168→173(59.4%) |
| 7 | 322.4 | 31.02 | 3.846 | 0.0000 | 166→169(63.3%) |
| | | | | | 166→170(14.9%) |
| 8 | 320.1 | 31.24 | 3.874 | 0.0000 | 165→169(58.1%) |
| | | | | | 165→170(15.4%) |
| 9 | 318.5 | 31.39 | 3.892 | 0.0000 | 159→169(24.7%) |
| 10 | 315.3 | 31.72 | 3.933 | 0.0000 | 162→169(39.0%) |
| | | | | | 159→169(13.6%) |
| 11 | 311.2 | 32.13 | 3.983 | 0.0000 | 168→175(42.8%) |
| | | | | | 167→175(19.9%) |
| 12 | 307.5 | 32.52 | 4.032 | 0.0000 | 164→175(21.7%) |
| 13 | 305.4 | 32.75 | 4.060 | 0.0000 | 159→169(29.5%) |
| | | | | | 168→170(12.7%) |
| | | | | | 163→169(10.7%) |
| 14 | 303.6 | 32.94 | 4.083 | 0.0000 | 168→171(39.8%) |
| 15 | 300.3 | 33.30 | 4.129 | 0.0000 | 168→171(13.9%) |
| | | | | | 162→173(12.2%) |
| 16 | 299.3 | 33.41 | 4.143 | 0.0000 | 168→172(38.1%) |
| 17 | 292.1 | 34.23 | 4.244 | 0.0000 | 166→171(40.1%) |
| | | | | | 166→172(14.7%) |
| 18 | 289.7 | 34.51 | 4.279 | 0.0000 | 165→172(35.7%) |
| | | | | | 165→171(16.6%) |
| 19 | 285.6 | 35.02 | 4.341 | 0.0000 | 168→180(27.2%) |
| | | | | | 163→169(10.7%) |
| 20 | 283.6 | 35.26 | 4.372 | 0.0000 | no single transition contributes more than 10% |
| 21 | 282.5 | 35.40 | 4.389 | 0.0000 | 155→169(84.4%) |
| 22 | 278.7 | 35.89 | 4.449 | 0.0000 | 158→177(47.8%) |
| | | | | | 165→177(23.3%) |
| | | | | | 157→177(14.0%) |
| 23 | 277.3 | 36.06 | 4.471 | 0.0000 | 159→173(17.0%) |
| | | | | | 162→169(12.4%) |
| | | | | | 163→169(10.7%) |
| 24 | 266.7 | 37.50 | 4.650 | 0.0000 | 168→174(35.4%) |
| | | | | | 167→170(26.3%) |
| 25 | 262.3 | 38.13 | 4.728 | 0.0000 | 160→169(43.6%) |
| | | | | | 160→170(23.4%) |
| | | | | | 160→172(13.9%) |
| | | | | | 160→171(11.4%) |

**Table 4.7.** Composition of Franck-Condon singlet excited states.

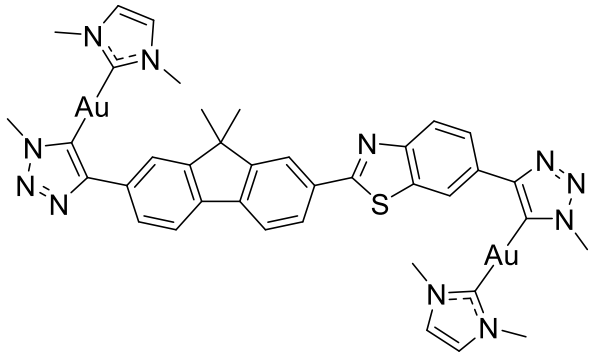

198 = HOMO; 199 = LUMO

| # | nm | 1000 cm-1 | eV | f | Assignment |
|---|---|---|---|---|---|
| 1 | 380.8 | 26.26 | 3.256 | 1.8237 | 198→199(95.7%) |
| 2 | 338.8 | 29.52 | 3.660 | 0.0168 | 197→199(91.5%) |
| 3 | 314.4 | 31.81 | 3.944 | 0.0236 | 198→200(75.8%) |
| | | | | | 197→201(10.0%) |
| 4 | 308.6 | 32.40 | 4.017 | 0.0972 | 198→201(69.9%) |
| | | | | | 197→200(18.9%) |
| 5 | 297.8 | 33.58 | 4.163 | 0.0127 | 198→202(47.3%) |
| | | | | | 198→203(21.7%) |
| 6 | 293.9 | 34.02 | 4.218 | 0.0057 | 196→199(65.1%) |
| | | | | | 198→204(10.1%) |
| 7 | 285.7 | 35.00 | 4.340 | 0.0393 | 197→200(30.8%) |
| | | | | | 198→203(26.8%) |
| | | | | | 198→201(11.5%) |
| 8 | 281.6 | 35.51 | 4.402 | 0.0761 | 198→202(31.3%) |
| | | | | | 197→200(23.3%) |
| | | | | | 198→203(15.2%) |
| 9 | 277.1 | 36.08 | 4.474 | 0.0033 | 198→204(14.4%) |
| | | | | | 198→206(13.4%) |
| | | | | | 194→199(11.4%) |
| | | | | | 197→201(10.2%) |
| 10 | 274.3 | 36.45 | 4.520 | 0.1012 | 198→204(22.3%) |
| | | | | | 196→199(21.1%) |
| | | | | | 197→204(17.1%) |
| | | | | | 198→206(12.0%) |
| 11 | 271.5 | 36.83 | 4.567 | 0.0130 | 197→201(59.3%) |
| 12 | 267.1 | 37.44 | 4.642 | 0.0320 | 197→202(65.7%) |
| 13 | 265.8 | 37.62 | 4.665 | 0.0956 | 195→199(68.6%) |
| 14 | 261.3 | 38.27 | 4.745 | 0.0265 | 194→199(22.8%) |
| | | | | | 198→206(18.8%) |
| | | | | | 197→203(13.7%) |
| 15 | 259.7 | 38.50 | 4.774 | 0.1218 | 198→209(10.6%) |
| | | | | | 197→203(10.3%) |
| 16 | 256.6 | 38.97 | 4.832 | 0.0115 | 193→199(65.4%) |

| | | | | | |
|---|---|---|---|---|---|
| | | | | | 193→200(12.9%) |
| 17 | 255.8 | 39.09 | 4.847 | 0.0430 | 197→203(45.5%) |
| 18 | 255.3 | 39.18 | 4.857 | 0.0064 | 192→199(65.4%) |
| | | | | | 194→199(10.2%) |
| 19 | 254.8 | 39.24 | 4.866 | 0.0010 | 198→205(88.7%) |
| 20 | 253.0 | 39.53 | 4.901 | 0.0330 | 198→207(12.1%) |
| | | | | | 188→199(11.1%) |
| 21 | 252.5 | 39.61 | 4.911 | 0.0031 | 198→207(60.9%) |
| | | | | | 198→206(15.3%) |
| 22 | 251.5 | 39.76 | 4.930 | 0.0142 | 198→208(17.9%) |
| | | | | | 198→209(15.9%) |
| 23 | 249.9 | 40.02 | 4.962 | 0.0397 | 196→200(28.3%) |
| | | | | | 191→199(18.0%) |
| 24 | 249.2 | 40.12 | 4.974 | 0.0102 | 198→210(42.1%) |
| | | | | | 198→209(22.7%) |
| 25 | 248.5 | 40.24 | 4.989 | 0.0136 | 198→211(14.1%) |
| | | | | | 190→199(13.2%) |
| | | | | | 183→199(11.7%) |
| 26 | 247.7 | 40.37 | 5.006 | 0.0345 | 197→204(17.4%) |
| | | | | | 190→199(11.6%) |
| | | | | | 191→199(11.0%) |
| | | | | | 198→204(10.8%) |
| 27 | 246.8 | 40.53 | 5.024 | 0.0323 | 183→199(23.9%) |
| | | | | | 189→199(16.8%) |
| | | | | | 190→199(13.9%) |
| 28 | 246.0 | 40.65 | 5.040 | 0.0186 | 197→204(27.2%) |
| | | | | | 196→200(16.3%) |
| | | | | | 191→199(11.0%) |
| 29 | 244.5 | 40.91 | 5.072 | 0.0657 | 198→211(20.7%) |
| 30 | 241.2 | 41.46 | 5.141 | 0.0191 | 188→199(15.1%) |
| | | | | | 197→206(14.7%) |
| 31 | 240.7 | 41.54 | 5.151 | 0.0205 | 198→212(21.7%) |
| | | | | | 188→199(10.2%) |
| 32 | 240.0 | 41.67 | 5.166 | 0.0450 | 190→199(23.8%) |
| | | | | | 192→201(14.0%) |
| | | | | | 194→201(13.0%) |
| 33 | 239.2 | 41.81 | 5.184 | 0.0262 | 193→200(14.6%) |
| 34 | 238.6 | 41.92 | 5.197 | 0.0261 | 198→212(27.4%) |
| | | | | | 197→206(19.3%) |
| | | | | | 197→211(10.1%) |
| 35 | 237.2 | 42.16 | 5.227 | 0.0003 | 197→207(75.8%) |
| | | | | | 197→206(11.6%) |
| 36 | 236.6 | 42.26 | 5.239 | 0.1047 | 196→201(13.5%) |
| | | | | | 195→201(13.3%) |
| | | | | | 187→199(12.2%) |
| 37 | 236.0 | 42.38 | 5.254 | 0.0197 | 196→202(25.0%) |

| | | | | | |
|---|---|---|---|---|---|
| 38 | 235.0 | 42.55 | 5.276 | 0.0004 | 197→205(89.6%) |
| 39 | 234.4 | 42.66 | 5.289 | 0.0205 | 187→199(24.2%) |
| | | | | | 198→213(12.3%) |
| 40 | 233.4 | 42.84 | 5.312 | 0.0036 | 197→208(17.7%) |
| | | | | | 198→208(14.9%) |
| 41 | 232.5 | 43.01 | 5.332 | 0.0269 | 198→213(15.4%) |
| | | | | | 191→200(11.2%) |
| 42 | 231.9 | 43.13 | 5.347 | 0.0085 | 187→199(10.3%) |
| 43 | 231.8 | 43.15 | 5.350 | 0.0355 | 196→202(14.8%) |
| | | | | | 197→208(12.0%) |
| 44 | 230.7 | 43.34 | 5.374 | 0.1471 | 198→214(18.4%) |
| | | | | | 198→213(16.4%) |
| | | | | | 187→199(14.8%) |
| 45 | 230.2 | 43.44 | 5.386 | 0.0389 | 198→214(14.0%) |
| | | | | | 196→201(13.1%) |
| 46 | 229.5 | 43.57 | 5.402 | 0.0580 | 198→215(13.0%) |
| 47 | 228.9 | 43.68 | 5.416 | 0.0096 | 198→215(16.5%) |
| | | | | | 195→200(12.9%) |
| 48 | 227.4 | 43.98 | 5.453 | 0.0181 | no single transition |
| | | | | | contributes more than 10% |
| 49 | 226.7 | 44.11 | 5.468 | 0.0111 | 197→209(19.8%) |
| | | | | | 197→212(15.0%) |
| 50 | 226.1 | 44.23 | 5.483 | 0.0049 | 186→199(12.1%) |

**Table 4.8.** Composition of Franck-Condon triplet excited states.

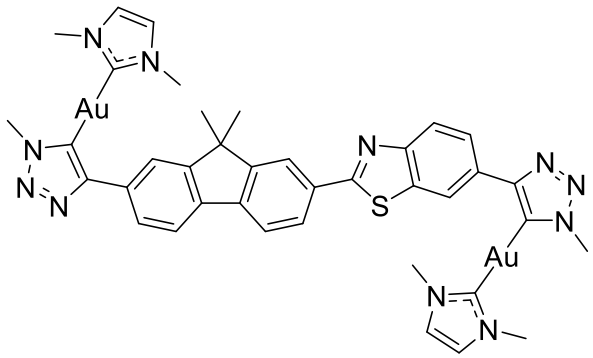


198 = HOMO; 199 = LUMO

| # | nm | 1000 cm-1 | eV | f | Assignment |
|---|---|---|---|---|---|
| 1 | 509.9 | 19.61 | 2.432 | 0.0000 | 198→199(71.4%) |
| 2 | 453.3 | 22.06 | 2.735 | 0.0000 | 197→199(46.4%) |
| | | | | | 198→200(14.9%) |
| 3 | 363.6 | 27.50 | 3.410 | 0.0000 | 197→200(17.6%) |
| | | | | | 198→201(14.3%) |
| 4 | 342.0 | 29.24 | 3.625 | 0.0000 | 198→200(18.8%) |
| | | | | | 197→201(17.9%) |

| | | | | | |
|---|---|---|---|---|---|
| | | | | | 198→202(15.1%) |
| 5 | 337.4 | 29.64 | 3.675 | 0.0000 | 196→199(12.8%) |
| | | | | | 198→203(11.8%) |
| | | | | | 198→200(10.3%) |
| 6 | 331.4 | 30.18 | 3.741 | 0.0000 | 196→199(30.8%) |
| 7 | 327.2 | 30.56 | 3.789 | 0.0000 | 196→199(12.4%) |
| 8 | 323.9 | 30.87 | 3.828 | 0.0000 | 197→199(20.5%) |
| | | | | | 198→203(10.2%) |
| 9 | 315.7 | 31.67 | 3.927 | 0.0000 | 198→199(10.6%) |
| 10 | 308.7 | 32.40 | 4.017 | 0.0000 | 198→204(16.6%) |
| | | | | | 197→204(14.9%) |
| 11 | 305.7 | 32.71 | 4.056 | 0.0000 | 194→199(23.7%) |
| 12 | 302.1 | 33.10 | 4.104 | 0.0000 | 195→199(10.7%) |
| 13 | 297.5 | 33.62 | 4.168 | 0.0000 | 189→199(15.5%) |
| | | | | | 188→199(15.1%) |
| | | | | | 198→200(12.6%) |
| 14 | 294.7 | 33.93 | 4.207 | 0.0000 | 185→205(33.4%) |
| | | | | | 187→205(27.2%) |
| 15 | 294.4 | 33.96 | 4.211 | 0.0000 | 186→207(30.0%) |
| | | | | | 189→207(11.6%) |
| 16 | 294.4 | 33.97 | 4.211 | 0.0000 | no single transition contributes more than 10% |
| 17 | 288.7 | 34.64 | 4.295 | 0.0000 | 195→199(15.0%) |
| 18 | 287.4 | 34.80 | 4.314 | 0.0000 | 198→201(28.2%) |
| | | | | | 197→200(11.0%) |
| 19 | 282.8 | 35.37 | 4.385 | 0.0000 | no single transition contributes more than 10% |
| 20 | 282.0 | 35.46 | 4.396 | 0.0000 | 198→202(14.1%) |
| | | | | | 198→200(13.6%) |
| 21 | 281.0 | 35.58 | 4.412 | 0.0000 | no single transition contributes more than 10% |
| 22 | 278.9 | 35.85 | 4.445 | 0.0000 | 187→201(11.0%) |
| | | | | | 198→201(10.8%) |
| 23 | 277.8 | 36.00 | 4.464 | 0.0000 | 183→199(22.8%) |
| 24 | 274.4 | 36.44 | 4.519 | 0.0000 | 183→199(12.7%) |
| 25 | 273.2 3 | 6.60 | 4.537 | 0.0000 | 192→199(17.9%) |

Optimized Cartesian coordinates (Å) (*xyz* format).

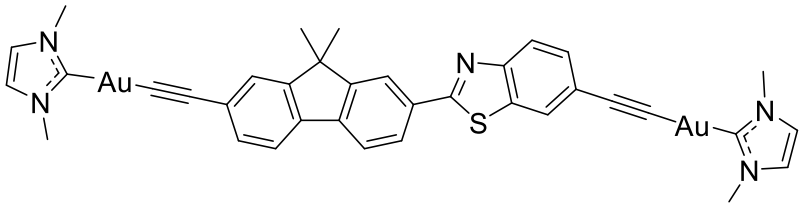


71

| | | | |
|---|---|---|---|
| P | 12.502745 | 21.975273 | -4.927990 |
| C | 11.556466 | 23.310274 | -4.111029 |
| H | 11.542414 | 23.141224 | -3.030441 |
| H | 12.004843 | 24.287995 | -4.318208 |
| H | 10.524189 | 23.302277 | -4.472586 |
| C | 14.215099 | 22.221555 | -4.334661 |
| H | 14.883637 | 21.520053 | -4.841983 |
| H | 14.550410 | 23.245992 | -4.529250 |
| H | 14.262490 | 22.023797 | -3.259910 |
| C | 12.564778 | 22.486940 | -6.682673 |
| H | 11.556905 | 22.463724 | -7.107133 |
| H | 12.974785 | 23.498028 | -6.778691 |
| H | 13.190253 | 21.788658 | -7.246232 |
| Au | 11.661358 | 19.845272 | -4.583137 |
| P | 2.826404 | -2.473837 | -0.023828 |
| C | 2.312531 | -3.075906 | 1.624953 |
| H | 1.976818 | -4.117172 | 1.570995 |
| H | 3.153232 | -3.002815 | 2.320961 |
| H | 1.497663 | -2.453096 | 2.005127 |
| C | 1.375701 | -2.807860 | -1.086199 |
| H | 1.618113 | -2.566069 | -2.125045 |
| H | 1.080706 | -3.860623 | -1.018928 |
| H | 0.538430 | -2.177204 | -0.773676 |
| C | 4.065959 | -3.700511 | -0.574632 |
| H | 4.947699 | -3.646153 | 0.070305 |
| H | 3.652288 | -4.714026 | -0.537455 |
| H | 4.376015 | -3.474323 | -1.598908 |
| Au | 3.564990 | -0.279063 | -0.058045 |
| C | 5.568224 | 6.953817 | -3.578533 |
| H | 4.637100 | 7.403639 | -3.219470 |
| H | 5.975452 | 7.590949 | -4.371831 |
| H | 5.332107 | 5.977077 | -4.015925 |
| C | 4.201000 | 1.601952 | -0.083441 |
| C | 4.595216 | 2.764931 | -0.092733 |
| C | 5.054525 | 4.112738 | -0.107062 |
| C | 5.008369 | 4.894147 | 1.066012 |
| C | 5.561713 | 4.682852 | -1.292212 |
| C | 5.452842 | 6.209008 | 1.071626 |
| H | 4.615894 | 4.446123 | 1.973907 |
| C | 6.004502 | 5.993168 | -1.286008 |
| H | 5.596026 | 4.078183 | -2.194772 |
| C | 5.952859 | 6.760545 | -0.108417 |
| H | 5.408544 | 6.793572 | 1.987189 |
| C | 6.583708 | 6.799666 | -2.437102 |
| C | 6.481452 | 8.088013 | -0.399978 |
| C | 6.855819 | 8.131316 | -1.756872 |

| | | | |
|---|---|---|---|
| C | 6.648313 | 9.209639 | 0.411719 |
| C | 7.392123 | 9.281051 | -2.302416 |
| C | 7.188287 | 10.364913 | -0.138889 |
| H | 6.363016 | 9.189952 | 1.460083 |
| C | 7.564582 | 10.417085 | -1.490277 |
| H | 7.688656 | 9.338557 | -3.345817 |
| H | 7.317049 | 11.239635 | 0.494134 |
| C | 7.880103 | 6.168461 | -2.965155 |
| H | 8.616390 | 6.051634 | -2.163594 |
| H | 7.678337 | 5.180136 | -3.393622 |
| H | 8.320659 | 6.794416 | -3.749492 |
| C | 8.134799 | 11.623871 | -2.084854 |
| N | 8.476100 | 11.721139 | -3.334863 |
| S | 8.414674 | 13.083248 | -1.119598 |
| C | 8.985722 | 12.961938 | -3.624728 |
| C | 9.039614 | 13.866790 | -2.539754 |
| C | 9.441658 | 13.380564 | -4.882595 |
| C | 9.531710 | 15.158083 | -2.681875 |
| C | 9.932269 | 14.663049 | -5.032249 |
| H | 9.402284 | 12.690406 | -5.719821 |
| C | 9.986406 | 15.568212 | -3.943483 |
| H | 9.570745 | 15.847486 | -1.844991 |
| H | 10.288699 | 14.999912 | -6.000627 |
| C | 10.498870 | 16.883542 | -4.130304 |
| C | 10.941826 | 18.016408 | -4.297071 |

Optimized Cartesian coordinates (Å) (*xyz* format).

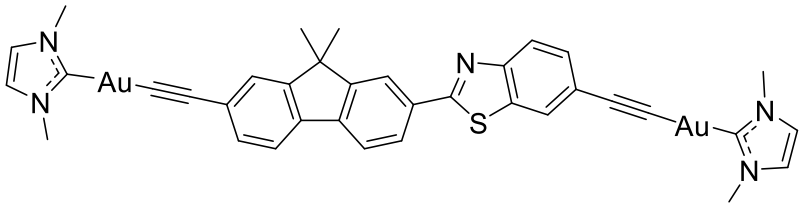


75

| | | | |
|---|---|---|---|
| C | 12.276926 | 21.747794 | -4.892171 |
| N | 11.880192 | 22.911791 | -4.323972 |
| N | 13.304710 | 22.097199 | -5.702632 |
| C | 12.644489 | 23.967163 | -4.770243 |
| C | 13.545475 | 23.452010 | -5.641933 |
| H | 12.483207 | 24.979802 | -4.433668 |
| H | 14.326374 | 23.926035 | -6.216614 |
| C | 14.061618 | 21.174772 | -6.527562 |

| | | | |
|---|---|---|---|
| H | 13.648578 | 20.174751 | -6.390465 |
| H | 13.980553 | 21.460349 | -7.579668 |
| H | 15.112591 | 21.177831 | -6.226497 |
| C | 10.793753 | 23.042224 | -3.371661 |
| H | 10.369823 | 22.052421 | -3.198436 |
| H | 11.169045 | 23.446989 | -2.428077 |
| H | 10.020893 | 23.703278 | -3.772721 |
| Au | 11.500367 | 19.884124 | -4.594205 |
| C | 2.776599 | -2.164102 | 0.023726 |
| N | 3.245532 | -3.324158 | -0.495477 |
| N | 1.589095 | -2.497204 | 0.584277 |
| C | 2.368912 | -4.361069 | -0.264099 |
| C | 1.321375 | -3.838168 | 0.418695 |
| C | 4.501895 | -3.467153 | -1.206375 |
| H | 4.995154 | -2.494690 | -1.228593 |
| H | 5.142936 | -4.188127 | -0.692326 |
| H | 4.317756 | -3.804481 | -2.229868 |
| C | 0.707527 | -1.572244 | 1.271030 |
| H | 0.567977 | -1.887156 | 2.308551 |
| H | 1.166777 | -0.583226 | 1.251316 |
| H | -0.261241 | -1.532722 | 0.766049 |
| H | 2.563815 | -5.367822 | -0.600447 |
| H | 0.420854 | -4.298023 | 0.796098 |
| Au | 3.660261 | -0.324984 | -0.024033 |
| C | 4.807572 | 7.388275 | -2.800165 |
| H | 4.265953 | 7.789727 | -1.937767 |
| H | 4.859562 | 8.168364 | -3.568243 |
| H | 4.232023 | 6.549263 | -3.207512 |
| C | 4.514025 | 1.462085 | -0.065530 |
| C | 5.039971 | 2.572270 | -0.085352 |
| C | 5.645793 | 3.860515 | -0.110701 |
| C | 6.320343 | 4.355381 | 1.025134 |
| C | 5.578998 | 4.660725 | -1.269568 |
| C | 6.914493 | 5.609737 | 1.019814 |
| H | 6.367403 | 3.732496 | 1.913397 |
| C | 6.170883 | 5.910789 | -1.274371 |
| H | 5.058874 | 4.277738 | -2.143790 |
| C | 6.839495 | 6.390916 | -0.133908 |
| H | 7.428971 | 5.970932 | 1.906942 |
| C | 6.217715 | 6.929051 | -2.402264 |
| C | 7.355873 | 7.722328 | -0.428735 |
| C | 7.002044 | 8.056085 | -1.750488 |
| C | 8.082492 | 8.620660 | 0.352207 |
| C | 7.367429 | 9.273197 | -2.290894 |
| C | 8.449234 | 9.844296 | -0.193453 |
| H | 8.361737 | 8.376301 | 1.373596 |

| | | | |
|---|---|---|---|
| C | 8.100651 | 10.185584 | -1.509724 |
| H | 7.105685 | 9.553098 | -3.307330 |
| H | 9.014462 | 10.544758 | 0.416752 |
| C | 6.956624 | 6.372090 | -3.627714 |
| H | 7.965447 | 6.040390 | -3.362179 |
| H | 6.413039 | 5.517963 | -4.047377 |
| H | 7.039441 | 7.137682 | -4.407585 |
| C | 8.477333 | 11.468850 | -2.098108 |
| N | 8.159099 | 11.832306 | -3.304349 |
| S | 9.423702 | 12.658236 | -1.186599 |
| C | 8.640186 | 13.083485 | -3.599298 |
| C | 9.367537 | 13.715991 | -2.565124 |
| C | 8.465011 | 13.756876 | -4.816377 |
| C | 9.914250 | 14.983878 | -2.718253 |
| C | 9.005442 | 15.017974 | -4.976408 |
| H | 7.907022 | 13.276880 | -5.614583 |
| C | 9.734696 | 15.650965 | -3.939063 |
| H | 10.471574 | 15.463305 | -1.920267 |
| H | 8.876800 | 15.550427 | -5.913609 |
| C | 10.279275 | 16.951742 | -4.135166 |
| C | 10.747045 | 18.074418 | -4.307504 |

Optimized Cartesian coordinates (Å) (*xyz* format).

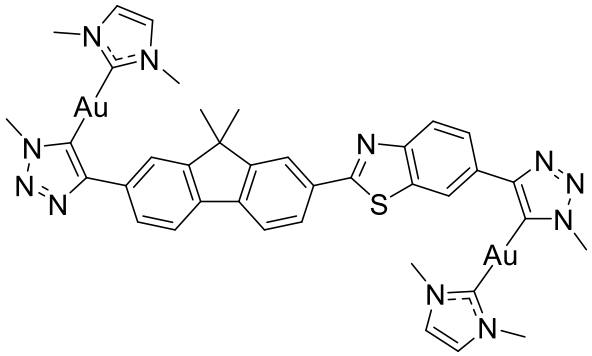


89

| | | | |
|---|---|---|---|
| C | 10.964297 | 18.396929 | 1.451696 |
| N | 11.996923 | 19.010366 | 2.126954 |
| N | 10.604813 | 17.320948 | 2.230578 |
| C | 12.283039 | 18.322526 | 3.324858 |
| C | 11.406807 | 17.259254 | 3.388776 |
| H | 13.052852 | 18.634970 | 4.000239 |
| H | 11.290702 | 16.494389 | 4.130393 |
| C | 9.553392 | 16.362605 | 1.924653 |

| | | | |
|---|---|---|---|
| H | 9.005623 | 16.664612 | 1.001320 |
| H | 9.978188 | 15.355654 | 1.746170 |
| H | 8.815783 | 16.309769 | 2.746978 |
| C | 12.706870 | 20.198861 | 1.688190 |
| H | 12.303134 | 20.550155 | 0.714287 |
| H | 12.590199 | 21.019892 | 2.420837 |
| H | 13.784175 | 19.985586 | 1.551635 |
| Au | 10.012211 | 18.875801 | -0.498594 |
| C | 0.727205 | 2.440612 | 0.959456 |
| N | -0.281443 | 1.532967 | 1.198025 |
| N | 0.147655 | 3.445779 | 0.218556 |
| C | -1.487943 | 1.966560 | 0.609393 |
| C | -1.217087 | 3.170129 | -0.007206 |
| C | -0.146482 | 0.298028 | 1.950259 |
| H | 0.893839 | 0.188645 | 2.325331 |
| H | -0.824827 | 0.293505 | 2.824564 |
| H | -0.371945 | -0.577775 | 1.312541 |
| C | 0.823139 | 4.635203 | -0.277145 |
| H | 0.360459 | 5.550999 | 0.136175 |
| H | 1.897263 | 4.632947 | 0.028146 |
| H | 0.793607 | 4.672403 | -1.382565 |
| H | -2.397392 | 1.405251 | 0.676666 |
| H | -1.853528 | 3.827136 | -0.565289 |
| Au | 2.878442 | 2.455974 | 1.518915 |
| C | 7.857088 | 7.554290 | -1.564565 |
| H | 6.969253 | 7.375406 | -2.184054 |
| H | 8.490253 | 8.273637 | -2.095053 |
| H | 8.405710 | 6.606985 | -1.496520 |
| C | 4.981051 | 2.622506 | 1.960874 |
| C | 5.896585 | 3.686510 | 1.852922 |
| N | 5.743023 | 1.540506 | 2.320594 |
| N | 7.073059 | 1.912933 | 2.440309 |
| N | 7.168048 | 3.160020 | 2.161004 |
| C | 5.340131 | 0.169775 | 2.588322 |
| H | 4.572503 | 0.138869 | 3.383289 |
| H | 4.920962 | -0.296212 | 1.677112 |
| H | 6.216976 | -0.424964 | 2.917854 |
| C | 5.700412 | 5.071401 | 1.495151 |
| C | 4.477508 | 5.699620 | 1.760119 |
| C | 6.743064 | 5.785296 | 0.870065 |
| C | 4.254920 | 7.030130 | 1.396225 |
| H | 3.690051 | 5.137286 | 2.263756 |
| C | 6.520081 | 7.095728 | 0.510609 |
| H | 7.698661 | 5.293972 | 0.687987 |
| C | 5.274629 | 7.721842 | 0.767359 |
| H | 3.304354 | 7.508332 | 1.611422 |

| | | | |
|---|---|---|---|
| C | 7.468579 | 8.067825 | -0.178712 |
| C | 5.329945 | 9.093370 | 0.274724 |
| C | 6.612705 | 9.321958 | -0.287539 |
| C | 4.373944 | 10.093360 | 0.283314 |
| C | 6.938864 | 10.544579 | -0.831877 |
| C | 4.702390 | 11.335594 | -0.267924 |
| H | 3.388746 | 9.921178 | 0.706278 |
| C | 5.970045 | 11.563722 | -0.808741 |
| H | 7.917083 | 10.709901 | -1.279144 |
| H | 3.960024 | 12.135550 | -0.283810 |
| C | 8.699135 | 8.325304 | 0.690524 |
| H | 8.411808 | 8.697477 | 1.682081 |
| H | 9.275239 | 7.403951 | 0.843117 |
| H | 9.362363 | 9.068295 | 0.235950 |
| C | 6.277064 | 12.876560 | -1.347305 |
| N | 5.522117 | 13.582336 | -2.134192 |
| S | 7.831419 | 13.711983 | -0.889671 |
| C | 6.086051 | 14.831186 | -2.452971 |
| C | 7.346596 | 15.093206 | -1.864168 |
| C | 5.486263 | 15.780545 | -3.287172 |
| C | 8.004424 | 16.291312 | -2.087151 |
| C | 6.143662 | 16.980850 | -3.501780 |
| H | 4.523559 | 15.565744 | -3.749291 |
| C | 7.391690 | 17.253673 | -2.899338 |
| H | 8.982743 | 16.498453 | -1.649784 |
| H | 5.702170 | 17.742234 | -4.151899 |
| C | 8.029918 | 18.527941 | -3.118817 |
| C | 9.002977 | 19.224371 | -2.374684 |
| N | 7.712779 | 19.339980 | -4.229543 |
| N | 8.403358 | 20.417028 | -4.201375 |
| N | 9.207060 | 20.388556 | -3.070397 |
| C | 10.109013 | 21.493963 | -2.790434 |
| H | 9.839435 | 21.982843 | -1.835779 |
| H | 11.152736 | 21.135704 | -2.719901 |
| H | 10.047072 | 22.247383 | -3.602786 |

**References.**


1 J. J. Mihaly, D. J. Stewart, T. A. Grusenmeyer, A. T. Phillips, J. E. Haley, M. Zeller and T. G. Gray, Photophysical properties of organogold(i) complexes bearing a benzothiazole-2,7-fluorenyl moiety: Selection of ancillary ligand influences white light emission, *Dalt. Trans.*, 2019, **48**, 15917–15927.

2 J. J. Mihaly, A. T. Phillips, J. T. Malloy, Z. M. Marsh, M. Zeller, J. E. Haley, K. De La Harpe, T. A. Grusenmeyer and T. G. Gray, Synthesis and Photophysical Properties of Laterally Asymmetric Digold(I) Alkynyls and Triazolyl: Ancillary Ligand and Organic Functionality Dictate Excited-State Dynamics, *Organometallics*, 2020, **39**, 489–494.

3 D. V Partyka, T. J. Robilotto, M. Zeller, A. D. Hunter and T. G. Gray, Dialkylbiarylphosphine Complexes of Gold(I) Halides. Gold−Aryl π-Interactions in the Solid State, *Organometallics*, 2008, **27**, 28–32.

4 J. E. Heckler, N. Deligonul, A. L. Rheingold and T. G. Gray, Gold(i) triazolyls: Organometallic synthesis in air and aqueous media, *Chem. Commun.*, 2013, **49**, 5990–5992.; L. Gao, D. V. Partyka, J. B. Updegraff, N. Deligonul and T. G. Gray, Synthesis, structures, and excited-state geometries of alkynylgold(I) complexes, *Eur. J. Inorg. Chem.*, 2009, **2009**, 2711–2719.

5 G. M. Sheldrick, A short history of SHELX, *Acta Crystallogr. Sect. A*, 2008, **64**, 112–122.

6 G. M. Sheldrick, Crystal structure refinement with SHELXL, *Acta Crystallogr. Sect. C*, 2015, **71**, 3–8.

7 C. B. Hübschle, G. M. Sheldrick and B. Dittrich, ShelXle: a Qt graphical user interface for SHELXL, *J. Appl. Crystallogr.*, 2011, **44**, 1281–1284.

8 L. Krause, R. Herbst-Irmer, G. M. Sheldrick and D. Stalke, Comparison of silver and molybdenum microfocus X-ray sources for single-crystal structure determination, *J. Appl. Crystallogr.*, 2015, **48**, 3–10.

9 Gaussian 16, Revision A.03, M. J. Frisch, G. W. Trucks, H. B. Schlegel, G. E. Scuseria, M. A. Robb, J. R. Cheeseman, G. Scalmani, V. Barone, G. A. Petersson, H. Nakatsuji, X. Li, M. Caricato, A. V Marenich, J. Bloino, B. G. Janesko, R. Gomperts, B. Mennucci, H. P. Hratchian, J. V Ortiz, A. F. Izmaylov, J. L. Sonnenberg, D. Williams-Young, F. Ding,

F. Lipparini, F. Egidi, J. Goings, B. Peng, A. Petrone, T. Henderson, D. Ranasinghe, V. G. Zakrzewski, J. Gao, N. Rega, G. Zheng, W. Liang, M. Hada, M. Ehara, K. Toyota, R. Fukuda, J. Hasegawa, M. Ishida, T. Nakajima, Y. Honda, O. Kitao, H. Nakai, T. Vreven, K. Throssell, J. A. Montgomery Jr., J. E. Peralta, F. Ogliaro, M. J. Bearpark, J. J. Heyd, E. N. Brothers, K. N. Kudin, V. N. Staroverov, T. A. Keith, R. Kobayashi, J. Normand, K. Raghavachari, A. P. Rendell, J. C. Burant, S. S. Iyengar, J. Tomasi, M. Cossi, J. M. Millam, M. Klene, C. Adamo, R. Cammi, J. W. Ochterski, R. L. Martin, K. Morokuma, O. Farkas, J. B. Foresman and D. J. Fox, Gaussian, Inc., Wallingford CT, 2016.

10 M. Dolg, U. Wedig, H. Stoll and H. Preuss, Energy-adjusted ab initio pseudopotentials for the first row transition elements, *J. Chem. Phys.*, 1987, **86**, 866–872.

11 J. P. Perdew, K. Burke and M. Ernzerhof, Generalized Gradient Approximation Made Simple, *Phys. Rev. Lett.*, 1996, **77**, 3865–3868.

12 N. Godbout, D. R. Salahub, J. Andzelm and E. Wimmer, Optimization of Gaussian-type basis sets for local spin density functional calculations. Part I. Boron through neon, optimization technique and validation, *Can. J. Chem.*, 1992, **70**, 560–571.

13 S. Miertuš, E. Scrocco and J. Tomasi, Electrostatic interaction of a solute with a continuum. A direct utilizaion of AB initio molecular potentials for the prevision of solvent effects, *Chem. Phys.*, 1981, **55**, 117–129.

14 J. Tomasi, B. Mennucci and R. Cammi, Quantum Mechanical Continuum Solvation Models, *Chem. Rev.*, 2005, **105**, 2999–3094.

15 E. Cancès, B. Mennucci and J. Tomasi, A new integral equation formalism for the polarizable continuum model: Theoretical background and applications to isotropic and anisotropic dielectrics, *J. Chem. Phys.*, 1997, **107**, 3032–3041.

16 B. Mennucci, E. Cancès and J. Tomasi, Evaluation of Solvent Effects in Isotropic and Anisotropic Dielectrics and in Ionic Solutions with a Unified Integral Equation Method: Theoretical Bases, Computational Implementation, and Numerical Applications, *J. Phys. Chem. B*, 1997, **101**, 10506–10517.

17 S. I. Gorelsky and A. B. P. Lever, Electronic structure and spectra of ruthenium diimine complexes by density functional theory and INDO/S. Comparison of the two methods, *J. Organomet. Chem.*, 2001, **635**, 187–196.

18 S. I. Gorelsky, AOMix: Program for Molecular Orbital Analysis, http://www.sg-chem.net.

## Chapter 5: Synthesis and Photophysics for a Series of Mononuclear Gold(I) complexes bearing a Diphenylamino Fluorenyl Moiety (DPA).

In chapters 2-4, a library of strucutre-property realtionships regarding gold(I) BTF complexes was established. The effect of ancillary ligand, nature of the gold-chromophore bond, as well as the number of metal centers on excited-state dynamics was described.[1-3] The benzothiazole-2,7-fluorenyl (BTF) moiety is considered an electron acceptor, due to the electron withdrawing character of the benzothiazole. Synthetically modifiying the benzothiazole to an electron donor such as diphenylamine (DPA), allows for stratigic tuning of the electronic environment of the fluorene based ligand. Of particular interest is structure-property relationships in the gold(I) DPA complexes as well as how ancillary ligand and gold-chromophore bond affect photophysical characteristics (Figure 5.1). This will serve to expand the toolbox of strucuture-property realtionships for gold(I) complexes as photoactive triplet materials.

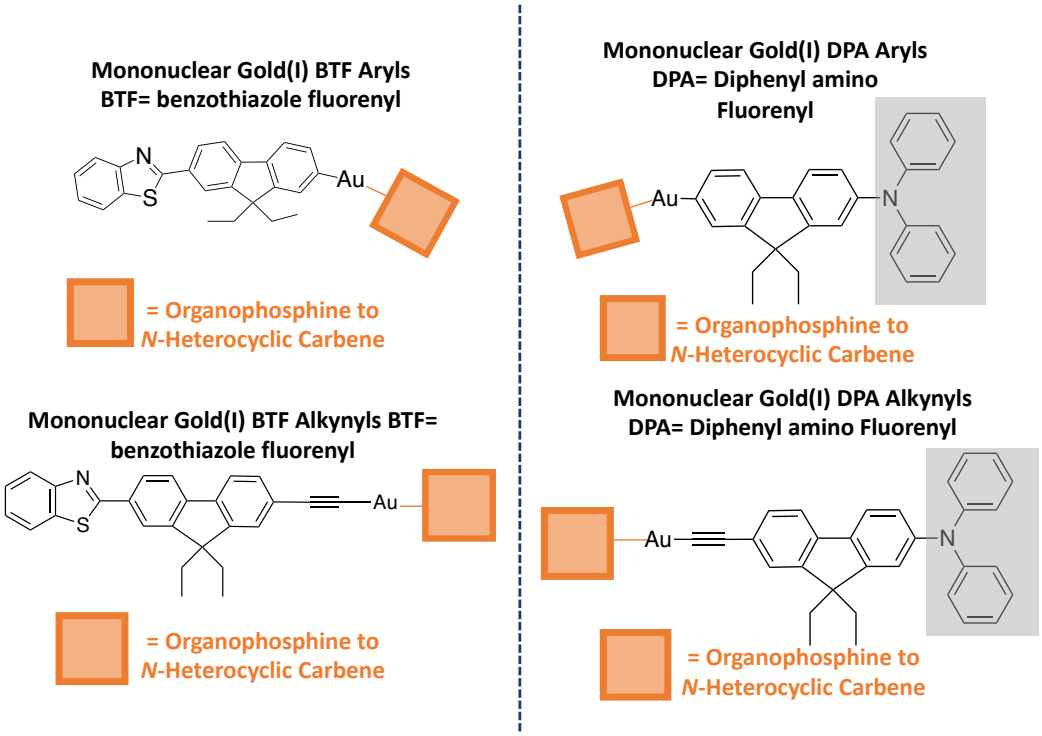


**Figure 5.1** Comparision gold(I) aryls and alkynyls with variation in ancillary ligand (BTF (left), DPA (right))

Five new gold(I) diphenylamino-fluorenyl complexes have been synthesized. Two gold(I) DPA aryl complexes (**Au-DPA 0,2**) were prepared by reaction of the corresponding gold(I) halide with known pinacolboronate ester ligand precursor.[4] This base-assisted boron transmetallation afforded the complexes **Au-ADPA(0,2)**) in 67 and 55 percent isolated yields, respectively (Scheme 5.1). Gold(I) alkynyls **Au-ADPA(0,2)** were obtained by *in situ* deprotonation of the known alkyne[5] and subsequent addition of this solution to a suspension of (phosphine-) or (*N*-heterocyclic carbene)gold(I) chloride.[6] **Au-ADPA(0,2)** were recovered in 60 and 78 percent isolated yields, respectively (Scheme 5.1). **Au-ADPA2** was then further functionalized through a copper-catalyzed [3+2] azide-alkynyl cycloaddition reaction to produce **Au-ADPA3** in 82 percent isolated yield (Scheme 5.1).[6]

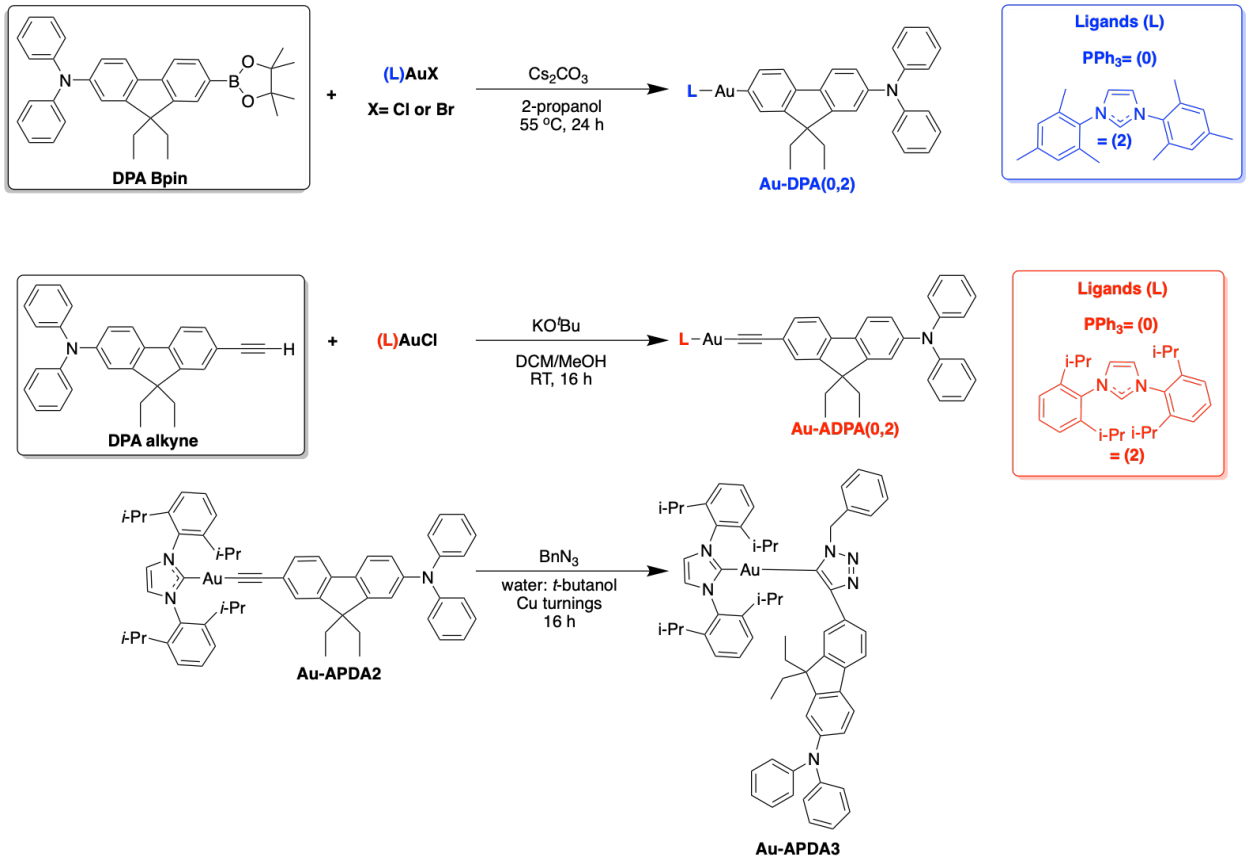


**Scheme 5.1** Synthesis of gold(I) DPA aryls (**Au-DPA (0,2)**), gold(I) DPA alkynyls (**Au-ADPA (0,2)**), and gold(I) DPA triazolyl **Au-ADPA3**.

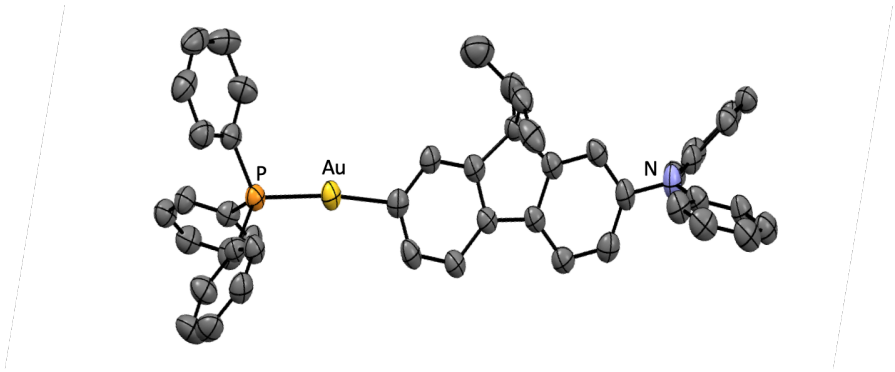

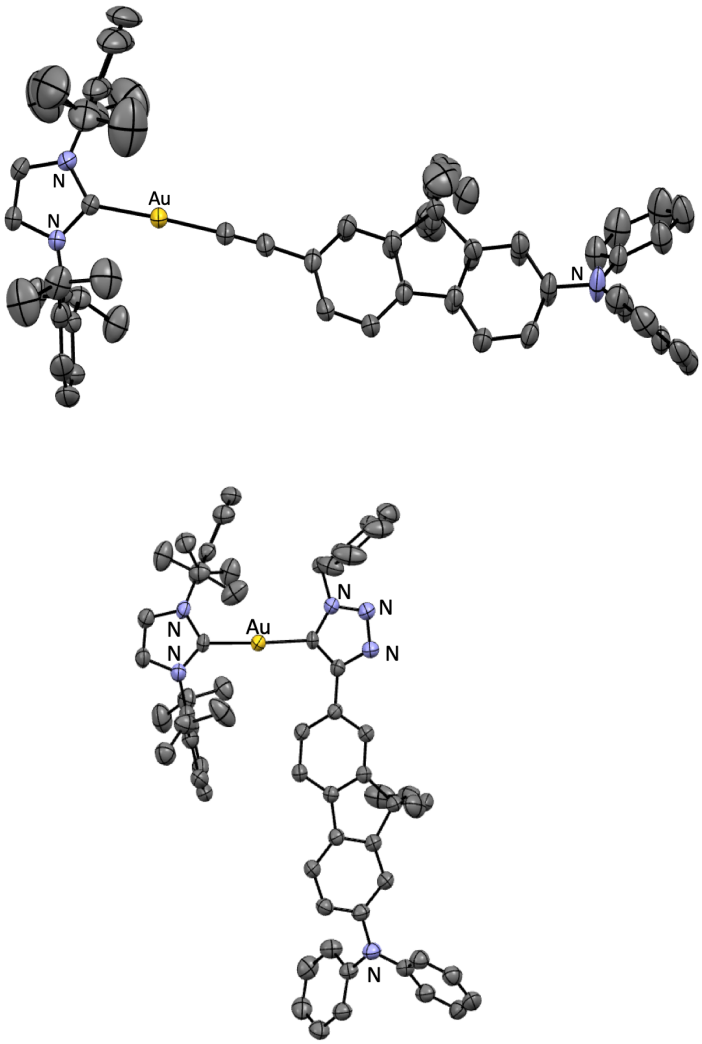


**Figure 5.2.** Crystal structures of **Au-DPA0** (top), **Au-ADPA2** (middle), **Au-ADPA2** (bottom). (50% probability level, 150 K). Hydrogen atoms are omitted for clarity. A partial atom labeling scheme appears; unlabeled atoms are carbon.

Crystal structures of **Au-DPA0**, **Au-ADPA2**, and **Au-ADPA3** appear in Figure 5.2; the structure of **Au-ADPA0** appears in the supporting information (Figure 5.11). Gold(I) centers are approximately linear and two-coordinate. Inspection of crystallographic packing diagrams reveals that none of the compounds exhibit aurophilic interactions or π-stacking. **Au-DPA0** has an Au-C bond length of 2.052(7) and an Au-P length of 2.203(2) and **Au-ADPA0** has an Au-C bond length

of 2.008(3) and an Au-P length of 2.28(1) demonstrating little variation in these both lengths between the phosphine aryl and alkynyl complexes. **Au-ADPA2** has an Au-$C_{carbene}$ length of 2.009(2) and an Au-$C_{alkyne}$ length of 1.975(2). **Au-ADPA3** has an Au-$C_{carbene}$ length of 2.039(3) and an Au-triazole length of 2.042(2).

**Ground-state absorption and steady-state luminescence spectroscopy.**

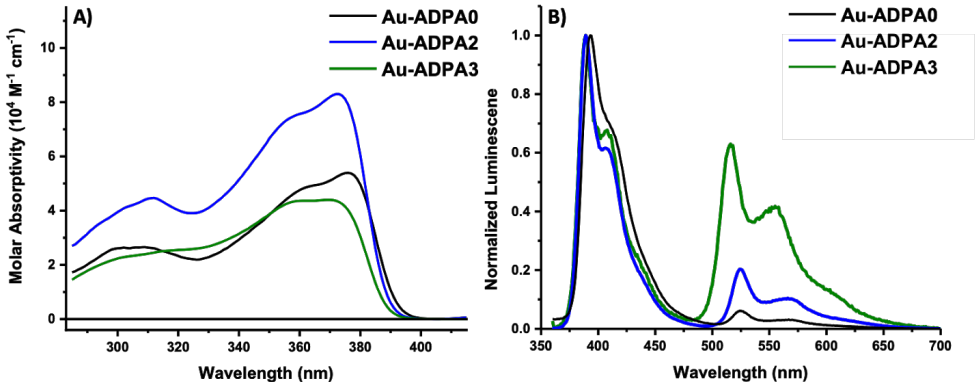


**Figure 5.3.** (a) Ground-state absorption spectra in molar absorptivity units. (b) Normalized luminescence spectra in freeze-pump-thaw degassed toluene. Coloring scheme for complexes: **Au-ADPA0**-black, **Au-DPA2**-blue, **Au-ADPA3**-green.

Ground-state absorption spectra in molar absorptivity units and steady-state luminescence spectra of **Au-ADPA0**, **Au-ADPA2**, and **Au-ADPA3** collected in toluene are shown in Figure 5.3. The luminescence spectra were collected at room temperature followed three freeze-pump-thaw degassing cycles. All three alkynyl complexes have comparable ground-state absorption spectra, and are characterized by two distinct absorption transitions. The low energy absorption transition occurs around 370 nm, displays vibronic structure, and has a molar absorptivity on the order of 4 x $10^4$ $M^{-1}$ $cm^{-1}$. A higher energy transition is found at approximately 310 nm. It is broad and has a

molar absorptivity value that is roughly half of the low energy absorption transition. The ground-state absorption spectra of the **Au-ADPA** complexes are nearly identical in energy, bandshape, and molar absorptivity values to the free alkyne.[5] Combined, these observations suggest that these ground-state absorption transitions are $\pi$-$\pi^*$ in character. The low energy ground-state absorption maxima experience a hypsochromic shift as the ancillary ligand is changed from a phosphine in **Au-ADPA0** (376 nm) to an *N*-heterocyclic carbene in **Au-ADPA2** (373 nm). A further hypsochromic shift is observed when the bridging moiety is converted to a triazole in **Au-ADPA3** (369 nm). We have previously observed a bathochromic shift when following this same structural progression in Au(I) alkynyl BTF complexes.[3] All three complexes display dual-luminescence in freeze-pump-thaw degassed toluene. The fluorescence and phosphorescence spectra of all three **Au-ADPA** complexes are highly structured. The vibronic structure of the observed luminescence transitions again suggests that they are $\pi$-$\pi^*$ in character. The fluorescence maxima generally follow the same energy trend as the ground-state absorption spectra with **Au-ADPA0** (392 nm) > **Au-ADPA2** (388 nm) = **Au-ADPA3** (388 nm). Phosphorescence intensity increases from **Au-ADPA0** to **Au-ADPA3**: **Au-ADPA0** exhibits the weakest phosphorescence at 525, 570 nm, with **Au-ADPA2** being at 525, 568 nm. This is the converse of what is observed in the aryl complexes **Au-DPA0** and **Au-DPA2**, where the phosphine complex has significantly more phosphorescence in comparison to the carbene complex. Converting the alkyne linkage in **Au-ADPA2** to a triazole (**Au-ADPA3**) leads to a further increase in phosphorescence intensity at 515, 556 nm. Taken together, these data demonstrate that both absorption and emission can be strategically tuned by changing either ancillary ligand or the gold-chromophore linkage in this synthetically new collection of gold(I) complexes.

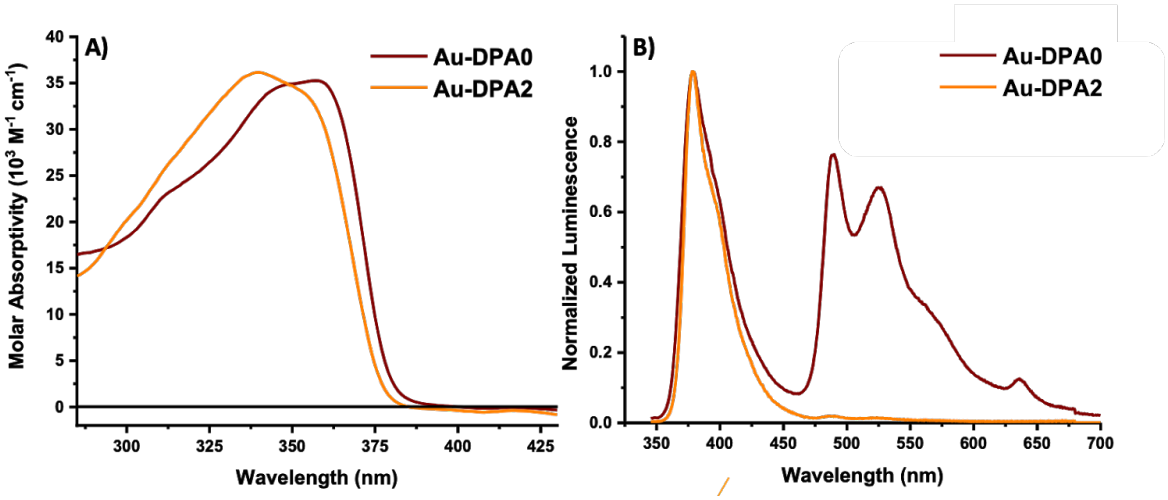


**Figure 5.4.** (a) Ground-state absorption spectra in molar absorptivity units. (b) Normalized luminescence spectra in freeze-pump-thaw deaerated toluene. Coloring scheme for complexes: **Au-DPA0**-wine red, **Au-DPA2**-orange.

Ground-state absorption spectra in molar absorptivity units and steady-state luminescence spectra of **Au-DPA0** and **Au-DPA2** collected in toluene are shown in Figure 5.4. The luminescence spectra were collected following three freeze-pump-thaw degas cycles. Both complexes have extinction coefficients on the order of 3.5 x $10^3$ $M^{-1}$ $cm^{-1}$. The absorption spectra for both complexes are similar in bandshape; with **Au-DPA0** having a more distinct high-energy shoulder, both spectra lack significant structure. **Au-DPA0**, containing a phosphine ancillary ligand displays an absorption maximum at 357 nm. Changing the ancillary from an organophosphine to an *N*-heterocyclic carbene (**Au-DPA2**) blue shifts the absorption maximum to 340 nm. Both complexes exhibit dual-luminescence at room temperature in freeze-pump-thaw degassed toluene. **Au-DPA0** (organophosphine ancillary ligand) exhibits narrow, structureless fluorescence at 379 nm and highly structured, intense phosphorescence at 489, 525, 635 nm. Changing the ancillary ligand to an *N*-heterocyclic carbene (**Au-DPA2**) also leads to dual-

emission: structureless fluorescence with maximum at 379 nm and weak phosphorescence at 486, 524 nm. Taken together, these data demonstrate that both absorption and emission can be strategically tuned by changing either ancillary ligand or the gold-chromophore linkage in this synthetically new collection of gold(I) complexes.

| | Au Complex | Experimental Results | | | | |
|---|---|---|---|---|---|---|
| | | $\lambda_{ABS}$/nm ($10^4$ $M^{-1}cm^{-1}$) | $\lambda_{FL}$[A] (nm) | $\lambda_{PHOS}$[A] (nm) | $\Phi_F$ | $\Phi_P$[C] |
| Alkynyl | **Au-ADPA0** | 376 (5.4) | 393 | 525 | 0.20 ± 0.02 | 0.02 |
| | **Au-ADPA1** | 373 (8.3) | 389 | 525 | 0.13 ± 0.01 | 0.04 |
| | **Au-ADPA2** | 369 (4.4) | 389 | 516 | < 0.01[B] | < 0.01 |
| Aryl | **Au-DPA0** | 357 (3.5) | 378 | 490 | 0.06 ± 0.01 | 0.09 |
| | **Au-DPA2** | 340 (3.6) | 378 | 488 | 0.07 ± 0.01 | < 0.01 |

**Table 5.1.** Photophysical data for **Au-DPA** and **Au-ADPA** series.
Data collected in toluene. Fluorescence lifetime data are not reported for any of the compounds because all lifetimes are shorter than the instrument response time of our time correlated single photon counting instrumentation.[A]Estimated from the luminescence maximum.[B]Value was deemed to be between 0.005 and 0.01 after two trials. The detection limit of the instrument is 0.05. [C]Phosphorescence quantum yields were determined using a relative method.

Table 5.1 collects absorption, fluorescence, and phosphorescence maxima as well as molar absorptivity values and quantum yields. Absorption and emission energy trends as well as molar absorptivity values were discussed earlier in the chapter. Regarding fluorescence and phosphorescence quantum yields, there are no clear trends in the data.

**Future Directions.**

Further investigation into the photophysical properties of these new gold(I) DPA complexes. This includes fluorescence and phosphorescence lifetimes as well as triplet-state quantum yields. This will allow for calculation of excited-state rate constants and insight into the

excited-state dynamics of these complexes. Computational support will lead to a more complete understanding as to the photophysical data we are observing.

**Experimental Details.**

**General Considerations.** All experimental procedures were carried out under an inert atmosphere of argon using standard Schlenk line techniques. Microanalyses (C, H, and N) were undertaken by Atlantic Microlab. Mass spectrometry was performed at the University of Cincinnati Mass Spectrometry facility. (Phosphine)gold(I) chlorides and (NHC)gold(I) chlorides were prepared according to literature procedures.[4] The corresponding gold(I) bromides were prepared by reacting one equivalent of gold(I) chloride with five equivalents of potassium bromide in a 1:1 mixture of dichloromethane/water, extraction in dichloromethane yielded the bromides quantitatively. **DPA alkyne** ligand was synthesized according to literature procedure.[5]

Dry methanol, dichloromethane, pentane, diethyl ether, Copper turnings, and potassium *tert*-butoxide *was* purchased from Sigma Aldrich and used as received. *Tert*-butanol was purchased from Fisher Scientific. Benzyl azide was purchased from Alfa Aesar. $^{1}$H NMR experiments were performed on a Bruker-500 Ascend Advanced III HD NMR spectrometer operating at 500.24 MHz. $^{1}$H chemical shifts are reported in parts per million ($\delta$) with integration and multiplicity (s = singlet, d = doublet, t = triplet, q = quartet, dd = doublet of doublets, dt = doublet of triplets, td = triplet of doublets, ddd = doublet of doublet of doublets, and m = muliplet), measured from tetramethylsilane (0 ppm) and are referenced to residual solvent in $CDCl_3$ (7.26 ppm). $^{31}P\{^{1}H\}$ NMR, chemical shifts were determined relative to concentrated $H_3PO_4$.

**DPA Bpin** : To a flame-dried 25 mL round bottom flask equipped with a stir bar was added

haloarene (1.0 mmol, 487 mg), $PdCl_2$dppf (0.03 mmol, 22 mg), KOAc (294 mg, 3.0 mmol), and bis(pinacolato) diboron 1 (279 mg, 1.1 mmol). The flask was then flushed with argon for 20 min. Dry dioxane (6 mL) was then added via syringe and the contents of the flask were heated at 80 °C for 24 h. The contents were then concentrated on a roto-evaporator and dichloromethane was added. The suspension was filtered over Celite to yield a yellowish-brown solution. The crude mixture was purified using flash column chromatography: solvent, 7:3 Pentanes:DCM. Desired compound was isolated as a white solid in 70% yield.

**Instrumentation.** Detailed instrument components and setup has been reported in the literature.[1-3]

**Relative Phosphorescence Quantum Yield Calculation:**

To determine the phosphorescence quantum yields of the Au-DPA and Au-ADPA compounds, a relative method was employed. Normalized, deaerated luminescence spectra were used to measure the area corresponding to fluorescence emission and the area corresponding to phosphorescence emission. This relative method was utilized on the Au-BTF compounds and compared to the experimental phosphorescence quantum yield to determine the accuracy of the calculation. Provided below in *Table 1* are the results for the Au-BTF series.

**Table 5.2.** Au-BTF Relative and Experimental Phosphorescence Quantum Yield Comparison.

| Compound: | Fl Integration Range (nm) | Phos. Integration Range (nm) | Fl. Area | Phos. Area | $\Phi_{Fl}$ | Relative $\Phi_{Phos}$ | Exp. $\Phi_{Phos}$ | STDEV |
|---|---|---|---|---|---|---|---|---|
| **Au-BTF0** | 360-499 | 499-750 | 55.52 | 61.2197 | 0.08 | 0.09 | 0.09 | 0.001263 |
| **Au-BTF1** | 360-499 | 500-750 | 55.214 | 45.5412 | 0.09 | 0.07 | 0.07 | 0.002994 |
| **Au-BTF2** | 360-499 | 499-750 | 63.471 | 25.5979 | 0.22 | 0.09 | 0.11 | 0.015043 |

The relative calculated phosphorescence quantum yield appears to be within agreement of the experimental phosphorescence quantum yield with little standard deviation. Because of this, the relative method was utilized for the Au-DPA and Au-ADPA compounds. Provided in Table 5.3 below are the calculated relative phosphorescence quantum yields.

**Table 5.3.** Relative Phosphorescence Quantum Yield Calculation for Au-DPA and Au-ADPA Complexes.

| Compound: | Fl Integration Range (nm) | Phos. Integration Range (nm) | Fl. Area | Phos. Area | $\Phi_{Fl}$ | Relative $\Phi_{Phos}$ |
|---|---|---|---|---|---|---|
| **Au-DPA0** | 345-459 | 459-700 | 41.463 | 62.67498 | 0.06 | 0.09 |
| **Au-DPA2** | 362.5-470 | 470-700 | 35.3625 | 1.75841 | 0.07 | 0.00 |
| **Au-ADPA0** | 360-500 | 500-700 | 42.2692 | 3.66422 | 0.2 | 0.02 |
| **Au-ADPA2** | 360-493 | 493-700 | 35.3999 | 10.6947 | 0.13 | 0.04 |
| **Au-ADPA3** | 360-477 | 477-700 | 54.1497 | 59.21636 | 0.01 | 0.01 |

**Synthesis, NMR, Mass Spectrometry, and Elemental Analysis**

**Au-DPA0:**

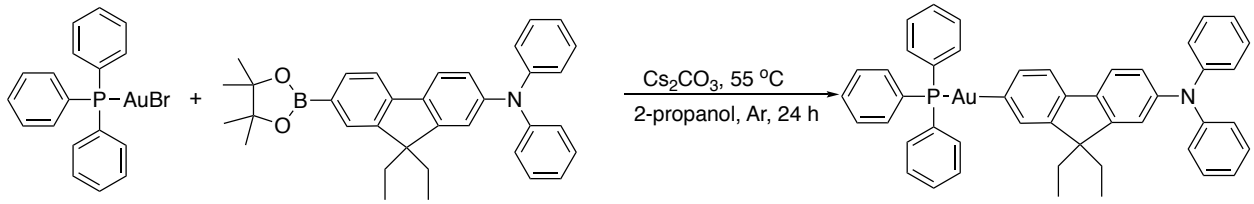


To flame-dried 25 mL RBF equipped with a stir bar was added (69.5 mg, 0.129 mmol, 1 equiv) of $Ph_3PAuBr$, (100 mg, 0.193 mmol, 1.5 equiv) of Dpa-Bpin ligand, (126 mg, 0.368 mmol, 2.85 equiv) of cesium carbonate. The flask was then purged for 15 min with argon, after which 5 mL of dry 2-propanol was added via syringe. The flask was then shielded from light and allowed to stir at 55 degrees $^{o}$C for 24 hours. The flask was then cooled and concentrated on roto-evaporator. 5 X 5 mL portions of benzene were then added and the suspension was filtered over Celite. The

light-yellow solution was then concentrated *in vacuo.* Analytically pure material was obtained by vapor diffusion of pentanes into a concentrated dichloromethane solution in a freezer. (73 mg, 67 % yield). $^{1}$H NMR (500 MHz, Chloroform-*d*) δ 7.66 – 7.43 (m, 19H), 7.24 – 7.17 (m, 4H), 7.14 – 7.06 (m, 5H), 6.96 (m, 3H), 1.92 (m, 7.3 Hz, 4H), 0.39 (t, $J$ = 7.3 Hz, 6H). $^{31}$P NMR (202 MHz, $CDCl_3$) δ 43.72. HRMS (FT-ICR, $[M]^+$) m/z calcd for $M^+$ $C_{47}H_{41}NPAu^+$ 847.26367 found 847.26397. Anal. Calcd for: $C_{47}H_{41}AuNP$: C, (66.59); H, (4.87); N, (1.65). Found: C, (66.85); H, (4.99); N, (1.69).

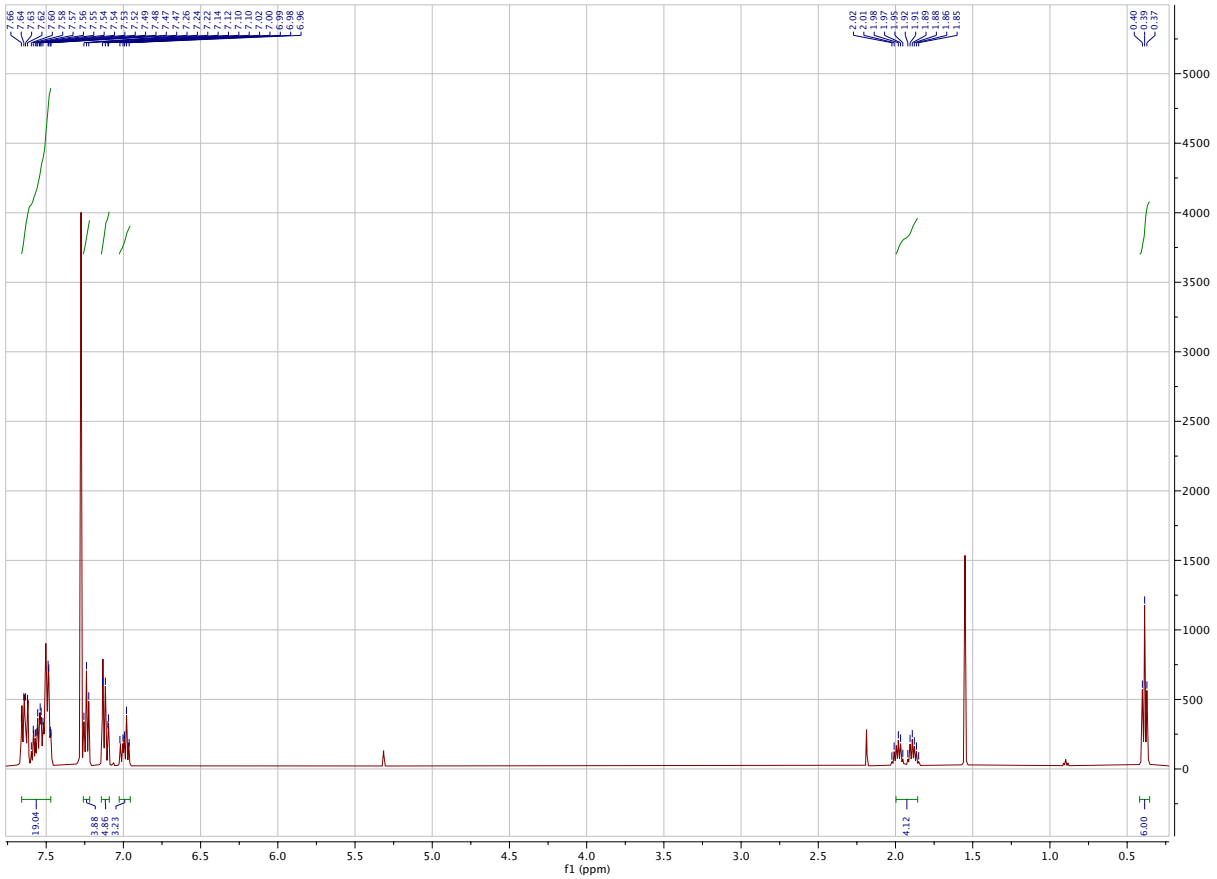


**Figure 5.5.** $^{1}$H NMR Spectrum of **Au-DPA0**

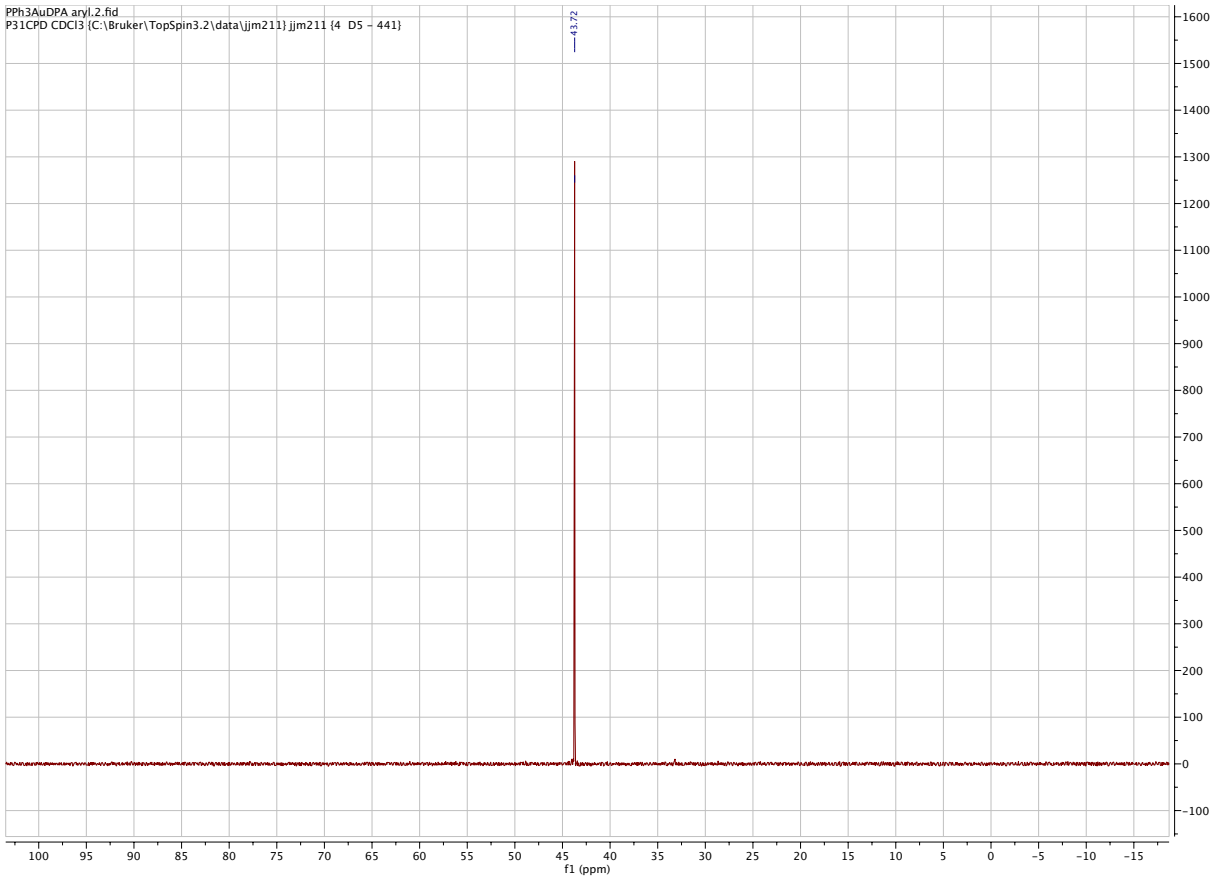


**Figure 5.6.** $^{31}P\{^{1}H\}$ NMR Spectrum of **Au-DPA0**

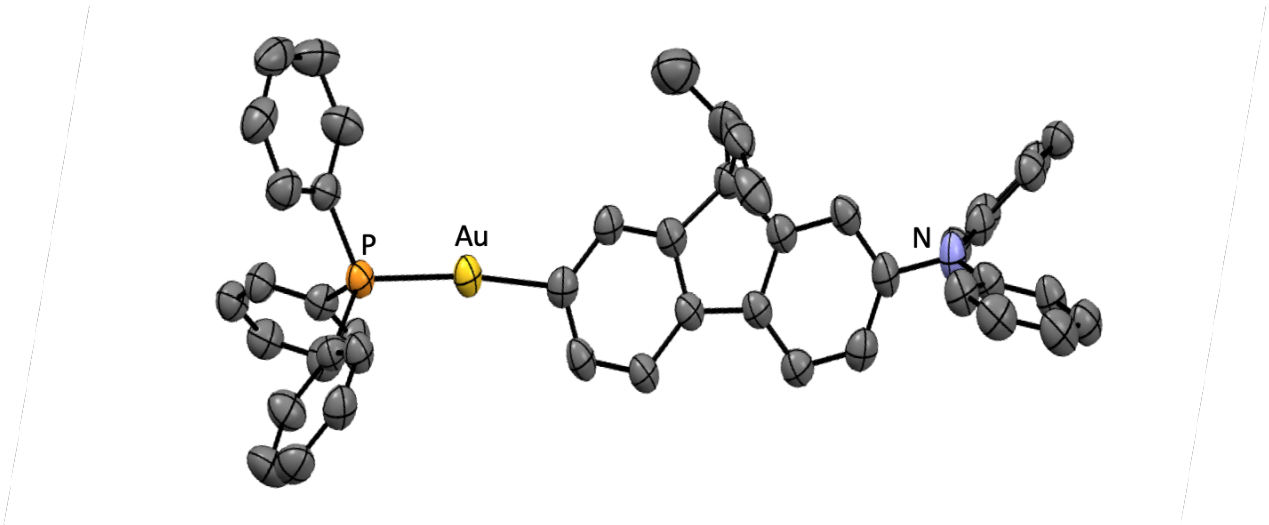


**Figure 5.7.** Thermal ellipsoid representation of **Au-DPA0** (50% probability, 150 K). Unlabeled atoms are carbon and hydrogen (disordered atom deleted for clarity).

**Au-DPA2:**

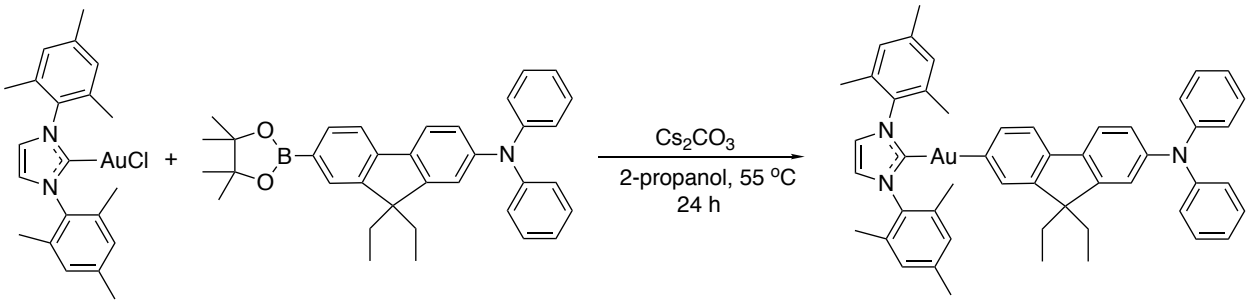


To flame-dried 25 mL RBF equipped with a stir bar was added (96.5 mg, 0.180 mmol, 1 equiv) of IMesAuCl, (173 mg, 0.333 mmol, 1.85 equiv) of Dpa-Bpin ligand, (126 mg, 0.66 mmol, 2.00 equiv) of cesium carbonate. The flask was then purged for 15 min with argon, after which 5 mL of dry 2-propanol was added via syringe. The flask was then shielded from light and allowed to stir at 55 degrees $^{o}$C for 24 hours. The flask was then cooled and concentrated on roto-evaporator. 5 X 5 mL portions of benzene were then added and the suspension was filtered over Celite. The light-yellow solution was then concentrated *in vacuo.* Analytically pure material was obtained by vapor diffusion of pentanes into a concentrated dichloromethane solution. (88 mg, 55 % yield). $^{1}$H NMR (500 MHz, Chloroform-*d*) δ 7.44 (d, *J* = 8.1 Hz, 1H), 7.34 (d, *J* = 7.3 Hz, 1H), 7.22 (t, *J* = 7.9 Hz, 4H), 7.10 (d, *J* = 8.1 Hz, 6H), 7.05 (d, *J* = 11.3 Hz, 7H), 6.98 – 6.94 (m, 3H), 2.40 (s, 6H), 2.22 (s, 12H), 1.84 (dd, *J* = 13.4, 7.3 Hz, 2H), 1.77 (dq, *J* = 14.3, 7.3, 6.6 Hz, 2H), 0.33 (t, *J* = 7.3 Hz, 6H). HRMS (FT-ICR, $[M+H]^{+}$) m/z calcd for $MH^{+}$ $C_{50}H_{51}N_{3}Au^{+}$ 890.37430 found 890.37431. Anal. Calcd for: $C_{50}H_{50}AuN_{3}$: C, (67.48); H, (5.66); N, (4.72). Found: C, (67.50); H, (5.90); N, (4.79).

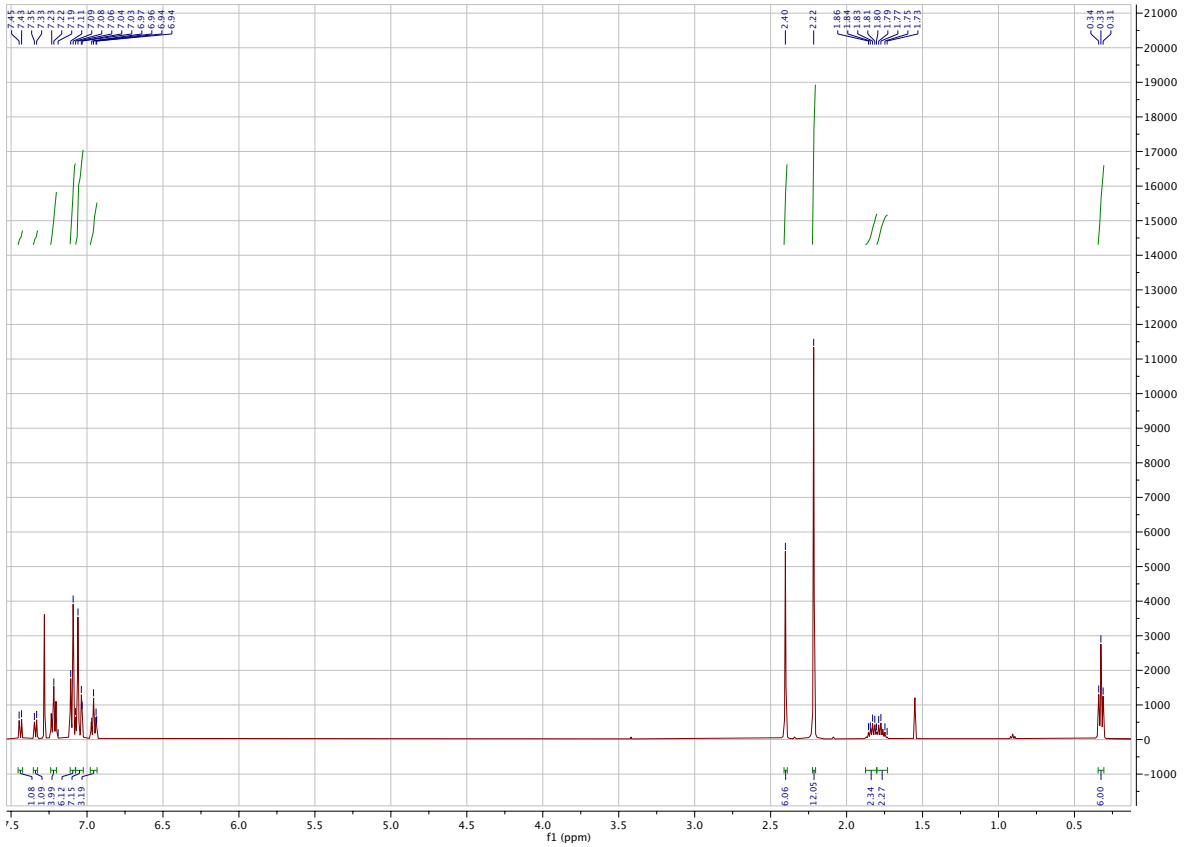

**Figure 5.8.** [1]H NMR Spectrum of **Au-DPA2**

**Au-ADPA0:**

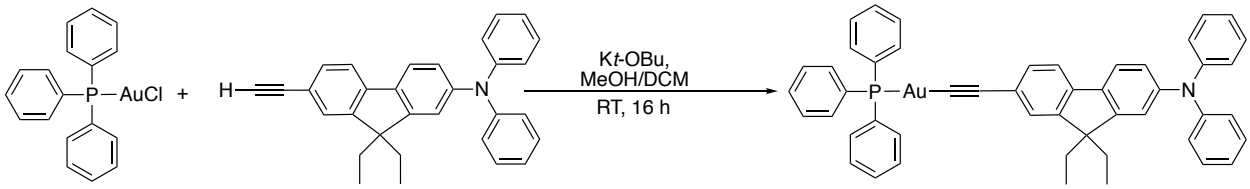


To 20 mL scintillation vial equipped with a stir bar was added (70 mg, 0.141 mmol, 1 equiv) of $PPh_3AuCl$ and 2 mL of MeOH. To a separate vial equipped with a stir bar was added (93 mg, 0.226 mmol, 1.60 equiv) of DPA alkyne ligand and (25 mg, 0.226 mmol, 1.60 equiv) of potassium tert-butoxide. 2 mL of DCM and 2 mL of MeOH were added and the solution was allowed to stir for 15 min. This solution was added via syringe to the suspension of $PPh_3AuCl$ creating a yellow/brown solution, which was allowed to stir for 16 h. Concentrated to dryness, added

dichloromethane and filtered over Celite. Analytically pure material was obtained by vapor diffusion of pentanes into a concentrated dichloromethane solution (73 mg, 60 % yield). $^{1}$H NMR $^{1}$H NMR (500 MHz, Chloroform-d) δ 7.59 – 7.44 (m, 19H), 7.25 – 7.22 (m, 4H), 7.12 – 7.06 (m, 5H), 7.00 (d, J = 6.1 Hz, 3H), 1.87 (m, J =7.0 Hz, 4H), 0.32 (t, J = 7.3 Hz, 6H). $^{31}$P NMR (202 MHz, $CDCl_3$) δ 42.41. HRMS (FT-ICR, $[M]^+$) m/z calcd for $M^+$ $C_{49}H_{41}NPAu^+$ 890.37430 found 890.37431. Anal. Calcd for: $C_{49}H_{41}AuNP$: C, (67.51); H, (4.74); N, (1.61). Found: C, (67.75); H, (4.96); N, (1.73).

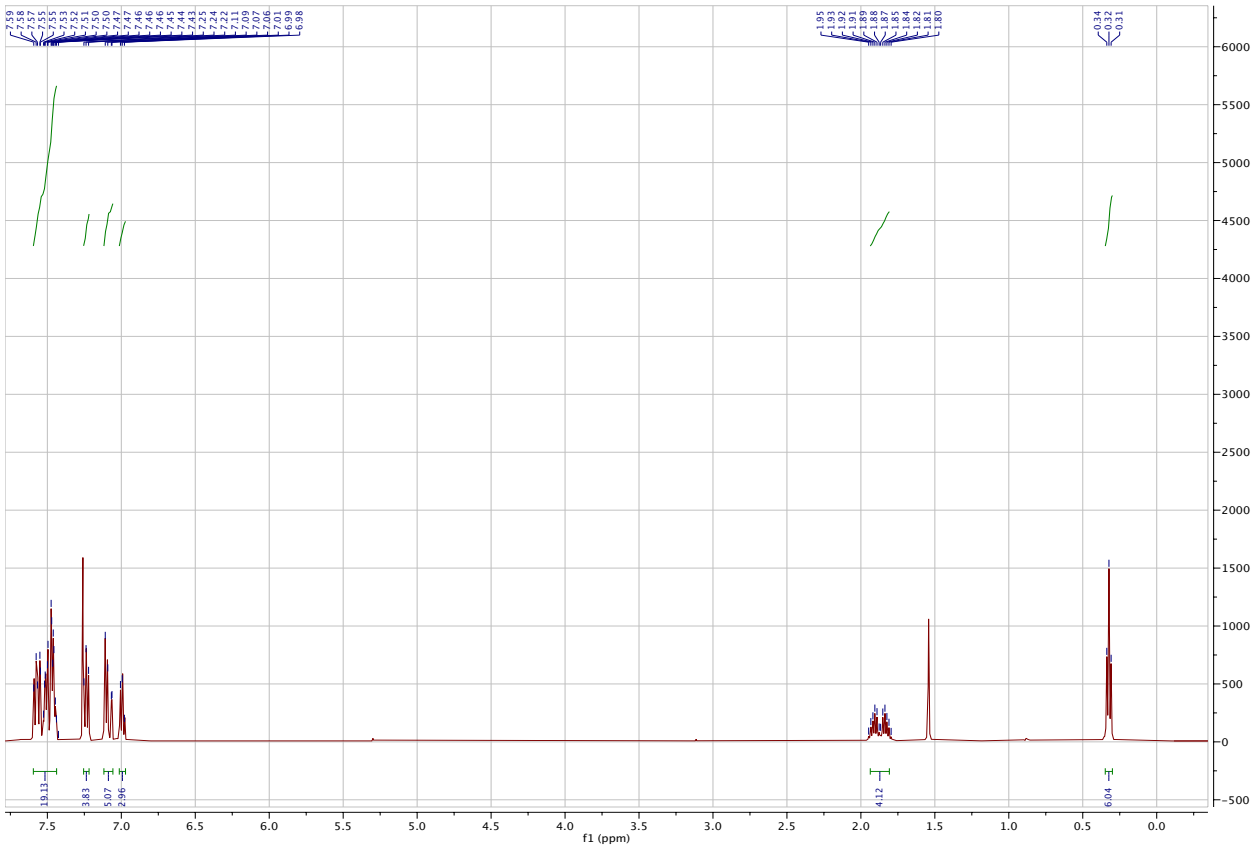


**Figure 5.9** $^{1}$H NMR Spectrum of **Au-ADPA0**

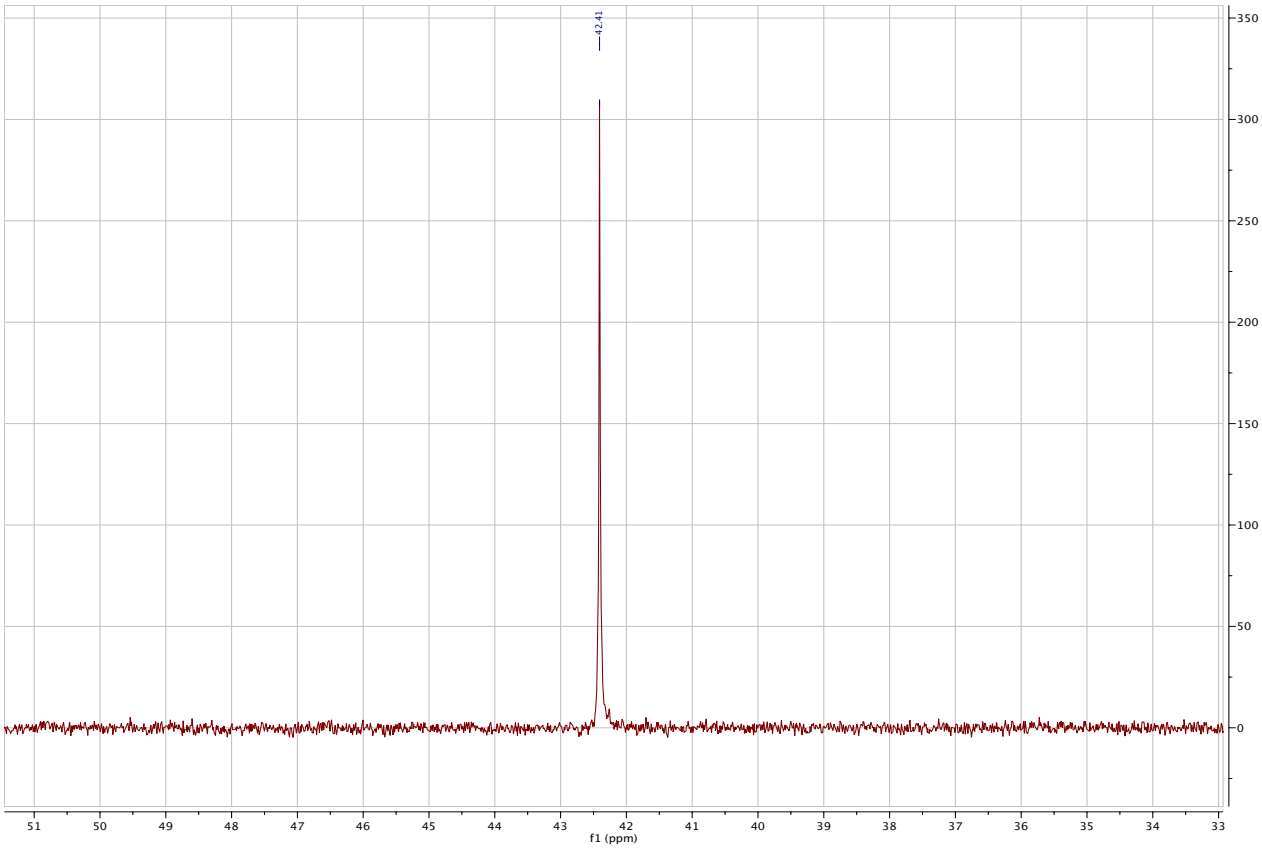


**Figure 5.10.** $^{31}P\{^{1}H\}$ NMR Spectrum of **Au-ADPA0**

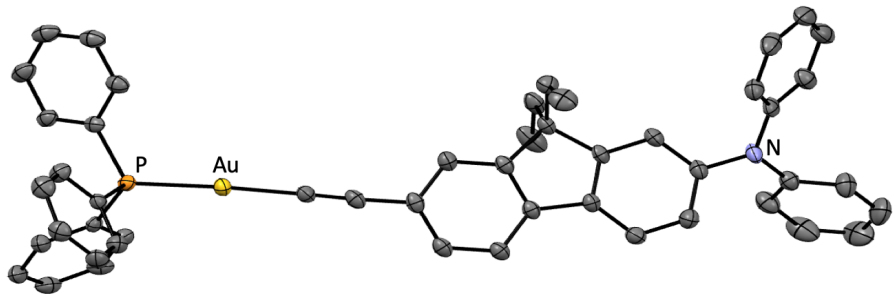


**Figure 5.11.** Thermal ellipsoid representation of **Au-ADPA0** (50% probability, 150 K).

Unlabeled atoms are carbon and hydrogen

**Au-ADPA2:**

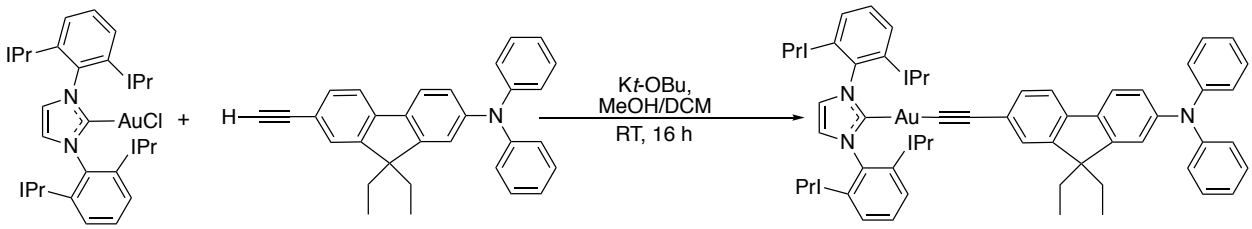


To 20 mL scintillation vial equipped with a stir bar was added (140 mg, 0.225 mmol, 1 equiv) of IPrAuCl and 2 mL of MeOH. To a separate vial equipped with a stir bar was added (141 mg, 0.372 mmol, 1.65 equiv) of DPA alkyne ligand and (43 mg, 0.380 mmol, 1.69 equiv) of potassium *tert*-butoxide. (2 mL of DCM and 2 mL of MeOH were added and the solution was allowed to stir for 15 min). This solution was added via syringe to the suspension of IPrAuCl creating a yellow solution, which was allowed to stir for 16 h. Concentrated to dryness, added dichloromethane and filtered over Celite. Analytically pure material was obtained by dissolving sample in 10 mL of Benzene and allowing slow evaporation to occur. (175 mg, 78 % yield). $^1$H NMR (500 MHz, Chloroform-*d*) δ 7.51 (t, *J* = 7.8 Hz, 2H), 7.46 (d, *J* = 8.2 Hz, 1H), 7.38 (d, *J* = 7.9 Hz, 1H), 7.32 (d, *J* = 7.8 Hz, 5H), 7.27 (s, 1H), 7.22 (t, *J* = 7.9 Hz, 4H), 7.14 (s, 2H), 7.08 (d, *J* = 7.8 Hz, 4H), 7.04 – 7.02 (m, 1H), 6.98 (t, *J* = 7.4 Hz, 3H), 2.64 (p, *J* = 6.9 Hz, 4H), 1.82 (ddd, *J* = 29.6, 13.6, 6.8 Hz, 4H), 1.41 (d, *J* = 6.9 Hz, 12H), 1.24 (d, *J* = 6.9 Hz, 12H), 0.23 (t, *J* = 7.3 Hz, 6H). HRMS (FT-ICR, $[M+H]^+$) m/z calcd for $MH^+$ $C_{58}H_{63}N_3Au^+$ 871.26367 found 871.26364. Anal. Calcd for: $C_{58}H_{62}AuN_3$: C, (69.79); H, (6.26); N, (4.21). Found: C, (70.03); H, (6.26); N, (4.33).


**Figure 5.12.** $^{1}$H NMR Spectrum of **Au-ADPA2**

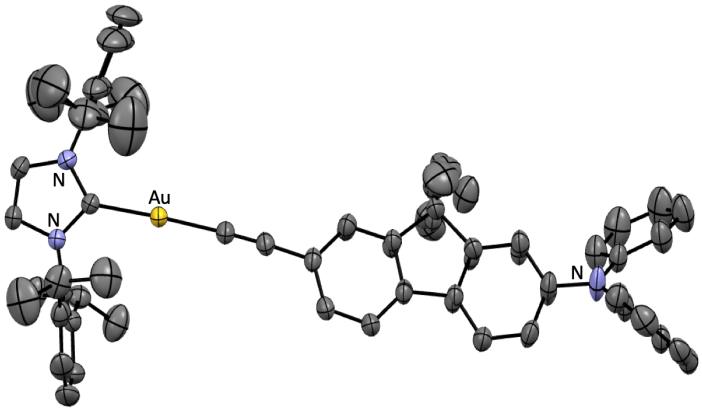


**Figure 5.13.** Thermal ellipsoid representation of **Au-ADPA2** (50% probability, 150 K). Unlabeled atoms are carbon and hydrogen.

**Au-ADPA3:**

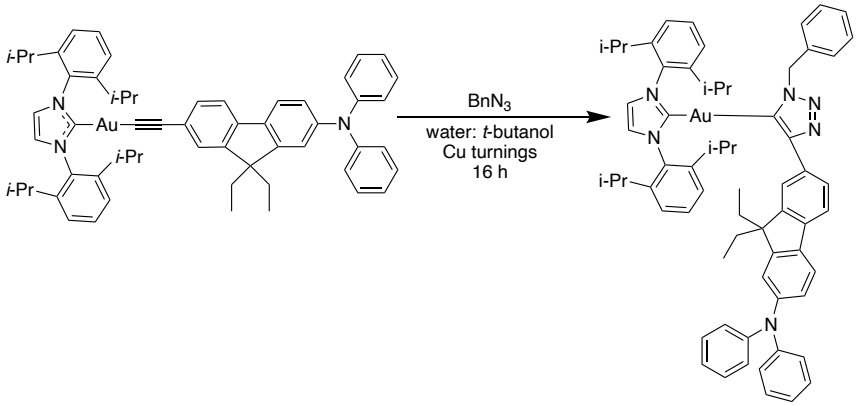


To a 25 mL flask equipped with a stir bar was added (32 mg, 0.0323 mmol) of **Au-ADPA3**. 5 mL of *tert*-butanol was then added along with 2.5 mL of DI water. (0.129 mL, 0.0903 mmol) of benzyl azide was then added dropwise and allowed to stir for 5 min. An excess of copper turnings was then added and the suspension was allowed to stir overnight. After 16 h, dichloromethane was added and an extraction was performed twice. These extracts were dried over magnesium sulfate and filtered. Concentrated *in vacuo* to yield an off-white solid which was washed with diethyl ether and dried. The compound was purified by slow diffusion of pentanes into a concentrated solution of $CDCl_3$ to yield white crystals (30 mg, 82 %). $^1$H NMR (500 MHz, Chloroform-*d*) δ 8.02 (s, 1H), 7.58 – 7.45 (m, 8H), 7.30 (d, *J* = 7.8 Hz, 3H), 7.22 (d, *J* = 12.3 Hz, 4H), 7.15 – 7.12 (m, 5H), 7.10 – 7.04 (m, 3H), 7.00 (d, *J* = 7.3 Hz, 2H), 6.94 (s, 1H), 6.77 – 6.73 (m, 2H), 5.03 (s, 2H), 2.62 (dt, *J* = 13.8, 6.9 Hz, 4H), 1.98 (d, *J* = 7.3 Hz, 2H), 1.83 (dd, *J* = 13.7, 7.2 Hz, 2H), 1.21 (dd, *J* = 6.7, 4.6 Hz, 24H), 0.30 (t, *J* = 7.3 Hz, 6H). HRMS (FT-ICR, $[M+H]^+$) m/z calcd for $MH^+$ $C_{65}H_{70}N_6Au^+$ 1131.53220 found 1131.53232. Anal. Calcd for: $C_{65}H_{69}AuN_6$: C, (69.01); H, (6.15); N, (7.43). Found: C, (68.97); H, (6.13); N, (7.60).

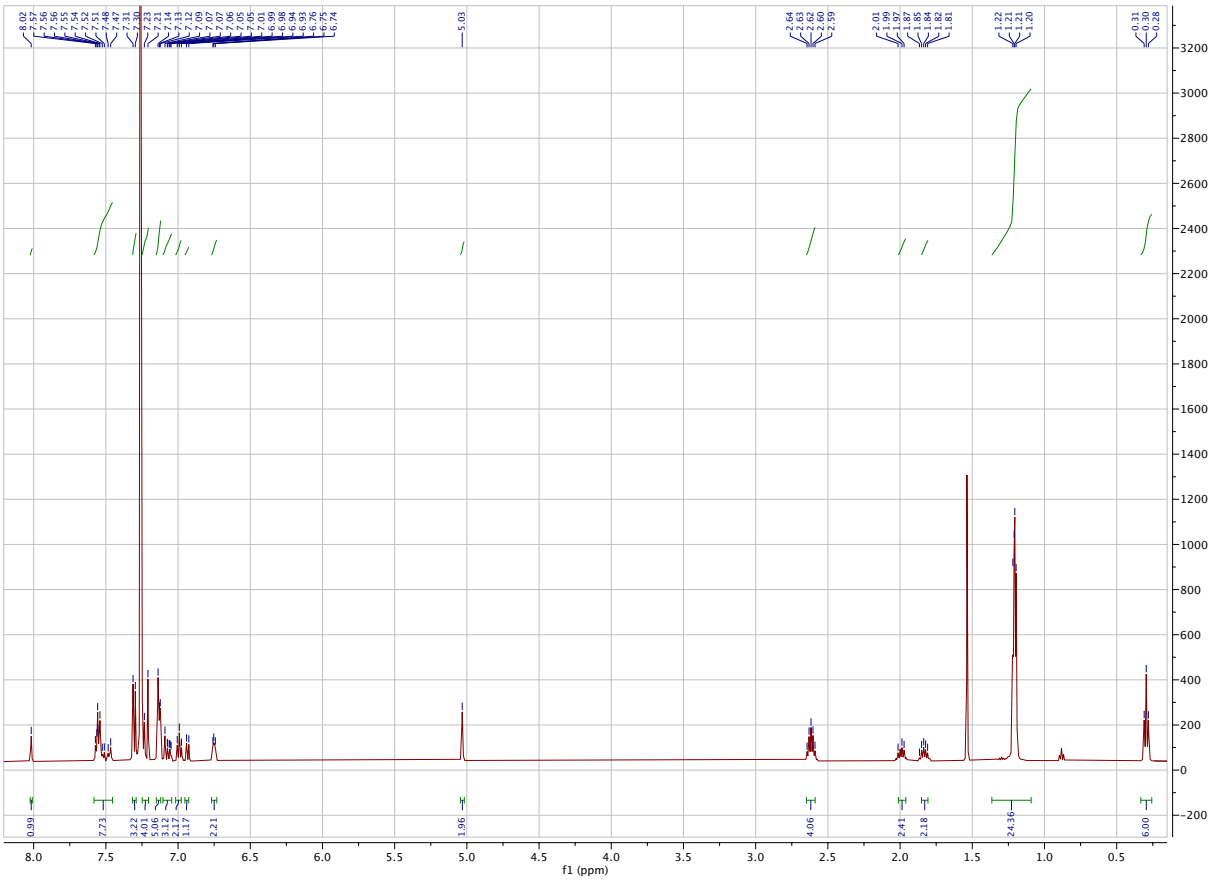


**Figure 5.14.** $^{1}$H NMR Spectrum of **Au-ADPA3**

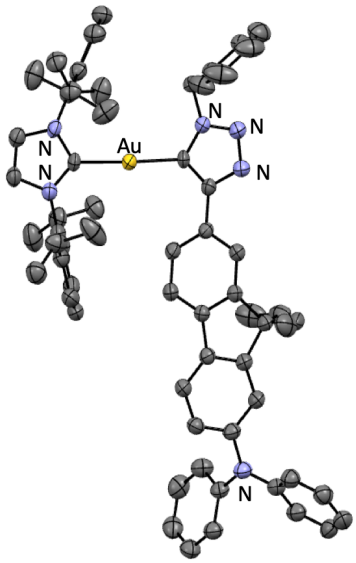


**Figure 5.15.** Thermal ellipsoid representation of **Au-ADPA2** (50% probability, 150 K). Unlabeled atoms are carbon and hydrogen.

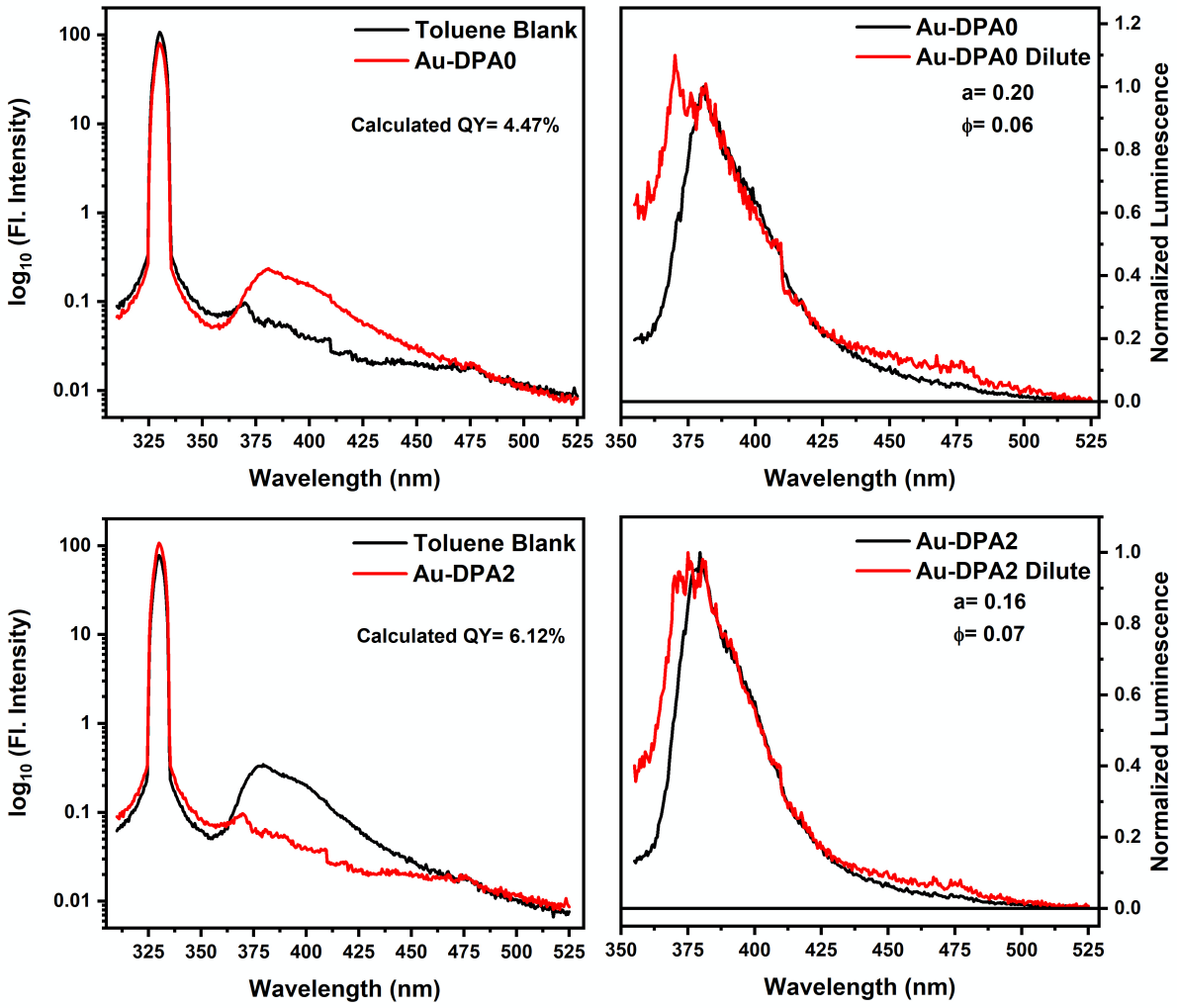
Toluene Blank
Au-DPA0
Calculated QY= 4.47%
log10 (Fl. Intensity)
Wavelength (nm)
Au-DPA0
Au-DPA0 Dilute
a= 0.20
ϕ= 0.06
Normalized Luminescence
Wavelength (nm)
Toluene Blank
Au-DPA2
Calculated QY= 6.12%
log10 (Fl. Intensity)
Wavelength (nm)
Au-DPA2
Au-DPA2 Dilute
a= 0.16
ϕ= 0.07
Normalized Luminescence
Wavelength (nm)

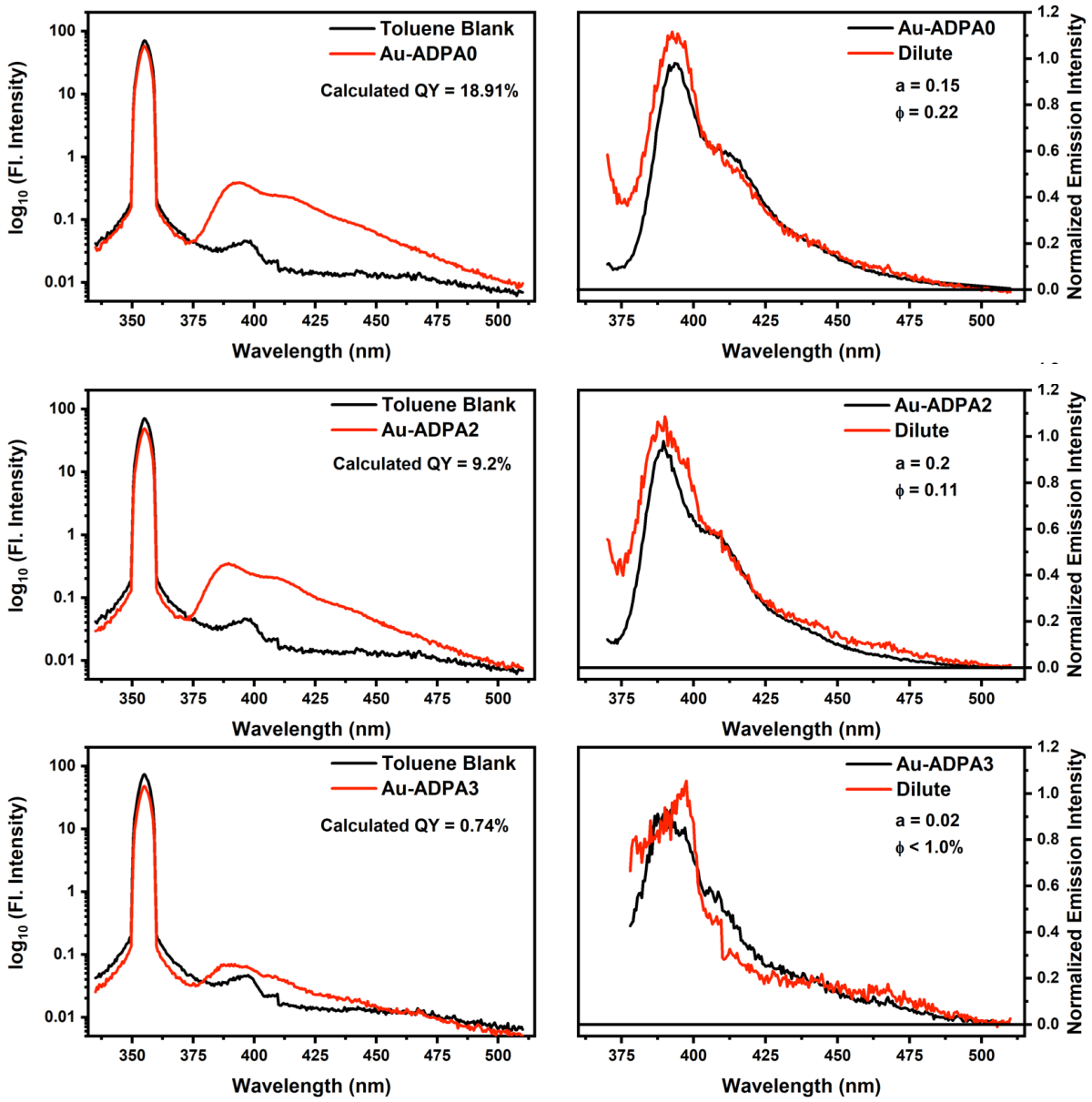


**Figure 5.16.** Raw Fluorescence Quantum Yields (Left) and Corrected Quantum Yields (Right) of **Au-DPA0** (1st), **Au-DPA2** (2nd), **Au-ADPA0** (3rd), **Au-ADPA2** (4$^{th}$), **Au-ADPA3 (5$^{th}$)** in Toluene. Quantum yields were collected in duplicate. The average of two trials is reported in Table 5.1.

**Single Crystal X-ray Structural Analysis**

Single crystals of the investigated compounds were coated with a trace of Fomblin oil and were transferred to the goniometer head of a Bruker Quest diffractometer with a fixed chi angle, a Mo Kα wavelength (λ = 0.71073 Å) $^{sealed}$ tube fine focus X-ray tube, single crystal curved graphite incident beam monochromator, a Photon100 CMOS area detector (**JJM_1_259_0m**, **jjm_1_288_2_0m_sq**), or onto a Bruker Quest diffractometer with kappa geometry, a Cu Kα wavelength (λ = 1.54178 Å) I-μ-S microsource X-ray tube, laterally graded multilayer (Goebel) mirror for monochromatization, a Photon2 CMOS area detector (**JJM_1_297_0m**, **JJM_1_204_0m**). Both instruments were equipped with an Oxford Cryosystems low temperature device and examination and data collection were performed at 150 K. Data were collected, reflections were indexed and processed, and the files scaled and corrected for absorption using APEX3 and SADABS[7]. The space groups were assigned and the structures were solved by direct methods using XPREP within the SHELXTL suite of programs[8] and refined by full matrix least squares against $F^2$ with all reflections using Shelxl2018[9] using the graphical interface Shelxle[10]. H atoms attached to carbon were positioned geometrically and constrained to ride on their parent atoms. C-H bond distances were constrained to 0.95 Å for aromatic C-H moieties, and to 1.00, 0.99 and 0.98 Å for aliphatic C-H, $CH_2$ and $CH_3$ moieties, respectively. Methyl $CH_3$ were allowed to rotate but not to tip to best fit the experimental electron density. $U_{iso}(H)$ values were set to a multiple of $U_{eq}(C)$ with 1.5 for $CH_3$, and 1.2 for C-H and $CH_2$ units, respectively. Additional data including description of disorder are given below for each structure, and in the tables below.

Complete crystallographic data, in CIF format, have been deposited with the Cambridge Crystallographic Data Centre. CCDC contains the supplementary crystallographic data for this paper. These data can be obtained free of charge from The Cambridge Crystallographic Data Centre via www.ccdc.cam.ac.uk/data_request/cif.

**JJM_1_297_0m**:

A chloroform molecule is disordered in a general position, and another chloroform molecule is disordered around an inversion center and also with a pentane molecule, also disordered around the inversion center.

The three disordered chloroform moieties were restrained to have similar geometries. The bond distances and angles of the pentane molecule were restrained to target values. $U^{ij}$ components of ADPs for disordered atoms closer to each other than 2.0 Å were restrained to be similar. Subject to these conditions the occupancy ratio for the chloroform disorder refined to 0.657(9) to 0.343(9), the occupancy rates for the chloroform / pentane disorder to two times 0.1453(13) for chloroform, and two times 0.3547(13) for pentane.

**JJM_1_259_0m**:

The triphenyl phosphine unit is disordered over two equally occupied moieties due to close contacts between neighboring molecules across inversion centers. The geometries of major and minor phenyl groups were restrained to be similar, and equivalent bond lengths around the P atoms were restrained to be similar. $U^{ij}$ components of ADPs for disordered atoms closer to each other than 2.0 Å were restrained to be similar.

**jjm_1_288_2_0m_sq**:

Crystals break up into multiple pieces upon cooling to 200 K or below. They desolvate slowly at room temperature. Data were thus collected at 250 K.

The two ethyl substituents and directly adjacent atoms are disordered induced by a different torsion angle of one of the ethyl groups. The two disordered moieties were restrained to have similar geometries. Atoms C30, C33, C34, C35 and C42 as well as C30, C33B, C34B, C35B and C42B were restrained to lie in a common plane. Atoms in close to identical positions were constrained to have identical ADPs (C33 and C33B, C34 and C34B, C35 and C35B, C36 and C36B, and C39 and C39B). $U^{ij}$ components of ADPs for disordered atoms closer to each other than 2.0 Å were restrained to be similar. Subject to these conditions the occupancy ratio refined to 0.575(5) to 0.425(5).

The structure contains additional independent solvent accessible voids of 410 $Å^3$ combined. No substantial electron density peaks were found in the solvent accessible voids (less than one electron per cubic Angstrom) and the residual electron density peaks are not arranged in an interpretable pattern. The structure factors were instead augmented via reverse Fourier transform methods using the SQUEEZE routine (P. van der Sluis & A.L. Spek (1990). Acta Cryst. A46, 194-201) as implemented in the program Platon. The resultant FAB file containing the structure factor contribution from the electron content of the void space was used in together with the original hkl file in the further refinement. (The FAB file with details of the Squeeze results is appended to the cif file). The Squeeze procedure corrected for 37 electrons within the solvent accessible voids.

**Table 5.4.** Crystallography experimental details

| | JJM_1_297_0m | JJM_1_204_0m |
|---|---|---|

| Crystal data | | |
|---|---|---|
| Chemical formula | $C_{65}H_{69}AuN_6 \cdot 0.355(C_5H_{12}) \cdot 1.145(CHCl_3)$ | $C_{47}H_{41}AuNP$ |
| $M_r$ | 1293.53 | 847.74 |
| Crystal system, space group | Triclinic, $P\bar{1}$ | Triclinic, $P\bar{1}$ |
| Temperature (K) | 150 | 150 |
| $a$, $b$, $c$ (Å) | 11.4227 (4), 14.9197 (6), 19.4470 (7) | 12.1299 (18), 12.4285 (19), 13.416 (2) |
| α, β, γ (°) | 69.9202 (11), 88.3028 (11), 84.9331 (12) | 105.454 (6), 90.588 (6), 107.654 (6) |
| $V$ (Å$^3$) | 3100.6 (2) | 1848.4 (5) |
| $Z$ | 2 | 2 |
| $F$(000) | 1323 | 848 |
| $D_x$ (Mg m$^{-3}$) | 1.386 | 1.523 |
| Radiation type | Cu $K\alpha$ | Cu $K\alpha$ |
| No. of reflections for cell measurement | 9754 | 9060 |
| θ range (°) for cell measurement | 3.2–80.4 | 3.8–72.2 |
| μ (mm$^{-1}$) | 6.16 | 8.14 |
| Crystal shape | Block | Plate |
| Colour | Colourless | Yellow |
| Crystal size (mm) | 0.21 × 0.17 × 0.14 | 0.42 × 0.35 × 0.15 |
| | | |
| Data collection | | |
| Diffractometer | Bruker AXS D8 Quest CMOS diffractometer with PhotonII charge-integrating pixel array detector (CPAD) | Bruker AXS D8 Quest CMOS diffractometer with PhotonII charge-integrating pixel array detector (CPAD) |
| Radiation source | I-mu-S microsource X-ray tube | I-mu-S microsource X-ray tube |
| Monochromator | Laterally graded multilayer (Goebel) mirror | Laterally graded multilayer (Goebel) mirror |
| Detector resolution (pixels mm$^{-1}$) | 7.4074 | 7.4074 |

| | | |
|---|---|---|
| Scan method | ω and phi scans | ω and phi scans |
| Absorption correction | Multi-scan (*SADABS* 2016/2, Krause *et al.*, 2015) | Numerical (SADABS 2016/2, Krause et al., 2015) |
| $T_{min}$, $T_{max}$ | 0.049, 0.179 | 0.052, 0.598 |
| No. of measured, independent and observed [$I > 2\sigma(I)$] reflections | 49041, 12866, 12319 | 62750, 8005, 7222 |
| $R_{int}$ | 0.038 | 0.139 |
| θ values (°) | $\theta_{max}$ = 81.0, $\theta_{min}$ = 2.4 | $\theta_{max}$ = 81.2, $\theta_{min}$ = 3.4 |
| $(\sin \theta/\lambda)_{max}$ (Å$^{-1}$) | 0.641 | 0.641 |
| Range of *h*, *k*, *l* | $h$ = -14→14, $k$ = -18→18, $l$ = -24→24 | $h$ = -15→15, $k$ = -15→15, $l$ = -17→17 |
| | | |
| Refinement | | |
| Refinement on | $F^2$ | $F^2$ |
| $R[F^2 > 2\sigma(F^2)]$, $wR(F^2)$, $S$ | 0.032, 0.081, 1.14 | 0.054, 0.146, 1.06 |
| No. of reflections | 12866 | 8005 |
| No. of parameters | 817 | 453 |
| No. of restraints | 212 | 0 |
| H-atom treatment | H-atom parameters constrained | H-atom parameters constrained |
| Weighting scheme | $w = 1/[\sigma^2(F_o^2) + (0.0191P)^2 + 5.0278P]$ where $P = (F_o^2 + 2F_c^2)/3$ | $w = 1/[\sigma^2(F_o^2) + (0.0771P)^2 + 3.0188P]$ where $P = (F_o^2 + 2F_c^2)/3$ |
| $(\Delta/\sigma)_{max}$ | 0.004 | 0.001 |
| $\Delta\rho_{max}$, $\Delta\rho_{min}$ (e Å$^{-3}$) | 1.10, -0.91 | 2.41, -1.61 |

Computer programs: Apex3 v2017.3-0 (Bruker, 2017), *SAINT* V8.38A (Bruker, 2016), *SHELXS97* (Sheldrick, 2008), *SHELXL2018*/3 (Sheldrick, 2015, 2018), SHELXLE Rev946 (Hübschle *et al.*, 2011).

| | JJM_1_259_0m | jjm_1_288_2_0m_sq |
|---|---|---|
| Crystal data | | |
| Chemical formula | $C_{49}H_{41}AuNP$ | $C_{58}H_{62}AuN_3$ |

| | | |
|---|---|---|
| $M_r$ | 871.76 | 998.07 |
| Crystal system, space group | Monoclinic, $P2_1/n$ | Triclinic, $P\bar{1}$ |
| Temperature (K) | 150 | 250 |
| $a$, $b$, $c$ (Å) | 8.8631 (7), 48.080 (4), 9.2630 (7) | 9.2778 (10), 16.4270 (15), 18.834 (2) |
| β (°) | 92.1118 (17) | 85.154 (4), 86.127 (4), 76.171 (3) |
| $V$ (Å$^3$) | 3944.6 (5) | 2773.9 (5) |
| $Z$ | 4 | 2 |
| $F$(000) | 1744 | 1020 |
| $D_x$ (Mg m$^{-3}$) | 1.468 | 1.195 |
| Radiation type | Mo $K\alpha$ | Mo $K\alpha$ |
| No. of reflections for cell measurement | 9995 | 9589 |
| θ range (°) for cell measurement | 2.3–30.5 | 2.3–33.1 |
| μ (mm$^{-1}$) | 3.81 | 2.69 |
| Crystal shape | Plate | Plate |
| Colour | Yellow | Colourless |
| Crystal size (mm) | 0.33 × 0.20 × 0.03 | 0.35 × 0.25 × 0.09 |
| | | |
| Data collection | | |
| Diffractometer | Bruker AXS D8 Quest CMOS diffractometer | Bruker AXS D8 Quest CMOS diffractometer |
| Radiation source | fine focus sealed tube X-ray source | fine focus sealed tube X-ray source |
| Monochromator | Triumph curved graphite crystal | Triumph curved graphite crystal |
| Detector resolution (pixels mm$^{-1}$) | 10.4167 | 10.4167 |
| Scan method | ω and phi scans | ω and phi scans |
| Absorption correction | Multi-scan (*SADABS* 2016/2, Krause *et al.*, 2015) | Multi-scan (*SADABS* 2016/2, Krause *et al.*, 2015) |
| $T_{min}$, $T_{max}$ | 0.549, 0.746 | 0.504, 0.747 |
| No. of measured, independent and observed [$I > 2\sigma(I)$] | 26077, 11844, 9942 | 105489, 21123, 17341 |

| | | |
|---|---|---|
| reflections | | |
| $R_{int}$ | 0.026 | 0.046 |
| θ values (°) | $\theta_{max}$ = 30.5, $\theta_{min}$ = 2.2 | $\theta_{max}$ = 33.3, $\theta_{min}$ = 2.3 |
| $(\sin \theta/\lambda)_{max}$ (Å$^{-1}$) | 0.715 | 0.772 |
| Range of *h*, *k*, *l* | *h* = -12→11, *k* = -52→68, *l* = -12→13 | *h* = -14→14, *k* = -25→24, *l* = -29→28 |
| | | |
| Refinement | | |
| Refinement on | $F^2$ | $F^2$ |
| $R[F^2 > 2\sigma(F^2)]$, $wR(F^2)$, $S$ | 0.036, 0.066, 1.14 | 0.029, 0.072, 1.03 |
| No. of reflections | 11844 | 21123 |
| No. of parameters | 636 | 650 |
| No. of restraints | 616 | 396 |
| H-atom treatment | H-atom parameters constrained | H-atom parameters constrained |
| Weighting scheme | $w = 1/[\sigma^2(F_o^2) + (0.0025P)^2 + 6.7128P]$ where $P = (F_o^2 + 2F_c^2)/3$ | $w = 1/[\sigma^2(F_o^2) + (0.0352P)^2 + 0.517P]$ where $P = (F_o^2 + 2F_c^2)/3$ |
| $(\Delta/\sigma)_{max}$ | 0.001 | 0.002 |
| $\Delta\rho_{max}$, $\Delta\rho_{min}$ (e Å$^{-3}$) | 1.62, -1.21 | 2.50, -1.54 |

Computer programs: Apex3 v2017.3-0 (Bruker, 2017), *SAINT* V8.38A (Bruker, 2016), *SHELXS97* (Sheldrick, 2008), *SHELXL2018*/3 (Sheldrick, 2015, 2018), SHELXLE Rev946 (Hübschle *et al.*, 2011).

**References.**


1 J. J. Mihaly, D. J. Stewart, T. A. Grusenmeyer, A. T. Phillips, J. E. Haley, M. Zeller and T. G. Gray, Photophysical properties of organogold(i) complexes bearing a benzothiazole-2,7-fluorenyl moiety: Selection of ancillary ligand influences white light emission, *Dalt. Trans.*, 2019, **48**, 15917–15927.

2 J. J. Mihaly, A. T. Phillips, J. T. Malloy, Z. M. Marsh, M. Zeller, J. E. Haley, K. De La Harpe, T. A. Grusenmeyer and T. G. Gray, Synthesis and Photophysical Properties of Laterally Asymmetric Digold(I) Alkynyls and Triazolyl: Ancillary Ligand and Organic Functionality Dictate Excited-State Dynamics, *Organometallics*, 2020, **39**, 489–494.

3 J. J. Mihaly, A. T. Phillips, D. J. Stewart, Z. M. Marsh, C. L. McCleese, J. E. Haley, M. Zeller, T. A. Grusenmeyer and T. G. Gray, Synthesis and photophysics of gold( i ) alkynyls bearing a benzothiazole-2,7-fluorenyl moiety: a comparative study analyzing influence of ancillary ligand, bridging moiety, and number of metal centers on photophysical properties , *Phys. Chem. Chem. Phys.*, 2020, 11915–11927.

4 D. V Partyka, T. J. Robilotto, M. Zeller, A. D. Hunter and T. G. Gray, Dialkylbiarylphosphine Complexes of Gold(I) Halides. Gold−Aryl π-Interactions in the Solid State, *Organometallics*, 2008, **27**, 28–32.

5 J. E. Rogers, J. E. Slagle, D. M. Krein, A. R. Burke, B. C. Hall, A. Fratini, D. G. McLean, P. A. Fleitz, T. M. Cooper, M. Drobizhev, N. S. Makarov, A. Rebane, K. Y. Kim, R. Farley and K. S. Schanze, Platinum acetylide two-photon chromophores, *Inorg. Chem.*, 2007, **46**, 6483–6494.

6 J. E. Heckler, N. Deligonul, A. L. Rheingold and T. G. Gray, Gold(i) triazolyls: Organometallic synthesis in air and aqueous media, *Chem. Commun.*, 2013, **49**, 5990–5992.;L. Gao, D. V. Partyka, J. B. Updegraff, N. Deligonul and T. G. Gray, Synthesis, structures, and excited-state geometries of alkynylgold(I) complexes, *Eur. J. Inorg. Chem.*, 2009, **2009**, 2711–2719.

7 G. M. Sheldrick, A short history of SHELX, *Acta Crystallogr. Sect. A*, 2008, **64**, 112–122.

8 G. M. Sheldrick, Crystal structure refinement with SHELXL, *Acta Crystallogr. Sect. C*, 2015, **71**, 3–8.

9 C. B. Hübschle, G. M. Sheldrick and B. Dittrich, ShelXle: a Qt graphical user interface for SHELXL, *J. Appl. Crystallogr.*, 2011, **44**, 1281–1284.

10 L. Krause, R. Herbst-Irmer, G. M. Sheldrick and D. Stalke, Comparison of silver and molybdenum microfocus X-ray sources for single-crystal structure determination, *J. Appl. Crystallogr.*, 2015, **48**, 3–10.

## Chapter 6: Synthesis and Photophysics for a Series of Gold(III) complexes bearing either a Diphenylamino or Benzothiazole Fluorenyl Moiety.

After synthesizing and photophysically analyzing a collection of gold(I) compounds with variation in ancillary ligand, gold-chromphore linkage, number of metal centers, as well as capping moiety (on the fluorene), the next logical step was to expand to gold(III) chemistry. The end goal was to synthesize molecules where we can examine the affect gold-chromophore linkage as well as the nature of the capping moiety have on photophysical properties.

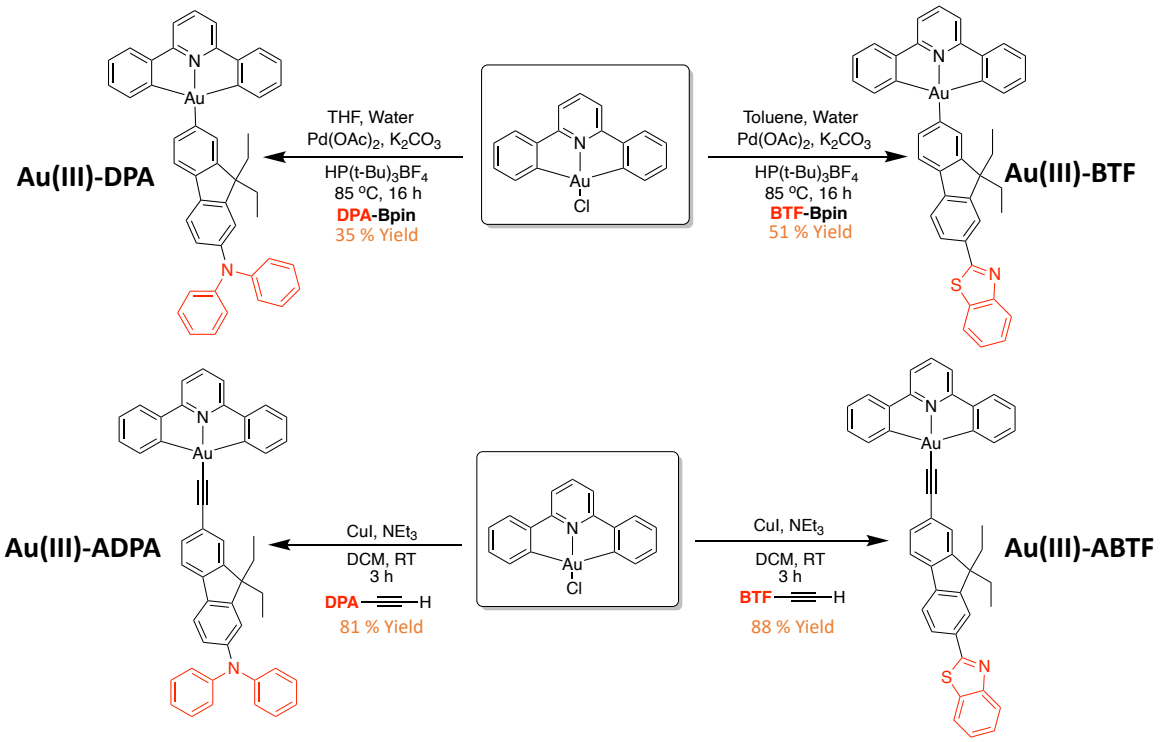


**Figure 6.1.** Synthesis of **Au(III)-BTF**, **Au(III)-ABTF**, **Au(III)-DPA**, **Au(III)-ADPA**.

Four new gold(III) complexes were synthesized by methods reported by Yam and co-workers.[1,2] The two gold(III) aryl complexes; **Au(III)-DPA** and **Au(III)-BTF**, were isolated in a palladium catalyzed coupling reaction between gold(III) chloride[3] and pinacolatoboron ester in 35 and 51 percent isolated yields, respectively (Figure 6.1).[1] The two new alkynyl complexes; **Au-ABTF** and **Au-ADPA**, were obtained in a copper assisted deprotonation by triethylamine with

subsequent nucleophilic attack of the gold(III) chloride starting material to yield the new complexes in 88 and 81 percent isolated yields, respectively (Figure 6.1).[2]

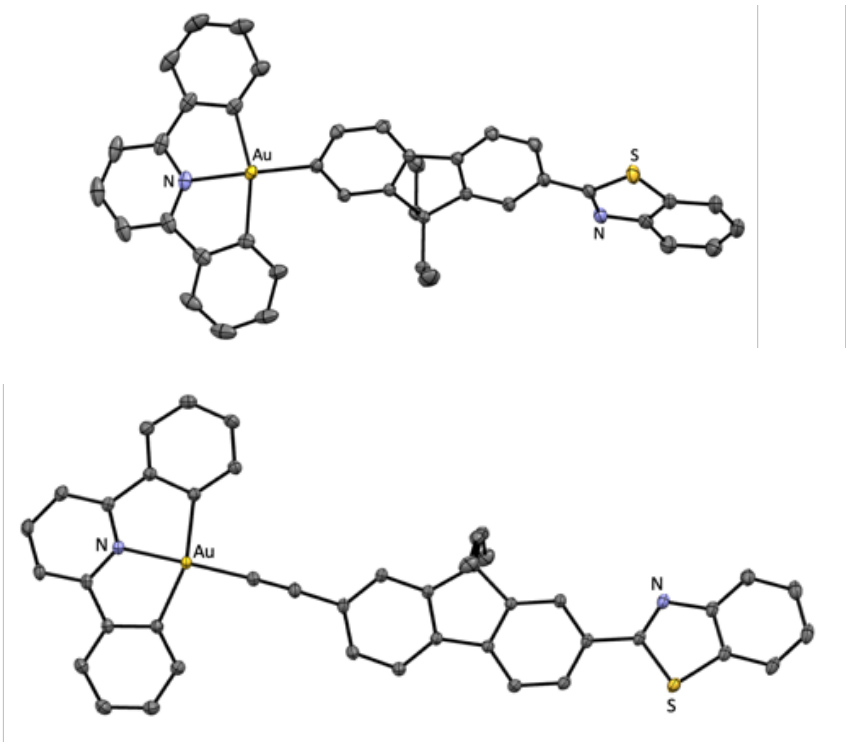


**Figure 6.2.** Crystal structures of **Au(III)-BTF** (top), **Au(III)-ABTF** (bottom). (50% probability level, 150 K). Hydrogen atoms are omitted for clarity. A partial atom labeling scheme appears; unlabeled atoms are carbon.

Thermal ellipsoid representations of all three complexes appear in Figure 6.2. In both structures, gold is four-coordinate and square planar; packing diagrams show no evidence of aurophilic interactions or π-π stacking. **Au(III)-BTF** has an Au-N bond length 2.025(1) Å and an Au-$C_{aryl}$ length of 2.005(2) Å. **Au(III)-ABTF** has an Au-N bond length of 1.997(1) Å and an Au-$C_{alkyne}$ length of 1.959(1) Å.

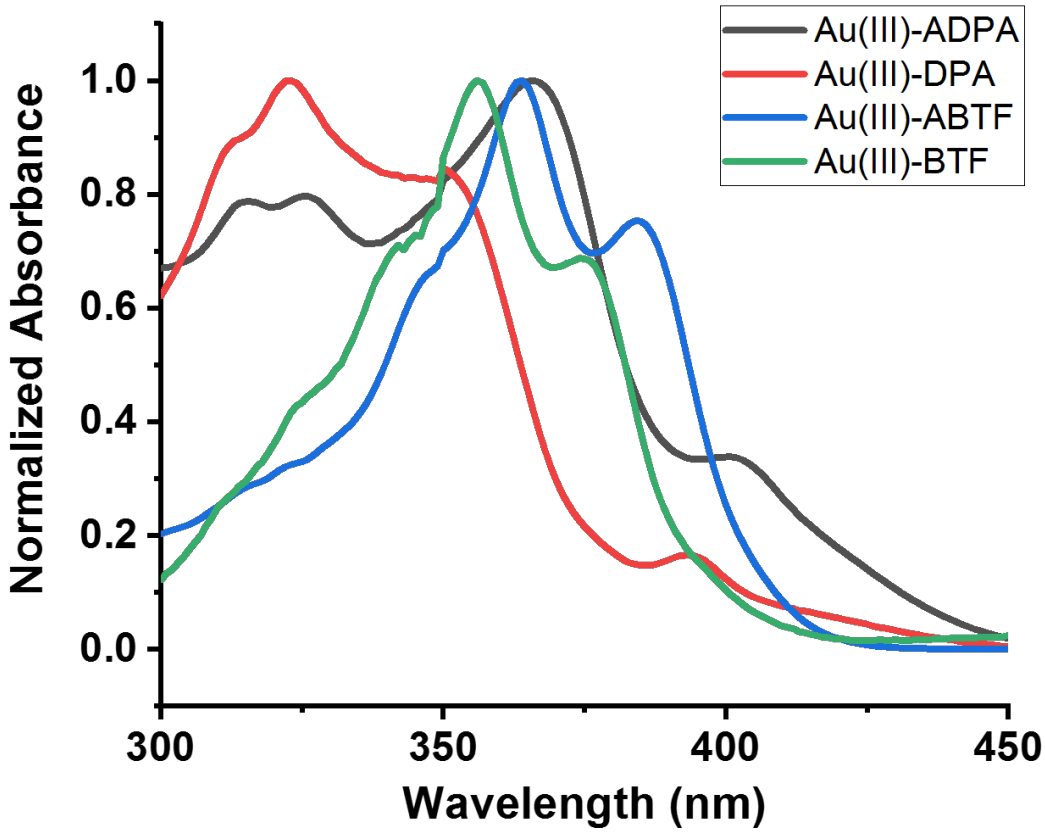


**Figure 6.3.** Ground state absortpion spectra of **Au(III)-BTF**, **Au(III)-ABTF**, **Au(III)-DPA**, **Au(III)-ADPA** in toluene at room temparature.

Normalized ground-state absorption spectra in toluene are show in Figure 6.3. **Au(III)-BTF** and **Au(III)-ABTF** are both structured and are similar in band-shape. The aryl complex; **Au(III)-BTF** has a maximum at 356 nm along with a distinct low energy shoulder at 375 nm and a less prononunced high energy shoulder. **Au(III)-ABTF** has a maximum at 364 nm and a distinct low energy shoulder at 385 nm with a high energy shoulder. These data suggest that changing the gold-chromphore linkage from and aryl to an alkynyl leads to a bathochromic shift in the absorption spectra. **Au(III)-DPA**, which contains an aryl linkage, displays a structured absorption spectrum with a maximum at 322 nm as well as a high energy shoulder at 312 nm and two lower energy shoulders at 351 and 393 nm. **Au(III)-ADPA**, which contains an alkynyl linkage, displays

an absorption spectrum that differs from the that of aryl complex **Au(III)-DPA**. **Au(III)-ADPA** exhibits a maximum at 366 nm with two low energy peaks at 315 and 326 nm, and a high energy peak at 402 nm. Interstingly, the BTF complexes have absorption spectra that are similar in band shape, but spectra of the DPA complexes differ. Comparing all four spectra, the trend recurs that the alkynyl complexes are red-shifted in comparision to aryls.

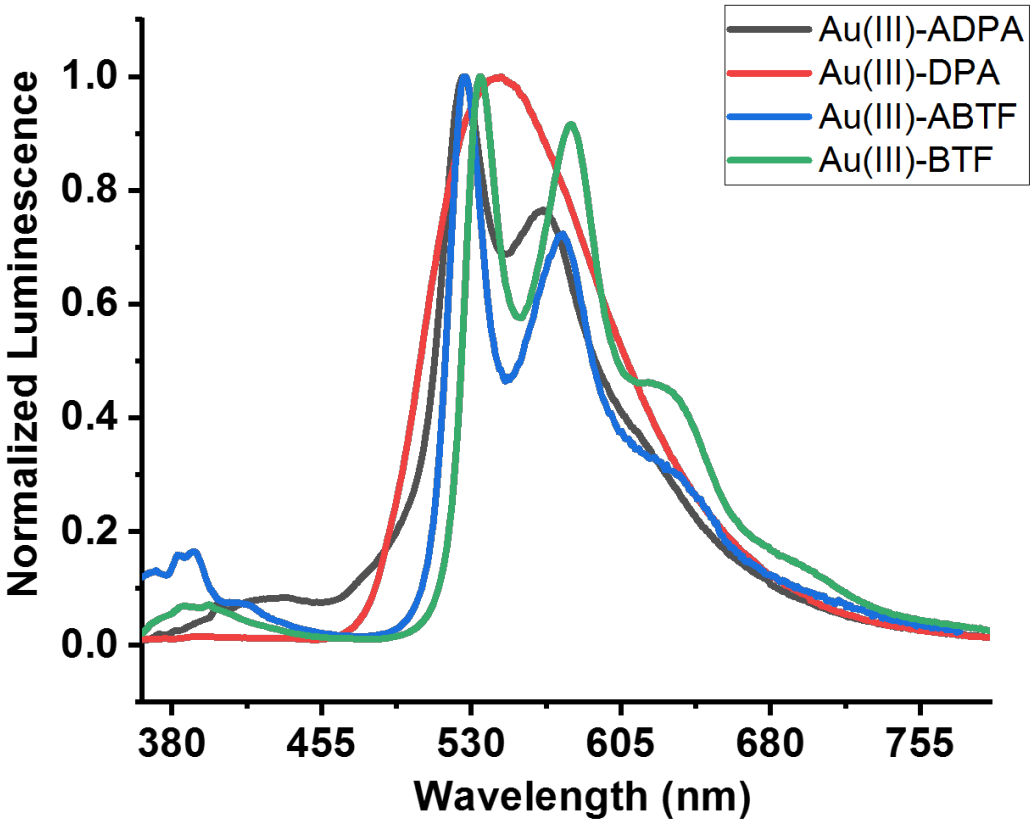


**Figure 6.4.** Luminescene spectra of **Au(III)-BTF**, **Au(III)-ABTF**, **Au(III)-DPA**, **Au(III)-ADPA** in degassed toluene at room temperature.

Luminescence spectra of of **Au(III)-BTF**, **Au(III)-ABTF**, **Au(III)-DPA**, **Au(III)-ADPA** in bubble-degassed toluene solutions at room temperature appear in Figure 6.4. All four complexes are characterized by almost strictly phosphorescence, with minor fluorescence. **Au(III)-BTF** and **Au(III)-ABTF** both exhibit highly structured phosphorescence that are similar in profile. **Au(III)-**

**BTF** display two distinct peaks 534 and 580 nm with a small shoulder at 634 nm; **Au(III)-ABTF** exhibits two distinct peaks at 527 and 576 nm with a small shoulder at 633 nm. The emission spectra of **Au(III)-ADPA** is also structured with two prominent peaks at 526 and 566 nm. Taken together, the alkynyl complexes are red-shifted in comparision to the aryl complexes. Interestingly, **Au(III)-DPA** exhibits structureless emission with a maximum at 545 nm. It is believed that **Au(III)-ADPA**, **Au(III)-BTF**, and **Au(III)-ABTF** exhibit structured emission from an intraligand transition of the cyclometallate, and that the origin of emission differs in **Au(III)-DPA** and is LLCT (ligand-to-ligand charge transfer) in nature.[4-14] However, a deeper understanding of the photophysical properties of these complexes as well as computational support is necessary. These studies are ongoing in the Gray laboratory.

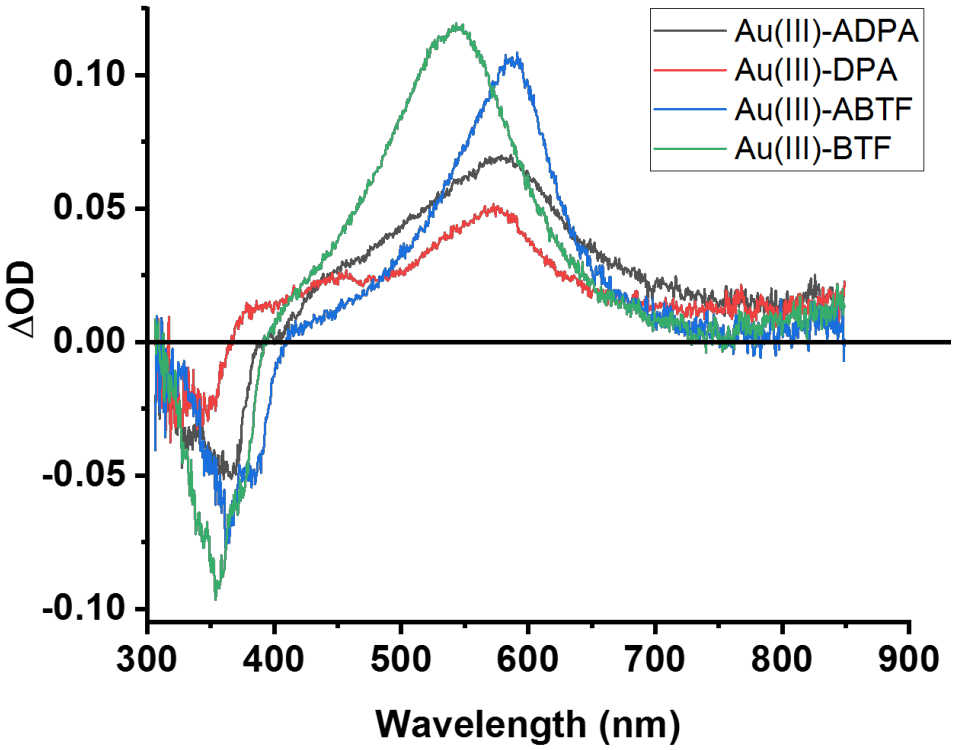

**Figure 6.5.** Nanosecond transient absoprtion spectra of **Au(III)-BTF**, **Au(III)-ABTF**, **Au(III)-DPA, Au(III)-ADPA** in degassed toluene at room temperature in deltaOD. All samples were excited at 355 nm. The spectra were collected 100 ns after the laser pulse.

Nanosecond transient absorption spectra of all four complexes appear in Figure 6.5. All four complexes are characterized by a bleach of the ground state, and positive absorption throughout the visible region. The two BTF complexes display stronger excited-state absoprtion compared to the two DPA complexes. Energy trends parallel those of the ground state absorption spectra: **Au(III)-BTF** displays a maximum at 544 nm, while **Au(III)-ABTF** peaks at 587 nm. **Au(III)-DPA** exhibits a maximum at 573 nm and **Au(III)-ADPA** exhibits a maximum at 580 nm. Taken together, the alkynyl complexes are red-shifted in comparision to the aryl complexes.

**Future Directions.**

Further investigation into the photophysical properties of these four new gold(III) complexes is necessary. These experiments include fluorescence and phosphorescence quantum yields and lifetimes as well as triplet-state quantum yields. This will allow for calculation of excited-state rate constants and insight into the excited-state dynamics of these complexes. Computational support as well as solvent dependent studies will lead to a more complete understanding as to why **Au(III)-DPA** produces structureless emission compared to the other three complexes. Lastly, publishing a study comparing the effect of gold-chromophore linkage on gold(III) complexes; which to my knowledge has never reported.

**Experimental Details.**

**General Considerations.** All experimental procedures were carried out under an inert atmosphere of argon using standard Schlenk line techniques. Microanalyses (C, H, and N) were undertaken by Atlantic Microlab. Mass spectrometry was performed at the University of Cincinnati Mass Spectrometry facility. Diphenylpyridine gold(III) chloride was synthesized via a previously described procedure.[3] Ligand syntheses have been reported previously in this dissertation.

Dry dichloromethane, tetrahydrofuran, toluene, pentane, and diethyl ether, tri-tert-butyl phosphonium tetrafluoroborate, and potassium carbonate were purchased from Sigma Aldrich and used as received. Mercury(II) acetate and triethyl amine were purchased from Alfa Aesar. Potassium tetrachloroaurate hydrate and palladium(II) acetate were purchased from Strem. 2,6-diphenylpyridine was purchased from TCI. Copper(I) Iodide was purchased from Honeywell. $^1$H NMR experiments were performed on a Bruker-500 Ascend Advanced III HD NMR spectrometer operating at 500.24 MHz. $^1$H chemical shifts are reported in parts per million ($\delta$) with integration and multiplicity (s = singlet, d = doublet, t = triplet, q = quartet, dd = doublet of doublets, dt = doublet of triplets, td = triplet of doublets, ddd = doublet of doublet of doublets, and m = multiplet), measured from tetramethylsilane (0 ppm) and are referenced to residual solvent in $CDCl_3$ (7.26 ppm).

**Instrumentation.** Detailed instrument components and setup has been reported in the literature prior to this summary.[15-17]

**Synthesis, NMR, Mass Spectrometry, and Elemental Analysis**

**Au(III)-BTF:**

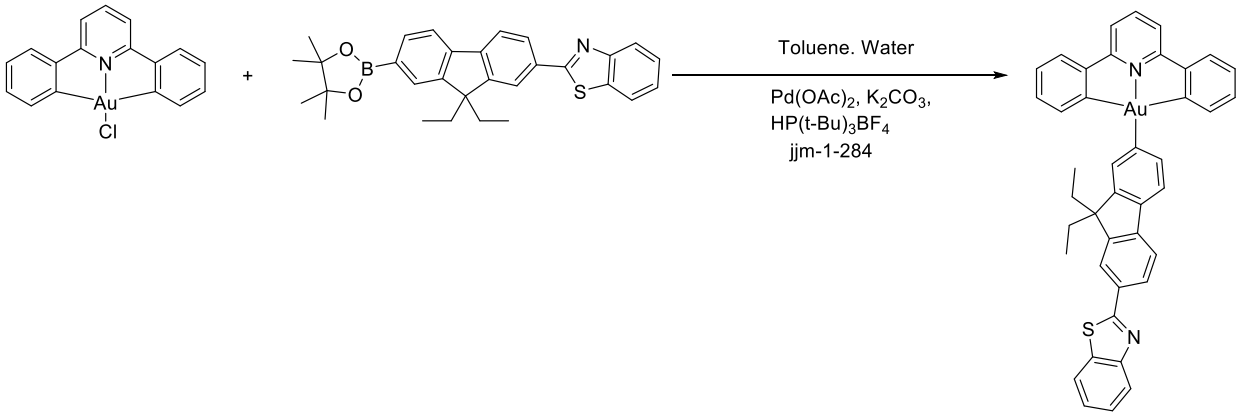


A flask containing [Au(C^N^C)Cl] (53.1 mg, 0.115 mmol), $K_2CO_3$ (550 mg, 0.43 mmol), $Pd(OAc)_2$ (7.2 mg, 0.023 mmol), $[HP(^tBu)_3]BF_4$ (13.3 mg, 0.046 mmol) and boronic acid (110.73 mg, 0.230 mmol) were added into degassed toluene and $H_2O$ (4 : 1, v/v) and the mixture was stirred at 80 °C for 12 hours under a nitrogen atmosphere. After removing the solvent, the crude product was purified by column chromatography on silica gel using hexane–dichloromethane (7 : 3, v/v) as the eluent. Subsequent crystallization by diffusion of diethyl ether vapor into a concentrated dichloromethane solution gave the product as a yellow solid. (46 mg, 51 % yield) $^1$H NMR (500 MHz, Chloroform-*d*) δ 8.14 (d, *J* = 1.5 Hz, 1H), 8.10 (d, *J* = 8.1 Hz, 1H), 8.05 (dd, *J* = 7.8, 1.6 Hz, 1H), 7.93 – 7.91 (m, 1H), 7.88 (d, *J* = 8.0 Hz, 1H), 7.73 – 7.65 (m, 5H), 7.58 (d, *J* = 8.0 Hz, 2H), 7.50 (ddd, *J* = 8.3, 7.2, 1.2 Hz, 1H), 7.42 – 7.37 (m, 3H), 7.31 (td, *J* = 7.3, 1.3 Hz, 2H), 7.27 (s, 1H), 7.24 (dd, *J* = 7.3, 1.3 Hz, 1H), 2.20 (dd, *J* = 13.9, 7.2 Hz, 2H), 2.12 (dd, *J* = 13.9, 7.1 Hz, 2H), 0.46 (t, *J* = 7.3 Hz, 6H). HRMS (FT-ICR, $[M+H]^+$) m/z calcd for $MH^+$ $C_{41}H_{32}N_2SAu^+$ 781.19462 found 781.19464. Anal. Calcd for: $C_{41}H_{51}AuN_2S$ x DCM: C, (58.27); H, (3.84); N, (3.24). Found: C, (58.49); H, (3.66); N, (3.52).

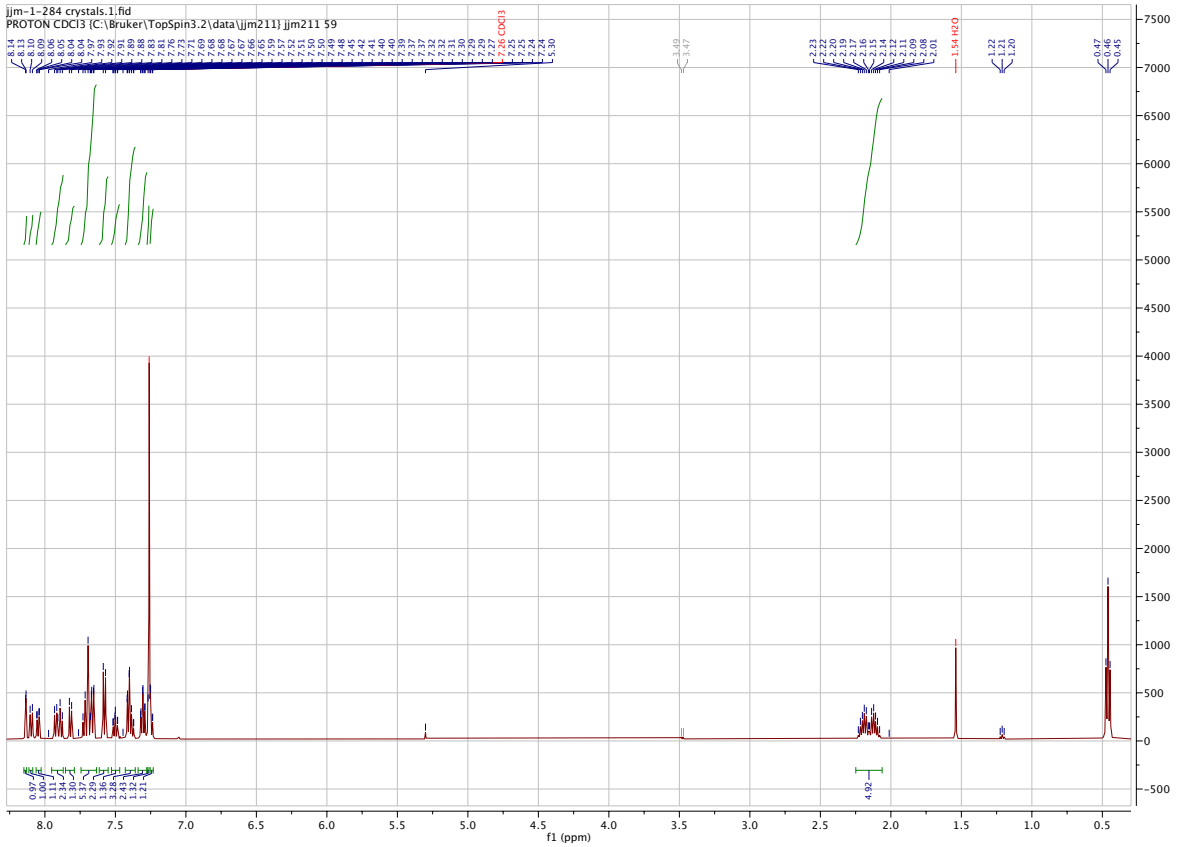


**Figure 6.6.** $^{1}$H NMR Spectrum of **Au(III)-BTF**.

**Au(III)-ABTF:**

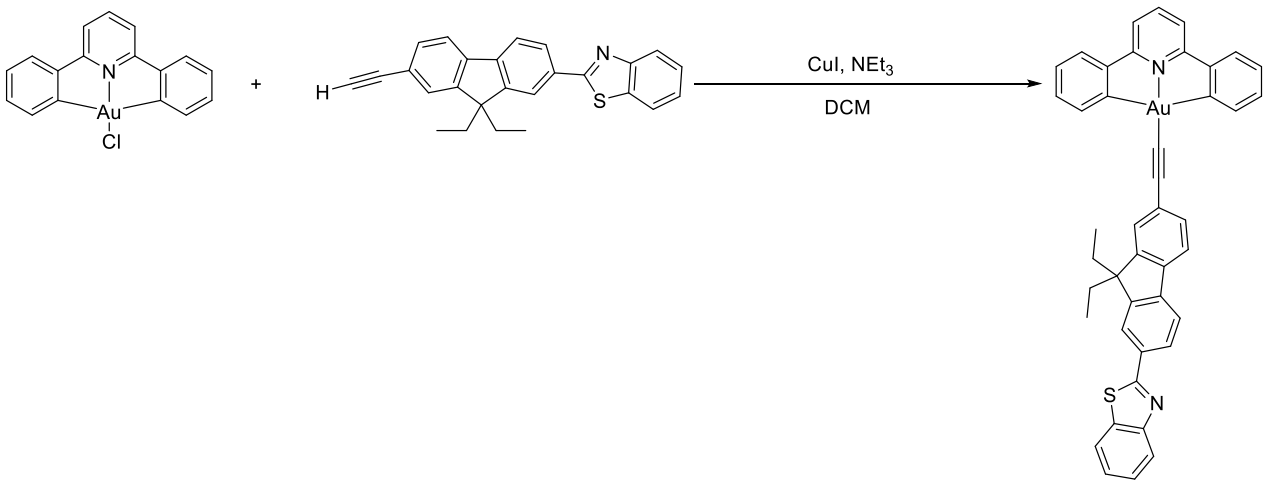

A mixture of [Au- (C∧N∧C)Cl] (99.3 mg, 0.215 mmol) and alkyne (123 mg, 0.325 mmol) in the presence of a catalytic amount of copper(I) iodide (9 mg) in triethylamine (2 mL) and dichloromethane (35 mL) was stirred at room temp overnight. After evaporation to dryness, the solid residue was purified by column chromatography on silica gel using dichloromethane as eluent. Subsequent recrystallization from slow diffusion of pentanes into the concentrated DCM solution yielded the product: (152 mg, 88 %). $^{1}$H NMR (500 MHz, Chloroform-*d*) δ 8.18 (d, *J* = 7.3 Hz, 2H), 8.14 (s, 1H), 8.10 (d, *J* = 8.1 Hz, 1H), 8.05 (d, *J* = 7.9 Hz, 1H), 7.94 – 7.87 (m, 3H), 7.80 (d, *J* = 7.9 Hz, 1H), 7.74 (d, *J* = 7.9 Hz, 1H), 7.66 (d, *J* = 7.8 Hz, 1H), 7.63 – 7.58 (m, 3H), 7.51 (t, *J* = 7.5 Hz, 3H), 7.45 (t, *J* = 7.3 Hz, 2H), 7.42 – 7.38 (m, 1H), 7.29 (t, *J* = 6.9 Hz, 3H), 2.18 (dq, *J* = 14.3, 6.8 Hz, 4H), 0.40 (t, *J* = 7.3 Hz, 6H).HRMS (FT-ICR, $[M+H]^{+}$) m/z calcd for $MH^{+}$ $C_{43}H_{32}N_{2}SAu^{+}$ 805.19462 found 805.19452. Anal. Calcd for: $C_{43}H_{31}AuN_{2}S$ x 0.5 DCM: C, (61.67); H, (3.81); N, (3.31). Found: C, (61.98); H, (3.90); N, (3.45).

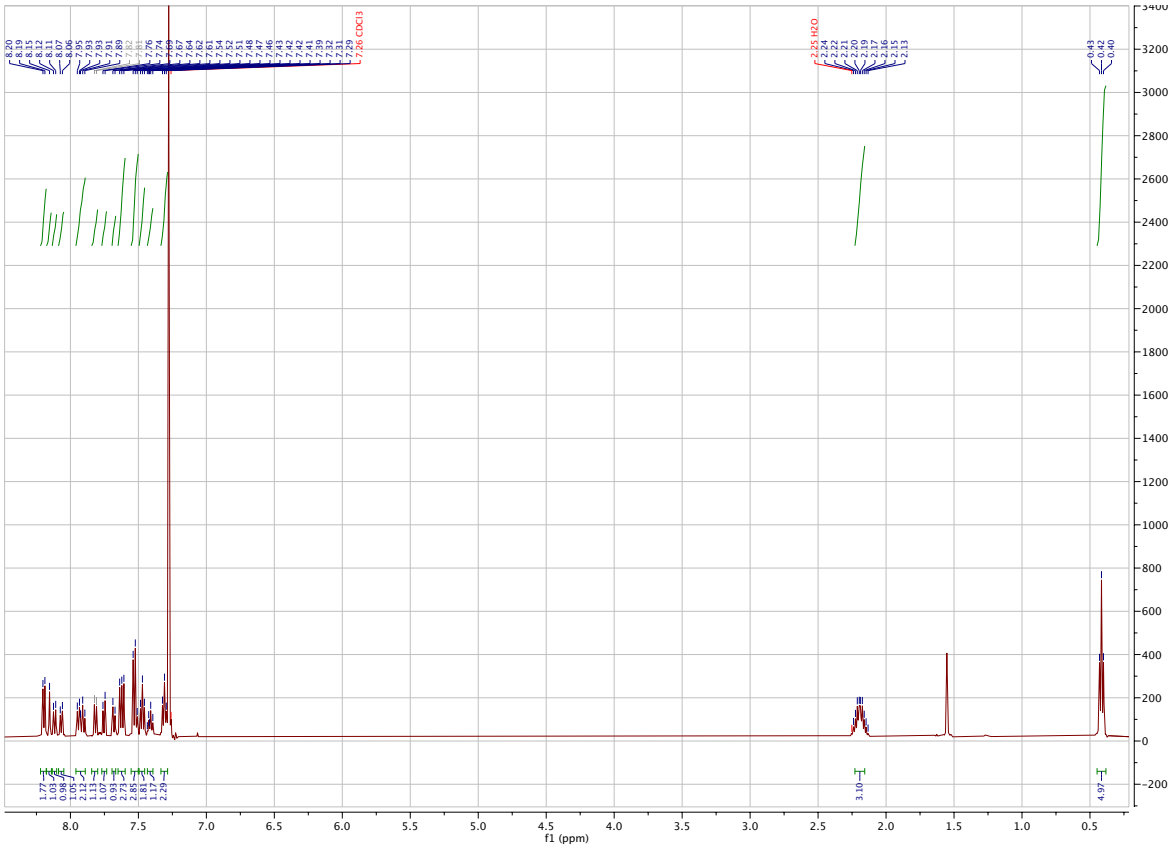


**Figure 6.7.** $^{1}$H NMR Spectrum of **Au(III)-ABTF**.

**Au(III)-ADPA:**

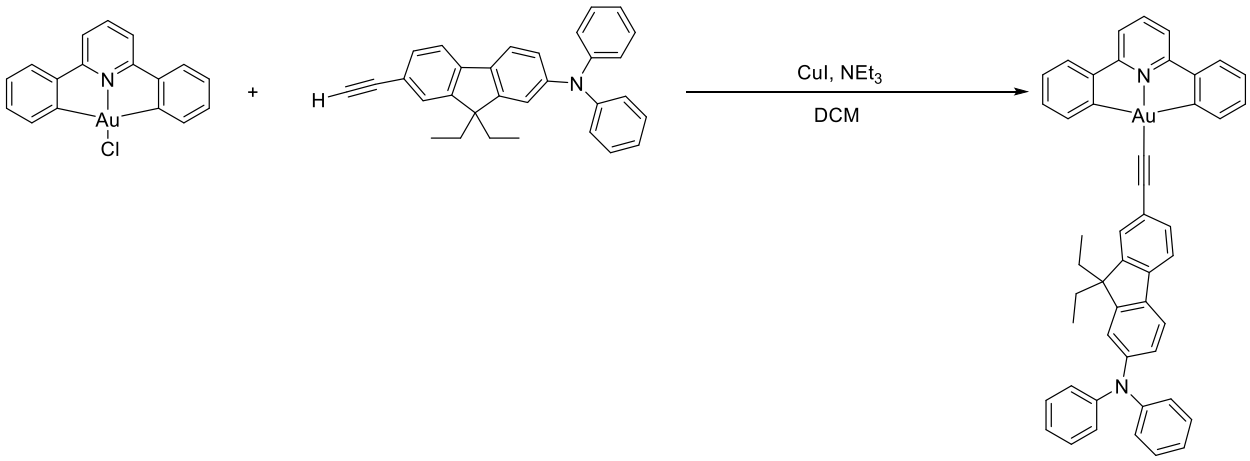


A mixture of [Au- (C∧N∧C)Cl] (99.3 mg, 0.215 mmol) and alkyne (134 mg, 0.325 mmol) in the presence of a catalytic amount of copper(I) iodide (9 mg) in triethylamine (2 mL) and dichloromethane (35 mL) was stirred at room temp overnight. After evaporation to dryness, the solid residue was purified by column chromatography on silica gel using dichloromethane as eluent. Subsequent recrystallization from slow diffusion of pentanes into the concentrated DCM solution yielded the product: (145 mg, 81 %). $^1$H NMR (500 MHz, Chloroform-*d*) δ 8.16 (d, *J* = 7.1 Hz, 2H), 7.87 (t, *J* = 7.9 Hz, 1H), 7.61 – 7.54 (m, 5H), 7.49 (d, *J* = 7.9 Hz, 2H), 7.43 (t, *J* = 7.2 Hz, 2H), 7.28 (s, 1H), 7.24 (s, 1H), 7.15 – 7.11 (m, 4H), 7.05 – 6.99 (m, 3H), 2.02 (dt, *J* = 13.6, 6.3 Hz, 2H), 1.91 (dt, *J* = 13.4, 6.1 Hz, 2H), 0.40 (t, *J* = 7.1 Hz, 6H). HRMS (FT-ICR, $[M]^+$) m/z calcd for $M^+$ $C_{48}H_{37}N_2Au^+$838.26168 found 838.26160. Anal. Calcd for: $C_{48}H_{36}AuN_2$: C, (68.73); H, (4.45); N, (3.34). Found: C, (68.54); H, (4.64); N, (3.35).

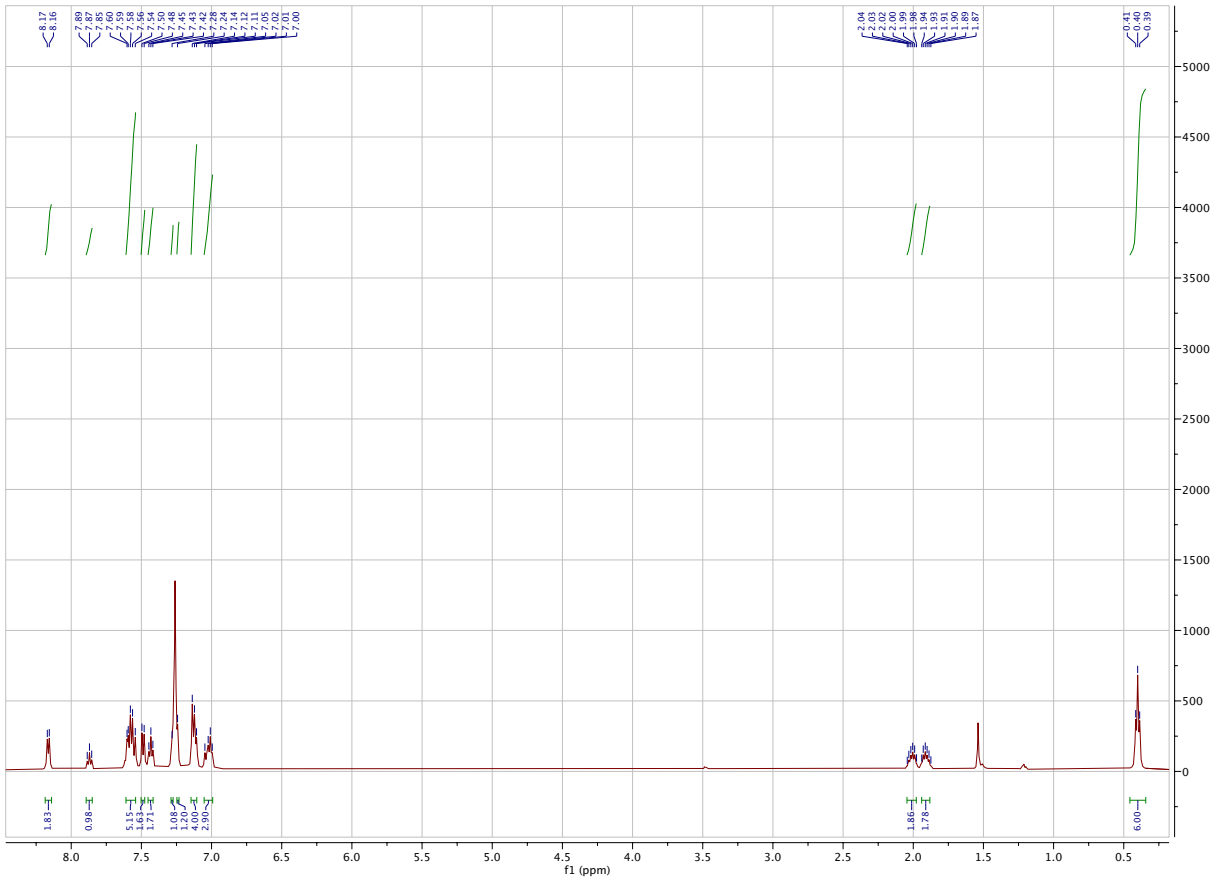

**Figure 6.8.** $^{1}$H NMR Spectrum of **Au(III)-ADPA**.

**Au(III)-DPA:**

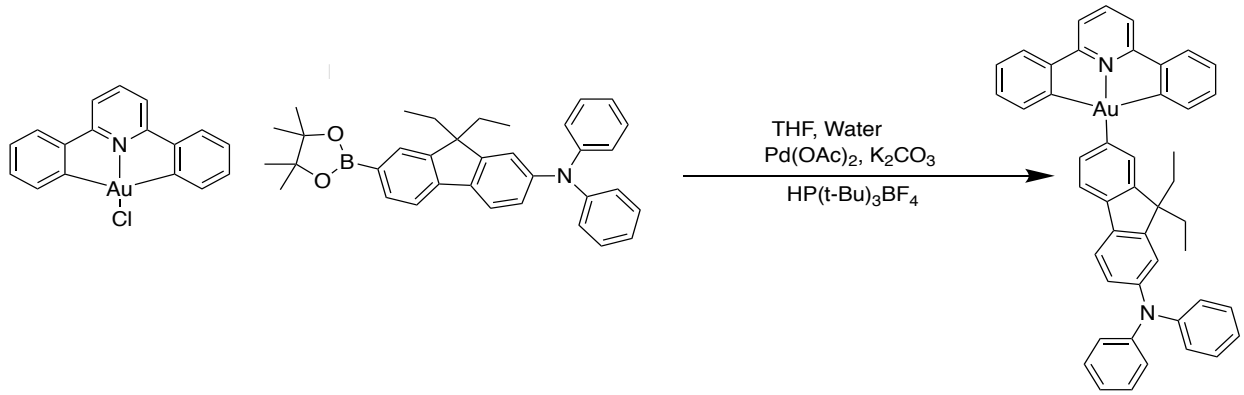


A flask containing [Au(C^N^C)Cl] (53.1 mg, 0.115 mmol), $K_2CO_3$ (550 mg, 0.43 mmol), $Pd(OAc)_2$ (7.2 mg, 0.023 mmol), $[HP(^tBu)_3]BF_4$ (13.3 mg, 0.046 mmol) and boronic acid (110 mg, 0.230 mmol) were added into degassed toluene and $H_2O$ (4 : 1, v/v) and the mixture was stirred

at 80 °C for 12 hours under a nitrogen atmosphere. After removing the solvent, the crude product was purified by column chromatography on silica gel using hexane–dichloromethane (7 : 3, v/v) as the eluent. Subsequent recrystallization by diffusion of diethyl ether vapor into a concentrated dichloromethane solution gave the product as a yellow solid (33 mg, 35 % Yield). $^{1}$H NMR (500 MHz, Chloroform-*d*) δ 7.88 (t, *J* = 8.0 Hz, 2H), 7.67 – 7.65 (m, 2H), 7.61 (t, *J* = 6.1 Hz, 3H), 7.57 (d, *J* = 8.0 Hz, 2H), 7.44 – 7.42 (m, 2H), 7.32 – 7.28 (m, 3H), 7.25 – 7.22 (m, 4H), 7.15 – 7.11 (m, 4H), 7.04 (d, *J* = 6.5 Hz, 2H), 7.01 – 6.96 (m, 3H), 2.00 – 1.95 (m, 2H), 1.93 – 1.89 (m, 2H), 0.46 (t, *J* = 7.3 Hz, 6H). HRMS (FT-ICR, $[M]^{+}$) m/z calcd for $M^{+}$ $C_{46}H_{37}N_{2}Au^{+}$ 814.26168 found 814.26267.

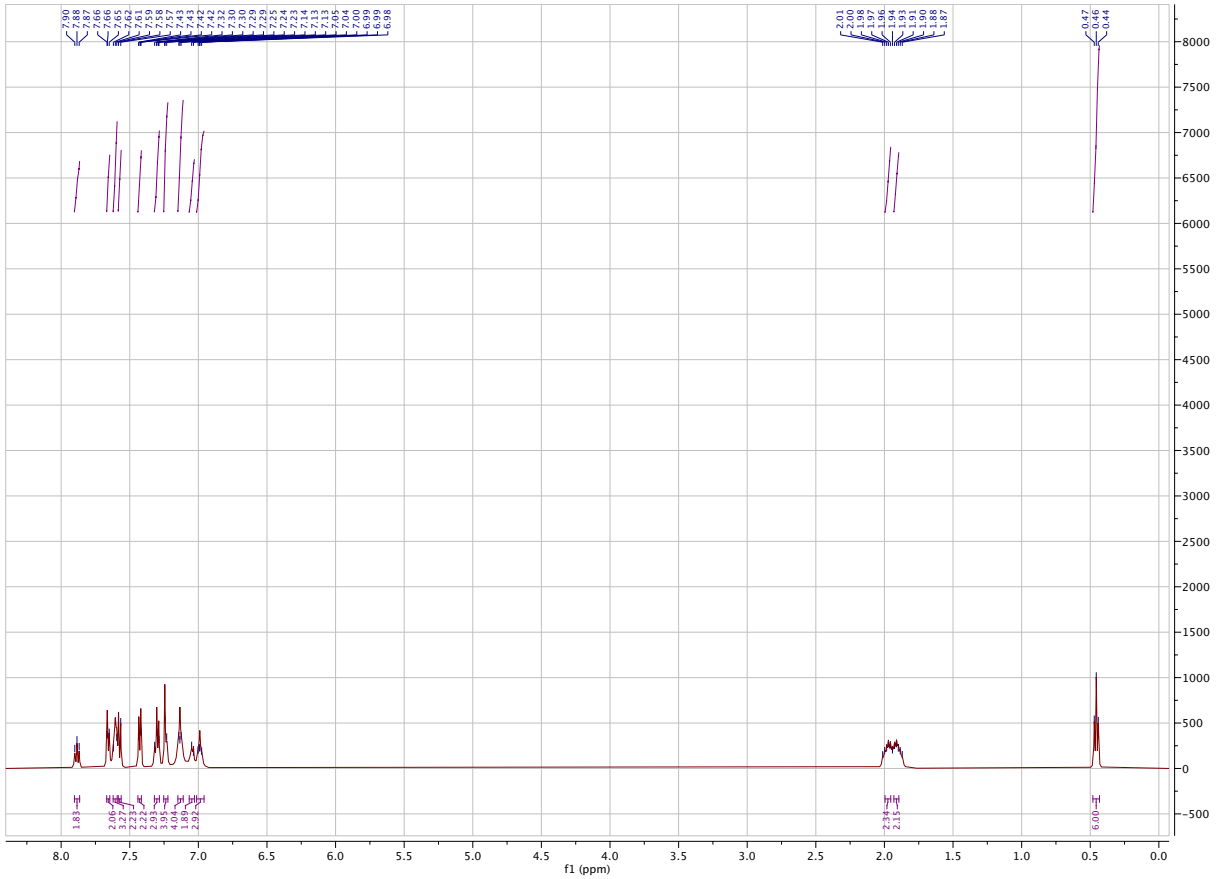


**Figure 6.9.** $^{1}$H NMR Spectrum of **Au(III)-DPA**.

**Single Crystal X-ray Structural Analysis**

Single crystals of the investigated compounds were coated with a trace of Fomblin oil and were transferred to the goniometer head of a Bruker Quest diffractometer with a fixed chi angle, a Mo Kα wavelength (λ = 0.71073 Å) sealed tube fine focus X-ray tube, single crystal curved graphite incident beam monochromator, a Photon100 CMOS area detector and equipped with an Oxford Cryosystems low temperature device and examination and data collection were performed at 150 K. Data were collected, reflections were indexed and processed, and the files scaled and corrected for absorption using APEX3 and SADABS[18]. The space groups were assigned and the structures were solved by direct methods using XPREP within the SHELXTL suite of programs[19] and refined by full matrix least squares against $F^2$ with all reflections using Shelxl2018[20] using the graphical interface Shelxle[21]. H atoms attached to carbon were positioned geometrically and constrained to ride on their parent atoms. C-H bond distances were constrained to 0.95 Å for aromatic C-H moieties, and to 0.99 and 0.98 Å for aliphatic $CH_2$ and $CH_3$ moieties, respectively. Methyl $CH_3$ were allowed to rotate but not to tip to best fit the experimental electron density. $U_{iso}(H)$ values were set to a multiple of $U_{eq}(C)$ with 1.5 for $CH_3$, and 1.2 for C-H and $CH_2$ units, respectively. Additional data are given in the tables below.

Complete crystallographic data, in CIF format, have been deposited with the Cambridge Crystallographic Data Centre. CCDC contains the supplementary crystallographic data for this paper. These data can be obtained free of charge from The Cambridge Crystallographic Data Centre via www.ccdc.cam.ac.uk/data_request/cif.

**Table 6.1.** Crystallography experimental details

| | jjm_1_281_0m | jjm_1_284_0m |
|---|---|---|
| Crystal data | | |
| Chemical formula | $C_{43}H_{31}AuN_2S{\cdot}CH_2Cl_2$ | $C_{41}H_{31}AuN_2S$ |
| $M_r$ | 889.65 | 780.70 |
| Crystal system, space group | Triclinic, $P\bar{1}$ | Triclinic, $P\bar{1}$ |
| Temperature (K) | 150 | 150 |
| *a*, *b*, *c* (Å) | 8.1901 (5), 9.0946 (5), 24.6657 (14) | 7.4390 (5), 14.2524 (9), 15.2855 (9) |
| α, β, γ (°) | 79.564 (2), 87.530 (2), 76.770 (2) | 80.116 (2), 81.972 (2), 88.066 (2) |
| *V* (Å$^3$) | 1758.89 (18) | 1580.84 (17) |
| *Z* | 2 | 2 |
| *F*(000) | 880 | 772 |
| $D_x$ (Mg m$^{-3}$) | 1.680 | 1.640 |
| Radiation type | Mo *K*α | Mo *K*α |
| No. of reflections for cell measurement | 9035 | 9942 |
| θ range (°) for cell measurement | 2.5–33.2 | 2.7–33.2 |
| μ (mm$^{-1}$) | 4.43 | 4.75 |
| Crystal shape | Block | Rod |
| Colour | Yellow | Yellow |
| Crystal size (mm) | 0.45 × 0.31 × 0.29 | 0.45 × 0.43 × 0.29 |
| | | |
| Data collection | | |
| Diffractometer | Bruker AXS D8 Quest CMOS diffractometer | Bruker AXS D8 Quest CMOS diffractometer |
| Radiation source | fine focus sealed tube X-ray source | fine focus sealed tube X-ray source |
| Monochromator | Triumph curved graphite crystal | Triumph curved graphite crystal |
| Detector resolution (pixels mm$^{-1}$) | 10.4167 | 10.4167 |
| Scan method | ω and phi scans | ω and phi scans |
| Absorption correction | Multi-scan (*SADABS* 2016/2, | Multi-scan (*SADABS* 2016/2, |

| | | |
|---|---|---|
| | Krause *et al.*, 2015) | Krause *et al.*, 2015) |
| $T_{min}$, $T_{max}$ | 0.484, 0.747 | 0.457, 0.747 |
| No. of measured, independent and observed [$I > 2\sigma(I)$] reflections | 67093, 13438, 12886 | 106913, 12128, 11157 |
| $R_{int}$ | 0.027 | 0.035 |
| θ values (°) | $\theta_{max}$ = 33.2, $\theta_{min}$ = 2.5 | $\theta_{max}$ = 33.3, $\theta_{min}$ = 2.7 |
| $(\sin \theta/\lambda)_{max}$ (Å$^{-1}$) | 0.771 | 0.772 |
| Range of *h*, *k*, *l* | $h$ = -12→12, $k$ = -14→14, $l$ = -37→37 | $h$ = -11→11, $k$ = -21→21, $l$ = -23→23 |
| | | |
| Refinement | | |
| Refinement on | $F^2$ | $F^2$ |
| $R[F^2 > 2\sigma(F^2)]$, $wR(F^2)$, $S$ | 0.015, 0.036, 1.05 | 0.019, 0.042, 1.09 |
| No. of reflections | 13438 | 12128 |
| No. of parameters | 454 | 409 |
| No. of restraints | 0 | 0 |
| H-atom treatment | H-atom parameters constrained | H-atom parameters constrained |
| Weighting scheme | $w = 1/[\sigma^2(F_o^2) + (0.0148P)^2 + 0.8616P]$ where $P = (F_o^2 + 2F_c^2)/3$ | $w = 1/[\sigma^2(F_o^2) + (0.0133P)^2 + 1.3786P]$ where $P = (F_o^2 + 2F_c^2)/3$ |
| $(\Delta/\sigma)_{max}$ | 0.008 | 0.002 |
| $\Delta\rho_{max}$, $\Delta\rho_{min}$ (e Å$^{-3}$) | 0.95, -1.06 | 3.36, -1.12 |
| Extinction method | *SHELXL2018*/3 (Sheldrick 2018), $Fc^*=kFc[1+0.001xFc^2\lambda^3/\sin(2\theta)]^{-1/4}$ | *SHELXL2018*/3 (Sheldrick 2018), $Fc^*=kFc[1+0.001xFc^2\lambda^3/\sin(2\theta)]^{-1/4}$ |
| Extinction coefficient | 0.00500 (15) | 0.00312 (15) |

Computer programs: Apex3 v2018.1-0 (Bruker, 2018), *SAINT* V8.38A (Bruker, 2016), *SHELXS97* (Sheldrick, 2008), *SHELXL2018*/3 (Sheldrick, 2015, 2018), SHELXLE Rev946 (Hübschle *et al.*, 2011).

**References.**


1 M. C. Tang, W. K. Kwok, S. L. Lai, W. L. Cheung, M. Y. Chan and V. Wing-Wah Yam, Rational molecular design for realizing high performance sky-blue-emitting gold(iii) complexes with monoaryl auxiliary ligands and their applications for both solution-processable and vacuum-deposited organic light-emitting devices, *Chem. Sci.*, 2019, **10**, 594–605.

2 V. K. M. Au, K. M. C. Wong, D. P. K. Tsang, M. Y. Chan, N. Zhu and V. W. W. Yam, High-efficiency green organic light-emitting devices utilizing phosphorescent bis-cyclometalated alkynylgold(III) complexes, *J. Am. Chem. Soc.*, 2010, **132**, 14273–14278.

3 S. Jürgens, V. Scalcon, N. Estrada-Ortiz, A. Folda, F. Tonolo, C. Jandl, D. L. Browne, M. P. Rigobello, F. E. Kühn and A. Casini, Exploring the C^N^C theme: Synthesis and biological properties of tridentate cyclometalated gold(III) complexes, *Bioorg. Med. Chem.*, 2017, **25**, 5452–5460.

4 K. M. Wong, X. Zhu, L. Hung, N. Zhu, V. W. Yam and H. Kwok, A novel class of phosphorescent gold ( III ) alkynyl-based organic light-emitting devices with tunable colour, 2005, **2**, 2906–2908.

5 V. W. Yam, Bipolar Gold(III) Complexes for Solution-Processable Organic Light-Emitting Devices with a Small E ffi ciency Roll-O ff, 2014, 17861–17868.

6 L. Li, M. Tang, W. Cheung, S. Lai, M. Ng, C. K. Chan, M. Chan and V. W. Yam, Rational Design Strategy for the Realization of Red- to Near- Infrared-Emitting Alkynylgold(III) Complexes and Their Applications in Solution-Processable Organic Light-Emitting Devices, , DOI:10.1021/acs.chemmater.9b01208.

7 C. H. Lee, M. C. Tang, W. L. Cheung, S. L. Lai, M. Y. Chan and V. W. W. Yam, Highly luminescent phosphine oxide-containing bipolar alkynylgold(iii) complexes for solution-processable organic light-emitting devices with small efficiency roll-offs, *Chem. Sci.*, 2018, **9**, 6228–6232.

8 V. K. M. Au, K. M. C. Wong, D. P. K. Tsang, M. Y. Chan, N. Zhu and V. W. W. Yam, High-efficiency green organic light-emitting devices utilizing phosphorescent bis-cyclometalated alkynylgold(III) complexes, *J. Am. Chem. Soc.*, 2010, **132**, 14273–14278.

9 M. C. Tang, D. P. K. Tsang, Y. C. Wong, M. Y. Chan, K. M. C. Wong and V. W. W. Yam, Bipolar gold(III) complexes for solution-processable organic light-emitting devices

with a small efficiency roll-off, *J. Am. Chem. Soc.*, 2014, **136**, 17861–17868.

10 M. Tang, C. Lee, S. Lai, M. Ng, M. Chan and V. W. Yam, Versatile Design Strategy for Highly Luminescent Vacuum-Evaporable and Solution-Processable Tridentate Gold(III) Complexes with Monoaryl Auxiliary Ligands and Their Applications for Phosphorescent Organic Light Emitting Devices, *J. Am. Chem. Soc.*, 2017, **139**, 9341–9349.

11 M. C. Tang, D. P. K. Tsang, M. M. Y. Chan, K. M. C. Wong and V. W. W. Yam, Dendritic luminescent gold(III) complexes for highly efficient solution-processable organic light-emitting devices, *Angew. Chemie - Int. Ed.*, 2013, **52**, 446–449.

12 D. Zhou, W. P. To, G. S. M. Tong, G. Cheng, L. Du, D. L. Phillips and C. M. Che, Tetradentate Gold(III) Complexes as Thermally Activated Delayed Fluorescence (TADF) Emitters: Microwave-Assisted Synthesis and High-Performance OLEDs with Long Operational Lifetime, *Angew. Chemie - Int. Ed.*, 2020, **59**, 6375–6382.

13 C. H. Lee, M. C. Tang, F. K. W. Kong, W. L. Cheung, M. Ng, M. Y. Chan and V. W. W. Yam, Isomeric Tetradentate Ligand-Containing Cyclometalated Gold(III) Complexes, *J. Am. Chem. Soc.*, 2020, **142**, 520–529.

14 M. Y. Leung, M. C. Tang, W. L. Cheung, S. L. Lai, M. Ng, M. Y. Chan and V. Wing-Wah Yam, Thermally Stimulated Delayed Phosphorescence (TSDP)-Based Gold(III) Complexes of Tridentate Pyrazine-Containing Pincer Ligand with Wide Emission Color Tunability and Their Application in Organic Light-Emitting Devices, *J. Am. Chem. Soc.*, 2020, **142**, 2448–2459.

15 J. J. Mihaly, D. J. Stewart, T. A. Grusenmeyer, A. T. Phillips, J. E. Haley, M. Zeller and T. G. Gray, Photophysical properties of organogold(i) complexes bearing a benzothiazole-2,7-fluorenyl moiety: Selection of ancillary ligand influences white light emission, *Dalt. Trans.*, 2019, **48**, 15917–15927.

16 J. J. Mihaly, A. T. Phillips, J. T. Malloy, Z. M. Marsh, M. Zeller, J. E. Haley, K. De La Harpe, T. A. Grusenmeyer and T. G. Gray, Synthesis and Photophysical Properties of Laterally Asymmetric Digold(I) Alkynyls and Triazolyl: Ancillary Ligand and Organic Functionality Dictate Excited-State Dynamics, *Organometallics*, 2020, **39**, 489–494.

17 J. J. Mihaly, A. T. Phillips, D. J. Stewart, Z. M. Marsh, C. L. McCleese, J. E. Haley, M. Zeller, T. A. Grusenmeyer and T. G. Gray, Synthesis and photophysics of gold( i ) alkynyls bearing a benzothiazole-2,7-fluorenyl moiety: a comparative study analyzing

influence of ancillary ligand, bridging moiety, and number of metal centers on photophysical properties , *Phys. Chem. Chem. Phys.*, 2020, 11915–11927.

18 G. M. Sheldrick, A short history of SHELX, *Acta Crystallogr. Sect. A*, 2008, **64**, 112–122.

19 G. M. Sheldrick, Crystal structure refinement with SHELXL, *Acta Crystallogr. Sect. C*, 2015, **71**, 3–8.

20 C. B. Hübschle, G. M. Sheldrick and B. Dittrich, ShelXle: a Qt graphical user interface for SHELXL, *J. Appl. Crystallogr.*, 2011, **44**, 1281–1284.

21 L. Krause, R. Herbst-Irmer, G. M. Sheldrick and D. Stalke, Comparison of silver and molybdenum microfocus X-ray sources for single-crystal structure determination, *J. Appl. Crystallogr.*, 2015, **48**, 3–10.

## Chapter 7. Dissertation Summary and Future Directions

This dissertation describes the synthesis, photophysics, and in some chapters; computational studies for a variety of new gold organometallics. The effects of oxidation state, gold-chromophore linkage, ancillary ligand, capping moiety, and number of metal centers on photophysical properties are examined. In the Au-BTF aryl series, the complexes with phosphine ancillary ligand displayed blue-shifted absorption and emission spectra compared to the complexes with carbene ancillary ligand as well as larger phosphorescence intensities. The phosphine complexes also displayed shorter fluorescence lifetimes, smaller fluorescence quantum yields, larger triplet state quantum yields, and rates of intersystem crossing that are essentially four times that of the carbene complex. Excited-state absorption from both the singlet and triplet excited states is established as well as delayed fluorescence. Computational study accords with photophysical results for both DFT and TD-DFT. Taken together, in the Au-BTF series the phosphine complexes are the more desirable triplet photoactive materials.

Data for the Au-ABTF alkynyl series exhibits converse excited-state dynamics with variation in ancillary ligand. In the Au-ABTF series, the complexes with phosphine ancillary ligand displayed blue-shifted absorption and emission spectra compared to the complexes with carbene ancillary ligand; however, the carbene complex exhibits larger phosphorescence intensity. In this series, the carbene complex displayed a shorter fluorescence lifetime, smaller fluorescence quantum yield, larger triplet state quantum yield, and a rate of intersystem crossing that is essentially two times that of the phosphine complexes. Excited-state absorption from both the singlet and triplet excited states is established as well as delayed fluorescence. Computational

study accords with photophysical results for both DFT and TD-DFT. Taken together, in the Au-ABTF series the carbene complex is the more desirable triplet photoactive material.

When comparing the aryl and alkynyl series; the phosphine complexes display different excited-state dynamics, with the aryl complex being the more desirable photoactive material. The carbene aryl and alkynyl complex exhibit nearly identical excited-state dynamics.

In the dinuclear gold(I) series, alkynyls with variation in ancillary ligand show little effect on excited state dynamics; however, when gold chromophore linkage is altered from an alkynyl to a triazolyl we see increases in triplet state quantum yield and rate of intersystem crossing making the triazolyl complex the more desirable triplet photoactive material. We do not observe increased phosphorescence in these complexes. Computational study accords with photophysical results for both DFT and TD-DFT.

In the gold(I) DPA complexes as well as the gold(III) complexes, we observe trends in absorption and emission energies and band-shape. We observe almost strictly phosphoresce in the gold(III) complexes. Those data demonstrate the effect of ancillary ligand, gold-chromophore linkage, capping moiety, and oxidation state have on photophysical properties.

Future directions would include lifetime and quantum yield data for the gold(I) DPA complexes as well as the gold(III) complexes. This will allow for calculation of excited-state rate constants gaining insight into the excited-state dynamics for these complexes. Time-resolved photophysical experiments should also be performed. This will provide a more detailed understanding of excited-state dynamics. After completion of those projects, continued structure-property study is necessary. A more precise understanding of structure-property relationships in gold organometallics is essential for application purposes.

**Bibliography.**


1 D. M. Arias-Rotondo and J. K. Mccusker, in *Visible Light Photocatalysis in Organic Chemistry*, Wiley-VCH Verlag GmbH & Co. KGaA, Weinheim, Germany, 2017, pp. 1–24.

2 E. Zysman-Colman, Ed., *Iridium(III) in Optoelectronic and Photonics Applications*, John Wiley & Sons, Ltd, Chichester, UK, 2017.

3 H. Yersin, *Highly Efficient OLEDs with Phosphorescent Materials*, Wiley-VCH Verlag GmbH & Co. KGaA, Weinheim, Germany, 2008.

4 T. Y. Li, J. Wu, Z. G. Wu, Y. X. Zheng, J. L. Zuo and Y. Pan, *Coord. Chem. Rev.*, 2018, 374, 55–92.

5 C. M. Che, C. C. Kwok, C. F. Kui, S. L. Lai and K. H. Low, in *Comprehensive Inorganic Chemistry II (Second Edition): From Elements to Applications*, Elsevier, 2013, vol. 8, pp. 607–655.

6 C. K. Prier, D. A. Rankic and D. W. C. MacMillan, *Chem. Rev.*, 2013, **113**, 5322–5363.

7 Y. You and W. Nam, *Chem. Soc. Rev.*, 2012, 41, 7061–7084.

8 K. T. Chan, G. S. M. Tong, W. P. To, C. Yang, L. Du, D. L. Phillips and C. M. Che, *Chem. Sci.*, 2017, **8**, 2352–2364.

9 G. S. Ming Tong, K. T. Chan, X. Chang and C. M. Che, *Chem. Sci.*, 2015, **6**, 3026–3037.

10 M. C. Tang, C. H. Lee, M. Ng, Y. C. Wong, M. Y. Chan and V. W. W. Yam, Highly Emissive Fused Heterocyclic Alkynylgold(III) Complexes for Multiple Color Emission Spanning from Green to Red for Solution-Processable Organic Light-Emitting Devices, *Angew. Chemie - Int. Ed.*, 2018, **57**, 5463–5466.

11 M. C. Tang, M. Y. Leung, S. L. Lai, M. Ng, M. Y. Chan and V. Wing-Wah Yam, Realization of Thermally Stimulated Delayed Phosphorescence in Arylgold(III) Complexes and Efficient Gold(III) Based Blue-Emitting Organic Light-Emitting Devices, *J. Am. Chem. Soc.*, 2018, **140**, 13115–13124.

12 Y. Yuan, P. Gnanasekaran, Y. W. Chen, G. H. Lee, S. F. Ni, C. S. Lee and Y. Chi, Iridium(III) Complexes Bearing a Formal Tetradentate Coordination Chelate: Structural Properties and Phosphorescence Fine-Tuned by Ancillaries, *Inorg. Chem.*, 2019, **59**, 523–532.

13 Z. Hao, K. Zhang, P. Wang, X. Lu, Z. Lu, W. Zhu and Y. Liu, Deep Red Iridium(III) Complexes Based on Pyrene-Substituted Quinoxaline Ligands for Solution-Processed Phosphorescent Organic Light-Emitting Diodes, *Inorg. Chem.*, 2019, **59**, 332–342.

14 R. C. Evans, P. Douglas and C. J. Winscom, Coordination complexes exhibiting room-temperature phosphorescence: Evaluation of their suitability as triplet emitters in organic light emitting diodes, *Coord. Chem. Rev.*, 2006, **250**, 2093–2126.

15 G. M. Farinola and R. Ragni, Electroluminescent materials for white organic light emitting diodes, *Chem. Soc. Rev.*, 2011, **40**, 3467–3482.

16 M. E. Thompson, P. E. Burrows and S. R. Forrest, Electrophosphorescence in organic light emitting diodes, *Curr. Opin. Solid State Mater. Sci.*, 1999, **4**, 369–372.

17 M. C. Tang, C. H. Lee, S. L. Lai, M. Ng, M. Y. Chan and V. W. W. Yam, Versatile Design Strategy for Highly Luminescent Vacuum-Evaporable and Solution-Processable Tridentate Gold(III) Complexes with Monoaryl Auxiliary Ligands and Their Applications for Phosphorescent Organic Light Emitting Devices, *J. Am. Chem. Soc.*, 2017, **139**, 9341–9349.

18 P. T. Furuta, L. Deng, S. Garon, M. E. Thompson and J. M. J. Fréchet, Platinum-functionalized random copolymers for use in solution-processible, efficient, near-white organic light-emitting diodes, *J. Am. Chem. Soc.*, 2004, **126**, 15388–15389.

19 S. Lamansky, P. Djurovich, D. Murphy, F. Abdel-Razzaq, H. E. Lee, C. Adachi, P. E. Burrows, S. R. Forrest and M. E. Thompson, Highly phosphorescent bis-cyclometalated iridium complexes: Synthesis, photophysical characterization, and use in organic light emitting diodes, *J. Am. Chem. Soc.*, 2001, **123**, 4304–4312.

20 W. P. To, D. Zhou, G. S. M. Tong, G. Cheng, C. Yang and C. M. Che, Highly Luminescent Pincer Gold(III) Aryl Emitters: Thermally Activated Delayed Fluorescence and Solution-Processed OLEDs, *Angew. Chemie - Int. Ed.*, 2017, **56**, 14036–14041.

21 M. A. Baldo, D. F. O. an dY. You, A. Shoustikov, S. Sibley, M. E. Thompson and S. R. Forrest, Highly efficient phosphorescent emission from organic electroluminescent devices, *Nature*, 1998, **395**, 151.

22 C. Adachi, M. A. Baldo, M. E. Thompson and S. R. Forrest, Nearly 100% internal phosphorescence efficiency in an organic light emitting device, *J. Appl. Phys.*, 2001, **90**,

5048–5051.

23 J. Kalinowski, V. Fattori, M. Cocchi and J. A. G. Williams, Light-emitting devices based on organometallic platinum complexes as emitters, *Coord. Chem. Rev.*, 2011, **255**, 2401–2425.

24 Q. Zeng, F. Li, Z. Chen, K. Yang, Y. Liu, T. Guo, G.-G. Shan and Z.-M. Su, Rational Design of Efficient Organometallic Ir(III) Complexes for High-Performance Flexible Monochromatic and White Light-Emitting Electrochemical Cells, *ACS Appl. Mater. Interfaces*, 2020, **12**, 4649–4658.

25 X. Z. Shu, M. Zhang, Y. He, H. Frei and F. D. Toste, Dual visible light photoredox and gold-catalyzed arylative ring expansion, *J. Am. Chem. Soc.*, 2014, **136**, 5844–5847.

26 O. Reiser, G. Kachkovskyi, V. Kais, P. Kohls, S. Paria, M. Pirtsch, D. Rackl and H. Seo, Walter de Gruyter GmbH, 2013, p. 139.

27 M. H. Shaw, J. Twilton and D. W. C. MacMillan, Photoredox Catalysis in Organic Chemistry, *J. Org. Chem.*, 2016, **81**, 6898–6926.

28 Y. You and W. Nam, Photofunctional triplet excited states of cyclometalated Ir(III) complexes: Beyond electroluminescence, *Chem. Soc. Rev.*, 2012, **41**, 7061–7084.

29 C. K. Prier, D. A. Rankic and D. W. C. MacMillan, Visible light photoredox catalysis with transition metal complexes: Applications in organic synthesis, *Chem. Rev.*, 2013, **113**, 5322–5363.

30 M. D. Levin, S. Kim and F. D. Toste, Photoredox catalysis unlocks single-electron elementary steps in transition metal catalyzed cross-coupling, *ACS Cent. Sci.*, 2016, **2**, 293–301.

31 M. N. Hopkinson, A. Tlahuext-Aca and F. Glorius, Merging Visible Light Photoredox and Gold Catalysis, *Acc. Chem. Res.*, 2016, **49**, 2261–2272.

32 J. Zhao, W. Wu, J. Sun and S. Guo, Triplet photosensitizers: From molecular design to applications, *Chem. Soc. Rev.*, 2013, **42**, 5323–5351.

33 J. F. Longevial, K. El Cheikh, D. Aggad, A. Lebrun, A. van der Lee, F. Tielens, S. Clément, A. Morère, M. Garcia, M. Gary-Bobo and S. Richeter, Porphyrins Conjugated with Peripheral Thiolato Gold(I) Complexes for Enhanced Photodynamic Therapy, *Chem.*

- *A Eur. J.*, 2017, **23**, 14017–14026.

34 L. Zhou, X. Ge, J. Liu, J. Zhou, S. Wei, F. Li and J. Shen, Internal heavy atom effect of Au(III) and Pt(IV) on hypocrellin A for enhanced in vitro photodynamic therapy of cancer, *Bioorganic Med. Chem. Lett.*, 2013, **23**, 5317–5324.

35 E. Baggaley, J. A. Weinstein and J. A. G. Williams, Lighting the way to see inside the live cell with luminescent transition metal complexes, *Coord. Chem. Rev.*, 2012, **256**, 1762–1785.

36 L. K. McKenzie, H. E. Bryant and J. A. Weinstein, Transition metal complexes as photosensitisers in one- and two-photon photodynamic therapy, *Coord. Chem. Rev.*, 2019, **379**, 2–29.

37 X. Jiang, N. Zhu, D. Zhao and Y. Ma, New cyclometalated transition-metal based photosensitizers for singlet oxygen generation and photodynamic therapy, *Sci. China Chem.*, 2016, **59**, 40–52.

38 R. Vestberg, R. Westlund, A. Eriksson, C. Lopes, M. Carlsson, B. Eliasson, E. Glimsdal, M. Lindgren and E. Malmström, Dendron decorated platinum(II) acetylides for optical power limiting, *Macromolecules*, 2006, **39**, 2238–2246.

39 N. J. Long, Organometallic Compounds for Nonlinear Optics—The Search for En-light-enment!, *Angew. Chemie Int. Ed. English*, 1995, **34**, 21–38.

40 M. J. Miller, A. G. Mott and B. P. Ketchel, General optical limiting requirements, *Nonlinear Opt. Liq. Power Limiting Imaging*, 2003, **3472**, 24.

41 S. R. Marder, B. Kippelen, A. K. Y. Jen and N. Peyghambarian, Design and synthesis of chromophores and polymers for electro-optic and photorefractive applications, *Nature*, 1997, **388**, 845–851.

42 G. J. Zhou and W. Y. Wong, Organometallic acetylides of PtII, AuI and Hg II as new generation optical power limiting materials, *Chem. Soc. Rev.*, 2011, **40**, 2541–2566.

43 G. S. He, L.-S. Tan, Q. Zheng and P. N. Prasad, Multiphoton Absorbing Materials: Molecular Designs, Characterizations, and Applications, *Chem. Rev.*, 2008, **108**, 1245–1330.

44 B. Liu, Z. Tian, F. Dang, J. Zhao, X. Yan, X. Xu, X. Yang, G. Zhou and Y. Wu,

Photophysical and optical power limiting behaviors of Au(I) acetylides with diethynyl aromatic ligands showing different electronic features, *J. Organomet. Chem.*, 2016, **804**, 80–86.

45 P. B. Jacques Simon, Design of Molecular Materials: Supramolecular Engineering, *Wiley*, 2001, **15**, 197–199.

46 Y. Lin, C. Jiang, F. Hu, J. Yin, G. A. Yu and S. H. Liu, Synthesis, characterization, and properties of some bisacetylide and binuclear acetylide gold(I) compounds based on the photochromic dithienylethene unit, *Dye. Pigment.*, 2013, **99**, 995–1003.

47 Q. Zhao, C. Huang and F. Li, Phosphorescent heavy-metal complexes for bioimaging, *Chem. Soc. Rev.*, 2011, **40**, 2508–2524.

48 H. Xiang, J. Cheng, X. Ma, X. Zhou and J. J. Chruma, *Near-infrared phosphorescence: Materials and applications*, 2013, vol. 42.

49 K. K. W. Lo, A. W. T. Choi and W. H. T. Law, Applications of luminescent inorganic and organometallic transition metal complexes as biomolecular and cellular probes, *Dalt. Trans.*, 2012, **41**, 6021–6047.

50 D. L. Ma, H. Z. He, K. H. Leung, D. S. H. Chan and C. H. Leung, Bioactive luminescent transition-metal complexes for biomedical applications, *Angew. Chemie - Int. Ed.*, 2013, **52**, 7666–7682.

51 K. Li, G. S. Ming Tong, Q. Wan, G. Cheng, W. Y. Tong, W. H. Ang, W. L. Kwong and C. M. Che, Highly phosphorescent platinum(ii) emitters: photophysics, materials and biological applications, *Chem. Sci.*, 2016, **7**, 1653–1673.

52 M. Mydlak, C. Bizzarri, D. Hartmann, W. Sarfert, G. Schmid and L. De Cola, Positively charged iridium(lll) triazole derivatives as blue emitters for light-emitting electrochemical cells, *Adv. Funct. Mater.*, 2010, **20**, 1812–1820.

53 C. Ulbricht, B. Beyer, C. Friebe, A. Winter and U. S. Schubert, Recent developments in the application of phosphorescent iridium(III) complex systems, *Adv. Mater.*, 2009, **21**, 4418–4441.

54 H. C. Su, H. F. Chen, F. C. Fang, C. C. Liu, C. C. Wu, K. T. Wong, Y. H. Liu and S. M. Peng, Solid-state white light-emitting electrochemical cells using iridium-based cationic

transition metal complexes, *J. Am. Chem. Soc.*, 2008, **130**, 3413–3419.

55 R. D. Costa, E. Ortí, H. J. Bolink, F. Monti, G. Accorsi and N. Armaroli, Luminescent ionic transition-metal complexes for light-emitting electrochemical cells, *Angew. Chemie - Int. Ed.*, 2012, **51**, 8178–8211.

56 T. M. Monos and C. R. J. Stephenson, Photoredox Catalysis of Iridium(III)-Based Photosensitizers, *Iridium(III) Optoelectron. Photonics Appl.*, 2017, 541–581.

57 K. Teegardin, J. I. Day, J. Chan and J. Weaver, Advances in Photocatalysis: A Microreview of Visible Light Mediated Ruthenium and Iridium Catalyzed Organic Transformations, *Org. Process Res. Dev.*, 2016, **20**, 1156–1163.

58 C. Adachi, S. Lee, T. Nakagawa, K. Shizu, K. Goushi and W. Potscavage, 2015, pp. 43–73.

59 I. Eryazici, C. N. Moorefield and G. R. Newkome, Square-planar Pd(II), Pt(II), and Au(III) terpyridine complexes: Their syntheses, physical properties, supramolecular constructs, and biomedical activities, *Chem. Rev.*, 2008, **108**, 1834–1895.

60 V. W. W. Yam and A. S. Y. Law, Luminescent d8 metal complexes of platinum(II) and gold(III): From photophysics to photofunctional materials and probes, *Coord. Chem. Rev.*, 2020, **414**, 213298.

61 Q. Zhao, F. Li and C. Huang, Phosphorescent chemosensors based on heavy-metal complexes, *Chem. Soc. Rev.*, 2010, **39**, 3007–3030.

62 Q. Zhao, H. Huang and F. Li, Phosphorescent heavy-metal complexes for bioimaging, *Chem. Soc. Rev.*, 2011, **40**, 2508–2524.

63 G. S. He, L.-S. Tan, Q. Zheng and P. N. Prasad, Multiphoton Absorbing Materials: Molecular Designs, Characterizations, and Applications, *Chem. Rev.*, 2008, **108**, 1245–1330.

64 B. Liu, Z. Tian, F. Dang, J. Zhao, X. Yan, X. Xu, X. Yang, G. Zhou and Y. Wu, Photophysical and optical power limiting behaviors of Au(I) acetylides with diethynyl aromatic ligands showing different electronic features, *J. Organomet. Chem.*, 2016, **804**, 80–86.

65 S. Cekli, R. W. Winkel, E. Alarousu, O. F. Mohammed and K. S. Schanze, Triplet excited state properties in variable gap π-conjugated donor-Acceptor-donor chromophores, *Chem.*

*Sci.*, 2016, **7**, 3621–3631.

66 S. Goswami, G. Wicks, A. Rebane and K. S. Schanze, Photophysics and non-linear absorption of Au(i) and Pt(ii) acetylide complexes of a thienyl-carbazole chromophore, *Dalt. Trans.*, 2014, **43**, 17721–17728.

67 S. Goswami, R. W. Winkel and K. S. Schanze, Photophysics and Nonlinear Absorption of Gold(I) and Platinum(II) Donor-Acceptor-Donor Chromophores, *Inorg. Chem.*, 2015, **54**, 10007–10014.

68 R. Vestberg, R. Westlund, A. Eriksson, C. Lopes, M. Carlsson, B. Eliasson, E. Glimsdal, M. Lindgren and E. Malmström, Dendron decorated platinum(II) acetylides for optical power limiting, *Macromolecules*, 2006, **39**, 2238–2246.

69 W. Wu, C. Cheng, W. Wu, H. Guo, S. Ji, P. Song, K. Han, J. Zhao, X. Zhang, Y. Wu and G. Du, Tuning the emission colour of triphenylamine-capped cyclometallated platinum(II) complexes and their application in luminescent oxygen sensing and organic light-emitting diodes, *Eur. J. Inorg. Chem.*, 2010, 4683–4696.

70 R. Westlund, E. Malmström, C. Lopes, J. Öhgren, T. Rodgers, Y. Saito, S. Kawata, E. Glimsdal and M. Lindgren, Efficient nonlinear absorbing platinum(II) acetylide chrompphores in solid PMMA matrices, *Adv. Funct. Mater.*, 2008, **18**, 1939–1948.

71 T. M. Cooper, D. M. Krein, A. R. Burke, D. G. McLean, J. E. Rogers and J. E. Slagle, Asymmetry in platinum acetylide complexes: Confinement of the triplet exciton to the lowest energy ligand, *J. Phys. Chem. A*, 2006, **110**, 13370–13378.

72 J. E. Rogers, J. E. Slagle, D. M. Krein, A. R. Burke, B. C. Hall, A. Fratini, D. G. McLean, P. A. Fleitz, T. M. Cooper, M. Drobizhev, N. S. Makarov, A. Rebane, K. Y. Kim, R. Farley and K. S. Schanze, Platinum acetylide two-photon chromophores, *Inorg. Chem.*, 2007, **46**, 6483–6494.

73 K. D. Belfield, M. V. Bondar, F. E. Hernandez and O. V. Przhonska, Photophysical characterization, two-photon absorption and optical power limiting of two fluorenylperylene diimides, *J. Phys. Chem. C*, 2008, **112**, 5618–5622.

74 K. Y. Kim, A. H. Shelton, M. Drobizhev, N. Makarov, A. Rebane and K. S. Schanze, Optimizing simultaneous two-photon absorption and transient triplet-triplet absorption in platinum acetylide chromophores, *J. Phys. Chem. A*, 2010, **114**, 7003–7013.

75 E. Glimsdal, M. Carlsson, B. Eliasson, B. Minaev and M. Lindgren, Excited states and two-photon absorption of some novel thiophenyl Pt(II)-ethynyl derivatives, *J. Phys. Chem. A*, 2007, **111**, 244–250.

76 J. Kalinowski, V. Fattori, M. Cocchi and J. A. G. Williams, Light-emitting devices based on organometallic platinum complexes as emitters, *Coord. Chem. Rev.*, 2011, **255**, 2401–2425.

77 K. M. Wong, X. Zhu, L. Hung, N. Zhu, V. W. Yam and H. Kwok, A novel class of phosphorescent gold ( III ) alkynyl-based organic light-emitting devices with tunable colour, 2005, **2**, 2906–2908.

78 V. W. Yam, Bipolar Gold(III) Complexes for Solution-Processable Organic Light-Emitting Devices with a Small E ffi ciency Roll-O ff, 2014, 17861–17868.

79 L. Li, M. Tang, W. Cheung, S. Lai, M. Ng, C. K. Chan, M. Chan and V. W. Yam, Rational Design Strategy for the Realization of Red- to Near- Infrared-Emitting Alkynylgold(III) Complexes and Their Applications in Solution-Processable Organic Light-Emitting Devices, , DOI:10.1021/acs.chemmater.9b01208.

80 C. H. Lee, M. C. Tang, W. L. Cheung, S. L. Lai, M. Y. Chan and V. W. W. Yam, Highly luminescent phosphine oxide-containing bipolar alkynylgold(iii) complexes for solution-processable organic light-emitting devices with small efficiency roll-offs, *Chem. Sci.*, 2018, **9**, 6228–6232.

81 V. K. M. Au, K. M. C. Wong, D. P. K. Tsang, M. Y. Chan, N. Zhu and V. W. W. Yam, High-efficiency green organic light-emitting devices utilizing phosphorescent bis-cyclometalated alkynylgold(III) complexes, *J. Am. Chem. Soc.*, 2010, **132**, 14273–14278.

82 M. C. Tang, D. P. K. Tsang, Y. C. Wong, M. Y. Chan, K. M. C. Wong and V. W. W. Yam, Bipolar gold(III) complexes for solution-processable organic light-emitting devices with a small efficiency roll-off, *J. Am. Chem. Soc.*, 2014, **136**, 17861–17868.

83 M. Tang, C. Lee, S. Lai, M. Ng, M. Chan and V. W. Yam, Versatile Design Strategy for Highly Luminescent Vacuum-Evaporable and Solution-Processable Tridentate Gold(III) Complexes with Monoaryl Auxiliary Ligands and Their Applications for Phosphorescent Organic Light Emitting Devices, *J. Am. Chem. Soc.*, 2017, **139**, 9341–9349.

84 M. C. Tang, D. P. K. Tsang, M. M. Y. Chan, K. M. C. Wong and V. W. W. Yam,

Dendritic luminescent gold(III) complexes for highly efficient solution-processable organic light-emitting devices, *Angew. Chemie - Int. Ed.*, 2013, **52**, 446–449.

85 D. Zhou, W. P. To, G. S. M. Tong, G. Cheng, L. Du, D. L. Phillips and C. M. Che, Tetradentate Gold(III) Complexes as Thermally Activated Delayed Fluorescence (TADF) Emitters: Microwave-Assisted Synthesis and High-Performance OLEDs with Long Operational Lifetime, *Angew. Chemie - Int. Ed.*, 2020, **59**, 6375–6382.

86 C. H. Lee, M. C. Tang, F. K. W. Kong, W. L. Cheung, M. Ng, M. Y. Chan and V. W. W. Yam, Isomeric Tetradentate Ligand-Containing Cyclometalated Gold(III) Complexes, *J. Am. Chem. Soc.*, 2020, **142**, 520–529.

87 M. Y. Leung, M. C. Tang, W. L. Cheung, S. L. Lai, M. Ng, M. Y. Chan and V. Wing-Wah Yam, Thermally Stimulated Delayed Phosphorescence (TSDP)-Based Gold(III) Complexes of Tridentate Pyrazine-Containing Pincer Ligand with Wide Emission Color Tunability and Their Application in Organic Light-Emitting Devices, *J. Am. Chem. Soc.*, 2020, **142**, 2448–2459.

88 D. V. Partyka, A. J. Esswein, M. Zeller, A. D. Hunter and T. G. Gray, Gold(I) pyrenyls: Excited-state consequences of carbon-gold bond formation, *Organometallics*, 2007, **26**, 3279–3282.

89 L. Gao, M. A. Peay, D. V. Partyka, J. B. Updegraff, T. S. Teets, A. J. Esswein, M. Zeller, A. D. Hunter and T. G. Gray, Mono- and di-gold(I) naphthalenes and pyrenes: Syntheses, crystal structures, and photophysics, *Organometallics*, 2009, **28**, 5669–5681.

90 Y. Dong, J. Zhang, A. Li, J. Gong, B. He, S. Xu, J. Yin, S. H. Liu and B. Z. Tang, Structure-tuned and thermodynamically controlled mechanochromic self-recovery of AIE-active Au( i ) complexes , *J. Mater. Chem. C*, 2020, 894–899.

91 I. D. Strelnik, V. V. Sizov, V. V. Gurzhiy, A. S. Melnikov, I. E. Kolesnikov, E. I. Musina, A. A. Karasik and E. V. Grachova, Binuclear Gold(I) Phosphine Alkynyl Complexes Templated on a Flexible Cyclic Phosphine Ligand: Synthesis and Some Features of Solid-State Luminescence, *Inorg. Chem.*, 2019, **59**, 244–253.

92 T. Seki, K. Kashiyama and H. Ito, Luminescent mechanochromism of gold N - heterocyclic carbene complexes with hypso- and bathochromic spectral shifts, *Dalt. Trans.*, 2019, **48**, 7105–7109.

93 N. M. W. Wu, M. Ng and V. W. W. Yam, Photochromic Benzo[b]phosphole Alkynylgold(I) Complexes with Mechanochromic Property to Serve as Multistimuli-Responsive Materials, *Angew. Chemie - Int. Ed.*, 2019, **58**, 3027–3031.

94 V. Fernández-Moreira, C. Val-Campillo, I. Ospino, R. P. Herrera, I. Marzo, A. Laguna and M. C. Gimeno, Bioactive and luminescent indole and isatin based gold(i) derivatives, *Dalt. Trans.*, 2019, **48**, 3098–3108.

95 E. Y. H. Hong and V. W. W. Yam, Triindole-tris-alkynyl-bridged trinuclear gold(I) complexes for cooperative supramolecular self-assembly and small-molecule solution-processable resistive memories, *ACS Appl. Mater. Interfaces*, 2017, **9**, 2616–2624.

96 M. C. Blanco, J. Cámara, V. Fernández-Moreira, A. Laguna and M. C. Gimeno, Gold(I), Phosphanes, and Alkynyls: The Perfect Allies in the Search for Luminescent Compounds, *Eur. J. Inorg. Chem.*, 2018, **2018**, 2762–2767.

97 J. J. González, E. Ortega, M. Rothemund, M. Gold, C. Vicente, C. De Haro, D. Bautista, R. Schobert and J. Ruiz, Luminescent Gold(I) Complexes of 1-Pyridyl-3-anthracenylchalcone Inducing Apoptosis in Colon Carcinoma Cells and Antivascular Effects, *Inorg. Chem.*, 2019, **58**, 12954–12963.

98 M. Głodek, S. Pawlędzio, A. Makal and D. Plażuk, The Impact of Crystal Packing and Aurophilic Interactions on the Luminescence Properties in Polymorphs and Solvate of Aroylacetylide–Gold(I) Complexes, *Chem. - A Eur. J.*, 2019, **25**, 13131–13145.

99 K. T. Chan, G. S. M. Tong, W. P. To, C. Yang, L. Du, D. L. Phillips and C. M. Che, The interplay between fluorescence and phosphorescence with luminescent gold(i) and gold(iii) complexes bearing heterocyclic arylacetylide ligands, *Chem. Sci.*, 2017, **8**, 2352–2364.

100 Montalti, A. Credi, L. Prodi and M. Teresa Gandolfi, *Handbook of Photochemistry, Third Edition*, CRC Press, 3rd Editio., 2006.

101 V. W. W. Yam, S. W. K. Choi and K. K. Cheung, Synthesis, photophysics and thermal redox reactions of a [{Au(dppn)Cl}2]2+ dimer with an unsupported AuII-AuII bond, *Chem. Commun.*, 1996, **3**, 1173–1174.

102 V. W. W. Yam, S. W. K. Choi and K. K. Cheung, Synthesis and design of novel tetranuclear and dinuclear gold(I) phosphine acetylide complexes. First X-ray crystal

structures of a tetranuclear ([Au4(tppb)(C≡CPh)4]) and a related dinuclear ([Au2(dppb)(C≡CPh)2]) complex, *Organometallics*, 1996, **15**, 1734–1739.

103 V. W. W. Yam, Luminescent coinage metal clusters of acetylides and chalcogenides, *J. Photochem. Photobiol. A Chem.*, 1997, **106**, 75–84.

104 V. W. W. Yam, C. K. Li and C. L. Chan, Proof of potassium ions by luminescence signaling based on weak gold - Gold interactions in dinuclear gold(I) complexes, *Angew. Chemie - Int. Ed.*, 1998, **37**, 2857–2859.

105 V. W. W. Yam and K. K. W. Lo, Luminescent polynuclear d10 metal complexes, *Chem. Soc. Rev.*, 1999, **28**, 323–334.

106 V. W. W. Yam, K. K. W. Lo and K. M. C. Wong, Luminescent polynuclear metal acetylides, *J. Organomet. Chem.*, 1999, **578**, 3–30.

107 B. C. Tzeng, K. K. Cheung and C. M. Che, Photoluminescent two-dimensional gold(I) polymers bearing a macrocyclic tetraaza cavity, *Chem. Commun.*, 1996, **0**, 1681–1682.

108 B. Tzeng and S. Pengb, Gl Y, 1996, 181–182.

109 B. C. Tzeng, C. M. Che and S. M. Peng, Luminescent gold(I) supermolecules with trithiocyanuric acid. Crystal structure, spectroscopic and photophysical properties, *Chem. Commun.*, 1997, **130**, 1771–1772.

110 Y. Ma, C. M. Che, H. Y. Chao, X. Zhou, W. H. Chan and J. Shen, High luminescence gold(I) and copper(I) complexes with a triplet excited state for use in light-emitting diodes, *Adv. Mater.*, 1999, **11**, 852–857.

111 K. H. Leung, D. L. Phillips, M. C. Tse, C. M. Che and V. M. Miskowski, Resonance raman investigation of the Au(I) - Au(I) interaction of the 1[dσ*pσ] Excited state of Au2(dcpm)2(ClO4)2 (dcpm = bis(dicyclohexylphosphine)methane), *J. Am. Chem. Soc.*, 1999, **121**, 4799–4803.

112 W. F. Fu, K. C. Chan, K. K. Cheung and C. M. Che, Substrate-binding reactions of the 3[dσ*pσ] excited state of binuclear gold(I) complexes with bridging bis(dicyclohexylphosphino)methane ligands: Emission and time-resolved absorption spectroscopic studies, *Chem. - A Eur. J.*, 2001, **7**, 4656–4664.

112 C. M. Che, H. Y. Chao, V. M. Miskowski, Y. Li and K. K. Cheung, Luminescent μ-ethynediyl and μ-butadiynediyl binuclear gold(I) complexes: Observation of 3(ππ*) emissions from bridging Cn2- units, *J. Am. Chem. Soc.*, 2001, **123**, 4985–4991.

114 W. Lu, H. F. Xiang, N. Zhu and C. M. Che, The 3(ππ*) Emission of Cy3PAu(C≡C)nAuPCy3 (n = 3, 4). Effect of chain length upon acetylenic 3(ππ*) emission, *Organometallics*, 2002, **21**, 2343–2346.

115 W. Lu, N. Zhu and C. M. Che, Polymorphic Forms of a Gold(I) Arylacetylide Complex with Contrasting Phosphorescent Characteristics, *J. Am. Chem. Soc.*, 2003, **125**, 16081–16088.

116 B. H. Xia, H. X. Zhang, C. M. Che, K. H. Leung, D. L. Phillips, N. Zhu and Z. Y. Zhou, Metal-metal interactions in heterobimetallic d8-d10 complexes. Structures and spectroscopic investigation of [M′M″(μ-dcpm)2(CN)2]+ (M′ = Pt, Pd; M″ = Cu, Ag, Au) and related complexes by UV-vis absorption and resonance Raman spectroscopy and ab initio calculations, *J. Am. Chem. Soc.*, 2003, **125**, 10362–10374.

117 T. Zou, C. T. Lum, C. N. Lok, W. P. To, K. H. Low and C. M. Che, A binuclear gold(I) complex with mixed bridging diphosphine and bis(N-heterocyclic carbene) ligands shows favorable thiol reactivity and inhibits tumor growth and angiogenesis in vivo, *Angew. Chemie - Int. Ed.*, 2014, **53**, 5810–5814.

118 X. S. Xiao, C. Zou, X. Guan, C. Yang, W. Lu and C. M. Che, Homoleptic gold(i) N-heterocyclic allenylidene complexes: Excited-state properties and lyotropic chromonics, *Chem. Commun.*, 2016, **52**, 4983–4986.

119 E. C. C. Cheng, K. H. Leung, V. M. Miskowski, V. W. W. Yam and D. L. Phillips, Electronic and resonance Raman spectra of [Au2(CS3)2]2-. Spectroscopic properties of a 'short' Au(I)-Au(I) bond, *Inorg. Chem.*, 2000, **39**, 3690–3695.

120 V. W. W. Yam, C. K. Li, C. L. Chan and K. K. Cheung, Synthesis, structural characterization, and photophysics of dinuclear gold(II) complexes [{Au(dppn)Br}2](PF6)2 and [{Au(dppn)I}2](PF6)2 with an unsupported AuII-AuII bond, *Inorg. Chem.*, 2001, **40**, 7054–7058.

121 V. W. W. Yam and E. C. C. Cheng, Design of luminescent sulfur-containing polynuclear gold(I) complexes for advanced nanomaterials and chemosensors, *Gold Bull.*, 2001, **34**, 20–23.

122 V. W. W. Yam, Molecular design of transition metal alkynyl complexes as building blocks for luminescent metal-based materials: Structural and photophysical aspects, *Acc. Chem. Res.*, 2002, **35**, 555–563.

123 V. W. W. Yam, K. L. Cheung, S. K. Yip and K. K. Cheung, Synthesis, characterization, structure and luminescence studies of mono-, di- and trinuclear gold(I) phosphine alkynyl complexes, *J. Organomet. Chem.*, 2003, **681**, 196–209.

124 V. W. W. Yam, S. K. Yip, L. H. Yuan, K. L. Cheung, N. Zhu and K. K. Cheung, Synthesis, structure, and ion-binding properties of luminescent gold(I) alkynylcalix[4]crown-5 complexes, *Organometallics*, 2003, **22**, 2630–2637.

125 C. K. Li, X. X. Lu, K. M. C. Wong, C. L. Chan, N. Zhu and V. W. W. Yam, Molecular design of luminescence ion probes for various cations based on weak gold(I)···gold(I) interactions in dinuclear gold(I) complexes, *Inorg. Chem.*, 2004, **43**, 7421–7430.

126 V. W. W. Yam, Luminescent metal alkynyls - From simple molecules to molecular rods and materials, *J. Organomet. Chem.*, 2004, **689**, 1393–1401.

127 H. S. Tang, N. Zhu and V. W. W. Yam, Tetranuclear macrocyclic gold(I) alkynyl phosphine complex containing azobenzene functionalities: A dual-input molecular logic with photoswitching behavior controllable via silver(I) coordination/decoordination, *Organometallics*, 2007, **26**, 22–25.

128 X. He, F. Herranz, E. C. C. Cheng, R. Vilar and V. W. W. Yam, Design, synthesis, photophysics, and anion-binding studies of bis(dicyclohexylphosphino)methane-containing dinuclear gold(I) thiolate complexes with urea receptors, *Chem. - A Eur. J.*, 2010, **16**, 9123–9131.

129 X. He and V. W. W. Yam, Design, synthesis, photophysics, and ion-binding studies of a ditopic receptor based on goid(i) phosphine thiolate complex functionalized with crown ether and urea binding units, *Inorg. Chem.*, 2010, **49**, 2273–2279.

130 X. He and V. W. W. Yam, Luminescent gold(I) complexes for chemosensing, *Coord. Chem. Rev.*, 2011, **255**, 2111–2123.

131 E. Y. H. Hong, H. L. Wong and V. W. W. Yam, From spherical to leaf-like morphologies: Tunable supramolecular assembly of alkynylgold(I) complexes through variations of the alkyl chain length, *Chem. - A Eur. J.*, 2015, **21**, 5732–5735.

132 F. K. W. Hau and V. W. W. Yam, Synthesis and cation-binding studies of gold(i) complexes bearing oligoether isocyanide ligands with ester and amide as linkers, *Dalt. Trans.*, 2015, **45**, 300–306.

133 F. C. M. Leung and V. W. W. Yam, Cation- and Solvent-Induced Supramolecular

Aggregation Studies of Crown Ether-Containing Dinuclear Alkynylgold(I) Isocyanide Complexes, *Eur. J. Inorg. Chem.*, 2017, **2017**, 5271–5278.

134 A. Chu, F. K. W. Hau and V. W. W. Yam, AuI···AuI Interaction Assisted Host–Guest Interactions and Stimuli-Responsive Self-Assembly in Tetranuclear Alkynylgold(I) Calix[4]arene-Based Isocyanide Complexes, *Chem. - A Eur. J.*, 2017, **23**, 11076–11084.

135 E. Y. H. Hong and V. W. W. Yam, Triindole-tris-alkynyl-bridged trinuclear gold(I) complexes for cooperative supramolecular self-assembly and small-molecule solution-processable resistive memories, *ACS Appl. Mater. Interfaces*, 2017, **9**, 2616–2624.

136 F. C. M. Leung and V. W. W. Yam, Photophysical and ion-binding studies of a tetranuclear alkynylgold(I) isonitrile complex, *J. Photochem. Photobiol. A Chem.*, 2018, **355**, 212–219.

137 A. Chu, F. K.-W. Hau, L.-Y. Yao and V. W.-W. Yam, Decanuclear Gold(I) Sulfido Pseudopolymorphs Displaying Stimuli-Responsive RGBY Luminescence Changes, *ACS Mater. Lett.*, 2019, **1**, 277–284.

138 N. M. W. Wu, M. Ng and V. W. W. Yam, Photochromic Benzo[b]phosphole Alkynylgold(I) Complexes with Mechanochromic Property to Serve as Multistimuli-Responsive Materials, *Angew. Chemie - Int. Ed.*, 2019, **58**, 3027–3031.

139 J. E. Heckler, N. Deligonul, A. L. Rheingold and T. G. Gray, Gold(i) triazolyls: Organometallic synthesis in air and aqueous media, *Chem. Commun.*, 2013, **49**, 5990–5992.

140 R. A. Vogt, T. G. Gray and C. E. Crespo-Hernández, Subpicosecond intersystem crossing in mono- and Di(organophosphine)gold(I) naphthalene derivatives in solution, *J. Am. Chem. Soc.*, 2012, **134**, 14808–14817.

141 L. Gao, D. S. Niedzwiecki, N. Deligonul, M. Zeller, A. D. Hunter and T. G. Gray, Gold(I) styrylbenzene, distyrylbenzene, and distyrylnaphthalene complexes: High emission quantum yields at room temperature, *Chem. - A Eur. J.*, 2012, **18**, 6316–6327.

142 D. V. Partyka, T. S. Teets, M. Zeller, J. B. Updegraff, A. D. Hunter and T. G. Gray, Constrained digold(I) diaryls: Syntheses, crystal structures, and photophysics, *Chem. - A Eur. J.*, 2012, **18**, 2100–2112.

143 R. A. Vogt, M. A. Peay, T. G. Gray and C. E. Crespo-Hernández, Excited-state dynamics of (Organophosphine)gold(I) pyrenyl isomers, *J. Phys. Chem. Lett.*, 2010, **1**, 1205–1211.

144 D. V. Partyka, L. Gao, T. S. Teets, J. B. Updegraff, N. Deligonul and T. G. Gray, Copper-catalyzed huisgen [3 + 2] cycloaddition of gold(I) alkynyls with benzyl azide. Syntheses, structures, and optical properties, *Organometallics*, 2009, **28**, 6171–6182.

145 L. Gao, M. A. Peay, D. V. Partyka, J. B. Updegraff, T. S. Teets, A. J. Esswein, M. Zeller, A. D. Hunter and T. G. Gray, Mono- and di-gold(I) naphthalenes and pyrenes: Syntheses, crystal structures, and photophysics, *Organometallics*, 2009, **28**, 5669–5681.

146 T. J. Robilotto, N. Deligonul, J. B. Updegraff and T. G. Gray, Azido, triazolyl, and alkynyl complexes of gold(I): Syntheses, structures, and ligand effects, *Inorg. Chem.*, 2013, **52**, 9659–9668.

147 K. T. Chan, G. S. M. Tong, W. P. To, C. Yang, L. Du, D. L. Phillips and C. M. Che, The interplay between fluorescence and phosphorescence with luminescent gold(i) and gold(iii) complexes bearing heterocyclic arylacetylide ligands, *Chem. Sci.*, 2017, **8**, 2352–2364.

148 S. Goswami, R. W. Winkel and K. S. Schanze, Photophysics and Nonlinear Absorption of Gold(I) and Platinum(II) Donor-Acceptor-Donor Chromophores, *Inorg. Chem.*, 2015, **54**, 10007–10014.

149 G. J. Zhou and W. Y. Wong, Organometallic acetylides of PtII, AuI and Hg II as new generation optical power limiting materials, *Chem. Soc. Rev.*, 2011, **40**, 2541–2566.

150 Y. Lin, C. Jiang, F. Hu, J. Yin, G. A. Yu and S. H. Liu, Synthesis, characterization, and properties of some bisacetylide and binuclear acetylide gold(I) compounds based on the photochromic dithienylethene unit, *Dye. Pigment.*, 2013, **99**, 995–1003.

151 B. Liu, Z. Tian, F. Dang, J. Zhao, X. Yan, X. Xu, X. Yang, G. Zhou and Y. Wu, Photophysical and optical power limiting behaviors of Au(I) acetylides with diethynyl aromatic ligands showing different electronic features, *J. Organomet. Chem.*, 2016, **804**, 80–86.

152 P. J. Conaghan, C. S. B. Matthews, F. Chotard, S. T. E. Jones, N. C. Greenham, M. Bochmann, D. Credgington and A. S. Romanov, Highly efficient blue organic light-emitting diodes based on carbene-metal-amides, *Nat. Commun.*, 2020, **11**, 1–8.

153 R. Hamze, S. Shi, S. C. Kapper, D. S. M. Ravinson, L. Estergreen, M. C. Jung, A. C. Tadle, R. Haiges, P. I. Djurovich, J. L. Peltier, R. Jazzar, G. Bertrand, S. E. Bradforth and M. E. Thompson, 'Quick-Silver' from a Systematic Study of Highly Luminescent, Two-

Coordinate, d10 Coinage Metal Complexes, *J. Am. Chem. Soc.*, 2019, **141**, 8616–8626.

154 A. S. Romanov, S. T. E. Jones, Q. Gu, P. J. Conaghan, B. H. Drummond, J. Feng, F. Chotard, L. Buizza, M. Foley, M. Linnolahti, D. Credgington and M. Bochmann, Carbene metal amide photoemitters: Tailoring conformationally flexible amides for full color range emissions including white-emitting OLED, *Chem. Sci.*, 2020, **11**, 435–446.

155 C. R. Hall, A. S. Romanov, M. Bochmann and S. R. Meech, Ultrafast Structure and Dynamics in the Thermally Activated Delayed Fluorescence of a Carbene-Metal-Amide, *J. Phys. Chem. Lett.*, 2018, **9**, 5873–5876.

156 D. Di, A. S. Romanov, L. Yang, J. M. Richter, J. P. H. Rivett, S. Jones, T. H. Thomas, M. A. Jalebi, R. H. Friend, M. Linnolahti, M. Bochmann and D. Credgington, High-performance light-emitting diodes based on carbene-metal-amides, 2017, **163**, 159–163.

157 T. Y. Li, D. S. Muthiah Ravinson, R. Haiges, P. I. Djurovich and M. E. Thompson, Enhancement of the Luminescent Efficiency in Carbene-Au(I)-Aryl Complexes by the Restriction of Renner-Teller Distortion and Bond Rotation, *J. Am. Chem. Soc.*, 2020, **142**, 6158–6172.

158 C. C. Beto, C. J. Zeman, Y. Yang, J. D. Bullock, E. D. Holt, A. Q. Kane, T. A. Makal, X. Yang, I. Ghiviriga, K. S. Schanze and A. S. Veige, An Application Exploiting Aurophilic Bonding and iClick to Produce White Light Emitting Materials, *Inorg. Chem.*, 2020, **59**, 1893–1904.

159 C. J. Zeman, Y.-H. Shen, J. K. Heller, K. A. Abboud, K. S. Schanze and A. S. Veige, Excited-State Turn-On of Aurophilicity and Tunability of Relativistic Effects in a Series of Digold Triazolates Synthesized via iClick, *J. Am. Chem. Soc.*, 2020, **142**, 8331–8341.

160 (a) J. E. Rogers, J. E. Slagle, D. M. Krein, A. R. Burke, B. C. Hall, A. Fratini, D. G. McLean, P. A. Fleitz, T. M. Cooper, M. Drobizhev, N. S. Makarov, A. Rebane, K. Y. Kim, R. Farley and K. S. Schanze, Platinum acetylide two-photon chromophores, *Inorg. Chem.*, 2007, **46**, 6483–6494.(b) J. E. Rogers, J. E. Slagle, D. G. McLean, R. L. Sutherland, M. C. Brant, J. Heinrichs, R. Jakubiak, R. Kannan, L. S. Tan and P. A. Fleitz, Insight into the nonlinear absorbance of two related series of two-photon absorbing chromophores, *J. Phys. Chem. A*, 2007, **111**, 1899–1906.

161 D. V Partyka, T. J. Robilotto, M. Zeller, A. D. Hunter and T. G. Gray, Dialkylbiarylphosphine Complexes of Gold(I) Halides. Gold−Aryl π-Interactions in the

Solid State, *Organometallics*, 2008, **27**, 28–32.;

162 J. J. Mihaly, D. J. Stewart, T. A. Grusenmeyer, A. T. Phillips, J. E. Haley, M. Zeller and T. G. Gray, Photophysical properties of organogold(i) complexes bearing a benzothiazole-2,7-fluorenyl moiety: Selection of ancillary ligand influences white light emission, *Dalt. Trans.*, 2019, **48**, 15917–15927.

163 Gaussian 16, Revision A.03, M. J. Frisch, G. W. Trucks, H. B. Schlegel, G. E. Scuseria, M. A. Robb, J. R. Cheeseman, G. Scalmani, V. Barone, G. A. Petersson, H. Nakatsuji, X. Li, M. Caricato, A. V Marenich, J. Bloino, B. G. Janesko, R. Gomperts, B. Mennucci, H. P. Hratchian, J. V Ortiz, A. F. Izmaylov, J. L. Sonnenberg, D. Williams-Young, F. Ding, F. Lipparini, F. Egidi, J. Goings, B. Peng, A. Petrone, T. Henderson, D. Ranasinghe, V. G. Zakrzewski, J. Gao, N. Rega, G. Zheng, W. Liang, M. Hada, M. Ehara, K. Toyota, R. Fukuda, J. Hasegawa, M. Ishida, T. Nakajima, Y. Honda, O. Kitao, H. Nakai, T. Vreven, K. Throssell, J. A. Montgomery Jr., J. E. Peralta, F. Ogliaro, M. J. Bearpark, J. J. Heyd, E. N. Brothers, K. N. Kudin, V. N. Staroverov, T. A. Keith, R. Kobayashi, J. Normand, K. Raghavachari, A. P. Rendell, J. C. Burant, S. S. Iyengar, J. Tomasi, M. Cossi, J. M. Millam, M. Klene, C. Adamo, R. Cammi, J. W. Ochterski, R. L. Martin, K. Morokuma, O. Farkas, J. B. Foresman and D. J. Fox, Gaussian, Inc., Wallingford CT, 2016.

164 M. Dolg, U. Wedig, H. Stoll and H. Preuss, Energy-adjusted ab initio pseudopotentials for the first row transition elements, *J. Chem. Phys.*, 1987, **86**, 866–872.

165 J. P. Perdew, K. Burke and M. Ernzerhof, Generalized Gradient Approximation Made Simple, *Phys. Rev. Lett.*, 1996, **77**, 3865–3868.

166 N. Godbout, D. R. Salahub, J. Andzelm and E. Wimmer, Optimization of Gaussian-type basis sets for local spin density functional calculations. Part I. Boron through neon, optimization technique and validation, *Can. J. Chem.*, 1992, **70**, 560–571.

167 S. Miertuš, E. Scrocco and J. Tomasi, Electrostatic interaction of a solute with a continuum. A direct utilizaion of AB initio molecular potentials for the prevision of solvent effects, *Chem. Phys.*, 1981, **55**, 117–129.

168 J. Tomasi, B. Mennucci and R. Cammi, Quantum Mechanical Continuum Solvation Models, *Chem. Rev.*, 2005, **105**, 2999–3094.

169 E. Cancès, B. Mennucci and J. Tomasi, A new integral equation formalism for the polarizable continuum model: Theoretical background and applications to isotropic and

anisotropic dielectrics, *J. Chem. Phys.*, 1997, **107**, 3032–3041.

170 B. Mennucci, E. Cancès and J. Tomasi, Evaluation of Solvent Effects in Isotropic and Anisotropic Dielectrics and in Ionic Solutions with a Unified Integral Equation Method: Theoretical Bases, Computational Implementation, and Numerical Applications, *J. Phys. Chem. B*, 1997, **101**, 10506–10517.

171 S. I. Gorelsky and A. B. P. Lever, Electronic structure and spectra of ruthenium diimine complexes by density functional theory and INDO/S. Comparison of the two methods, *J. Organomet. Chem.*, 2001, **635**, 187–196.

172 S. I. Gorelsky, AOMix: Program for Molecular Orbital Analysis, http://www.sg-chem.net.

173 L. Gao, D. V. Partyka, J. B. Updegraff, N. Deligonul and T. G. Gray, Synthesis, structures, and excited-state geometries of alkynylgold(I) complexes, *Eur. J. Inorg. Chem.*, 2009, **2009**, 2711–2719.

174 G. M. Sheldrick, A short history of SHELX, *Acta Crystallogr. Sect. A*, 2008, **64**, 112–122.

175 G. M. Sheldrick, Crystal structure refinement with SHELXL, *Acta Crystallogr. Sect. C*, 2015, **71**, 3–8.

176 C. B. Hübschle, G. M. Sheldrick and B. Dittrich, ShelXle: a Qt graphical user interface for SHELXL, *J. Appl. Crystallogr.*, 2011, **44**, 1281–1284.

177 L. Krause, R. Herbst-Irmer, G. M. Sheldrick and D. Stalke, Comparison of silver and molybdenum microfocus X-ray sources for single-crystal structure determination, *J. Appl. Crystallogr.*, 2015, **48**, 3–10.

178 S. Parsons, H. D. Flack and T. Wagner, Use of intensity quotients and differences in absolute structure refinement, *Acta Crystallogr. Sect. B*, 2013, **69**, 249–259.

179 J. J. Mihaly, A. T. Phillips, J. T. Malloy, Z. M. Marsh, M. Zeller, J. E. Haley, K. De La Harpe, T. A. Grusenmeyer and T. G. Gray, Synthesis and Photophysical Properties of Laterally Asymmetric Digold(I) Alkynyls and Triazolyl: Ancillary Ligand and Organic Functionality Dictate Excited-State Dynamics, *Organometallics*, 2020, **39**, 489–494.

180 J. E. Heckler, N. Deligonul, A. L. Rheingold and T. G. Gray, Gold(i) triazolyls: Organometallic synthesis in air and aqueous media, *Chem. Commun.*, 2013, **49**, 5990–5992.; L. Gao, D. V. Partyka, J. B. Updegraff, N. Deligonul and T. G. Gray, Synthesis, structures, and excited-state geometries of alkynylgold(I) complexes, *Eur. J. Inorg.*

*Chem.*, 2009, **2009**, 2711–2719.

181 J. J. Mihaly, A. T. Phillips, D. J. Stewart, Z. M. Marsh, C. L. McCleese, J. E. Haley, M. Zeller, T. A. Grusenmeyer and T. G. Gray, Synthesis and photophysics of gold( i ) alkynyls bearing a benzothiazole-2,7-fluorenyl moiety: a comparative study analyzing influence of ancillary ligand, bridging moiety, and number of metal centers on photophysical properties , *Phys. Chem. Chem. Phys.*, 2020, 11915–11927.

182 M. C. Tang, W. K. Kwok, S. L. Lai, W. L. Cheung, M. Y. Chan and V. Wing-Wah Yam, Rational molecular design for realizing high performance sky-blue-emitting gold(iii) complexes with monoaryl auxiliary ligands and their applications for both solution-processable and vacuum-deposited organic light-emitting devices, *Chem. Sci.*, 2019, **10**, 594–605.

183 V. K. M. Au, K. M. C. Wong, D. P. K. Tsang, M. Y. Chan, N. Zhu and V. W. W. Yam, High-efficiency green organic light-emitting devices utilizing phosphorescent bis-cyclometalated alkynylgold(III) complexes, *J. Am. Chem. Soc.*, 2010, **132**, 14273–14278.

184 S. Jürgens, V. Scalcon, N. Estrada-Ortiz, A. Folda, F. Tonolo, C. Jandl, D. L. Browne, M. P. Rigobello, F. E. Kühn and A. Casini, Exploring the C^N^C theme: Synthesis and biological properties of tridentate cyclometalated gold(III) complexes, *Bioorg. Med. Chem.*, 2017, **25**, 5452–5460.

185 K. M. Wong, X. Zhu, L. Hung, N. Zhu, V. W. Yam and H. Kwok, A novel class of phosphorescent gold ( III ) alkynyl-based organic light-emitting devices with tunable colour, 2005, **2**, 2906–2908.

185 V. W. Yam, Bipolar Gold(III) Complexes for Solution-Processable Organic Light-Emitting Devices with a Small E ffi ciency Roll-O ff, 2014, 17861–17868.

186 L. Li, M. Tang, W. Cheung, S. Lai, M. Ng, C. K. Chan, M. Chan and V. W. Yam, Rational Design Strategy for the Realization of Red- to Near- Infrared-Emitting Alkynylgold(III) Complexes and Their Applications in Solution-Processable Organic Light-Emitting Devices, , DOI:10.1021/acs.chemmater.9b01208.

187 C. H. Lee, M. C. Tang, W. L. Cheung, S. L. Lai, M. Y. Chan and V. W. W. Yam, Highly luminescent phosphine oxide-containing bipolar alkynylgold(iii) complexes for solution-processable organic light-emitting devices with small efficiency roll-offs, *Chem. Sci.*, 2018, **9**, 6228–6232.

188 V. K. M. Au, K. M. C. Wong, D. P. K. Tsang, M. Y. Chan, N. Zhu and V. W. W. Yam, High-efficiency green organic light-emitting devices utilizing phosphorescent bis-cyclometalated alkynylgold(III) complexes, *J. Am. Chem. Soc.*, 2010, **132**, 14273–14278.

189 M. C. Tang, D. P. K. Tsang, Y. C. Wong, M. Y. Chan, K. M. C. Wong and V. W. W. Yam, Bipolar gold(III) complexes for solution-processable organic light-emitting devices with a small efficiency roll-off, *J. Am. Chem. Soc.*, 2014, **136**, 17861–17868.

190 M. Tang, C. Lee, S. Lai, M. Ng, M. Chan and V. W. Yam, Versatile Design Strategy for Highly Luminescent Vacuum-Evaporable and Solution-Processable Tridentate Gold(III) Complexes with Monoaryl Auxiliary Ligands and Their Applications for Phosphorescent Organic Light Emitting Devices, *J. Am. Chem. Soc.*, 2017, **139**, 9341–9349.

191 M. C. Tang, D. P. K. Tsang, M. M. Y. Chan, K. M. C. Wong and V. W. W. Yam, Dendritic luminescent gold(III) complexes for highly efficient solution-processable organic light-emitting devices, *Angew. Chemie - Int. Ed.*, 2013, **52**, 446–449.

192 D. Zhou, W. P. To, G. S. M. Tong, G. Cheng, L. Du, D. L. Phillips and C. M. Che, Tetradentate Gold(III) Complexes as Thermally Activated Delayed Fluorescence (TADF) Emitters: Microwave-Assisted Synthesis and High-Performance OLEDs with Long Operational Lifetime, *Angew. Chemie - Int. Ed.*, 2020, **59**, 6375–6382.

193 C. H. Lee, M. C. Tang, F. K. W. Kong, W. L. Cheung, M. Ng, M. Y. Chan and V. W. W. Yam, Isomeric Tetradentate Ligand-Containing Cyclometalated Gold(III) Complexes, *J. Am. Chem. Soc.*, 2020, **142**, 520–529.

194 M. Y. Leung, M. C. Tang, W. L. Cheung, S. L. Lai, M. Ng, M. Y. Chan and V. Wing-Wah Yam, Thermally Stimulated Delayed Phosphorescence (TSDP)-Based Gold(III) Complexes of Tridentate Pyrazine-Containing Pincer Ligand with Wide Emission Color Tunability and Their Application in Organic Light-Emitting Devices, *J. Am. Chem. Soc.*, 2020, **142**, 2448–2459.